Hydro-Mechanical Behaviour of Bentonite-Based Materials Used for Disposal of Radioactive Wastes

Dissertation

as a requirement of the degree of
Doktor-Ingenieur (Dr.-Ing.)

at the Faculty of
Civil and Environmental Engineering
Ruhr-Universität Bochum

submitted by
Linzhi Lang
from Shandong, China

Reviewers
Prof. Dr. Jörg Renner
Dr. Snehasis Tripathy
Prof. Dr. Maria Datcheva
Prof. Dr. Wei Xiang

Bochum, February 2019

This work is dedicated to my beloved

parents, sister and brother.

Vorwort des Herausgebers

Das Thema der Promotionsarbeit von Herrn Linzhi Lang liegt im Bereich der Forschung zur Entsorgung von wärmentwickelnden radioaktiven bzw. toxischen Abfällen in tiefen geologischen Formationen bis zu 1000 m Tiefe. Das Ablagerungskonzept besteht in einem Multibarrierenkonzept, bei dem der mögliche Transport der Giftstoffe und Radionukleide in die Biosphäre durch redundante Barrieren verhindert werden soll. Zu diesen Barrieren gehören neben dem Behälter selbst eine an ihn angrenzende Pufferzone aus quellfähigem Bentonit oder Bentonit-Sand Gemischen und sogenannte Verschlussbauwerke ebenfalls aus vorverdichteten Bentonit-Sand-Gemischen, welche als Schacht- oder Streckenverschluss den gesamten Einlagerungsbereich abdichten.

Die vorliegende Arbeit beschäftigt sich mit dem Verhalten hochverdichteter Bentonite und Bentonit-Sand-Gemische. Aus der Anwendung dieser Bentonit basierten Baustoffe entweder als Puffer im Nahbereich des Behälters oder innerhalb der Abschlussbauwerke ergeben sich mechanische (M), hydraulische (H), thermische (T) und chemische (C) Einwirkungen, welche eine Materialantwort des Dichtmaterials erzeugen. Die mechanische Belastung resultiert aus dem umgebenden Gebirgsdruck, die hydraulische Einwirkung z.B. aus dem Zutritt von Wasser aus dem umgebenden Gebirge. Thermische Beanspruchungen gehen infolge des radioaktiven Zerfalls vom Abfall aus. Eine chemische Beanspruchung auf die Bentonitbaustoffe kann sich aus salzhaltigen Wasserzutritt ergeben. In der Realität treten diese Einwirkungen und die resultierenden Prozesse im Bentonitmaterial zeitlich überlagernd und gekoppelt auf. Aus diesem Grund ist das Verständnis der durch diese Einwirkungen hervorgerufenen Prozesse entscheidend für eine realistische Beschreibung.

Herr Lang greift in seiner Arbeit spezielle Einwirkungen bzw. Einwirkungskombinationen heraus und untersucht deren Effekte auf das Materialverhalten, vorwiegend anhand von experimentellen Analysen, welche durch numerische Untersuchungen und theoretische Betrachtungen ergänzt werden. So untersucht er die Auswirkung der volumetrischen Randbedingung auf die Wasseraufnahmefähigkeit des Bentonit-Sand-Gemisches, den Einfluss einer vorherigen Trocknung auf die spätere Quelldruck- und Permeabilitätsentwicklung als auch den Einfluss einer erhöhten Salzkonzentration auf das Quellverhalten. Zusätzlich hat er durch seinen experimentellen Datensatz eine verwendbare Grundlage zur Parameterkalibrierung geschaffen, welche zukünftig im Rahmen weiterführender Untersuchungen bei numerischen Modellierungen von Randwertproblemen von Nutzen sein wird.

Bochum, Februar 2019 Dr.-Ing. Wiebke Baille

Acknowledgements

This research was performed at the Chair of Foundation Engineering, Soil and Rock Mechanics, Ruhr-Universität Bochum (RUB). First and foremost, I would like to thank my supervisor, Prof. Tom Schanz, who provided a chance of doing research in RUB to me and gave me a lot of precious scientific support during my research work. His wisdom and personality deeply impress me. I am grateful to him for his support and am sorry that he has not lived to attend my graduation. The memory of him will remain forever with me.

I am grateful to Prof. Jörg Renner (RUB) and Dr. Snehasis Tripathy (Cardiff University) for their continuous support during my PhD work after Prof. Schanz' life was taken prematurely.

I am grateful to Prof. Maria Datcheva (Bulgarian Academy of Sciences) and Prof. Wei Xiang (China University of Geosciences) for acting as reviewers of my thesis. Their critical and constructive comments will significantly improve this work.

I would like to express my gratitude to Dr. Wiebke Baille and Dr. Diethard König for their continuous help and numerous constructive suggestions during my research work, which guide me through the long academic puzzlement to a sudden enlightenment. In addition, I also thank the other colleagues in RUB who provide me so much help in my work and life.

I gratefully acknowledge the financial support from China Scholarship Council (CSC), Deutsche Forschungsgemeinschaft (DFG) and Ruhr-Universität Bochum Research School PLUS (Germany's Excellence Initiative [DFG GSC 98/3]) during my PhD study.

Last but not least, I am sincerely graduate to my parents, sister, brother-in-law, brother, sister-in-law, nieces and nephews for their endless love and amazing support during my PhD study.

Bochum, February 2019 Linzhi Lang

Abstract

Compacted bentonite-based materials (bentonite and bentonite-sand mixtures) are often selected as buffer, backfill and sealing materials in the geological repository for the disposal of radioactive wastes because these materials exhibit several valuable properties (e.g. adequate swelling capacity, low water permeability). The aim of the present thesis is to advance the understanding of the influence of the thermo-hydro-mechanical-chemical (THMC) boundary conditions prevailing in the geological repository on the hydro-mechanical behaviour of compacted bentonite-based materials.

To study the effect of the THMC boundary conditions prevailing in the geological repository on the hydro-mechanical behaviour of buffer, backfill and sealing materials, laboratory tests under controlled-boundary condition were performed on bentonite-based materials. Water retention measurements were carried out under different confinement conditions (unconfined, constant vertical stress and constant volume conditions) on bentonite-sand (50/50) mixtures to investigate the effect of mechanical boundary conditions on the hydration of backfill and sealing materials. Multi-step swelling pressure tests were performed on compacted bentonite-sand (50/50) mixtures to examine the effect of hydraulic boundary conditions (water phase and suction) on the swelling capacity of backfill and sealing materials. Swelling pressure tests and suction measurements were carried out on bentonite-based materials to explore the quantitative effect of hydro-chemical boundary conditions on the swelling capacity of buffer, backfill and sealing materials. Swelling pressure and permeability tests were performed on desiccated bentonite samples and reference sample to study the effect of the desiccation due to the thermo-hydraulic boundary conditions on the swelling capacity and the permeability of bentonite buffer.

Experimental results from the water retention measurements showed that the confinement conditions (unconfined condition, constant vertical stress condition and constant volume condition) significantly affects the wetting water retention curves (WRCs) of bentonite-sand (50/50) mixtures. Moreover, the hysteresis loop of the wetting-drying WRCs is also affected by the confinement conditions. The effect of the confinement conditions on the WRCs of bentonite-sand mixtures (50/50) is due to their influence on the macrostructural voids of bentonite-sand (50/50) mixtures.

The magnitudes of the swelling pressure of compacted bentonite-sand (50/50) mixtures upon wetting are strongly affected by not only the magnitude of applied suction but also

water phase (water vapour and liquid water). For the applied suction range greater than 3 MPa, the swelling pressures due to the hydration with liquid water are greater than those due to the hydration with water vapour. The effect of suction and water phase on the swelling pressure is related to swelling mechanisms.

Based on the experimental results from this study and those reported in the literature it was found that the difference between the total suction of saturated bentonite-based materials and the suction of the aqueous solutions used to saturate the bentonite-based materials is nearly equal to the swelling pressure of saturated bentonite-based materials. The linkage between these three parameters indicates that the total suction of bentonite-based materials caused by the adsorptive and osmotic forces will not dissipate when the bentonite-based materials are saturated with aqueous solutions under constant volume condition. The link between these three parameters provides the framework for establishing a quantitative link between the swelling capacity of buffer, backfill and sealing materials and the chemical boundary condition in the geological repository.

The experimental results from the swelling pressure and the permeability measurements on desiccated bentonite samples showed that desiccation slightly increases the swelling pressure and the hydraulic conductivity of compacted bentonite, especially when the compacted bentonite undergoes the extreme desiccation at the applied suction greater than 700 MPa. Therefore, the desiccation due to the thermo-hydraulic boundary conditions in the geological repository could slightly increase the swelling capacity and the permeability of the bentonite buffer.

Contents

List of Figures

List of Tables

Nomenclature

μ	Total water potential
ψ_{a}	Applied suction
ψ_{t}	Total suction
σ_{v}	Vertical stress
$\sigma_{\mathrm{v}} - u_{\mathrm{a}}$	Vertical net stress
P_{s}	Swelling pressure
ATT	Axis translation technique
MWCO	Molecular weight cut-off
MW	Molecular weight
OT	Osmotic technique
PEG	Polyethelene glycol
RH	Relative humidity
VET	Vapour equilibrium technique
C_{c}	Compression index
C_{s}	Swelling index
e_{M}	Macro-structural void ratio
e_{m}	Micro-structural void ratio
e	Total void ratio

G_{s}	Specific gravity of soil particles
k	Coefficient of permeability
S	Degree of saturation
u_{a}	Air pressure
u_{w}	Pore water pressure
w_{M}	Macro-structural water content
w_{m}	Micro-structural water content
w	Water content

1 Introduction

1.1 Background

The disposal of high-level radioactive wastes (HLW) or spent fuel (SF) in geological repositories is an internationally accepted solution which provides long-term safe containment and isolation of radioactive wastes (OECD, 1995, 2003). The geological repository (Figure 1.1) refers to a facility in a geological environment at a depth from 300 to 1000 m and is usually used for disposal of HLW or SF.

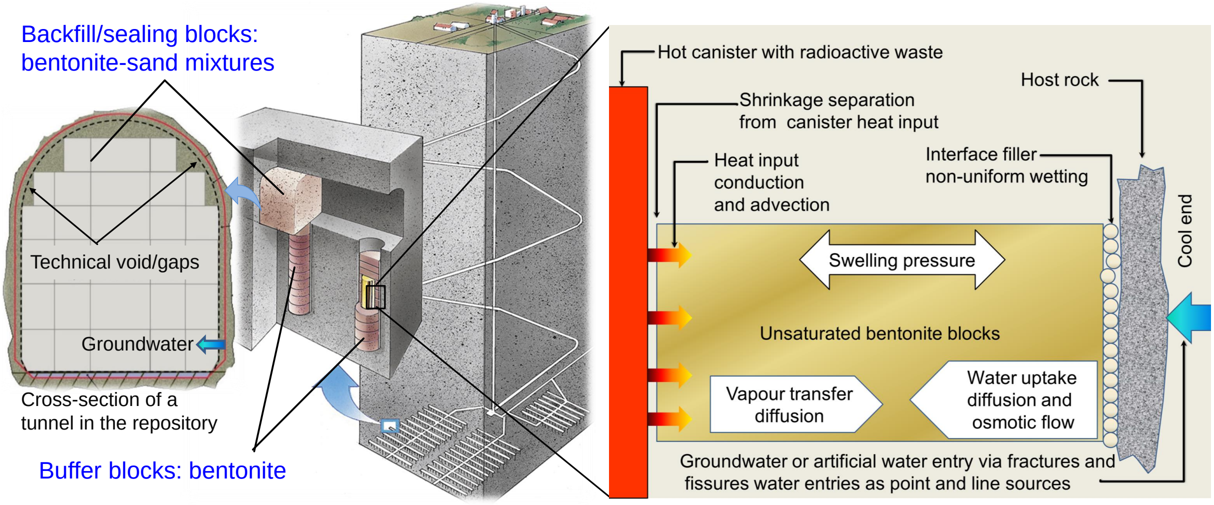

Figure 1.1: Sketch of the geological repository for high level radioactive wastes (HLW) or spent fuel (SF) (modified after Pusch & Yong (2006) and Sellin & Leupin (2013))

The geological repository generally relies on a multi-barrier system to isolate the radioactive wastes from the biosphere (OECD, 2003). Such a multi-barrier system typically consists of the natural geological barrier provided by the repository host rock and its surrounding and an engineered barrier system (EBS). The multi-barrier system creates overall robustness of the system that enhances the confidence that the waste will be successfully contained. The EBS comprises the artificial, engineered materials placed within a repository, including the waste form, waste canisters, buffer materials, backfill and seals (Figure 1.1). As one part of the EBS concept, the buffer materials, backfill and seals are designed to stabilise the repository excavations and the thermo-hydro-mechanical-chemical conditions, and to provide low permeabilities and/or diffusivities, and/or long-term retardation. Compacted bentonites are often selected as the buffer materials between the waste canister and the host rock and compacted bentonite-sand mixtures are often selected as backfill and sealing materials in excavated disposal galleries, drifts, shafts and tunnel (OECD, 2003; Sellin & Leupin, 2013).

Compacted bentonite-based materials (bentonite and bentonite-sand mixtures) are often selected as the buffer, backfill and sealing materials in the geological repository because these materials exhibit several valuable properties, e.g. the low transport capacity of radioisotopes, adequate swelling capacity and low water permeability (Pusch & Yong, 2006). The hydro-mechanical behaviour (e.g. water permeability, swelling capacity) of compacted bentonite-based materials is closely related to the boundary conditions which may occur in the geological repository. For instance, the swelling capacity of the compacted bentonite-based materials may significantly decrease when they are in contact with the groundwater with high salinity. The boundary conditions in the geological repository are very complex and may include thermal (temperature), hydraulic (suction and water phase), mechanical (stress and strain), chemical (solutes in groundwater) and even biological boundary conditions (Pusch & Yong, 2006; Johannesson et al., 2014). Moreover, these thermo-hydro-mechanical-chemical (THMC) boundary conditions are changeable during the operation of the geological repository. Therefore, studying the effect of the prevailing THMC boundary conditions in the geological repository on the hydro-mechanical behaviour of compacted bentonite-based materials is essential for assessing the long-term safety of the EBS.

Since there are technical voids/gaps between backfill/sealing materials and the host rock in the geological repository (Figure 1.1), the hydration of backfill and sealing materials may occur under different mechanical boundary conditions, i.e. unconfined, partially confined and completely confined conditions (Pusch & Yong, 2006; Villar, 2007). To study the effect of the mechanical boundary conditions on the hydration of backfill and sealing materials, it is necessary to determine the water retention curves (WRCs) of backfill and sealing materials under different mechanical boundary conditions. WRCs define the relationship between the water content of soil/material and matric and/or total suction and are necessary to analyse water permeability and volume change of unsaturated soil or materials. However, the measurement of WRCs is generally performed under unconfined condition through increasing or decreasing matric and/or total suction. Thus, determination of the WRCs of bentonite-sand mixtures under different mechanical boundary conditions is necessary to study the effect of the mechanical boundary conditions on the hydration of backfill and sealing materials.

Because the backfill and sealing materials in the geological repository may be gradually hydrated with either liquid water or water vapour, hydraulic boundary condition such as suction and water phase would affect the swelling capacity of the backfill and sealing materials. To estimate the influence of the hydraulic boundary condition on the swelling capacity of the backfill and sealing materials, it is necessary to determine the effect of suction and water phase on the swelling pressure of the backfill and sealing materials. The literature review on the swelling pressure of bentonite-based materials indicates that though some researchers have studied the swelling pressure-suction relationship of bentonite-based materials, few researchers have investigated the effect of water phase on the swelling pressure of bentonite-based materials. Thus, investigating the effect of suction and water phase on the swelling pressure of bentonite-sand mixtures is still essential for understanding the influence of the hydraulic boundary condition on the swelling capacity of the backfill and sealing materials.

The groundwater in the geological repository may include solutes such as salts and salt solution could strongly affect the swelling capacity of compacted bentonite-based materials (Pusch, 1980*b*; Karnland et al., 2005; Castellanos et al., 2008; Villar & Lloret, 2008). Therefore, the chemical boundary condition due to the solutes in the groundwater could significantly influence the swelling capacity of buffer, backfill and sealing materials used in the geological repository. The literature review on the swelling pressure of bentonite-based materials shows that the main focus of previous studies has been set on qualitatively illustrating the effect of chemical boundary condition on swelling pressure. However, no systematic studies have been made in the past to explore the quantitative link between swelling pressure and chemical boundary condition.

In the geological repository, either the HLW or the SF in deposition holes generates heat and thus leads to the thermal boundary condition. The elevated temperature results in the desiccation of bentonite buffer before the deposition holes are sealed (Johannesson et al., 2014). Johannesson et al. (2014) stated that the bentonite buffer blocks will be under thermal gradient for about three months before finalizing the backfill of deposition holes in the floor of the disposal tunnel. The hydro-mechanical behaviour of compacted bentonite buffer under the thermal gradient has been studied using column tests, mock-up and full-scale tests (Åkesson et al., 2009; Johannesson et al., 2014; Villar et al., 2016; Tripathy et al., 2017). These researchers found that under the thermal gradient, water in the unsaturated bentonite migrates from high temperature (hot zone) to low temperature (cold zone). This water migration finally results in dehydration and shrinkage of the bentonite buffer close to the heat source. The desiccation due to the thermal gradient may further affect the swelling ability and permeability of the bentonite buffer close to the heat source. The effect of desiccation on the swelling behaviour and the permeability of clays have been only addressed in the frame of studies regarding cyclic wetting-drying behaviour (Osipov et al., 1987; Day, 1994; Al-Homoud et al., 1995; Alonso et al., 1999; Albrecht & Benson, 2001; Akcanca & Aytekin, 2014). However, the influence of the desiccation at elevated temperature on the swelling capacity and the permeability of compacted bentonite has not been explored in the past.

1.2 Objectives

The aim of the present work is to advance the understanding of the influence of the THMC boundary conditions prevailing in the geological repository on the hydro-mechanical behaviour of compacted bentonite-based materials. The materials used in the present investigation are Calcigel bentonite and Calcigel bentonite-sand (50/50) mixtures.

The objectives of this thesis are:

- To experimentally establish the WRCs of the selected bentonite-sand mixtures under different confinement conditions (unconfined, constant vertical stress and constant volume conditions) and to determine the microstructural characteristics from wetting WRCs based on the method proposed by Navarro et al. (2017b) on Na-bentonite. The WRCs and the microstructural characteristics under different confinement conditions enable assessing the influence of the mechanical boundary conditions on the hydration of backfill and sealing materials.
- To experimentally determine the effect of suction and water phase on the swelling pressure of the compacted bentonite-sand mixtures during the wetting process with the osmotic and vapour equilibrium techniques to control suction. The effect of suction and water phase on the swelling pressure of the compacted bentonite-sand mixtures enables studying the effect of hydraulic boundary condition in the geological repository on the swelling capacity of backfill and sealing materials.

- To experimentally determinate the one-dimensional swelling-compression-rebound behaviour of compacted bentonite-sand mixtures at different suctions. The suction-controlled compression test results and microstructural characteristics allow calibrating Barcelona expansive model (BExM) used in the numerical simulation of the multi-step swelling pressure test.
- To numerically simulate the multi-step swelling pressure test of compacted bentonite-sand mixtures based on the BExM for verifying the assumption that the method for determining microstructural characteristics from the wetting WRCs based on the method proposed by Navarro et al. (2017b) on Na-bentonite is reliable on Ca-rich bentonite.
- To theoretically and experimentally determine the linkage between swelling pressure, the total suction of the bentonite-based materials and applied suction (suction and suction of hydrating fluids). The linkage between swelling pressure, the total suction of bentonite-based materials and the applied suction allows quantitatively estimating the effect of hydro-chemical boundary conditions on the swelling capacity of buffer, backfill and sealing materials.
- To experimentally study the influence of the desiccation due to the thermo-hydraulic boundary condition on swelling pressure and hydraulic conductivity of compacted bentonite-based materials for assessing the effect of desiccation on the swelling capacity and permeability of bentonite buffer.

1.3 Layout of the thesis

This thesis consists of ten chapters. The first chapter presents the background, the objectives and the layout of the thesis. Following the first chapter, the second chapter presents the literature review on the hydro-mechanical behaviour of bentonite-based materials. Chapter 3 describes the basic and the physiochemical properties of materials used and the experimental methods (sample preparation, experimental techniques and experimental procedure).

Chapter 4 presents the experimental results and discussion with respect to the effect of different confinement conditions on WRCs of the bentonite-sand mixtures. The microstructural characteristics of the bentonite-sand mixtures determined from wetting WRCs are also presented in this chapter. In addition, chapter 4 presents the results of the total suction measurements after the suction controlled wetting tests.

Chapter 5 presents the experimental results and discussion with respect to the multi-step swelling pressure tests on the compacted bentonite-sand mixtures. In this chapter, the effect of suction and water phase on the swelling pressure of the compacted bentonite-sand mixtures is analysed based on the multi-step swelling pressure test results. An empirical method for determining swelling pressure-suction relationship from the wetting WRCs under constant volume condition is proposed and validated in this chapter. Moreover, chapter 5 presents the results of the total suction measurements after swelling pressure tests.

Chapter 6 presents the experimental results and discussion with respect to one-dimensional swelling-compression-rebound behaviour of compacted bentonite-sand mixtures. One-dimensional swelling-compression-rebound curves at different constant suctions are obtained to assess the changes in yield stress, swelling index and compression index with the applied suction. The effect of stress level during the wetting process on the yield stress, the compression index and the swelling index of saturated bentonite-sand mixtures is also examined in this chapter. In addition, chapter 6 presents the coefficient of permeability as a function of bentonite content and the results of the total suction measurements of the saturated bentonite-sand mixtures after unloading.

Chapter 7 presents the numerical simulation and simulation results of the multi-step swelling pressure test on the compacted bentonite-sand mixtures. The BExM is first introduced and parameters used in this mechanical model are then calibrated with the experimental data obtained in Chapters 4, 5 and 6. The hydro-mechanical responses of the compacted bentonite-sand mixtures upon hydrating are numerically simulated using Code_Bright (UPC, 2017). Finally, the numerical simulation results are compared with those measured by the laboratory tests.

Chapter 8 chapter examines the linkage between swelling pressure, total suction and applied suction in the case of saturated bentonite-based materials and unsaturated bentonite-based materials. In the case of saturated bentonite-based materials, an equation describing the linkage between the swelling pressure, the total suction of saturated bentonite-based materials and the suction of hydrating fluids (applied suction) is derived based on the thermodynamics of soil moisture. The derived equation is then validated according to laboratory tests involving swelling pressure tests and total suction measurements after the swelling pressure tests on the bentonite. In addition, the experimental data for bentonite-sand mixtures presented in chapters 4, 5 and 6 are also used to validate the derived equation. In the case of the unsaturated bentonite-based materials, the linkage between swelling pressure, the total suction of the bentonite-based materials and applied suction is experimentally examined based on the experimental data obtained in this thesis. Chapter 8 also presents a relationship between the measured total suction and water content in bentonite-based materials.

Chapter 9 presents the experimental results and discussion with respect to the effect of the desiccation at elevated temperature on the swelling pressure and the permeability of the compacted bentonite. Suction controlled desiccation test results are first presented in this chapter. Subsequently, the chapter presents the swelling pressure test results for reference bentonite specimens and desiccated bentonite specimens. Finally, the permeability test results for reference bentonite specimen and desiccated bentonite specimens are presented in the chapter.

Chapter 10 presents the main conclusions drawn according to the experimental results, the numerical simulation and the theoretical considerations. Moreover, several recommendations for further investigation are also drawn in this chapter.

2 Literature review

2.1 Introduction

The present chapter mainly presents a detailed literature review on the hydro-mechanical behaviour of compacted bentonite-based materials. Section 2.2 introduces the montmorillonite structure, waters in montmorillonite and swelling mechanisms of montmorillonite since bentonites are one expansive clay/material with montmorillonite as the principal clay mineral constituent. Section 2.3 shows fabric and structure of compacted bentonite-based materials. Section 2.4 presents a literature review with respect to soil suction, including components of soil suction, techniques for measuring soil suction, suction of saturated bentonite-based materials and techniques for controlling suction. Sections 2.5, 2.6 and 2.7 present literature review on water retention curves (WRCs), compressibility and swelling pressure of bentonite-based materials, respectively.

2.2 Montmorillonite

Bentonite is a highly colloidal, expansive alteration product of volcanic ash. From the perspective of soil science, bentonite is a highly plastic, swelling clay material (Mitchell & Soga, 2005).

In clay science, bentonite is one of swelling clay with montmorillonite as the principal clay mineral constituent (Bergaya et al., 2006). In addition, bentonites may also contain the other clay minerals, e.g. kaolinite, illite, chlorite, and the non-clay minerals, e.g. quartz, feldspar, mica, calcite, dolomite. For instance, Calcigel bentonite used in this study consisted of 60-70% montmorillonite, 6-9% quartz, 1-4% feldspar, 1-2% kaolinite, 1-6% mica, 2-4% calcite, 1-3% dolomite and 3% other minerals (see section 3.2.5). Since bentonites are one expansive clay with montmorillonite as the principal clay mineral constituent, the properties of bentonites are mainly dominated by this clay mineral. This section presents the montmorillonite structure, water in montmorillonite and swelling mechanisms of montmorillonite.

2.2.1 Montmorillonite structure

The diagrammatic sketch of montmorillonite structure is shown in Figure 2.3. The montmorillonite is a phyllosilicates mineral that comprises repeating 2:1 unit layers where one octahedral (O) sheet is sandwiched between two tetrahedral (T) sheets (Grim, 1968; Velde, 1992; Bergaya et al., 2006). The T sheet is composed of silicon in tetrahedral coordination with oxygens, whereas the O sheet is composed of aluminum and/or magnesium octahedral coordination with oxygens and hydroxyls. Each unit TOT layer of montmorillonite is nearly 0.96 nm thick in the absence of any polar molecules and is from 200 to 1000 nm wide in lateral dimensions (Van Olphen, 1977; Bergaya et al., 2006; Segad et al., 2012a). Several unit TOT layers are stacked one above the other, in a parallel arrangement, to form a quasi-crystal or particle. For each 2:1 unit layer of the montmorillonite, its two tetrahedral sheets are almost exclusively occupied by silicon. The charge imbalance is due to divalent ion substitutions, F_e or M_g, for the trivalent aluminum ions in the octahedral site. Because of the isomorphous substitution in the octahedral and even tetrahedral sheets, the unit layer has a negative charge that is balanced by interlayer exchangeable cations, e.g. Na^+, K^+, Mg^{2+}, Ca^{2+}.

An assembly of TOT layers are referred as a montmorillonite particle or quasi-crystal and an assembly of montmorillonite particles are referred as an aggregate (Bergaya et al., 2006). As a consequence, interlayer, inter-particle, and inter-aggregate pores could be distinguished in montmorillonite (Figure 2.2).

2.2.2 Water in montmorillonite

Montmorillonites contain water in several forms: free water, capillary water, adsorbed water (inter-particle pore water), interlayer water, and hydroxyl water (Velde, 1992; Bergaya et al., 2006). A schematic diagram showing water in montmorillonites is presented in Figure 2.3. The capillary and adsorbed water, held by macro-pores (inter-aggregate pore water), can be easily removed by drying under ambient conditions. The adsorbed water is attracted to the surfaces of montmorillonite particles and could be removed by heating to 80-90°C. The interlayer water is associated with the hydration of interlayer cations, the interaction of clay surfaces with water molecules, and interlayer cations and water

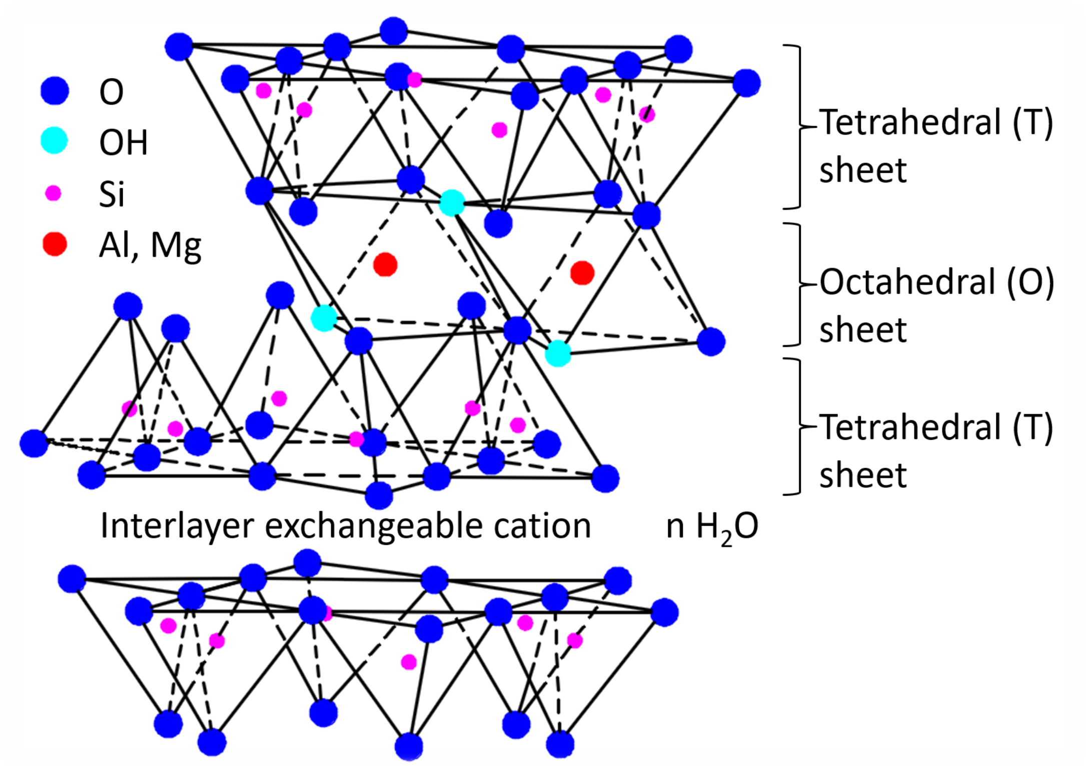

Figure 2.1: Sketch of montmorillonite structure (modified after Grim (1968))

activity in the clay-water system. It normally leaves the interlayer at 100-250°C, depending on the nature of the interlayer cations (Waclawska, 1984; Bray & Redfern, 1999; Önal & Sarıkaya, 2007; Środoń & MaCarty, 2008; Caglar et al., 2009; Derkowski et al., 2012; Lang et al., 2017). Hydroxyl water is also called crystalline water and is present in the form of OH units within the O sheet. The OH oxidises upon heating and forms H_2O (dehydroxylation reaction). The dehydroxylation reaction in montmorillonite occurs above 400°C.

2.2.3 Swelling mechanisms of montmorillonite

When montmorillonite is in contact with aqueous solutions or water either liquid water or water vapour, it can swell significantly. There are six separate processes which dominate the swelling of montmorillonite in aqueous solutions or water: crystalline swelling, diffuse double-layer (DDL) swelling, the breakup of the quasi-crystal or particle, cation demixing, co-volume swelling and Brownian swelling (Norrish, 1954; Van Olphen, 1977; Laird, 2006). The following sections present a literature review on the crystalline swelling,

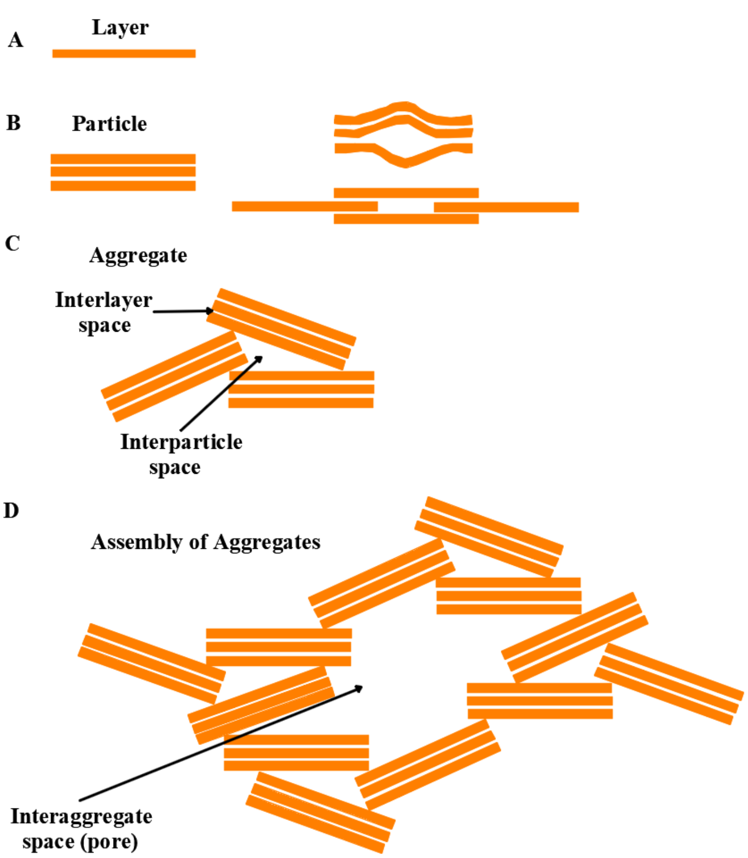

Figure 2.2: Diagram showing (A) a montmorillonite layer; (B) a particle, made up of stacked layers; layer translation and deformation can give rise to a lenticular pore; (C) an aggregate, showing an interlayer pore and an inter-particle pore; and (D) an assembly of aggregates, enclosing an inter-aggregate pore (copied from Bergaya et al. (2006))

DDL swelling, the breakup of the quasi-crystal or particle and cation demixing since the other two swelling processes would be insignificant in determining the swelling state of compacted bentonite-based materials (Van Olphen, 1977; Laird, 2006; Liu, 2013). In addition, it should be noted that the crystalline swelling and osmotic swelling are the main mechanisms and the other four swelling processes are actually the secondary effects of crystalline swelling and osmotic swelling.

2.2.3.1 Crystalline swelling

The crystalline swelling is a process whereby 0 to 4 discrete layers of water molecules are intercalated between the unit layers of a montmorillonite particle. The occurrence of the crystalline swelling is due to the hydration of ions and surfaces of the unit layer of the

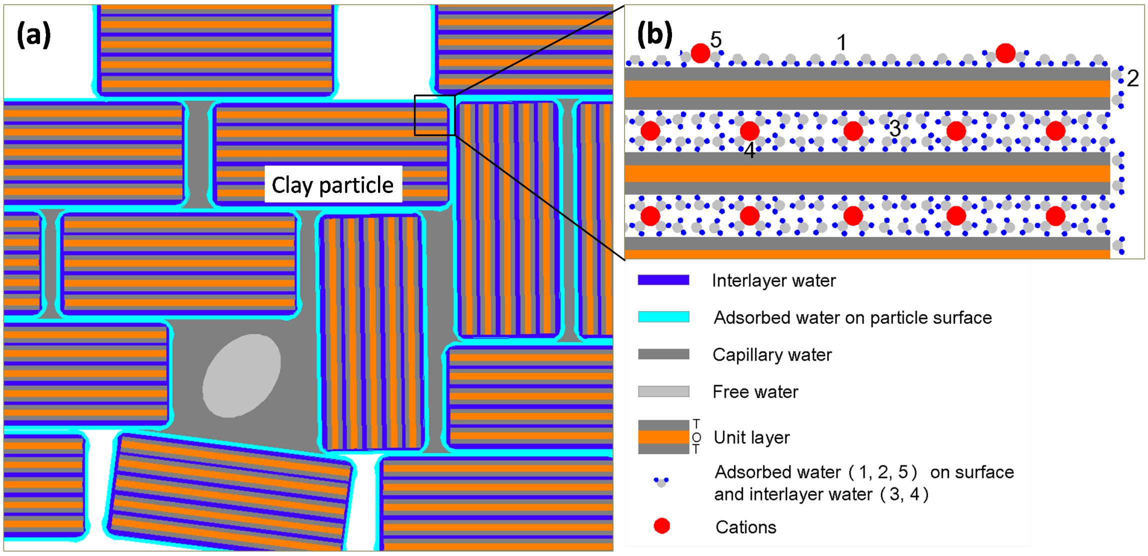

Figure 2.3: Schematic diagram showing water in montmorillonites in the case of (a) inter-particles and (b) particle

montmorillonite particle. Layer hydrates with 0, 1, 2, 3 and 4 layers of water molecules are distinguished by basal spacings of nearly 9.6, 12.6, 15.6, 18.6 and 21.6 Å. The crystalline swelling is dominated by a balance between strong forces of attraction and repulsion or a balance between potential energies of attraction and repulsion (Slade & Quirk, 1991; Laird, 1996, 2006).

Factors related to the hydration of the unit layer of the montmorillonite can affect the crystalline swelling of montmorillonite. These factors include layer charge, the nature of exchangeable cations in interlayer, temperature, relative humidity, concentration of aqueous solutions and so on. The extent of crystalline swelling of montmorillonite decreased with increasing layer charge (e.g. Norrish (1954), Slade & Quirk (1991), Laird (2006)). The magnitude of the crystalline swelling is affected by the nature of exchangeable cations in interlayer or the hydration energy of exchangeable cations in interlayer (e.g. Cases et al. (1997), Salles et al. (2010), Morodome & Kawamura (2011)). The extent of crystalline swelling decreases with an increase in temperature (e.g. Ferrage et al. (2007a), Morodome & Kawamura (2009), Morodome & Kawamura (2011)). The magnitude of crystalline swelling increases with an increase in relative humidity (Mooney et al., 1952), but decreases with an increase in concentration of aqueous solutions (Norrish, 1954; Slade & Quirk, 1991).

2.2.3.2 DDL swelling or osmotic swelling

The crystalline swelling is a process which takes place within particle or between the unit layers. However, the DDL swelling is a process which mainly takes place between particles (Van Olphen, 1977; Laird, 2006; Liu, 2013). As mentioned in the preceding section, the montmorillonite particle carries a net negative charge as a result of the isomorphous substitution. The net negative charge is compensated by the cations which are located on the layer surfaces. In the presence of water, these compensating cations tend to diffuse away from the layer surface because their concentration is smaller in the bulk solution. On the other hand, they are attracted electrostatically to the charged layers. The result of these opposing trends is the creation of an atmospheric distribution of the compensating cations in a diffuse electrical double layer on the exterior layer surfaces of the montmorillonite particle. The compensating cations between the layers of the stack are confined to the narrow space between the opposite layer surfaces. The DDL swelling is also called osmotic swelling because this swelling is due to the concentration differences of dissolved ions between the bulk solution and the mid-plane of two overlapped diffuse electrical double layers.

After the crystalline swelling has fully developed, the DDL may also develop within the interlayer space, especially the interlayer spaces of Na-and Li-saturated montmorillonites (Van Olphen, 1977; Segad et al., 2012a; Liu, 2013). For the case of Na- and Li-saturated montmorillonites in water or dilute solutions, they can be almost completely delaminated such that diffuse double layers form between all of the individual layers and each layer behaves as a separate colloid (Laird, 2006; Salles et al., 2010; Segad et al., 2012a). However, Ca-saturated montmorillonite particle still consists of several unit layers and their interlayer distances are limited to about 1 nm even it is in water or dilute solutions (Segad et al., 2012a,b).

In general, the DDL swelling occurs after the crystalline swelling has fully developed. Van Olphen (1977) stated that at the particle distances beyond four monomolecular layers of water (equivalent to about 10 Å), the crystalline swelling is no longer important and the DDL swelling becomes dominant. Slade & Quirk (1991) indicated that for Mg-, Ca- and La-saturated montmorillonites equilibrated with corresponding salt solutions, their crystalline swelling is limited to the basal spacing less than 15.5 Å and the transition from 15.5 to 19.0 Å spacings can be considered an osmotic process. Salles et al. (2010) studied the variation of inter-particle spaces in K-, Na-, Cs-, and Ca-saturated montmorillonites over relative humidity range from 11 to 97% using thermoporometry experiments. They found that for Li- and Na-saturated montmorillonites, the osmotic swelling occurs in inter-particle before the crystalline swelling fully developed. However, for Ca-montmorillonite, the osmotic swelling is strongly limited for all the range of relative humidity and apparent inter-particle swelling occurs as the relative humidity is greater than 97%. Moreover, Saiyouri et al. (2000, 2004) stated tat for the hydration of compacted Ca-rich bentonite, the full development of crystalline swelling arises at a suction of 3 MPa, whereas osmotic swelling arises at a suction of 26 MPa.

According to Gouy Chapman theory, there are several factors affecting the DDL swelling: electrolyte concentration, cation valency, dielectric constant, temperature, ion size and so on (Bolt, 1956; Van Olphen, 1977; Laird, 2006). An increase in the electrolyte concentration or the cation valency results in a decrease in the DDL thickness, whereas an increase in the dielectric constant leads to an increase in the DDL thickness. Temperature has a slight effect on the DDL thickness because an increase in temperature induces not only a direct increase in the DDL thickness but also a decrease in the dielectric constant. As a consequence, an increase in temperature decreases the DDL thickness slightly. An increase in the ion size results in an increase in the DDL thickness.

2.2.3.3 Formation and breakup of particles

Figure 2.4 shows the breakup and formation of particles (on the left the layers are grouped together in a single particle, in the middle the same layers are split into four particles and on the right the layers are completely delaminated). The dynamic nature of particles is a unique feature of montmorillonite suspensions. If two montmorillonite particles approach each other in an aqueous suspension with sufficient kinetic energy to overcome the DDL repulsion, the diffuse portions of their double layers will start to fuse. Simultaneously, anions, excess cations and water are expelled from the region between the two approaching DDLs. When the two DDLs approach each other enough (less than 4 nm) and sufficient anions and excess cations are expelled, the electrostatic forces will experience a complete reversal from being repulsive in the double layer region to attractive in the crystalline swelling region. Consequently, the two particles fuse together to form the one larger particle. Conversely, hydrodynamic forces due to shaking, stirring, raindrop effect and so on may divide a large particle into two smaller particles. For instance, Na- and Li-saturated montmorillonites in dilute aqueous systems can be almost completely delaminated such that diffuse double layers form between all of the individual layers. Unlike the Na- and Li-saturated montmorillonites, the Mg- and Ca-saturated montmorillonites in dilute aqueous systems do not spontaneously delaminate. The hydrodynamic forces due to shaking, stirring and even sonication may result in some large particles breaking up to form a suspension of smaller Mg- or Ca-saturated montmorillonite particles. However, most Mg- and Ca-saturated montmorillonites can not be completely delaminated.

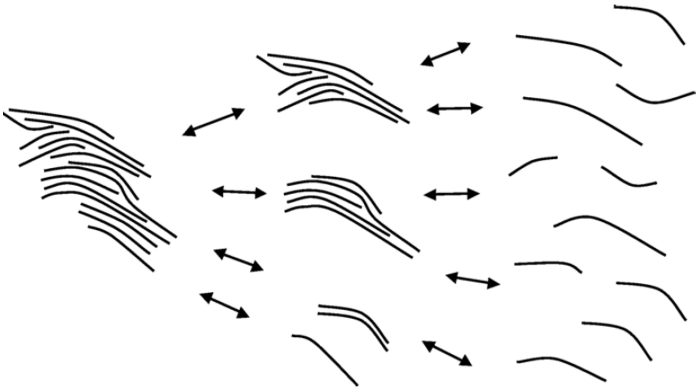

Figure 2.4: Diagram depicting the breakup and formation of particle (copied from Laird (2006))

2.2.3.4 Cation demixing

As two distinct types of cations (e.g. Na and Ca) occur in an aqueous montmorillonite system, the montmorillonite can exhibit difference preference for one cation over the other one. This cation exchange selectivity is controlled by a complex feed-back process by which the extent of the crystalline swelling governs selectivity for one cation over another. Selectivity as well as the composition of the equilibrating solution governs the mix of cations and other clay and solution properies govern the extent of the crystalline swelling. The demixing of cations is one result of such complex feed-back system. For instance, in a Na/Ca montmorillonite system, demixing means that Na cation will have a tendency to be segregated in certain interlayers when the competing Ca cations are segregated in to other interlayers. If the clay is shaken, the particles will readily break apart at interlayers dominated by Na (Figure 2.5). The phenomenon of demixing is a major reason why a relatively small amount of Na can be so disruptive to soil structure.

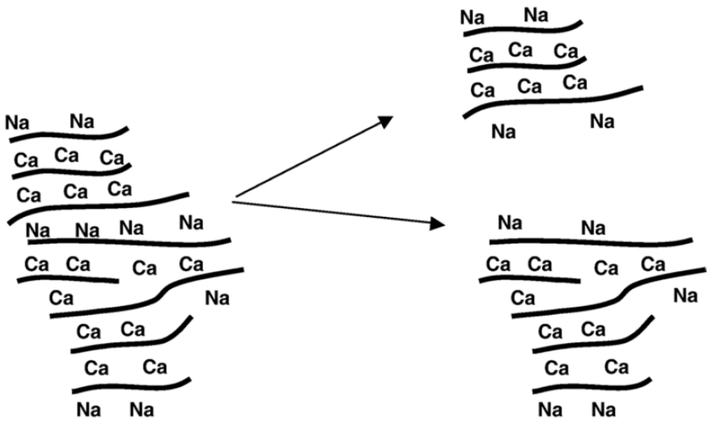

Figure 2.5: Schematic diagram depicting demixing of Ca and Na and the preferential breakup of montmorillonite particles along interlayers dominated by Na (copied from Laird (2006))

2.3 Fabric and structure of compacted bentonite-based materials

Microstructure refers to the arrangement of particles, particle assemblies and pore spaces in a soil (Collins & McGown, 1974; Sridharan et al., 1971; Mitchell & Soga, 2005; Romero & Simms, 2008). A possible microstructure representation of a compacted bentonite-based material is presented in Figure 2.6. The microstructure of a compacted bentonite-based material is composed of arrangements of clay aggregates, silts, sand grains and pores between them (Nagaraj & Murthy, 1985; Agus, 2005). The clay aggregate is composed of clay particles and intro-aggregate pores (interlayer pore and inter-particle pore). The clay particle is an arrangement of clay unit layers with interlayer pores in between. The inter-aggregate pores refer to the pore between inter-aggregate, the pore between the clay aggregate and silt, and the pore between the clay aggregate and sand grain.

The common methods for determining the microstructure of compacted bentonite-based materials are mercury intrusion porosimetry (MIP), scanning electron microscopy (SEM) and environmental scanning electron microscopy (ESEM) (Romero & Simms, 2008). Microstructural investigation into compacted bentonite-based materials shows that they have a double porosity structure, especially in unsaturated compacted bentonite-based materials (Cui et al., 2002; Lloret et al., 2003; Agus & Schanz, 2005*b*; Delage et al., 2006; Arifin, 2008; Romero et al., 2011; Wang et al., 2013a; Seiphoori et al., 2014; Manca et al., 2015).

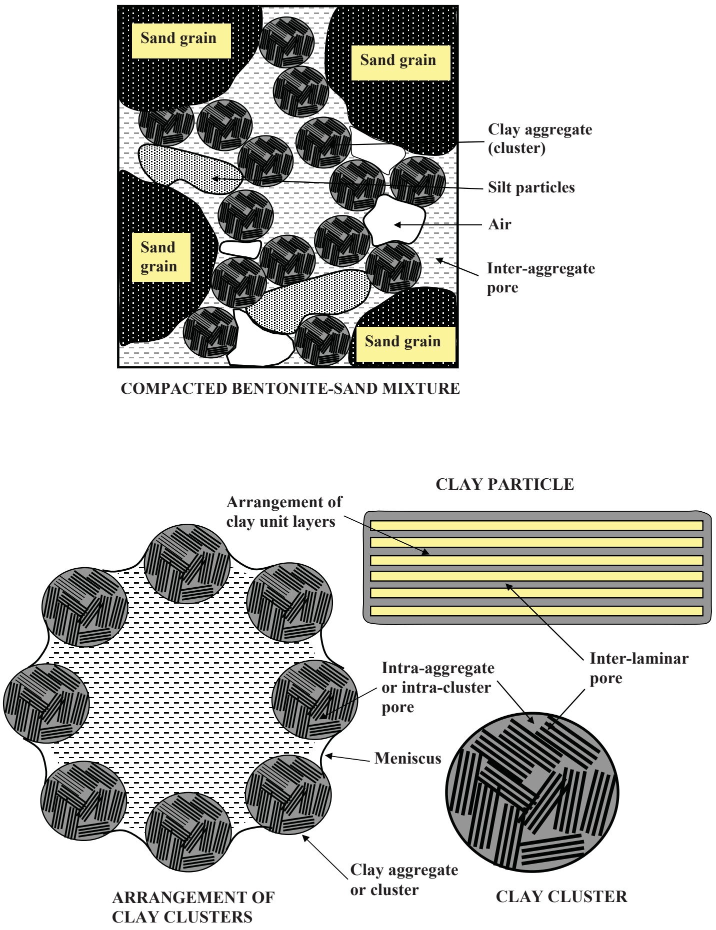

Figure 2.6: Schematic view of possible representation of a compacted bentonite-based material (copied from Agus (2005))

The double porosity structures of compacted bentonite-sand mixtures and compacted bentonite are shown in Figures 2.7 and 2.8, respectively.

Microstructure of compacted bentonite-based materials provides a good insight into hydro-mechanical behaviour of compacted bentonite-based materials. For instance, the changes in microstructural and macrostructural void ratios upon wetting can be used to explain swelling pressure and hydraulic conductivity (Lloret et al., 2003; Wang et al., 2013a; Seiphoori et al., 2014). In addition, microstructural parameters (i.e. microstructural and macrostructural void ratios) are necessary for simulating long-term hydro-mechanical behaviour of compacted bentonite-based materials used for disposing of HLWs (Gens & Alonso, 1992; Alonso et al., 1999, 2005; Sánchez et al., 2005; Wang et al., 2013b).

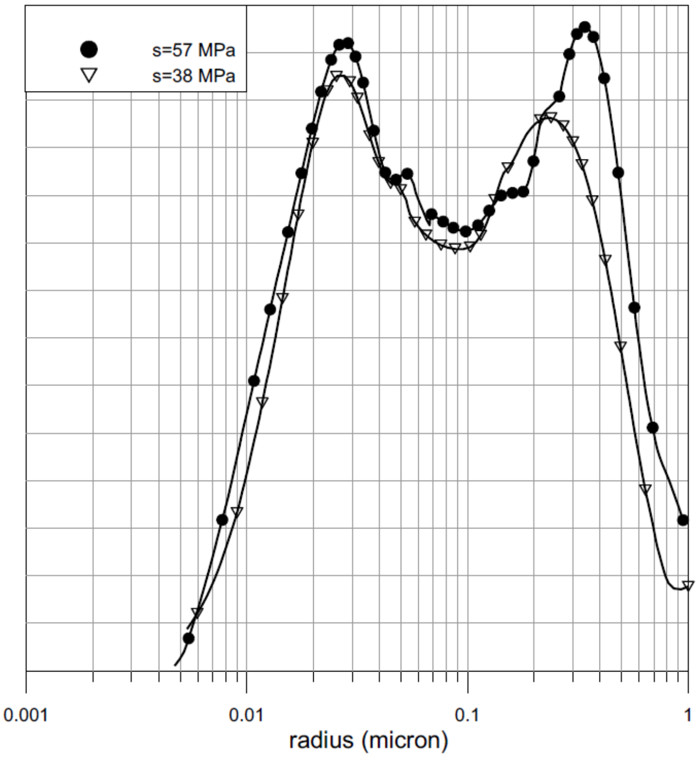

Figure 2.7: Pore-size distribution curves of compacted bentonite-sand mixtures (70/30) at 38 and 57 MPa suction obtained by mercury intrusion porosimetry (copied from Cui et al. (2002))

As mentioned in preceding paragraph, the MIP, SEM and ESEM are common techniques for obtaining the microstructural parameters of compacted bentonite-based materials. However, these techniques are generally costly and time-consuming. Navarro et al. (2017b) proposed a method for determining the intra-aggregate (microstructural) and inter-aggregate (macrostructural) water content of MX-80 bentonite using experimental data from wetting WRCs. This method is valid for the MX-80 bentonite, but the validation of the other types of clay has not been carried out (Navarro et al., 2017b). To validate their method, the microstructural and macrostructural void ratios of bentonite-sand mixtures are determined from wetting water retention curve (chapter 4) and simulation of the hydraulic-mechanical behaviour of compacted bentonite-sand mixtures based on Barcelona expansive model (chapter 7) is performed.

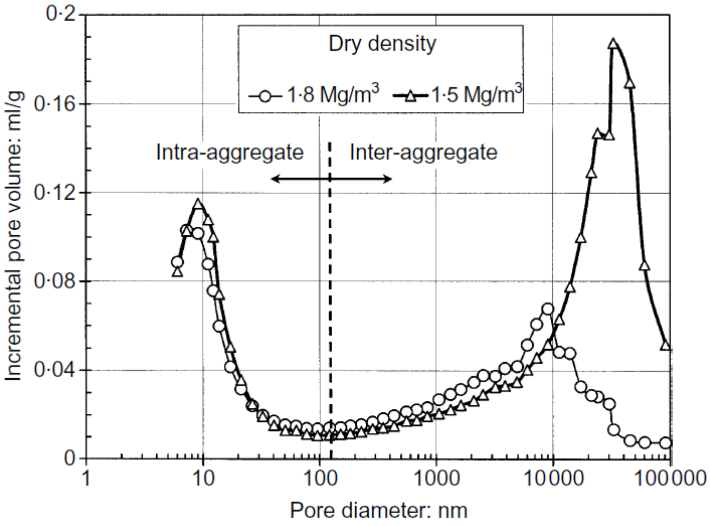

Figure 2.8: Distribution of incremental pore volume for two compacted bentonite samples at different dry densities. Mercury intrusion porosimeter test (copied from Lloret et al. (2003))

2.4 Soil suction

2.4.1 Components of soil suction

Soil suction is commonly referred to as the free-energy state of soil water (Edlefsen & Anderson, 1943). The free-energy of soil water can be measured in terms of the partial vapour of the soil water (Richards, 1965). The thermodynamic relationship between soil suction (ψ) and the partial pressure of the pore-water vapour ($\overline{u}_{\mathrm{v}}$) is given by Eq.(2.1) (Fredlund & Rahardjo, 1993)

$$\psi = -\frac{RT_{\mathrm{K}}}{M_{\mathrm{w}}\overline{\upsilon}_{\mathrm{w}}}\ln(\frac{\overline{u}_{\mathrm{v}}}{\overline{u}_{\mathrm{v0}}}) \tag{2.1}$$

where,

R is universal (molar) gas constant i.e., 8.31432 J/(mol K);

T_{K} is absolute temperature i.e., $T_{\mathrm{K}} = (273.15 + T)$ (K), T = temperature, °C;

$\overline{\upsilon}_{\mathrm{w}}$ is specific volume of water or the inverse of the density of water, m^3/kg;

M_{w} is molecular mass of water vapour (i.e., 18.016 kg/kmol);

$\overline{u}_{\mathrm{v0}}$ is the saturation pressure of water vapour over a flat surface of pure water at the same temperature, kPa.

The soil suction or total suction of unsaturated soils consists of matric and osmotic suctions (Fredlund & Rahardjo, 1993; Lu & Likos, 2004; Fredlund et al., 2012). Total suction is the equivalent suction derived from the measurement of the partial pressure of the water vapor in equilibrium with the soil-water relative to the partial pressure of the water vapour in equilibrium with free pure water (Fredlund & Rahardjo, 1993; Fredlund et al., 2012). Matric suction is the equivalent suction derived from the measurement of the partial pressure of the water vapour in equilibrium with the soil-water relative to the partial pressure of the water vapour in equilibrium with a solution identical in composition with the soil water (Fredlund & Rahardjo, 1993; Fredlund et al., 2012). Osmotic suction is the equivalent suction derived from the measurement of the partial pressure of water vapour in equilibrium with a solution identical in composition with the soil-water relative to the partial pressure of water vapour in equilibrium with free pure water (Fredlund & Rahardjo, 1993; Fredlund et al., 2012).

In clays, the matric suction is due to surface tension, adsorptive forces and osmotic forces (i.e. the electrical double layer forces), whereas the osmotic suction is due to the presence of dissolved solutes in the pore water (Yong & Warkentin, 1975; Fredlund & Rahardjo, 1993; Lu & Likos, 2004; Fredlund et al., 2012).

2.4.2 Techniques for meauring soil suction

Experimental techniques for measuring soil suction vary widely with suction components (i.e. total suction, matric suction and osmotic suction) and measurement ranges. The common experimental techniques for measuring total, matric and osmotic suctions are summarized in Table 2.1. In addition, measurement range for each experimental techniques is also listed in Table 2.1. The following sections present a literature review on the relative humidity sensor, chilled-mirror hygrometer and pore fluid squeezer since the others techniques listed in Table 2.1 are not involved in the thesis.

Relative humidity sensor

The relative humidity sensor is generally composed of a porous probe containing two electrodes separated by a thin polymer-coated substrate. This polymer-coated substrate is able to adsorb or release water when the relative humidity of the air in equilibrium with probe changes. There two types of relative humidity sensors: resistance and capacitance sensors. When the polymer-coated substrate adsorbs or releases water, the resistance and capacitance of the electrode-polymer system change. According to the known relationship between relative humidity and either sensor resistance or capacitance,

Table 2.1: Experimental techniques/devices for measuring soil suctions and their measurement ranges

Name of device/technique	Suction component measured	Range (kPa)	Reference
Psychrometers	Total	100-300000	R1
Non-contact filter paper	Total	1000-500000	R2
Relative humidity sensor	Total	Entire range	R3
Chilled-mirror hygrometer	Total	200-300000	R4
Tensiometers	Matric	0-100	R5
Null-type pressure plate	Matric	0-1500	R6
Thermal conductivity sensors	Matric	10-1500	R7
Contact filter paper	Matric	Entire range	R8
Pore fluid squeezer	Osmotic	Entire range	R9

R1: Spanner (1951), Richards & Ogata (1958); R2: McQUEEN & Miller (1968), Lu & Likos (2004); R3: Wiederhold (1997), Albrecht et al. (2003); R4: Gee et al. (1992), Agus & Schanz (2005*a*); R5: Stannard (1992); R6: Hilf (1956), Fredlund et al. (2012); R7: Phene et al. (1971a), Phene et al. (1971b); R8: McQUEEN & Miller (1968); R9: Manheim (1966), Krahn & Fredlund (1972).

the relative humidity can be determined for a either sensor resistance or capacitance measured. Polymer-based relative humidity sensors are generally applicable for relative humidity ranging from near 0% to near 100% (Wiederhold, 1997; Albrecht et al., 2003; Lu & Likos, 2004).

Wiederhold (1997) studied the difference between polymer resistance sensors and polymer capacitance sensors. He stated that resistance sensor tends to exhibit greater linearity over relative humidity range greater than 95%, whereas the capacitance sensor tends to exhibit greater linearity over relative humidity range less than 95%. In addition, he also indicated that both types of sensors exhibit fast response time (less than 15 s), low hysteresis (1-6%) and long-term stability.

Albrecht et al. (2003) assessed polymer capacitance sensors for measuring soil gas relative humidity and total suction in soils. They found that the capacitance sensors can be used to obtain unbiased estimates of relative humidity for a broad variety of soils with precision of approximately ±3%. In addition, they also stated that the capacitance sensors are non-hysteretic and relatively insensitive to temperature.

Because of their high reliability, little or no hysteresis, well-behaved response over a wide range of total suction, resistance to contaminants and little sensitivity to temperature, polymer-based capacitance relative humidity sensors have been widely applied in environmental and geotechnical engineering (Dueck et al., 2001; Albrecht et al., 2003; Agus & Schanz, 2005*a*; Arifin, 2008; Åkesson et al., 2009; Nguyen-Tuan, 2014; Cui et al., 2008; Ye et al., 2009; Mokni & Barnichon, 2016; Villar et al., 2016). For instance, polymer-based capacitance relative humidity sensors are used to monitor evolution of total suction of compacted bentonite-based materials while the compacted bentonite-based materials are wetted under coupled THM boundary conditions.

Chilled-mirror hygrometer

The chilled-mirror hygrometer uses the chilled-mirror dew point technique to measure the water activity or the relative humidity of a soil sample. In an instrument that uses the dew point technique, the soil sample is equilibrated with the head-space of a sealed chamber which contains a mirror and a means of detecting condensation on the mirror. At equilibrium, the relative humidity of the air in the chamber is the same as that of the soil sample. In the instrument, the mirror temperature is precisely controlled by a thermoelectic cooler. Detection of the exact point at which condensation first appears on the mirror is observed with a photoelectric cell. A beam of light is directed onto the mirror and reflected into a photo detector cell. The photo detector senses the changes in reflectance when condensation occurs on the mirror. A thermocouple attached to the mirror then records the temperature at which condensation occurs. The instrument then displays the final relative humidity and temperature and total suction of the soil sample can be finally determined based on Eq.(2.1).

Gee et al. (1992) described a chilled-mirror hygrometer or water activity meter for measuring total suction of soils. This device is capable of measuring total soil suction in the range from 300 to 300000 kPa and its repeatability of measurements is found to be equal or better than the rated precision (±0.3% relative humidity). Later, commercial chilled-mirror hygrometer or water activity meter occurs with a name of Aqualab-3, Aqualab-3TE, WP4, Aqualab-4TE and so on (Decagon Devices, 2003; Meter Group, 2018; Decagon Devices, 2010). The application of the commercial chilled-mirror hygrometers to measuring total suction of soils has been investigated by several researchers (Leong et al., 2003; Agus & Schanz, 2005*a*; Cardoso et al., 2007; Agus et al., 2010; Seiphoori et al., 2014). Leong et al. (2003) stated that for the chilled-mirror dew-point technique (WP4), its error in total suction measurement is less than 150 kPa for the suction range from 137 to 2500 kPa. Agus & Schanz (2005*a*); Agus et al. (2010) found that the chilled-mirror hygrometer technique (Aqualab-3TE) appears to provide the most accurate means of measuring total suction in the suction range from 200 to 30000 kPa for benonite-sand mixtures. In addition, they also indicated that this technique is deemed to be the most accurate compared with psychrometers, non-contact filter paper and relative humidity sensor.

Pore fluid squeezer

The pore fluid squeezer is a device for determining the osmotic suction of a soil according to the electrical conductivity of a small amount of pore water extracted from the soil (Manheim, 1966; Krahn & Fredlund, 1972; Arifin & Schanz, 2009; Fredlund et al., 2012). A pore fluid squeezer is mainly composed of a heavy-walled cylinder and piston squeezer. When a extraction pressure is applied on the piston squeezer, the pore water in the soil can be extracted and collected. Since pure water has a relatively low electrical conductivity compared with pore-water with dissolved salts, the electrical conductivity of the pore-water in the soil reflects the concentration of dissolved salts that is relevant to osmotic suction. For a small amount of pore-water extracted from a soil, its electrical conductivity can be measured. According to the calibration relationship between electrical conductivity and osmotic suction, the osmotic suction of the soil can be then determined based on a electrical conductivity measurement.

2.4.3 Suction of saturated bentonite-based materials

Following saturation of a compacted bentonite-based sample with deionized water, the matric and the total suction of the sample are generally assumed to be nearly equal to zero or 0.001 MPa. Although the suction of deionized water is approximately equal to zero, however, the assumptions with regard to a zero matric suction and a zero total suction in case of saturated bentonite-based materials may not be considered appropriate. Fredlund et al. (2012) stated that even when a soil is saturated with a positive pore-water pressure, the osmotic component of the total suction still remains. Tripathy et al. (2014a) found that the calculated osmotic suction in various bentonites increased from 2 MPa to more than 19 MPa during the drying process. In addition, they also stated that the magnitude of osmotic suction of bentonites depended on the nature of exchangeable cations and the water content. Total suction measurements after constant volume swelling pressure tests on a bentonite and on a sand-bentonite mixture that were saturated with deionized water and salt solutions have been reported by Karnland et al. (2005) and Arifin (2008), respectively. These studies have demonstrated that the measured total suctions after the release the swelling pressure in bentonite-based materials can significantly be greater than 0.001 MPa. The measured total suction after completion of swelling pressure tests was found to vary from several hundreds of kilopascal to 37 MPa for a Na-bentonite (Karnland et al., 2005) and up to about 3 MPa in case of a heavily compacted bentonite-sand mixtures (Arifin, 2008). These studies imply that the type and amount of exchangeable cations and the water content or the swollen dry density influence the total suction of saturated bentonites.

In addition to the water content, temperature and composition of the pore water, the overburden pressure influences the swelling clay suction (Croney, 1952; Kassiff & Shalom, 1971; Towenr, 1981). They stated that for saturated swelling clays, the overburden pressure was equal to the sum of effective suction and pore water pressure. The effective suction is the matric suction of an unloaded sample of the soil whose water content is the same as that of a loaded sample. The pore water pressure is the pore pressure of the loaded sample. Moreover, Lambe & Whitman (1969); Nagaraj et al. (1994); Singhal et al. (2015) indicated that removal of overburden pressure from clays can induce a negative pore water pressure or capillary suction.

A review of the literature presented herein suggested that an interdependency between the swelling pressure, total suction and suction of the hydrating fluid may be expected in case of swelling clays. However, no systematic studies have been made in the past to explore this aspect. Such studies are expected to advance the understanding of the changes in the swelling pressure and in total suction in response to a variation in the properties of the hydrating fluid. Additionally, understanding of the linkage between the various relevant parameters will enable developing models that in turn will facilitate evaluating the influence of hydro-mechanical-chemical boundary conditions on the stability of the deep geological repositories.

2.4.4 Techniques of controlling suction

This section presents literature review on suction control techniques which are commonly used during performing unsaturated soil experiments. There are three common techniques for controlling suction: axis translation technique (ATT), osmotic technique (OT) and vapour equilibrium technique (VET). The first two techniques are used to control matric suction, whereas the last one is used to control total suction.

2.4.4.1 Axis translation technique (ATT)

The ATT is the most common technique for controlling suction during carrying out unsaturated soil experiments. The ATT is related to the practice of increasing pore air pressure (u_{a}) while maintaining pore water pressure (u_{w}) at a reference value through a saturated, porous, high-air-entry ceramic plate or a cellulose acetate membrane (Richards, 1941; Hilf, 1956; Fredlund & Rahardjo, 1993; Lu & Likos, 2004). Because either ceramic plate or a cellulose acetate membrane is permeable to dissolved salts, this technique can only control matric suction ($u_{\mathrm{a}} - u_{\mathrm{w}}$). Figure 2.9 presents a schematic of cross section at the boundary between an unsaturated soil sample and a saturated high-air-entry ceramic plate. For drying test, the air pressure is elevated and water is drained from the sample through the high-air-entry ceramic plate. The drainage will continue until a equilibrium water content of the sample corresponding to the applied matric suction is established. The applied suction is recorded as the difference between the water pressure on the one side of the high-air-entry plate and the pore air pressure on the other side of the high-air-entry plate.

Many experimental instruments based on the ATT have been developed and evaluated for achieving the different objectives (Richards, 1941; Hilf, 1956; Bishop & Donald, 1961; Romero, 1999; Ng & Pang, 2000; Leong et al., 2004; Agus, 2005; Hoffmann et al., 2007; Lins et al., 2009; Fredlund et al., 2012). Bishop & Donald (1961) developed unsaturated triaxial device for investigating the behaviour of unsaturated soil. Romero (1999) and

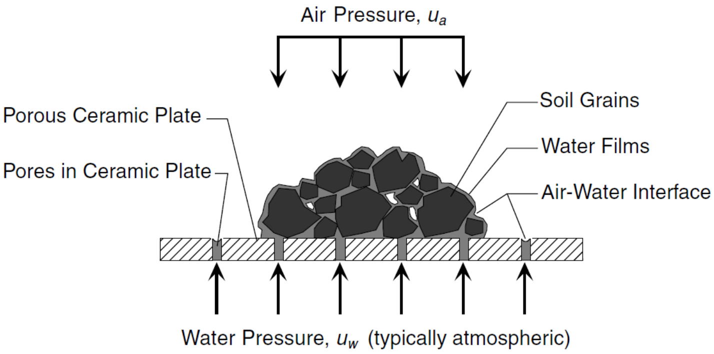

Figure 2.9: Schematic showing the enlarged cross section of the interface between unsaturated soil and high-air-entry plate for an axis translation measurement (copied from Lu & Likos (2004))

Lins et al. (2009) modified the common oedometer cells to allow performing suction-controlled oedometer test and obtaining WRCs under confinement conditions. Romero (1999); Agus (2005); Hoffmann et al. (2007) developed constant volume swelling pressure devices for studying changes in swelling pressure of expansive clays with decreasing the applied suction. Ng & Pang (2000) and Fredlund et al. (2012) developed a new stress controllable pressure plate apparatus to study the influence of the stress state on the soil-water characteristics. Leong et al. (2004) introduced a modified pressure plate device which allows determining both the drying and wetting soil-water characteristic curve.

Though the ATT has proved to be an efficient and reliable technique for controlling suction, there are still some experimental difficulties with respect to the application of the ATT (Delage et al., 2008c). The major experimental difficulties are the accumulation of diffused air beneath the high-air-entry ceramic plate, the control of the relative humidity of the air chamber to minimise evaporation or condensation effects on the sample, the application of the air pressurisation process at elevated degree of saturation and the estimation of the equilibrium time. In addition, controlled suction range of the ATT is generally from 0 to 1500 kPa, depending on the high-air-entry ceramic plates.

2.4.4.2 Osmotic technique (OT)

In addition to the ATT, the OT is another method of controlling matric suction (Kassiff & Shalom, 1971; Delage et al., 1998; Delage & Cui, 2008a). In this method, a soil sample and an aqueous solution consisting of the large size of polyethelene glycol (PEG) molecule and water are separated by a semi-permeable membrane (Figure 2.10). The semi-permeable membrane is permeable to water and ions but impermeable to PEG molecule and soil particles. Therefore, water molecule and ions are able to pass freely through the semi-permeable membrane. If there is a difference in free energy (water potential or suction or osmotic pressure) between the soil water and PEG solution, water will migrate from one side with high water potential to the side with low water potential. Water equilibrium between the soil and PEG solution is established until the difference in free energy between two sides dissipates. At equilibrium, the osmotic suction due to the dissolved salt is same on each side. Moreover, the osmotic suction due to PEG molecular is also equal to the matric suction of the soil. The magnitude of the suction of the PEG solution depends on the concentration of the PEG solution. The higher the concentration is, the greater the suction is. In practice, the concentration of the PEG solution is generally maintained constant by renewing the PEG solution at appropriate time intervals or circulating the PEG solution.

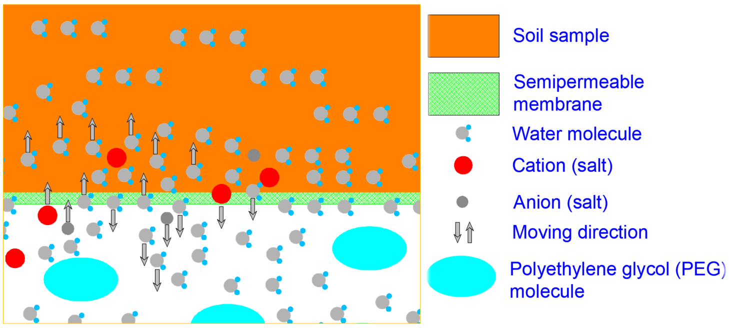

Figure 2.10: Schematic showing the enlarged cross section of the interface between unsaturated soil, semi-permeable membrane and polyethelene glycol (PEG) solution for osmotic technique

The semi-permeable membranes are generally characterized by the molecular weight cut off (MWCO) (Ballew et al., 2002). The MWCO of a membrane is determined by performing a comprehensive dialysis test with a set of solutes of known molecular weight. The MWCO of the membrane is determined as the molecular weight of the smallest solute which is at least 90% retained during this test (the smallest solute for which the permeation is 10% or less). In addition, the semi-permeable membranes may also be characterized by the rate at which a permeable species passes through the membrane. In general, the smaller the MWCO is, the higher the membrane permeability.

The selecting of MWCO of semi-permeable membrane is based on the molecular weight of PEG molecule that are going to be retained outside the membrane since soil particles is generally assumed to be unable to pass through the membrane. To avoiding PEG molecule infiltrating a soil, the ratio of the molecular weight of a PEG to the MWCO of a semi-permeable membrane should be at least 2 according to a rule of thumb (Ballew et al., 2002). A rule of thumb is to choose a MWCO by selecting an MWCO value about half of the molecular weight of the macromolecules to be retained in order to achieve a minimum 90% retention. For the osmotic technique used in geotechnical engineering, two types of membranes (i.e. the cellulotic and synthetic membranes) are commonly used and their MWCO ranges from 1500 to 14000. The common molecular weights of PEG molecules range from 1000 to 20000 (e.g. PEG 1000, PEG 2000, PEG 10000, PEG 20000), depending on the MWCO of membranes.

Compared to the ATT, the OT had several advantages. Since no artificial air pressure is required to apply, the OT can simulates the filed conditions and air diffusion issue can be avoided (Delage et al., 2008c). In addition, the OT is capable of controlling suction range from 0.01 to 10 MPa (Kassiff & Shalom, 1971; Delage et al., 1998, 2008c; Tripathy & Rees, 2013; Baille, 2014). As a consequence, the value of suction greater than 1.5 MPa can be easily applied through increasing the concentration of PEG solution.

The main disadvantage of the OT is related to the failure of the semi-permeable membrane in limiting the passage of PEG molecule (Delage & Cui, 2008b; Tripathy et al., 2011, 2014a). The cellulotic membrane that is most commonly used in geotechnical engineering is sensitive to bacteria attacks. The attacks may decrease the ability of the semi-permeable membrane in limiting the passage of PEG molecule. Tripathy et al. (2011) stated that the pore size of the semi-permeable membranes increased significantly, particularly at the higher applied suction based on the comparison of the atomic force microscope images of the semi-permeable membranes before and after the osmotic tests. To avoid the failure of the semi-permeable membrane, one solution is adding few drops of penicilin in the PEG solution (Kassiff & Shalom, 1971). Moreover, using a synthetic membrane instead of cellulotic membrane is found be possible to use the osmotic technique in a satisfactory manner to perform any desired test on partly saturated soils, regardless of its duration (Monroy et al., 2007).

For achieving the different experimental aims which can not be achieved by the ATT, several oedometers based on the OT have been developed and evaluated. (Kassiff & Shalom, 1971) developed an osmotic system coupled with the conventional consolidometer set-up to measure the swelling percentage and pressure under gradual and controlled moisture intake. Delage et al. (1992) modified the device developed by (Kassiff & Shalom, 1971) through introducing a closed circuit comprising a one litre bottle where the PEG solution was circulated by a pump. Afterwords, oedometers with the OT to controlling suction were improved by several researchers (Cuisinier & Masrouri, 2004; Yigzaw et al., 2016). The literature review shows that suction range of osmotic oedometers is limited from 0 to 8.5 MPa.

2.4.4.3 Vapour equilibrium technique (VET)

The VET is based on the equilibration of a closed space with a chemical system which produces the desired equilibrium vapour pressure or relative humidity. In other words, the VET is a technique for controlling the relative humidity of a closed system. The relative humidity of the chemical system can be controlled by using different saturated aqueous solutions (Greenspan et al., 1977; Delage et al., 1998; Tang & Cui, 2005). The values of the suction controlled by the VET can be determined by the psychometric law (Eq.(2.1)). In this technique, the exchange of water between the chemical system and a soil occurs in vapour phase and consequently, the total suction is controlled or applied by the VET. In general, the controlled suction range of the ATT is from 2 to 500 MPa, depending on the saturated aqueous solutions (Lloret et al., 2003; Delage et al., 1998; Tang & Cui, 2005; Agus, 2005).

In geotechnical engineering, the VET has been widely implemented during performing unsaturated soil experiments. The VET has been being used for determining the soil-water charactersitic curve or water retention curves by many researchers (e.g. Delage et al. (1998), Villar Galicia (2002), Agus (2005), Arifin (2008), Wang et al. (2012), Baille et al. (2014), Tripathy et al. (2014a), Gatabin et al. (2016), among others). To study the compressibility of unsaturated soils over high suction range, the VET coupled with the conventional oedometer was developed by several researchers (Lloret et al., 2003; Cuisinier & Masrouri, 2004; Agus, 2005; Wang et al., 2012). In addition, the VET coupled with the constant volume cells were also developed to measure the changes in swelling pressure of expansive clays with gradually decreasing the applied total suction (Hoffmann et al., 2007; Agus et al., 2013; Wang et al., 2014b; Yigzaw et al., 2016; Tripathy et al., 2017).

The main disadvantage of the VET is that the water equilibrium between a reference chemical system and a soil is extremely time-consuming. The equilibrium time can be from several weeks to several months, depending on several factors, e.g. the types of soils, initial suction of a soil sample, the applied suction (Ridley & Burland, 1993; Baille, 2014). The extremely slow equilibrium time is due to the fact that water exchange between the reference chemical system and the soil is water vapour and water transfer is controlled by diffusion (Delage et al., 2008c). To accelerate the water equalisation, a convection circuit driven by an air pump was used to force water vapour exchange between the reference chemical system and the soil by many researchers (e.g. Blatz & Graham (2000), Lloret et al. (2003), Agus (2005), Pintado et al. (2013)). However, the dynamic equilibrium achieved in this manner is not the same as the equilibrium in static conditions and thus, the applied suction is different the desired suction (Pintado et al., 2009, 2013).

2.5 Water retention curves (WRCs)

The WRCs define the relationship between suction and either water content or degree of saturation and are the measure of the water retention of a soil or material at for a given suction (Lu & Likos, 2004; Fredlund et al., 2012). In addition to the WRCs, the other terms used to refer to the relationship between the amount of water in the soil and soil suction are as follows: (a) soil-water characteristic curve (SWCC), (b) suction-water content relationship, (c) retention curves, (d) moisture retention curves and (e) soil moisture retention curves. These terms can be independently applied to describing the drying and wetting water content-suction curves.

Since the word "retention" is more closely related to the retention of water in materials other than soil (Fredlund et al., 2012), the term "WRC" has been generally preferred for bentonite-based materials (Pusch, 1982; Lloret et al., 2003; Villar & Lloret, 2004; Delage et al., 2006; Ye et al., 2009; Romero et al., 2011; Seiphoori et al., 2014; Tripathy et al., 2017). Because bentonite-based materials (i.e. bentonite, bentonite-sand mixtures) are used in the present investigation, the WRC is used to describe the retention of water in bentonite-based materials.

The WRC is generally presented by a plot of either water content or degree of saturation against the logarithm of the suction. For instance, Figure 2.11 shows a drying WRC: degree of saturation-suction relationship. A key feature of a WRC is the air-entry value for the drying WRC or the air-expulsion value for the wetting WRC. The air-entry value or air-expulsion value is equal to the soil suction of separation between the saturated and unsaturated states of soils (Vanapalli et al., 1999; Khalili et al., 2004; Lu & Likos, 2004). The drying WRCs are measured by subjecting saturated soil samples to an increasing suction, while the wetting WRCs are determined by subjecting unsaturated or oven-dried soil samples to a decreasing suction.

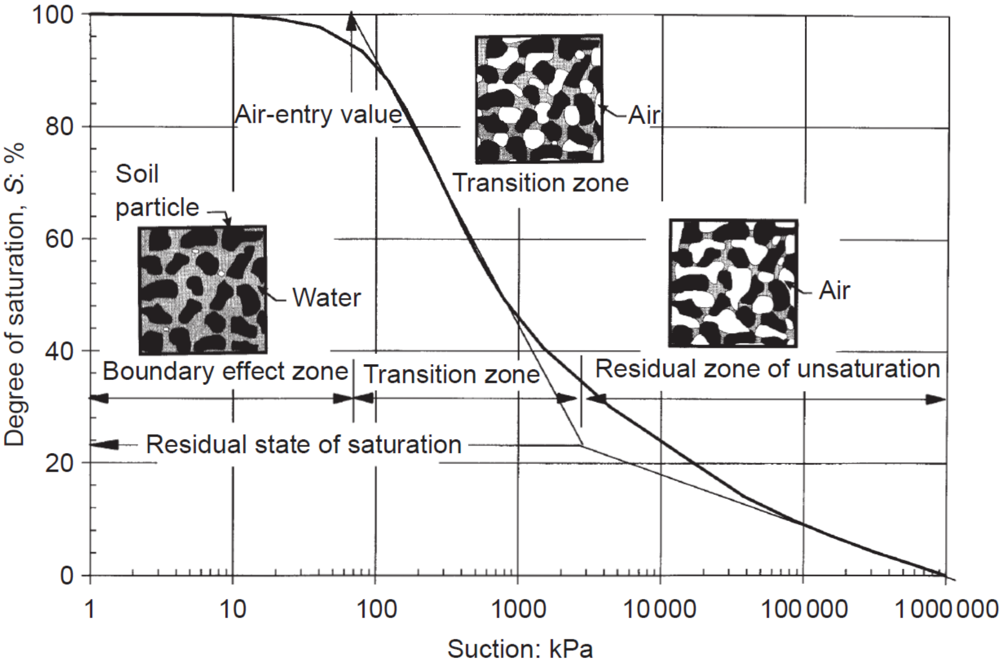

Figure 2.11: Typical drying water retention curve (copied from Vanapalli et al. (1999))

For a compacted bentonite-based material, its WRCs are closely related to its the mechanical properties, e.g. swelling pressure, permeability and compressibility (Agus et al., 2013; Ye et al., 2009; Wang et al., 2013; Marcial et al., 2002; Baille et al., 2014). In addition, the WRCs are also necessary to simulate the long-term hydro-mechanical behaviour of compacted bentonite-based materials used for disposing the nuclear wastes (Pusch & Yong, 2003; Sánchez et al., 2005; Wang et al., 2013b; Nguyen-Tuan, 2014; Mokni & Barnichon, 2016; Villar et al., 2016). The WRCs are the key to solving transient water and solute transport problems during the simulation. Thus, it is essential to determine the WRCs of compacted bentonite-based materials.

In general, there are several testing methods for determining the WRCs of compacted bentonite-based materials. These testing methods are based on the ATT, the OT and the VET which have been introduced in the preceding sections. Pressure plate devices based on ATT are usually used to apply the matric suction from 0.001 to 1.5 MPa (Fredlund et al., 2012; Lu & Likos, 2004). The OT using PEG solution and semi-permeable membrane allows to apply the matric suction from 0.01 to 10 MPa (Williams & Shaykewich, 1969; Kassiff & Shalom, 1971; Delage et al., 1998; Tripathy & Rees, 2013; Baille et al., 2014). Desiccator provided with a controlled relative humidity environment and based on VET is generally used to apply the total suction of 2 to several hundred MPa (Fredlund et al., 2012). In addition, chilled mirror hygrometer is also a method for determining WRCs by directly measuring total suction of soils (Leong et al., 2003; ASTM-D6836, 2003; Agus et al., 2010; Fredlund et al., 2012). This method is suitable for determining suctions in the range of 0.2 to several hundred MPa.

These conventional test devices for determining WRCs are not capable of applying a confining pressure to a compacted bentonite-based sample. However, the compacted bentonite-based materials in the field are usually under complex stress states. The hydration of bentonite-based materials used in the repositories occur under free swelling condition, partially restricted volume expansion condition and completely restricted volume expansion condition (constant volume condition) (Pusch & Yong, 2006; Villar, 2007; Sellin & Leupin, 2013; Johannesson et al., 2014).

To simulate field conditions in the laboratory, several test cells have been developed over the past few years. A suction controlled oedometer cell was developed at the Technical University of Catalonia (UPC) in Barcelona, Spain (Romero, 1999; Fredlund et al., 2012). The Barcelona oedometer cell can impose not only a vertical load but also matric or total suction on a soil specimen. In addition to the Barcelona oedometer, a Barcelona isochoric cell has been also developed to study hydro-mechanical behaviour of compacted bentonite-based materials (Hoffmann et al., 2007; Agus et al., 2013). The Barcelona cells are capable of applying matric suction based on ATT and total suction based on VET. Moreover, constant volume cells for specially determining WRCs of compacted bentonite-based materials have been also developed by many researchers e.g. Villar & Lloret (2004); Ye et al. (2012b); Wang et al. (2013a); Seiphoori et al. (2014); Gatabin et al. (2016). In this case, OT and VET are generally used to apply the matric suction and total suction, respectively.

The drawback of the VET is that the time to reach moisture equalisation is extremely long due to the fact that vapour transfer depends on diffusion (Delage et al., 2008c). Although forcing humid air to flow through a soil specimen could significantly reduce the equalisation time, the equilibrium suction in the soil specimen may be different from that of the applied suction (Pintado et al., 2009, 2013). In view of the equalisation time, both the ATT and the OT are reasonable techniques for controlling suction during determining the WRCs of compacted bentonite-based materials. In view of the controlled suction range, the OT is capable of controlling wider suction range than that of ATT. The OT is capable of controlling suction range of 0.01 to 10 MPa, whereas the ATT is only capable of controlling suction range of 0.001 to 1.5 MPa. Because the initial suction of the compacted bentonite-sand mixtures used as the engineered barrier in German repositories is in the range of 23 to 27 MPa, the OT is more appropriate. However, the current Barcelona oedometer and isochoric cell do not allow as-compacted samples to be wetted using osmotic technique to control suction.

Based on the developed or modified devices, the WRCs had been studied for several bentonite-based materials e.g. FEBEX bentonite, MX-80 bentonite, GMZ bentonite, Boom clay. Literature review indicates that the WRCs of bentonite-based materials vary considerably in shape, depending on the constraints of volume, or confining pressure applied to the specimen during the determination (Villar, 2007; Cui et al., 2008; Ye et al., 2009; Wang et al., 2013a; Romero et al., 2011; Gatabin et al., 2016; Tripathy et al., 2017). For instance, the effect of confinement conditions on the wetting WRCs of MX-80 bentonite-based materials is shown in Figure 2.12. Water content over the lower suction range (i.e. 4 MPa) is significantly greater on the WRCs determined in unconfined condition than on the WRCs determined in constant volume condition. Romero et al. (2011) found that the air-expulsion value of compacted Boom clay increased with the applied vertical net stress or decreasing the total void ratio.

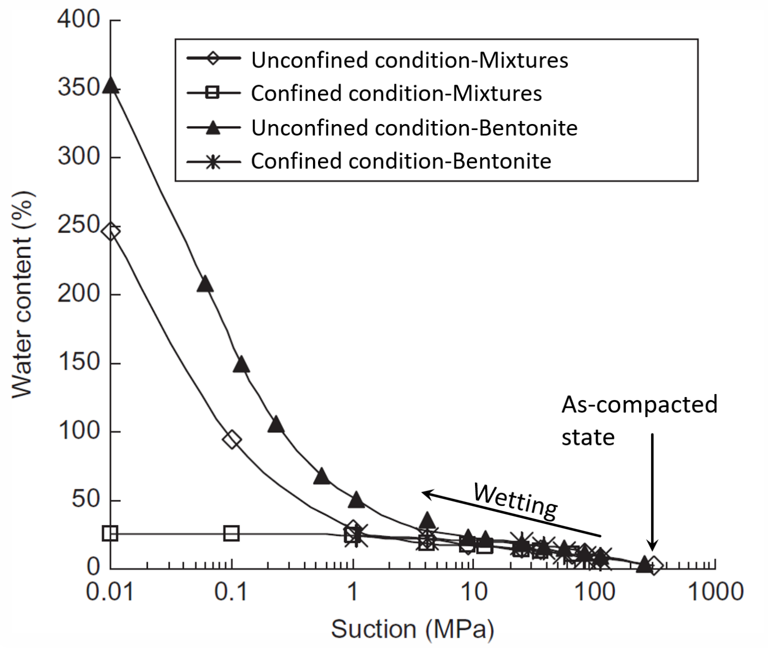

Figure 2.12: Water retention curves of bentonite-based materials (copied from Wang et al. (2013a))

Since compacted Calcigel bentonite-based materials (i.e. bentonite and bentonite-sand mixtures) have been selected as buffer, backfill and seals in German EBS concept for disposal of wastes (Rothfuchs et al., 2005, 2012; Xie et al., 2012; Jobmann et al., 2015, 2017), their WRCs had been investigated. Agus (2005); Arifin (2008); Nguyen-Tuan (2014) systematically studied the unconfined wetting-drying WRCs of compacted Calcigel bentonite-sand mixtures. Al-Badran (2011) investigated the drying WRCs determined under constant net stresses using slurry specimens made of Calcigel bentonite-sand mixtures. Agus et al. (2013) studied the wetting WRCs under constant volume condition using heavily compacted Calcigel bentonite-sand mixtures. Due to inefficiency of the vapour equilibrium technique to apply desired suctions in their study, wetting WRCs obtained over suction range above 2 MPa are questionable. However, no systematic investigation into the effect of confinement conditions on wetting WRCs of compacted bentonite-sand mixtures has been performed in the past.

2.6 Compressibility of bentonite-based materials

Compacted bentonite-based materials (i.e. bentonite and bentonite-sand mixtures) have been selected as buffer, backfill and seals in the deep geological repositories for disposal of HLWs. The deep geological repositories in many countries are planned to be located at great depths ranging from 300 m to about 1000 m below ground level surrounded by intact host rock. At such depths, the compacted bentonite based materials may undergo the compression (Tripathy & Schanz, 2007; Ye et al., 2012a). Thus, it is essential to investigate the compressibility of compacted bentonite-based materials for advancing the understanding of their hydro-mechanical behaviour. In addition, it is also necessary to obtain the compressibility of compacted bentonite-based materials for providing experimental evidences for constitutive models (Gens & Alonso, 1992; Villar, 1999).

One-dimensional compression behaviour of bentonite-based materials is generally obtained in laboratory by consolidation and suction controlled oedometer tests (Villar, 1999; Marcial et al., 2002; Lloret et al., 2003; Cuisinier & Masrouri, 2005; Baille et al., 2010; Ye et al., 2012a). The former provides the one dimensional compressive behaviour of saturated samples, whereas the latter provides the one dimensional compressive behaviour of unsaturated samples. From the one-dimensional consolidation and suction controlled oedometer tests, the relationship between void ration of the sample (e) with vertical net stress ($\sigma_{\mathrm{v}} - u_{\mathrm{a}}$) is directly determined. Their relationship is generally plotted on a plot of the void ratio against the logarithm of the vertical net stress (Lambe & Whitman, 1969; Alonso et al., 1990; Gens & Alonso, 1992; Mitchell & Soga, 2005). If the sample only undergoes the loading phase, the relationship between void ration with the vertical net stress is generally called compression curve. If the sample undergoes not only the loading phase but also the unloading phase, their relationship is called compression-rebound curve.

Based on the compression curve or compression-rebound curve, several hydro-mechanical parameters can be obtained: preconsolidation stress or yield stress, swelling index (C_s), compression index (C_c) and saturated coefficient of permeability (k). The preconsolidation stress or yield stress delimits the elastic and plastic branches of the compression curve. The swelling index corresponds to the slope of the elastic branch of the compression curve or rebound curve, whereas the compression index corresponded to the slope of the plastic branch of the compression curve. The saturated coefficient of permeability is calculated from the values of coefficient of volume compressibility and the coefficient of consolidation at each incremental vertical stress. The coefficient of consolidation is determined from the time-settlement curve during consolidation at each incremental vertical stress according to Casagrande or Taylor's method (Taylor, 1942; ASTM-D698, 1996; Mitchell & Soga, 2005).

The compression behaviour of saturated bentonite-based materials has been widely investigated in the past by many researchers, e.g. Mesri & Olson (1971), Sridharan & Rao (1973), Sridharan & Jayadeva (1982), Sridharan et al. (1986b), Yong & Mohamed (1992), Marcial et al. (2002), Tripathy & Schanz (2007), Baille et al. (2010) among others. Experimental results reveal that the compressive behaviour of saturated bentonite-based materials is affected by several factors: (a) nature of exchangeable cations, (b) specific surface area, (c) electrolyte concentrations, (d) pH of the fluids, (e) organic pore fluids, (f) initial compaction conditions, (g) temperature, (h) stress path and (I) stress history. For instance, Baille et al. (2010) indicated that the initial compaction conditions affect the swelling index, compression index and the permeability. In addition, experimental and theoretical investigations also reveal that physico-chemical forces, e.g. diffuse double layer repulsive forces, van der Waals attractive forces, controls the compression of saturated bentonite-based materials.

Meanwhile, studies with respect to the compressive behaviour of compacted unsaturated bentonite-based material have been also performed by several researchers. Villar (1999); Lloret et al. (2003) investigated the compressive/swelling behaviour of compacted unsaturated bentonite (FEBEX) through performing suction controlled oedometer tests. Examination of their experimental results revealed dependence of the yield stress on the applied suction and dependence of void ratio on stress paths. Cuisinier & Masrouri (2005) studied the influence of the controlled suction on the compressibility of compacted bentonite-silt mixture. They stated that the swelling index and compression index were not influenced significantly by the controlled suctions, whereas the preconsolidation stress was strongly affected by the applied suction. Similar experimental results on compacted bentonite-sand mixtures were also reported by Agus (2005) and Wang et al. (2013a). Ye et al. (2012a) investigated the compression behaviour of highly compacted GMZ01 bentonite with suction and temperature control. They found that with an increase in the applied suction, both the elastic compressibility and plastic compressibility decreased, while the preconsolidation stress increased considerably. With increasing temperature, the elastic compressibility changes insignificantly, but the plastic compressibility slightly decreased and the yield surface shrank. Similar experimental results on compacted bentonite-sand mixtures were also reported by Nguyen-Tuan (2014).

Compacted Calcigel bentonite-sand mixtures has been selected as the optimized sealing materials for construction of Germany underground repositories for radioactive wastes (Rothfuchs et al., 2005, 2012). More attentions in the past have been paid to the thermo-hydro-mechanical behaviour of compacted bentonite-sand mixtures with respect to the swelling capacity (swelling pressure and swelling strain), suction measurement, water permeability, the WCRs under unconfined condition and simulation (Rothfuchs et al., 2005; Agus, 2005; Arifin, 2008; Rothfuchs et al., 2012; Nguyen-Tuan, 2014). However, very limited studies of compressive behaviour of compacted unsaturated bentonite-sand mixtures have been performed. Two exceptions are perhaps the investigations carried out by Agus (2005) and Nguyen-Tuan (2014). Agus (2005) studied the effect of the suction on the compressibility of heavily compacted bentonite-sand (50/50) mixtures (dry density equal to 2.0 Mg/m^3). Nguyen-Tuan (2014) investigated the influence of the suction and temperature on the compressibility of slightly compacted bentonite-sand (50/50) mixtures (dry density equal to 1.4 Mg/m^3). However, the compressive behaviour of compacted unsaturated bentonite-sand (50/50) mixtures with a dry density of 1.8 Mg/m^3 has not been performed. This dry density approximately corresponds to the dry density of the compacted bentonite-sand block used in the field (Rothfuchs et al., 2005, 2012). In chapter 6, the one-dimensional compressive behaviour of compacted unsaturated bentonite-sand (50/50) mixtures with a dry density of 1.8 Mg/m^3 would be studied.

2.7 Swelling pressure

The swelling pressure of compacted bentonites has been considered as an important mechanical parameter for assessing the long-term stability of repositories for disposal of radioactive wastes. From the perspective of laboratory measurements, the swelling pressure is defined as the pressure required to hold a soil sample at constant volume when the soil sample takes in water either liquid water or water vapour, or aqueous solutions (Sridharan et al., 1986a; Gens & Alonso, 1992). Figure 2.13 presents the methods for measuring the swelling pressure in laboratory. Generally, there are three methods for measuring the swelling pressure: free swelling-load, swell-under-load and constant volume methods (Sridharan et al., 1986a).

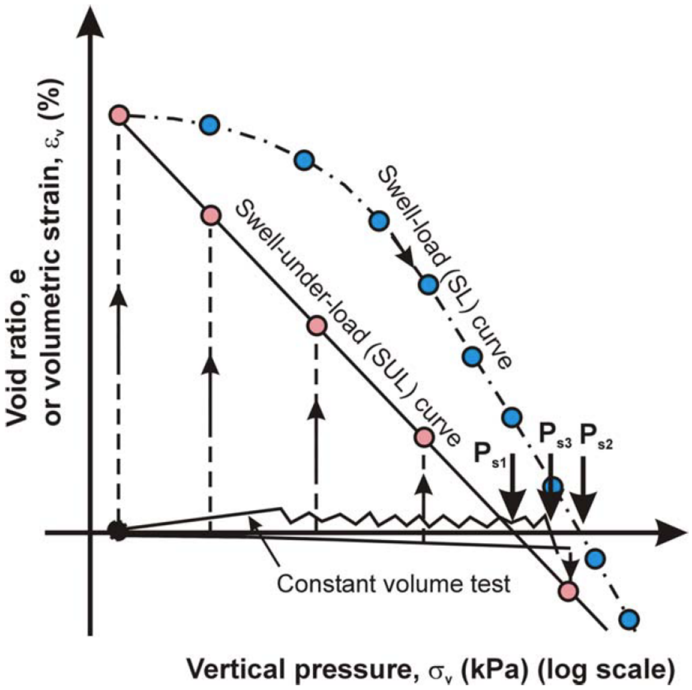

Figure 2.13: Testing methods for measuring swelling pressure (copied from Agus (2005))

For free swelling-load method, the sample is allowed, under a seating pressure to swelling on addition of water or aqueous solutions, to an equilibrium position. Afterwards, loads are applied in convenitent increments and the sample is consolidated at each load to obtain the compression curve (void ratio vs vertical stress). The vertical stress corresponding to the initial void ratio of the sample is defined as the swelling pressure (P_{s2} in Figure 2.12).

Unlike the free swelling-load method, the swelling-under-load method requires more than three identical samples. These identical samples are loaded at distinct vertical stress in oedometer apparatuses. After the deformations or void ratios of each samples reach equilibrium, water or aqueous solution is added to the oedometer apparatuses to flood the samples. The samples under the corresponding vertical stresses are allowed to swell or collapse until their deformations or void ratios reach the final equilibrium. For each sample, its final void ratio and the corresponding vertical net stress are plotted on a semi-logarithmic plot to form a compression curve (Figure 2.12). The vertical stress corresponding to the initial void ratio of the samples is defined as the swelling pressure ($P_{\mathrm{s}1}$ in Figure 2.12) determined by the swelling-under method.

For the constant volume method, a sample in the oedometer apparatus is allowed to take in water or aqueous solutions with gradually increasing or decreasing the vertical stress to maintain the sample at the original volume or void ratio. At equilibrium, the vertical stress corresponding to the original void ratio is defined as the swelling pressure ($P_{\mathrm{s}3}$ in Figure 2.12) determined by the constant volume method (Sridharan et al., 1986a). An alternative constant volume method is using the constant volume device which is equipped with a load cell to directly measure swelling pressure (Romero, 1999; Schanz & Tripathy, 2009). In the present investigation, the latter constant volume method is used to measure swelling pressures of compacted bentonite-based materials.

Several researchers compared these three methods for measuring swelling pressure. The "free swelling-load" method was consistently reported to give the maximum value of swelling pressure than the other methods (Sridharan et al., 1986a; El-Sohby et al., 1989; Agus, 2005). The constant volume method gives swelling pressures that have been reported to be intermediate between "free swelling-load" method and "swelling-under-load" (Sridharan et al., 1986a) method or to be the lowest values (El-Sohby et al., 1989; Agus, 2005). The phenomenon that the three methods determine different values of swelling pressures can be well explained according to stress-path dependency of swelling pressure introduced by Gens & Alonso (1992).

In addition to experimental methods, theoretical methods are also proposed by many researchers to estimate the swelling pressure of bentonite-based materials. Philip Low and his co-workers proposed a model based on thermodynamics of soil moisture to predict swelling pressure of saturated montmorillonites (Low & Anderson, 1958; Viani et al., 1983; Low, 1987). Yong & Warkentin (1975) introduced a method for calculating the swelling pressure by combining DDL model and Van't Hoff equation. They stated that the swelling pressure can be calculated as an osmotic pressure by means of the Van't Hoff equation. Komine & Ogata (1996, 2003) proposed a method for predicting the swelling strain and swelling pressure of bentonite-based buffer materials. This method combined the equations considering the influences of the sand-bentonite mass ratio and the exchangeable-cation compositions in bentonite with the theoretical equations of the Gouy-Chapman diffuse double layer theory and the van der Waals force. Sridharan & Choudhury (2002) proposed an equation based on DDL theory for obtain the swelling pressure of a given sodium montmorillonite clay-water electrolyte system for any void ratio and pore fluid properties. Tripathy et al. (2004) suggested equations for computing swelling pressures of compacted bentonites based on the diffuse double layer theory and the reported experimental data. Agus & Schanz (2008) proposed an approach for predicting swelling pressure of bentonites based on thermodynamic relationships between swelling pressure and suction. Their proposed method is found to be applicable for estimating the swelling pressures of saturated bentonite-sand mixtures and bentonites. Schanz & Tripathy (2009) investigated the applicability of the modified diffuse double-layer theory equations proposed by Tripathy et al. (2004) by comparing the prediction with laboratory test results on swelling pressures of compacted Calcigel bentonite. Schanz et al. (2013) introduced an alternative approach to estimate the swelling pressure of compacted bentonites using Gouy-Chapman diffuse double layer theory. Liu (2013) developed a mechanistic model to predict the swelling pressure of fully saturated, bentonite-based materials in distilled water or dilute saline solutions over a large range of final dry densities of bentonite. In this model, a thermodynamic relationship between swelling pressure and suction was applied to describing the contribution of crystalline swelling and the DDL model was used to describe the contribution of osmotic swelling. Moreover, this method also accounts for the demixing of exchangeable cations and the disintegration of the montmorillonite particles into small stacks of unit layers upon water uptake. Navarro et al. (2017a) suggested a calculation procedure to estimate the swelling pressure of bentonites. This calculation procedure is capable of quantitatively estimating the effect of environment salinity on swelling pressure of saturated MX-80 bentonite.

These theoretical methods are developed or modified to predict the swelling pressure of saturated bentonite-based materials. However, few methods for evaluating the swelling pressure of unsaturated expansive soil have been found in literature. Several exceptions are perhaps the investigations carried out by Vanapalli et al. (2010, 2012) and Tu & Vanapalli (2016) who studied semi-empirical models for estimating the swelling pressure of both natural and compacted expansive soils. The semi-empirical models establish the relationship between the initial suctions of unsaturated expansive soils and the swelling pressures of saturated expansive soils based on the WRCs. In fact, these semi-empirical models are the methods for evaluating the swelling pressures of saturated expansive soils rather than the swelling pressure of unsaturated expansive soils. Therefore, more investigations into predicting the swelling pressure of unsaturated bentonite-based materials used for disposing of radioactive wastes should be performed.

A proposal for methods for predicting the swelling pressure of unsaturated bentonite-based materials is generally based on experimental observation. Several researchers studied the changes in swelling pressure of compacted bentonite-based materials with gradually decreasing the applied suction. Kassiff & Shalom (1971) investigated the swelling pressure of an expansive clay mainly consisting of calcium montmorillonite upon gradually wetting, using the OT to decreasing the applied suction. They found that the swelling pressure is approximately equal to the difference between the suction a freshly prepared sample under zero load and the final suction of a sample continuously wetted and not allowed to change its volume. Lloret et al. (2003) studied the changes in swelling pressure of compacted FEBEX bentonite upon gradually wetting and found that its swelling pressure exhibited increase, decrease and again increase with decreasing the applied suction. Similar experimental phenomenon was also observed by Yigzaw et al. (2016) on compacted Greek and MX-80 bentonites. In addition, they also indicated that wetting modes involved with liquid water and vapour wetting caused different equilibrium swelling pressure values. Agus et al. (2013) investigated the variation of compacted Calcigel bentonite-sand mixtures as well as compacted bentonite with gradually decreasing the applied suction. They found that the swelling pressure of compacted Calcigel bentonite-based materials monotonically increased with decreasing the applied suction. Similar experimental results were also reported by Wang et al. (2014b) on compacted bentonite-claystone mixture, Seiphoori et al. (2014) on compacted bentonite-sand mixtures and Tripathy et al. (2017) on compacted MX-80 bentonite. Moreover, Agus et al. (2013) also found that the development of swelling pressure of compacted bentonite-sand mixtures while decreasing suction from 23 MPa (as-prepared state) to 2 MPa was insignificant. They stated that two reasons caused the insignificant development of swelling pressure within suction range of 23 to 2 MPa. The microstructural swelling possibly compensated for a great extent of the collapse of macro-structure, leading to only very small magnitudes of swelling pressure. Moreover, inefficiency of the VET to apply desired suction may be also held responsible for insignificant increase in the swelling pressure. To confirm these reasons, further investigation into changes in swelling pressure of compacted bentonite-sand mixtures with gradually decreasing the applied suction is required using both VET and OT to control suction above 2 MPa.

The literature review above shows that the swelling pressure of unsaturated bentonite-based materials is closely related to the applied suction. Since the WRCs define the relationship between the suction and either the water content or the degree of saturation, a linkage between the swelling pressure-suction relationship and WRCs may be exited. In addition, there may be a linkage between swelling pressure, applied suction and total suction of bentonite-based materials because the applied suction may be not equal to the total suction of bentonite-based materials at equilibrium. Thus, it is essential to study the linkage between the swelling pressure-suction relationship and WRCs, and the linkage between swelling pressure, the applied suction and total suction of bentonite-based material.

Unlike the swelling pressures of unsaturated bentonite-based materials, the swelling pressures of saturated bentonite-based materials have been widely studied in laboratory by numerous researchers. Kassiff & Shalom (1971); Villar & Lloret (2008); Baille et al. (2010) investigated the influence initial water content/suction on swelling pressures of saturated bentonite-based materials. Kassiff & Shalom (1971); Baille et al. (2010) stated that a decrease in initial water content or an increase in initial suction leaded to greater swelling pressures for a given dry density. However, Villar & Lloret (2008) indicated that the swelling pressure of saturated compacted FEBEX bentonite seems not to be affected by the initial water content. The dependency of swelling pressure on initial compaction dry density had been studied by many researchers, e.g. Pusch (1980*b*), Bucher & Max (1989), Madsen (1998), Karnland et al. (2005), Agus (2005), Villar & Lloret (2008), Yigzaw et al. (2016). They found that the initial dry density significantly affects the swelling pressure of saturated bentonite-based materials and the swelling pressure of saturated bentonite-based materials monotonically increases with their initial dry density or bentonite dry density. Arifin (2008); Villar et al. (2010); Bag (2011) studied the effect of temperature on swelling pressure of compacted bentonite-based materials. They found that the swelling pressure of saturated bentonites decreased with an increase in temperature. The influence of salinity of the water on swelling pressures of saturated bentonite-based materials had studied by some researchers, e.g. Pusch et al. (1990), Karnland et al. (2005), Castellanos et al. (2008), Zhu et al. (2013), Tripathy et al. (2014b). Their studies show that the salinity of the water used to saturating the bentonite-based materials can considerably influence the swelling pressure of compacted bentonite-based materials. The swelling pressure of saturated bentonite-based materials decreased with increasing the salinity of the water.

A review of the literature presented herein showed that the swelling pressure of saturated bentonite-based materials is a functional of their total suction (e.g. Kassiff & Shalom (1971), Karnland et al. (2005), Agus & Schanz (2008), Arifin (2008)) and the salinity of the water used to saturate the bentonite-based materials (Pusch et al., 1990; Karnland et al., 2005; Castellanos et al., 2008; Zhu et al., 2013; Tripathy et al., 2014b). Since the salinity of the water is a functional of its suction or chemical potential (Lu & Likos, 2004), an interdependency between the swelling pressure, total suction and suction of the hydrating fluid are expected in case of saturated bentonite-based material. However, few studies of the linkage between swelling pressure, total suction of saturated bentonite-based materials and the suction of hydrating fluid have been reported in the past. Such studies are expected to advance the understanding of the changes in the swelling pressure and in total suction in response to a variation in the properties of the hydrating fluid. Moreover, understanding of the linkage between the various relevant parameters will enable developing models that in turn will facilitate evaluating the influence of hydro-mechanical-chemical boundary conditions on the stability of the deep geological repositories.

In addition to initial compaction conditions, temperature and the salinity of water, the preliminary desiccation may also affect the swelling pressure as well as the water permeability of bentonite-based materials. The preliminary desiccation due to thermal gradient occurs before initiating the sealing the disposal hole. Compacted bentonite-based blocks, initially unsaturated, are installed in a disposal hole of a disposal tunnel. In the disposal hole, the compacted bentonite-based blocks are filled in the ring gap between the cold host rock and the hot canister containing HLWs. Sealing the disposal hole is generally initiated after all of buffer components and canisters are installed (Johannesson et al., 2014). Before sealing the disposal hole, a buffer protection made of a plastic or of rubber is installed in the technical gap between the host rock and buffer blocks. This protection is to prevent the buffer blocks to absorb water from the wet host rock before initiating the backfilling work. During the duration of protection (about three months), the bentonite-based buffer blocks are mainly under thermal gradient.

Hydro-mechanical behaviour of compacted bentonite-based materials under the thermal gradient has been studied using column tests, mock-up and full-scale tests (Åkesson et al., 2009; Johannesson et al., 2014; Villar et al., 2016; Tripathy et al., 2017). These researchers found that with increasing the distance between the measuring sites and the heater which simulates the hot canister, water content of the measuring sites increased, whereas the bulk density decreased. These results suggest that under the thermal gradient, water in the unsaturated bentonite-based materials migrates from high temperature (hot zone) to low temperature (cold zone). This water migration finally results in dehydration or shrinkage of the bentonite-based buffer close to the high temperature. Preliminary desiccation due to this thermal gradient may further affect the swelling ability and permeability of the bentonite buffer close to the high temperature.

The effect of the preliminary desiccation on the subsequent swelling behaviour and water permeability of clays have been only addressed in the frame of studies regarding cyclic wetting-drying behaviour (Osipov et al., 1987; Day, 1994; Al-Homoud et al., 1995; Alonso et al., 1999; Albrecht & Benson, 2001; Akcanca & Aytekin, 2014). However, little work has been done to study on influence of the preliminary desiccation at elevated temperature (i.e. 80°C) on the subsequent swelling behaviour and permeability of compacted bentonite-based materials.

2.8 Summary

A detailed literature review on the hydro-mechanical behaviour of compacted bentonite-based materials used for disposal of radioactive wastes is presented in this chapter. Section 2.2 presents the montmorillonite structure, waters in montmorillonite and swelling mechanisms of montmorillonite. Section 2.3 shows fabric and structure of compacted bentonite-based materials. Section 2.4 presents soil suction, including components of soil suction, techniques for measuring soil suction, suction of saturated bentonite-based materials and techniques for controlling suction. Sections 2.5 introduces water retention curves (WRCs), the methods for determining WRCs and features of WRCs of bentonite-based materials. Sections 2.6 presents a literature review on compressibility of bentonite-based materials including factors affecting the compressibility of bentonite-based materials. Sections 2.7 presents a detail literature review on experimental and theoretical methods for determining swelling pressure and factors affecting swelling pressure.

The detailed literature review on the hydro-mechanical behaviour of compacted bentonite-based materials indicated that some of the aspects pertaining to the use of bentonite-based materials as the buffer, backfill and seals require further investigations. These specific aspects include: (i) the influence of the confined conditions on wetting WRCs of bentonite-based materials, (ii) estimating microstructural characteristics from the wetting WRCs, (iii) the linkage between swelling pressure-suction relationship and the WRCs, (iv) the effect of suction decrease technique (the OT and VET) on swelling pressure development of compacted bentonite-sand mixtures within suction range of 23 to 2 MPa, (v) the compressibility of compacted bentonite-sand mixtures with intermediate dry density (1.8 Mg/m^3), (vi) the linkage between swelling pressure, total soil suction and applied suction in bentonite-based materials and (vii) the influence of preliminary desiccation due to the thermo-hydraulic boundary condition on swelling pressure and hydraulic conductivity of compacted bentonite-based materials.

3 Materials and experimental methods

3.1 Introduction

This chapter presents the properties of materials used, such as specific gravity, particle size distribution, Atterberg limits, mineral constituents, specific surface area and cation exchange capacity. Specific gravity, particle size distribution, Atterberg limits and specific surface area were determined from laboratory tests in this thesis, whereas the others were collected from previous studies.

In addition to the properties of materials, this chapter also presents the experimental methods used in this thesis. The laboratory tests performed in this thesis include water retention measurements, multi-step swelling pressure tests, one-dimensional swelling-compression-rebound tests, total suction measurements after swelling pressure tests, swelling pressure and permeability measurements after desiccation tests. The laboratory tests were designed according to two aspects of consideration. One is the possible THMC boundary conditions which may occur in the geological repository for the disposal of radioactive wastes. The other is to obtain the necessary parameters for performing the numerical simulation.

3.2 Materials

The materials used in this study were Calcigel bentonite and Hostun sand. Compacted Calcigel bentonite-based materials (bentonite and bentonite-sand mixtures) have been selected as buffer, backfill and seals in German EBS concept for the disposal of HLWs (Rothfuchs et al., 2005, 2012; Xie et al., 2012; Jobmann et al., 2015, 2017). Calcigel bentonite is a natural bentonite, from Bavaria, Germany and purchased from Süd-Chemie AG Moosburg, Germany. Hostun sand is a quartz sand, from France and purchased from Sibelco Europe.

3.2.1 Specific gravity and particle size distribution

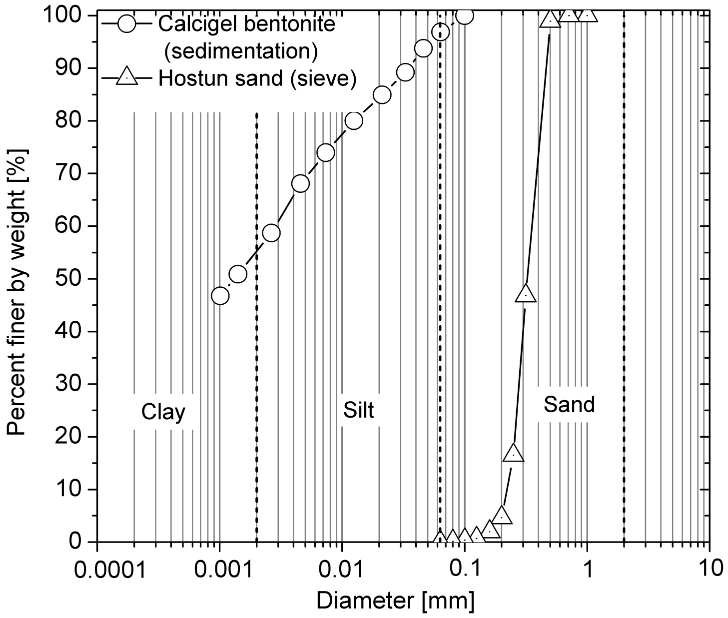

Figure 3.1: Particle size distributions of Calcigel bentonite and Hostun sand

The specific gravities of the bentonite and sand were determined by pycnometer method based on ASTM-D854 (2002). The specific gravity determined was found to be equal to 2.80 for the bentonite and 2.65 for the sand. The particle size distribution of the bentonite and sand was determined by sedimentation method (ASTM-D3977, 1997) and sieve method (ASTM-D422, 2007), respectively. The particle size distribution curves obtained are presented in Figure 3.1.

3.2.2 Atterberg limits

Liquid limit, plastic limit and plastic index were determined according to ASTM-D4318 (2000). Multipoint test method was used to determine the liquid limit. The liquid limit, plastic limit, plastic index and shrinkage limit of the bentonite were found to be equal to 119, 45, 74 and 10%, respectively. Mixtures of 50/50 bentonite-sand (dry mass ratio) was found to have a liquid limit of 62%, plastic limit of 26%, plastic index of 36% and shrinkage limit of 12%. The Atterberg limits of the bentonite-sand mixtures with the ratio of 50/50 were determined because this mixture is selected as the seals in the underground repositories for disposal of LILWs (Rothfuchs et al., 2005, 2012; Jobmann et al., 2017).

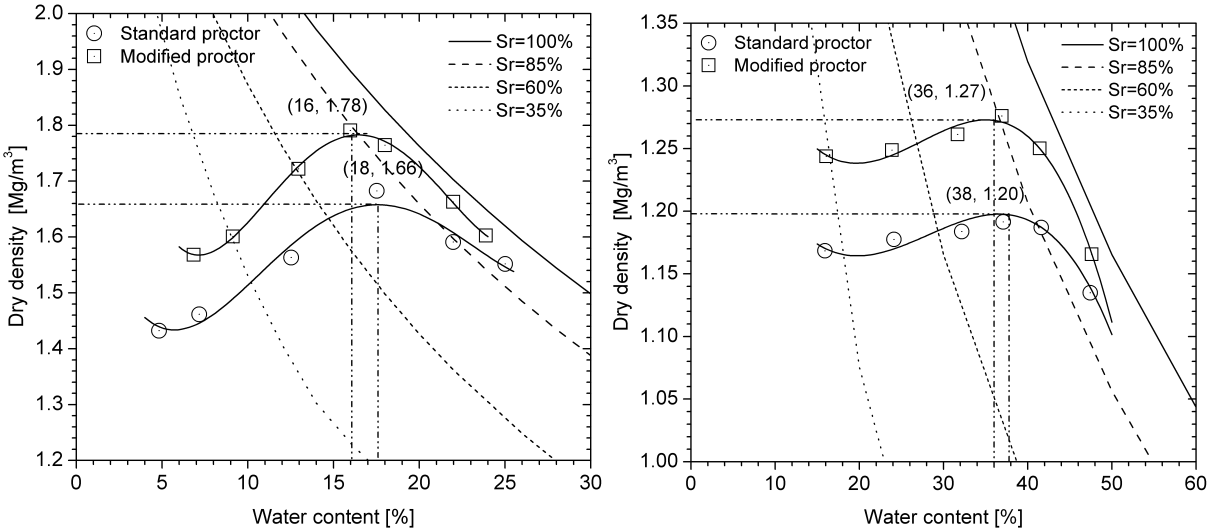

(a) (b)

Figure 3.2: Proctor curves of (a) bentonite-sand mixtures (50/50) and of (b) pure bentonite

3.2.3 Compaction characteristics

Proctor compaction curves of the bentonite-sand (50/50) mixtures and the bentonite were determined according to standard proctor method (ASTM-D698, 2007) and modified proctor method. Each mixture was dynamically compacted by the standard proctor method with a compaction energy of 600 kN-m/m^3 and by the modified proctor method with a compaction energy of 2700 kN-m/m^3. The standard and modified compaction curves are presented in Figure 3.2(a) for bentonite-sand mixtures (50/50) and in Figure 3.2(b) for pure bentonite. It should be noted that proctor compaction curves of bentonite were determined by Agus (2005) and Arifin (2008) for same bentonite. The optimum water content and the maximum dry density for each mixture are given in Table 3.1.

3.2.4 Specific surface area

The specific surface area was measured by ethylene glycol monoethyl ether (EGME) method (Cerato & Lutenegger, 2002). The specific surface area measured by this method represents total specific surface area. The total specific surface area was found be equal to 436 m^2/g for the bentonite and to 0.3 m^2/g for the sand.

Table 3.1: Optimum water content and maximum dry density of the materials used

Materials	Proctor	Optimum water content (%)	Maximum dry density (Mg/m^3)
Bentonite-sand (50/50)	Standard	18	1.66
	Modified	16	1.78
Pure bentonite	Standard	38	1.20
	Modified	36	1.27

3.2.5 Mineral constituents

Calcigel bentonite used in this study was composed of montmorillonite (60-70%), quartz (6-9%), feldspar (1-4%), kaolinite (1-2%), mica (1-6%), calcite (2-4%), dolomite (1-3%) and other minerals (3%). The amount of each mineral constituent shown in brackets was not measured in this study but provided by Süd-Chemie AG, Moosburg, Germany. The mineral constituents of the Calcigel bentonite used in this study were found to be similar to those of the Calcigel bentonite reported in the literature (Madsen, 1998; Agus, 2005; Steudel & Emmerich, 2013; Baille, 2014). A comparison of mineral constituents between the bentonite used in this study and those reported in the literature is shown in Table 3.2. The comparison demonstrates that the mineral constituents of Calcigel bentonite used in this study was very similar to those reported by Madsen (1998).

3.2.6 Cation exchange capacity

The cation exchange capacity (CEC) used in this study was not experimentally determined but selected from literature. Because the mineral constituents of Calcigel bentonite used in this study was very similar to those reported by Madsen (1998), the CEC and exchangeable cations from Madsen (1998) were used in this study. The CEC reported by Madsen (1998) was determined by the ammonium acetate method at pH 7 and found to equal to 62 cmol(+)/kg. Exchangeable cations were Na^+ (1.8 cmol(+)/kg), K^+ (0.2 cmol(+)/kg), Mg^{2+} (22.4 cmol(+)/kg) and Ca^{2+} (37.6 cmol(+)/kg).

In addition, the CEC of Calcigel bentonite has been also reported by the other researchers, e.g. Steudel & Emmerich (2013); Baille (2014). For comparison, the CECs reported by them were also summarized here. The CEC reported by Steudel & Emmerich

Table 3.2: Comparison of mineral constituents of Calcigel bentonites

Mineral constituents	Content [%]				
	Madsen (1998)	Agus (2005)	Steudel and Emmerich (2013)	Baille (2014)	This study
Montmorillonite	66.3	50-60	63.5	78	60-70
Quartz	8	5-10	5.9	4	6-9
Feldspar	2-4	5-8	-	-	1-4
Kaolinite	-	-	3.8	2	1-2
Illite	-	-	13.7	8	-
Mica	12-15	-	-	-	1-6
Calcite	3.8	1-5	3.3	3.5	2-4
Dolomite		10-15	7.3	3	1-3
Others	2-3	2-29	2.5	1.5	3

(2013) was measured with Cu-triethylenetetramine method (Lorenz, 1999) and equal to 63 cmol(+)/kg. The exchangeable cations were Na^+ (8 cmol(+)/kg), K^+ (2 cmol(+)/kg), Mg^{2+} (21 cmol(+)/kg) and Ca^{2+} (44 cmol(+)/kg). Similarly, the CEC given by Baille (2014) was also determined by Cu-triethylenetetramine method and similar experimental results were obtained. The value of CEC determined by Baille (2014) was 64 cmol(+)/kg and the exchangeable cations were Na^+ (3 cmol(+)/kg), K^+ (2 cmol(+)/kg), Mg^{2+} (21 cmol(+)/kg) and Ca^{2+} (50 cmol(+)/kg).

It should be noted that dissolved salts in Calcigel bentonite were very limited and could be neglected. Based on the measurements of osmotic suction using the squeezing technique (Fredlund et al., 2012), Arifin & Schanz (2009) found that the osmotic suction of Calcigel bentonite remained at about 0.05 MPa for a large range of water content. This indicates that the dissolved salts in Calcigel bentonite was minimal and could be neglected.

3.2.7 Summary of the properties of the materials used

According to the Unified Soil Classification System, both of the pure bentonite and bentonite-sand mixtures (50/50)) can be classified as inorganic clays of high plasticity

(CH). Hostun sand can be classified as silty sand. The main properties of the materials are summarized in Table 3.3

3.3 Experimental methods

This section presents sample preparation and experimental techniques and procedures. The laboratory tests conducted in this thesis include water retention measurements, multi-step swelling pressure tests, one-dimensional swelling-compression-rebound tests, swelling pressure tests and the total suction measurements after swelling pressure tests, swelling pressure and permeability measurements after desiccation tests.

3.3.1 Sample preparation

Slurry samples including bentonite and bentonite-sand (50/50) mixtures slurries are prepared for determining the drying-wetting WRCs under unconfined condition. The compacted bentonite-sand mixtures samples are prepared for determining the wetting WRCs under unconfined, constant vertical stress and constant volume conditions, performing one-dimensional swelling-compression-rebound tests and multi-step swelling pressure tests. The compacted bentonite samples are prepared for carrying out swelling pressure tests and total suction measurements after swelling pressure tests and as reference samples and for making desiccation samples. The swelling pressure and permeability tests were performed on the reference samples and desiccation samples.

3.3.1.1 Bentonite-sand mixtures samples

Slurry samples with a water content of 68% corresponding to $1.1\omega_L$ of bentonite-sand mixtures were prepared for obtaining the drying WRCs under unconfined condition. An adequate amount of water was added into the bentonite-sand mixtures with the water content of 5% at the ambient laboratory condition to reach the target water content of 68%. The bentonte-sand-water mixture was kept in a air-tight plastic container for two weeks to allow for water equilibrium. Prior to injecting the slurry into sample ring with 50 mm in diameter and 20 mm in height, a stirrer was used to sufficiently stirring the mixture to make homogeneous slurry samples.

To obtain the wetting WRCs under unconfined condition, the oven-dried samples were prepared following the procedure mentioned by Agus (2005); Fredlund et al. (2012). Slurry

Table 3.3: Summary of the main properties of the materials used

Properties	Materials		
	Calcigel bentonite	Hostun sand	Benonite-sand mixture (50/50)
Specific gravity G_s	2.80	2.65	2.73†
Liquid limit ω_L (%)	119	n/a	62
Plastic limit ω_P (%)	45	n/a	26
Shrinkage limit ω_S (%)	10	n/a	12
Plastic index I_P (%)	74	n/a	36
CEC (cmol(+)/kg)*	62	n/a	31†
Exchangeable cation (cmol(+)/kg)*: Ca^{2+}, Mg^{2+}, Na^+, and K^+	37.6, 22.4, 1.8 and 0.2	n/a	n/a
Montmorillonite content (%)	60-70	n/a	30-35†
Total specific surface area (m^2/g)	436	0.3	218†

$\star$ data were collected from Madsen (1998).

† data were weighted average values.

samples were placed at ambient laboratory condition (relative humidity of 56% and controlled temperature of 22°C) for two weeks to obtain air-dried samples. The air-dried samples were dried in the oven with a temperature of 105°C for 48 h.

The bentonite-sand mixtures (50/50, dry mass ratio) was prepared by mixing the bentonite and sand in ambient laboratory condition (relative humidity of 56% and controlled temperature of 22°C). At this ambient laboratory condition, the mixture obtained had a water content of 5%. Subsequently, an adequate amount of water was added into the bentonite-sand mixtures to reach a target water content of 9%. The mixtures were then kept in a air-tight plastic container for two weeks to allow for water equilibrium. After two weeks, water content and total suction of the sample were measured by the oven drying method (105°C) and a chilled-mirror hygrometer (Leong et al., 2003), respectively. Details for the chilled-mirror hygrometer would be introduced in section 3.3.5.2. Finally, the remaining bentonite-sand mixtures was statically compacted into the samples with 50 mm in diameter and 5 or 15 mm in height using the compaction device shown in Figure 3.3.

A constant volume mould consisting of a piston, a stainless steel sample ring and a hydraulic jack with loading capacity up to 15 t was used to obtain as-compacted samples (Figure 3.3). To reduce water equilibrium time, the as-compacted samples with 5 mm in height were used in the tests for determining wetting WRCs. However, the samples with 15 mm were used in the one-dimensional swelling-compression rebound tests and constant volume swelling pressure tests. All the as-compacted samples had the almost same initial conditions of water content (9%), dry density (1.8 Mg/m^3) and total suction (27 MPa). Since bentonite-based materials used as backfill and sealing materials are generally compacted on the dry side of optimum (Lloret et al., 2003; Romero et al., 2011), the water content 9% rather than the optimum water water content either 16 or 18% (Table 3.1) was used in the present investigation. The water content 9% was selected because it was approximately equal to the water content of compacted bentonite-sand bricks used in the filed (Agus, 2005). The dry density 1.8 Mg/m^3 was selected because it was nearly equal to the dry density of compacted bentonite-sand bricks used as backfill and sealing materials in the field (Rothfuchs et al., 2005, 2012; Jobmann et al., 2017).

3.3.1.2 Bentonite samples

Bentonite-water mixtures were prepared at two target water contents of 9% and 20% by adding the required amounts of deionized water to the bentonite. The mixing of

Figure 3.3: Compaction device using hydraulic pressure

bentonite and water was carried out in ambient laboratory conditions (relative humidity of 56% and controlled temperature of 22°C). The bentonite-water mixtures were kept in a two-layer plastic bag for about two weeks for moisture equilibration. The water contents of the mixtures were determined by oven drying method at a temperature of 105°C prior to preparing samples. The total suctions of the mixtures were determined by using AquaLab-3TE chilled-mirror hygrometer(Leong et al., 2003).

Compacted bentonite samples, 50 mm in diameter and 10/15 mm in height, were prepared by statically compacting bentonite-water mixtures by using a 15 t capacity compression testing machine shown in Figure 3.3. The samples were compacted as described in section 3.3.1.1. The compacted bentonite samples were prepared for carrying out total suction measurements after swelling pressure tests and swelling pressure and permeability measurements after desiccation tests. The water contents of bentonite were selected according to a rule of thumb that bentonites used as buffer material are generally compacted on the dry side of optimum (Lloret et al., 2003; Romero et al., 2011). The dry densities of compacted bentonite were selected according to the likely density of compacted bentonite to be applied in German repositories for the disposal of radioactive wastes (Xie et al., 2012; Jobmann et al., 2015).

In addition to compacted bentonite samples, slurry samples with a water content of 131% corresponding to $1.1\omega_{\mathrm{L}}$ of bentonite were also prepared. The slurry samples were prepared for obtaining the drying-wetting WRCs under unconfined condition. An adequate amount of water was added into the bentonite with the water content of 5% in the ambient laboratory condition to reach the target water content of 131%. The bentonte-water mixture was kept in a air-tight plastic container for two weeks to allow for water equilibrium. Prior to injecting the slurry into sample ring with 50 mm in diameter and 20 mm in height, a stirrer was used to sufficiently stirring the mixture to make homogeneous slurry samples.

3.3.2 Water retention measurements

The hydration of bentonite-based materials used in the repositories may occur under free swelling condition, partial restricted volume expansion condition and completely restricted volume expansion condition (Pusch & Yong, 2006; Villar, 2007; Sellin & Leupin, 2013; Johannesson et al., 2014). To reasonably simulate the field conditions in laboratory, the wetting WRCs were determined by employing wetting tests under unconfined, constant vertical stress and constant volume conditions on bentonite-sand mixtures. For comparison, the drying WRCs of bentonite-sand mixtures were also established by performing drying tests under unconfined condition on slurry samples and constant volume condition on compacted samples. The experimental techniques for determining WRCs include the ATT, the OT and the VET mentioned in chapter 2.

3.3.2.1 Pressure plate extractor based on the ATT

The pressure plate extractor shown in Figure 3.4 is generally used to apply matric suction range less than 1.5 MPa during determining drying WRCs. The pressure plate extractor are mainly composed of a high-air-entry disk, an air pressure chamber, an air supply system and a water compartment (Fredlund et al., 2012). Soil samples are placed on the top of the high-air-entry disk, and the airtight chamber is pressurized to a target matric suction. The high-air-entry disk does not allow the passage of air if the applied matric suction is less than the air-entry value of the disk. The air-entry value of the disk is related to the diameter of the pores in the ceramic disk. The air-entry value of the disk mainly controls the maximum air pressure which can be applied to a soil sample.

Prior to using, the high-air-entry disk must be saturated and is always in contact with water in the water compartment below the disk. The water compartment is connected

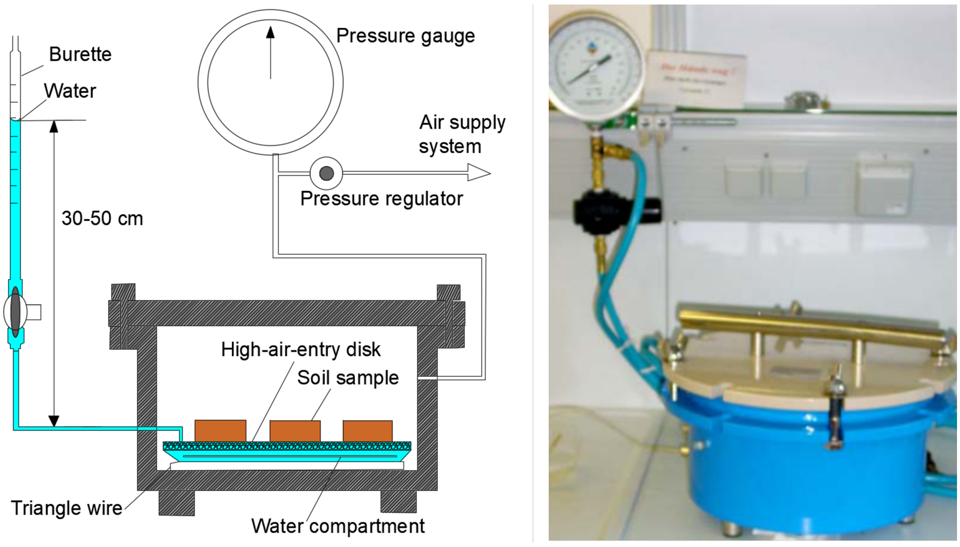

Figure 3.4: Pressure plate extractor: schematic and a photograph

to a burette for flushing bulbs and for collecting water expelled from a soil sample. The application of matric suction to a soil sample results in the pore water draining to the water compartment through the disk. At equilibrium, the soil will have a reduced water content corresponding to the increased matric suction. Because more than one soil samples are generally tested, it is necessary to dismantle the chamber and measure the weight of each sample after equilibrium at the applied pressure. The plot of equilibrium water content or degree of saturation versus the logarithm of the corresponding soil suction generates drying WRC.

In the present investigation, pressure plate extractors with disks with an air-entry value of 100, 500 and 1500 kPa were used and matric suctions of 0.06, 0.2, 0.4 and 0.8 MPa were applied. Prior to using, the high-air-entry disks were saturated following the procedure suggested by (ASTM-D6836, 2003). For each matric suction applied (i.e., 0.06, 0.2, 0.4 and 0.8 MPa), two replicate slurry samples with a water content of $1.1\omega_{\mathrm{L}}$ of the bentonite-based materials were used. In addition, all the pressure plate tests were performed at a temperature of $22 \pm 0.5°\mathrm{C}$.

3.3.2.2 Barcelona cells equipped with the OT

Barcelona oedometer and isochoric cells were developed at the Technical University of Barcelona (UPC) in Spain (Romero, 1999). They are generally used to determine one-dimensional swelling/compression deformation (Romero, 1999; Agus, 2005; Arifin, 2008)

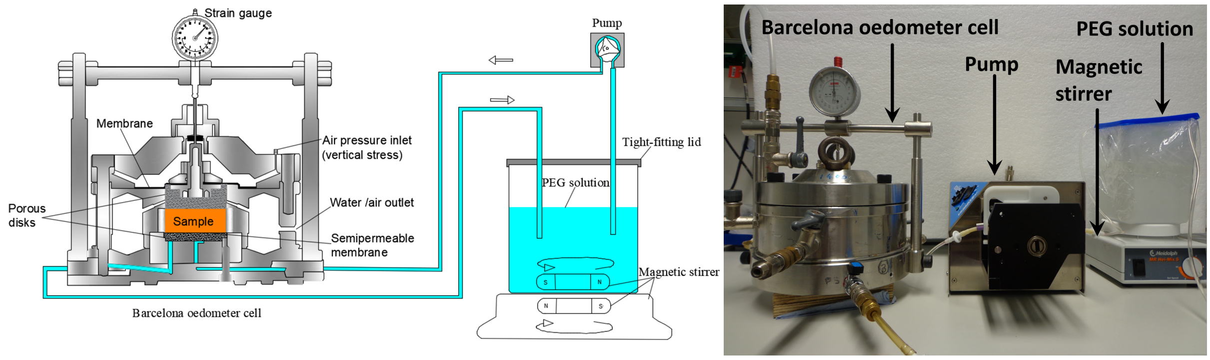

(a) (b)

Figure 3.5: (a) Schematic and (b) photograph of experimental set-up for determination of the wetting WRCs under laterally confined condition

and constant volume swelling pressure (Hoffmann et al., 2007; Schanz & Tripathy, 2009; Agus et al., 2013). In the present study, Barcelona oedometer and isochoric cells were modified to be capable of applying a matric suction from 0.01 to 13 MPa through the OT. The OT is generally capable of controlling suction range of 0.01 to 10 MPa (Kassiff & Shalom, 1971; Delage et al., 1998; Tripathy & Rees, 2013; Baille, 2014). The modified Barcelona oedometer cell shown in Figure 3.5 was used to obtain the wetting WRCs under laterally confined condition. The modified Barcelona isochoric cell presented in Figure 3.6 was employed to obtain the wetting-drying WRCs under constant volume condition. All the tests were performed at a temperature of 22.5 ± 0.1°C.

Figure 3.7 shows the enlarged cross section of the interface between a sample, semi-permeable membrane and polyethelene glycol (PEG) solution in the modified either oedomter cell or isochoric cell. In the modified Barcelona oedomter and isochoric cells, semi-permeable membrane could be embedded on their bases. The semi-permeable membrane is permeable to water and ions but impermeable to PEG molecule and soil particles and grain. Thus, water molecule and ions are able to pass freely through the semi-permeable membrane. If there is a difference in free energy (total potential) between the clay water and PEG solution, water will migrate from one side with high water potential to the side with low water potential. Water equilibrium between the clay sample and PEG solution is established until the difference in free energy between two sides dissipates. At equilibrium, the osmotic suction due to the dissolved salt is same on each side. Moreover, the osmotic suction due to PEG molecular is also equal to the matric suction of the clay sample (Kassiff & Shalom, 1971; Delage et al., 1998; Tripathy & Rees, 2013).

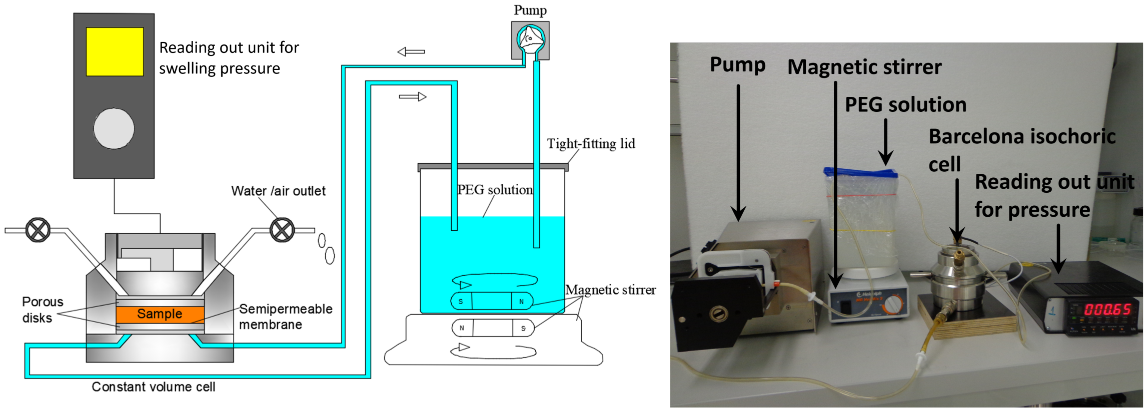

(a) (b)

Figure 3.6: (a) Schematic and (b) photograph of experimental set-up for determination the WRCs under constant volume condition

The magnitude of the suction of the PEG solution depends on the concentration of the PEG solution. The higher the concentration is, the greater the suction is. Thus, different values of matric suction could be applied through circulating PEG solution with different PEG concentrations.

In the present investigation, the PEG and semi-permeable membrane were selected according a rule of thumb mentioned in section 2.4.4.2. A PEG with the molecular weight (MW) values of 20000 was used in the present study. The relationships among mass ratio of PEG to water, refraction (brix) and suction of PEG solution are given in Figure 3.8(a) and 3.8(b). For a given PEG concentration, its Brix index and total suction were determined by a refractometer and the chilled-mirror hygrometer, respectively (Delage et al., 1998; Tripathy & Rees, 2013). The determined Brix index values at pre-measured PEG concentrations were found to agree very well with the values reported by (Delage et al., 1998; Tripathy & Rees, 2013). Moreover, the semi-permeable membrane used in this study was Spectra/Pro with a molecular weight cut-off (MWCO) of 1000.

3.3.2.3 Desiccator

Figure 3.9 shows the schematic of the desiccator with the VET to apply suction. Several soil samples are placed on the perforated porcelain desiccator plate that is fixed in the middle of the desiccator. At the bottom of the desiccator, there is a saturated salt solution which is able to maintain a constant relative humidity (RH) at a given temperature. When the RH of the saturated salt solution was greater than that of the soil samples, the water

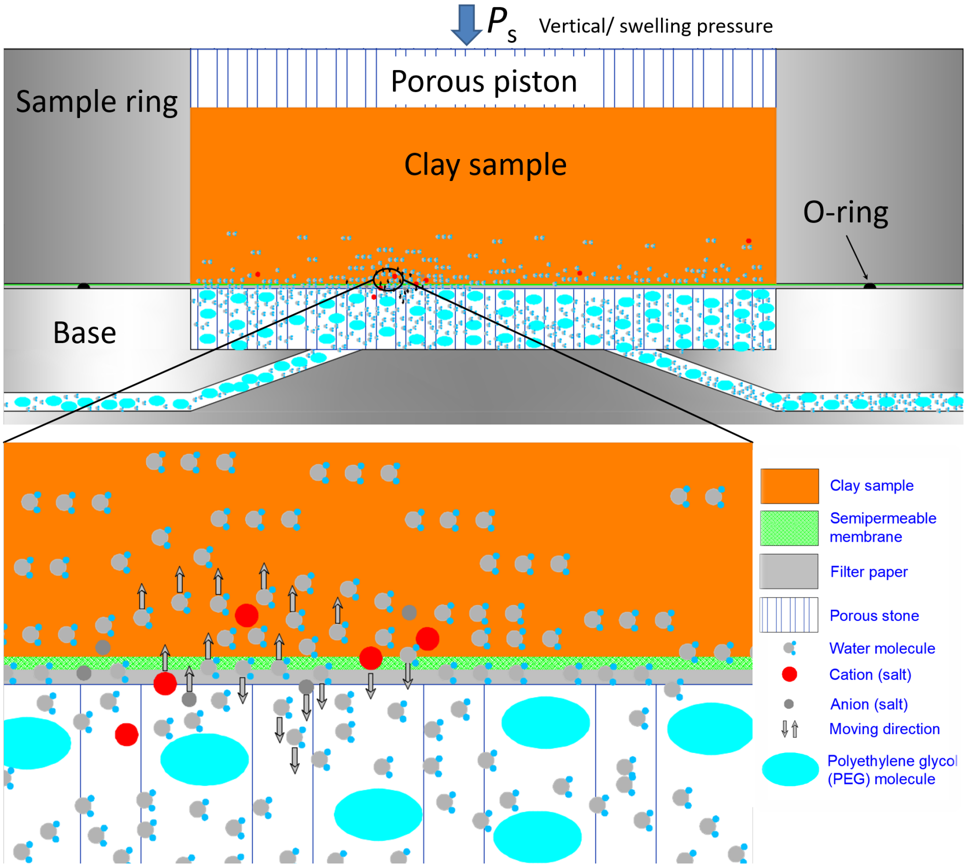

Figure 3.7: Schematic showing the enlarged cross section of the interface between a clay sample, semi-permeable membrane and the polyethelene glycol (PEG) solution in the modified either oedomter cell or isochoric cell

vapour in the soil samples diffuses into the saturated salt solution. As a consequence, the soil samples lose water and become dry. On the contrary, the soil samples adsorb water.

Total suction provided by a saturated aqueous solution in the desiccator could be determine by chilled-mirror hydrometer. Different values of RH or total suction could be applied by placing different saturated aqueous solutions in a desiccator at a controlled temperature. The saturated aqueous solutions used in the present study were summarized in Table 3.4 and the temperature during desiccator tests were controlled at 22.5 ± 0.1°C. The total suctions shown in Table 3.4 were measured by using AquaLab-3TE chilled-mirror hygrometer (Decagon Devices, 2003). For comparison, the suction values of the saturated aqueous solutions as given in ASTM-E104 (2007) are also shown in Table 3.4. The suction values of the saturated aqueous solutions measured in this study were found to agree very well with the values given in ASTM-E104 (2007).

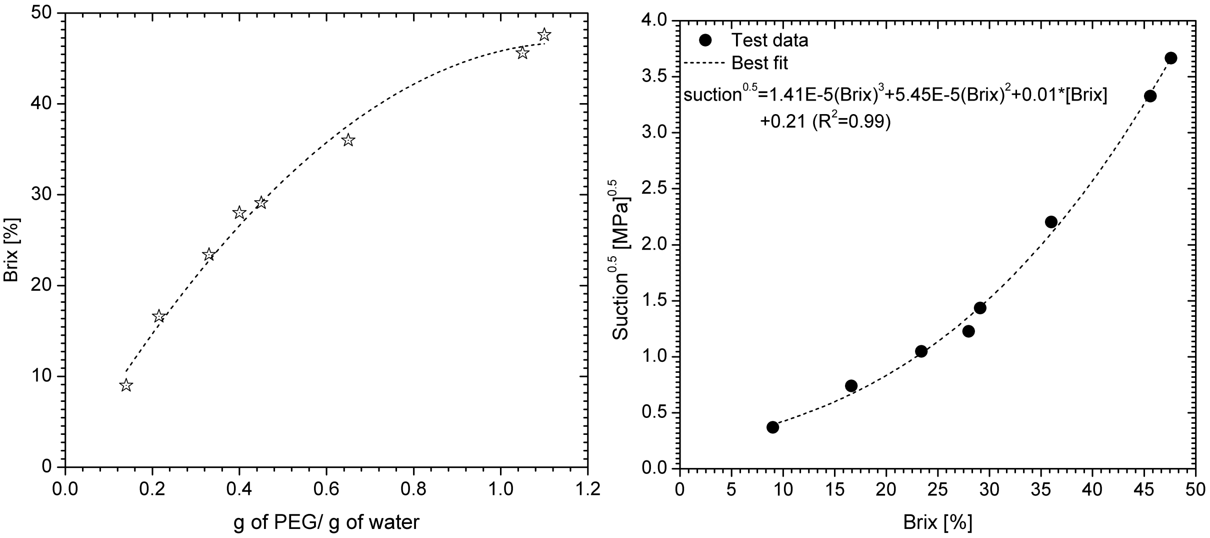

(a) (b)

Figure 3.8: Relationship between mass ratio and Brix (a) and that between Brix and suction (b) for the PEG used in this study

Table 3.4: Equilibrium total suction of saturated aqueous solutions

Total suction	Saturated solutions								
(MPa)	K_2SO_4	KNO_3	KCl	NaCl	$NaNO_2$	$Mg(NO_3)_2$	$MgCl_2$	LiCl	NaOH
ASTM†	3.1-4.5	8.2-10.0	22.9-23.9	38.7-39.1	-	86.8-87.9	152.1-153.8	-	-
Aqualab*	3.4	9.8	22.3	39.5	58	85.6	153.6	282	346

† determined based on the relative humidity at 25°C which are given in ASTM-E104 (2007), $*$ determined based on the relative humidity at 22.5°C which are measured by the AquaLab-3TE chilled-mirror hygrometer in the present investigation.

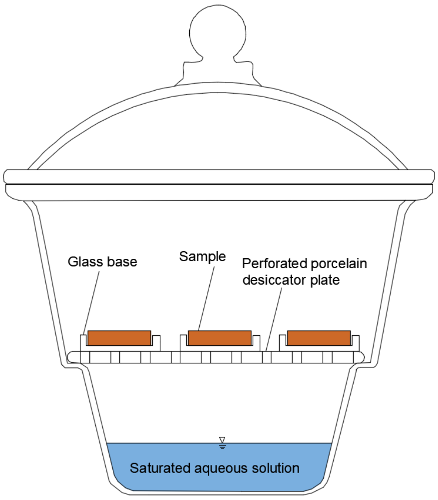

Figure 3.9: Schematic of the desiccator with vapour equilibrium technique to control suction

3.3.2.4 Experimental procedure for determining WRCs

Table 3.5 shows the initial condition of compacted bentonite-sand mixtures samples and applied suctions during the wetting tests under constant vertical stress condition. Samples BS-WL50-1 to BS-WL50-8 were first loaded to 50 kPa in the modified Barcelona oedometer cell described in section 3.3.2.2 and subsequently wetted under the applied suctions of 0.001, 0.15, 0.32 0.55, 2.26 10.94, 10.94 and 11.03 MPa, respectively. Unlike the samples BS-WL50-1 to BS-WL50-8 samples, samples BS-WL200-1 to BSWL200-6 were first loaded to 200 kPa in the oedometer cell and then wetted under the given suctions shown in Table 3.5. The applied suctions shown in Table 3.5 were controlled through circulating PEG solution with different PEG concentrations and the applied suction of 0.001 MPa corresponded to circulating deionized water. The swelling deformation upon wetting during tests was recorded by a strain gauge with a readability of 0.001 mm. The equilibrium was assumed to be reached when the swelling deformation was observed to be constant (changes in swelling strain less than 0.001 mm/day). At this point, the samples were removed from the cells and their water content and total suction were finally determined by the oven drying method (105°C) and the chilled-mirror hygrometer, respectively. The water content measured and the corresponding applied suction were used to generate the wetting WRCs under laterally confined conditions.

Table 3.5: Initial conditions of compacted bentonite-sand mixtures (50/50) samples and applied suction during the wetting tests under laterally confined condition

Sample no.	Initial compaction condition				Test types	Applied suction
-	Dry density (Mg/m^3)	Water content (%)	Degree of saturation (%)	Total suction $(\text{MPa})^{\alpha}$	-	MPa
BS-WL50-1	1.81	9	48.5	27	WL50	$0.001^{\dagger}$
BS-WL50-2	1.81	9	48.5	27		0.15
BS-WL50-3	1.81	9	48.5	27		0.32
BS-WL50-4	1.80	9	47.8	27		0.55
BS-WL50-5	1.80	9	47.9	27		2.26
BS-WL50-6	1.81	9	48.5	27		10.94
BS-WL50-7	1.81	9	48.5	27		10.94
BS-WL50-8	1.81	9	48.5	27		13.03
BS-WL200-1	1.80	9	48.1	27	WL200	$0.001^{\dagger}$
BS-WL200-2	1.80	9	48.1	27		0.55
BS-WL200-3	1.80	9	48.0	27		1.58
BS-WL200-4	1.80	9	48.0	27		1.58
BS-WL200-5	1.81	9	48.3	27		4.86
BS-WL200-6	1.81	9	48.3	27		10.91

BS represents bentonite-sand mixtures (50/50); WL50 means that the samples were wetted under a vertical pressure of 50 kPa, whereas WL200 means that the samples were wetted under a vertical pressure of 200 kPa; $*$ was determined by chilled-mirror technique; † correspond to the total suction of deionized water.

The wetting WRCs of bentonite-sand mixtures under constant volume condition was determined employing constant volume wetting tests on compacted samples. Table 3.6 presents the initial conditions of compacted bentonite-sand mixtures samples and applied suction during the wetting-drying tests. The compacted bentonite-sand mixtures samples with the almost same initial conditions were wetted in suction controlled condition. Samples BS-WCV-1 to BS-WCV-7 were placed in the modified Barcelona isochoric cell described in section 3.3.2.2 and subsequently wetted with the applied suctions of 0.001, 0.15, 0.55, 1.12, 3.78, 11.15 and 11.45 MPa, respectively. The applied suctions were controlled through circulating PEG solution with different PEG concentrations. Swelling pressures during the tests were recorded by a pressure reading unit with a readability of 0.001 kN. It is assumed that equilibrium was established when the swelling pressure was observed to reach equilibrium (changes in swelling pressure less than 0.01 kN/day). After the equilibrium was reached, tests were terminated and the samples were removed from the constant volume cell. Finally, the water content and total suction of each sample were measured. The water content measured and the corresponding applied suction were used to establish the wetting WRCs under constant volume conditions.

In addition to the wetting WRCs under constant volume conditions, the drying WRCs under constant volume condition were also determined. Samples BS-WCVD-1 to BS-WCVD-4 (Table 3.6) were placed in the modified Barcelona isochoric cell and were then saturated with deionized water. When swelling pressure reached equilibrium, the deionized water was replaced by PEG solution with different concentrations to dry samples. The applied suction was 0.15 MPa for BS-WCVD-1, 0.55 MPa for BS-WCVD-2, 7.7 MPa for BS-WCVD-3 and 10.9 MPa for BS-WCVD-4 to BS-WCVD-10. As the applied suction was higher than 10.9 MPa, swelling pressures were found to almost disappear and the samples almost lost the contact with the wall of the sample ring. Thus, further dehydration of samples BS-WDCV-5 to samples BS-WDCV-10 at the applied suction from 39.5 to 346.2 MPa actually occurred under unconfined condition using VET to apply suction.

The drying-wetting WRCs and the wetting WRCs under unconfined condition were determined employing ATT and VET techniques described in section 3.3.2 on slurry sample, oven-dried samples and as-compacted samples. For tests for determining the drying WRCs, the suction range less than 1.5 MPa was applied by ATT described in section 3.3.2.1, whereas the suction range greater than 2 MPa was applied by VET described in section 3.3.2.3. In the case of suction range below 1.5 MPa, suction values applied were 0.06, 0.2, 0.4, 0.8 MPa. In case of the suction range above 1.5 MPa, suction values applied were 3.4, 22.3, 39, 84, 184, 282, 346 MPa.

Table 3.6: Initial condition of compacted bentonite-sand mixtures (50/50) samples and applied suction during the wetting-drying tests under constant volume condition

Sample no.	Initial compaction condition				Test types	Applied suction
-	Dry density (Mg/m^3)	Water content (%)	Degree of saturation (%)	Total suction (MPa)[*]	-	MPa
BS-WCV-1	1.81	9	48.8	27	WCV	0.001[†]
BS-WCV-2	1.81	9	48.8	27		0.15
BS-WCV-3	1.81	9	48.8	27		0.55
BS-WCV-4	1.81	9	48.6	27		1.12
BS-WCV-5	1.81	9	48.6	27		3.78
BS-WCV-6	1.81	9	48.7	27		11.15
BS-WCV-7	1.81	9	48.7	27		11.45
BS-WCVD-1	1.80	9	48.0	27	WCVD	0.001→0.22
BS-WCVD-2	1.80	9	48.1	27		0.001→0.55
BS-WCVD-3	1.80	9	48.0	27		0.001→7.7
BS-WCVD-4	1.80	9	48.0	27		0.001→10.9
BS-WCVD-5	1.80	9	48.0	27		0.001→10.9→39.5
BS-WCVD-6	1.80	9	48.0	27		0.001→10.9→58
BS-WCVD-7	1.80	9	48.0	27		0.001→10.9→85.6
BS-WCVD-8	1.80	9	48.0	27		0.001→10.9→153.6
BS-WCVD-9	1.80	9	48.0	27		0.001→10.9→281.9
BS-WCVD-10	1.80	9	48.0	27		0.001→10.9→346.2

BS represents bentonite-sand mixtures; WCV means that the samples were wetted under constant volume condition; WCVD means that the samples were first wetted under constant volume condition and subsequently underwent drying under constant volume condition and/or unconfined condition; ∗ total suction was determined by chilled-mirror technique; Further drying of samples BS-WDCV-5 to BS-WDCV-10 over suction range from 39.5 to 346.2 MPa occurred in unconfined condition; † correspond to the total suction of deionized water.

For each suction applied, two replicate slurry samples were used. For the tests for measuring the wetting WRCs under unconfined condition, only the VET was used to apply suction and suction values applied were 0.28, 0.98, 3.4, 22.3, 39, 84, 156, 282 and 346 MPa. For the suction range less than 1.0 MPa, unsaturated KCl solution was used to apply the target suctions (ASTM-D5298, 2010). To maintain the constant suction, the unsaturated KCl solution was periodically renewed and the temperature was controlled at 22.5 ± 0.1°C. For the suction range greater than 1.0 MPa, saturated solutions mentioned in the section of 3.3.2.3 were used to apply the target suctions. For each suction above, two replicate oven-dried samples and one as-compacted sample were used.

For the drying test with ATT to apply suction, the volumes of outflow in the graduated cylinder were regularly monitored. When the outflow from the pressure plate has ceased for 96 h, the equilibrium has been established (ASTM-D6836, 2003). Monitoring the volume of the outflow with elapsed time in each test indicated that an equilibrium time was about less than 2 weeks for the applied suction less than 0.2 MPa. In the case of the applied suction of 0.4 and 0.8 MPa, the equilibrium time was about 4 weeks. For the test with VET to apply suction, the mass of the samples were regularly weighted by a balance with a readability of 0.001 g. Monitoring the mass of the samples with elapsed time in each test demonstrated that an equilibrium time more than 6 months was sufficient for drying the slurry samples or wetting the oven-dried samples at the applied suction range of 3-346 MPa.

Once the equilibrium in each test was reached, one of the replicate samples was used to determine water content by the oven drying method (105°C). The other sample was used to measure volume by the wax method (ASTM-D4943, 2010). In the case of as-compacted sample, the volume was determined by calliper and subsequently, the water content was determined by the oven drying method. The data measured and the corresponding applied suction were used to generate either the drying-wetting WRCs or the wetting WRCs (i.e. suction-water content relationship and suction-degree of saturation relationship) under unconfined condition.

3.3.3 Multi-step swelling pressure tests

To study the effect of suction and water phase on the swelling pressure of the compacted bentonite-sand mixtures, two multi-step swelling pressure tests on the compacted bentonite-sand mixtures were performed with OT and VET to reduce suction, respectively. In addition, a single-step swelling pressure test was also conducted for comparison. This section presents the experimental techniques and procedure for performing the swelling pressure tests on compacted bentonite-sand mixtures samples.

Barcelona isochoric cell was used to perform the single-step and multi-step swelling pressure tests on compacted bentonite-sand mixtures samples. The experimental set-up shown in Figure 3.10 was used for carrying out the single-step swelling pressure test. In this test, deionized water in a burette was used to directly saturate a sample. The modified Barcelona isochoric cell described in section 3.3.2.2 (Figure 3.6) was used for performing multi-step swelling pressure test with the OT to apply suction. The experimental set-up presented in Figure 3.15 was used to perform multi-step swelling pressure test with the VET to apply suction.

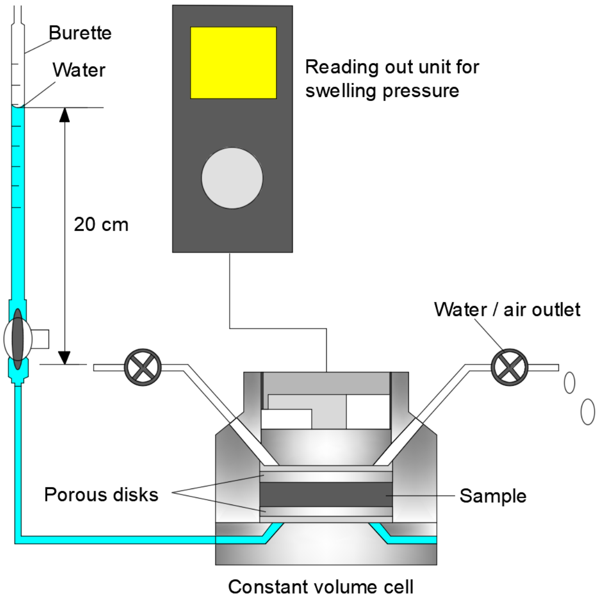

Figure 3.10: Schematic of experimental set-up for single-step swelling pressure test

Table 3.7 presents the initial conditions of the compacted bentonite-sand mixtures samples and suction control techniques for performing the swelling pressure tests. All the as-compacted samples had the same initial conditions, i.e. dry density of 1.8 Mg/m^3, water content of 9% and degree of saturation of 47.9%. Sample BS-CVPS-S-W was placed in the isochoric cell (Figure 3.10) and was saturated with deionized water (liquid water). The swelling pressure test was terminated until a variation of the swelling pressure was less than 5 kPa per day. The duration of the single-step swelling pressure test was 22 days. Sample BS-CVPS-M-OT in the modified isochoric cell was gradually hydrated by decreasing suction in a stepwise manner from the initial value (27 MPa) to a value close

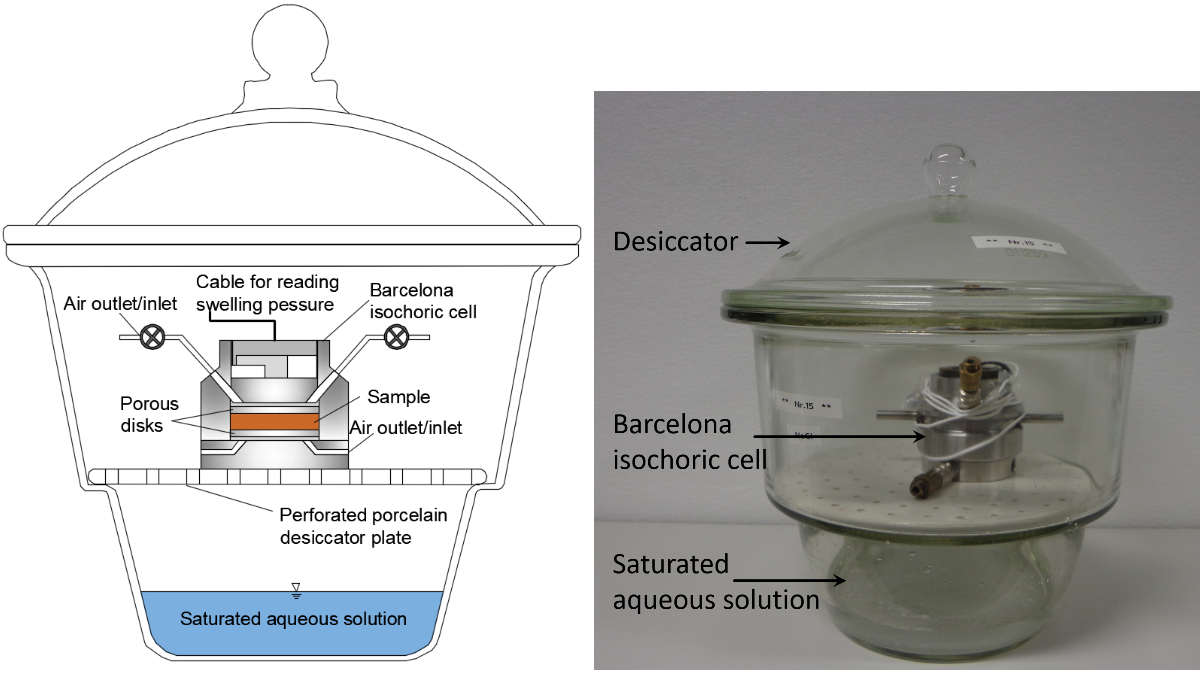

(a) (b)

Figure 3.11: Experimental set-up for multi-step swelling pressure test with the VET to control suction ((a) schematic and (b) photograph)

Table 3.7: Initial condition of the as compacted bentonite-sand mixtures (50/50) samples and the suction control techniques for performing the constant volume swelling pressure tests

Sample no.	Initial compaction condition				Wetting method	Applied suction
-	Dry density (Mg/m^3)	Water content (%)	Degree of saturation (%)	Total suction (MPa)$^{\alpha}$	-	MPa
BS-CVPS-S-W	1.80	9	47.9	27	Water	$0.001^{\dagger}$
BS-CVPS-M-OT	1.80	9	47.9	27	OT	13.06→4.7→1.02→0.55→0.15→$0.001^{\dagger}$
BS-CVPS-M-VET	1.80	9	47.9	27	VET	9.8→3.4→$0.001^{\dagger}$

BS represents bentonite-sand mixtures; CVPS represents constant volume swelling pressure test; S, M denote single-step and multi-step CVPS, respectively; W denotes liquid water; OT denotes osmotic technique; VET denotes vapour equilibrium technique; †, total suction of deionized water.

to zero (0.001 MPa). The suction was gradually decreased by applying the OT and the applied suction was 13.06, 4.7, 1.02, 0.55, 0.15 and 0.001 MPa. For each suction level, equilibrium was assumed to be reached when the variation of the swelling pressure was less than 5 kPa per day. Duration of the multi-step swelling pressure test with the OT to control suction was 102 days.

In the case of sample BS-CVPS-M-VET, it was gradually wetted in the isochoric cell (Figure 3.11) using the VET to decrease the sample suction. The applied suction was 9.8, 3.4 and 0.001 MPa. After sample BS-CVPS-M-VET was placed in the isochoric cell, the whole cell was transferred in to a desiccator with a target suction of 9.8 MPa. The swelling pressure and the mass of the whole cell were regularly measured during equilibrium. When both the swelling pressure and mass became constant, the whole cell was transferred into a desiccator with a suction of 3.4 MPa. Once both the swelling pressure and mass were found to be constant, the isochoric cell was taken out and connected with a burette filled with deionized water to saturate the samples. The duration of the multi-step swelling pressure test with the VET to control suction was about 560 days.

In addition, it should be noted that after the swelling pressure tests were completed, the isochoric cell was dismantled and total suction and water content of each saturated sample were determined. Prior to dismantling the device, pressurized humid air (relative humidity = 100%) generated by deionized water was used to flush the bottom and top fluid reservoirs to minimize fluid uptake by samples upon unloading. Subsequently, the samples were removed from the device for final total suction and water content measurements.

3.3.4 One-dimensional swelling-compression-rebound tests

To advance the understanding of compressibility of compacted bentonite-sand mixtures and to obtain parameter for performing numerical simulation, the one-dimensional swelling-compression-rebound tests were performed. This section presents the experimental techniques and procedure of the one-dimensional swelling-compression-rebound tests.

3.3.4.1 High stress oedometer device

The one-dimensional swelling-compression-rebound tests were carried out using the high stress oedometer device (Figure 3.12) which was developed by Baille et al. (2010). This cell was mainly composed of a bottom part with a stainless steal porous disk, a middle part and a top part where a load cell and a top cap with a stainless steel porous disk are connected. The load cell was capable of applying 60 kN load and had a precision of 0.001 kN. The cell was equipped with a strain gauge with a readability of 0.001 mm. The direct operation and calibration of this device was possible through a control unit with a keypad and liquid-crystal display.

3.3.4.2 Calibration of the deivce against deformation

Prior to testing the soil samples, deformation of the high stress oedometer device due to loading and unloading was calibrated. The calibration was performed using a dummy made of stainless steel. The dummy had a 50 mm in diameter and 15 mm in height which are same with the dimension of compacted bentonite-sand samples. The dummy together with dry filter papers and porous disks was subjected to increasing and decreasing vertical stress in the high stress oedometer device. In addition, deformation calibration with wet filter papers and porous disks was also performed. The deformation characteristics of the high stress oedometer device are presented in Figure 3.13.

3.3.4.3 Experimental techniques

The one-dimensional swelling-compression-rebound tests were performed on the as-compacted bentonite-sand mixtures samples. The initial conditions of the as-compacted bentonite

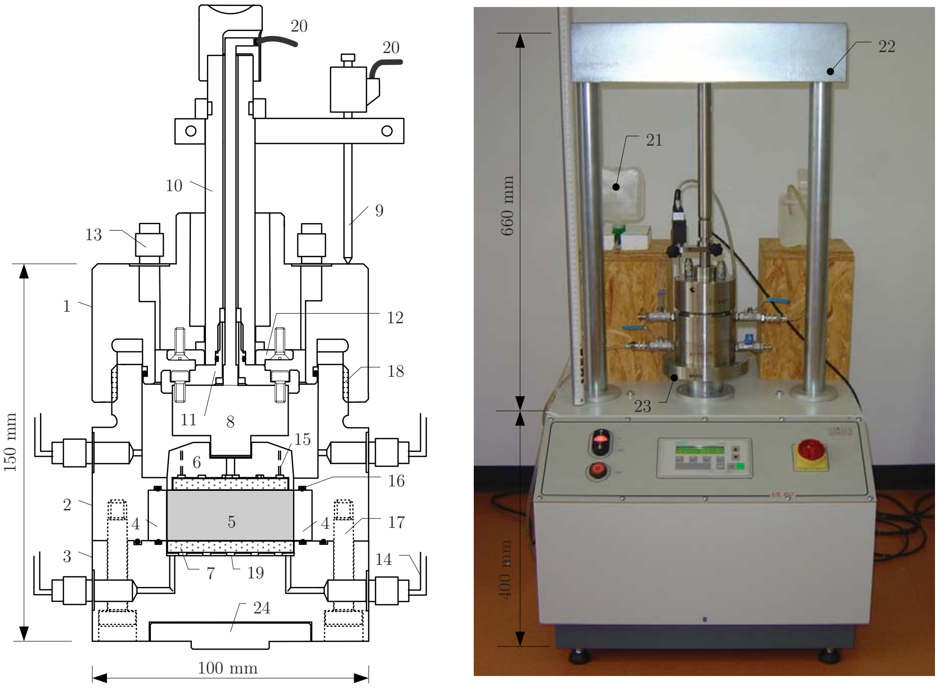

1 Top part
2 Central part
3 Bottom part
4 Specimen ring
5 Soil specimen
6 Pressure pad with top porous plate
7 Bottom porous plate
8 Force transducer
9 Strain gauge
10 Loading piston
11 Adapter for 8
12 Upper restraint
13 Provision for vapour supply
14 Water or vapour supply
15 Vent
16 O-ring
17 Heavy screw
18 Thread
19 Water chamber
20 Electrical cables
21 Fluid reservoir
22 Loading frame
23 Base plate
24 Adapter for 23

Figure 3.12: High stress oedometer device (collected from Baille et al. (2010))

samples are presented in Table 3.7. As can be seen from this table, all the as-compacted bentonite-sand mixtures samples had the almost same initial conditions, i.e. dry density of 1.8 Mg/m^3, water content of 9% and degree of saturation of 47%.

Stress paths which the as-compacted samples followed during the tests are shown in Figure 3.14. Sample BS-SCR-1 together with filter papers was placed in the high stress oedometer device and a sealing pressure of about 2.5 kPa was applied. Deionized water in a burette was supplied from the bottom of the samples through the water inlet at the bottom of the device (Figure 3.15(a)). The air/water outlets at the top of the device were kept open to allow air to escape during the test. Vertical deformation of sample BS-SCR-1 upon wetting was recorded. When the vertical deformation was observed to be constant (changes less than 0.001 mm/day), the loading-unloading was performed following the stress paths shown in Figure 3.14. Load increment was applied until the change in the vertical deformation was less than 0.001 mm/day.

Prior to being placed in the high stress oedometer device, samples BS-SCR-2 and BS-SCR-3 held by sample rings were stored in desiccators at the applied suction of 3.4 and

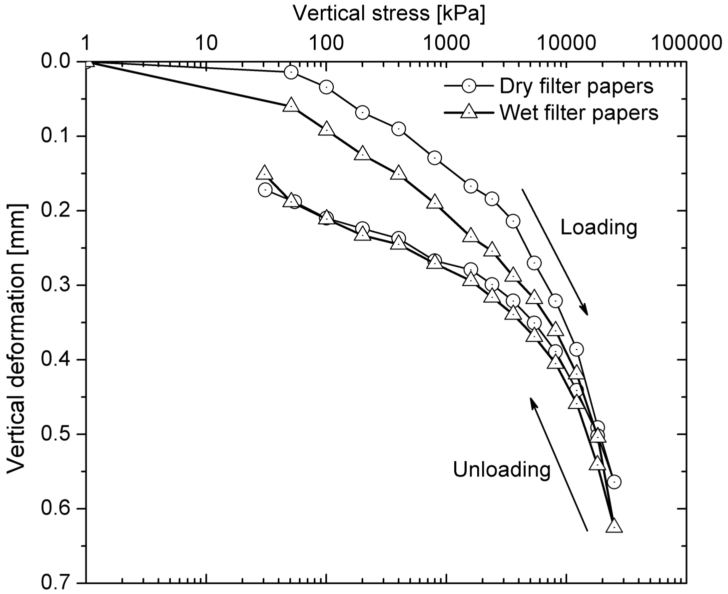

Figure 3.13: Deformation characteristics of the high stress oedometer device

10 MPa, respectively. The VET described in section 3.3.2.3 was used to apply the target suction. Mass and vertical deformation of each sample were regularly monitored until the mass of the samples became constant. Afterwards, samples BS-SCR-2 and BS-SCR-3 were transferred to the oedometer device for performing suction controlled loading-unloading following the stress paths shown in Figure 3.14. The experimental set-up is presented in Figure 3.15(b). The water vapour above the saturated salt solutions in the bottle is capable of providing the suction of 3.4 and 10 MPa during the loading-unloading tests. The bottle was connected to the air inlet at the top and air outlets at the bottom of the oedometer device and the air outlet at bottom was connected to the air inlet at top. In this study, air pump was not used to cycle the vapour in above close system because the failed tests implied that heat generated by the air pump could increase the applied suction. In addition, the rebound test on sample BS-SCR-3 was not performed due to power failure.

In the case of sample BS-SCR-4, the compression and rebound test was performed under as-compacted condition. Unlike sample BS-SCR-4, samples BS-SCR-5, BS-SCR-6 and BS-SCR-7 were first loaded to 0.05, 2.4 and 12.15 MPa under as-compacted condition, respectively (Figure 3.14). Subsequently, they were saturated with deionized water at constant vertical stresses. Finally, samples BS-SCR-5 and BS-SCR-6 were loaded and unloaded following the stress paths presented in Figure 3.14. Load increment was applied until the change in the vertical deformation was less than 0.001 mm/day.

Table 3.8: Initial conditions of the as-compacted bentonite-sand mixtures (50/50) samples used in the one-dimensional swelling-compression-rebound tests

Sample no.	Initial compaction condition			
-	Dry density (Mg/m^3)	Water content (%)	Degree of saturation (%)	Total suction (MPa)$^{\alpha}$
BS-SCR-1	1.79	9	47.2	27
BS-SCR-2	1.79	9	47.1	27
BS-SCR-3	1.79	9	47.1	27
BS-SCR-4	1.79	9	47.0	27
BS-SCR-5	1.79	9	47.1	27
BS-SCR-6	1.79	9	47.4	27
BS-SCR-7	1.79	9	47.2	27

BS represents bentonite-sand mixtures, SCR represents that the samples were used to perform the swelling-compression-rebound test.

After the swelling-compression-rebound tests were completed, the device was dismantled and total suction and water content of all the samples were determined. For the samples (i.e., BS-SCR-2, BS-SCR-5, BS-SCR-6 and BS-SCR-7) saturated with deionized water, some special care were taken. Prior to dismantling the device, pressurized humid air (relative humidity = 100%) generated by deionized water was used to flush the bottom and top fluid reservoirs to minimize fluid uptake by samples upon unloading. Afterwards, the samples were removed from the device for final total suction and water content measurements.

3.3.5 Swelling pressure tests and subsequent total suction measurements

To examine the linkage between swelling pressure, total soil suction and applied suction in bentonite-based materials, constant volume swelling pressure tests and total suction measurements after the swelling pressure tests were carried out on bentonite samples. This section describes the experimental techniques and procedure for performing constant volume swelling pressure tests and subsequent total suction suction measurements. The experimental techniques and/or equipments for determining swelling pressure of saturated and unsaturated bentonite and total suction after swelling pressure tests mainly include Barcelona isochoric cell and chilled-mirror hygrometer technique.

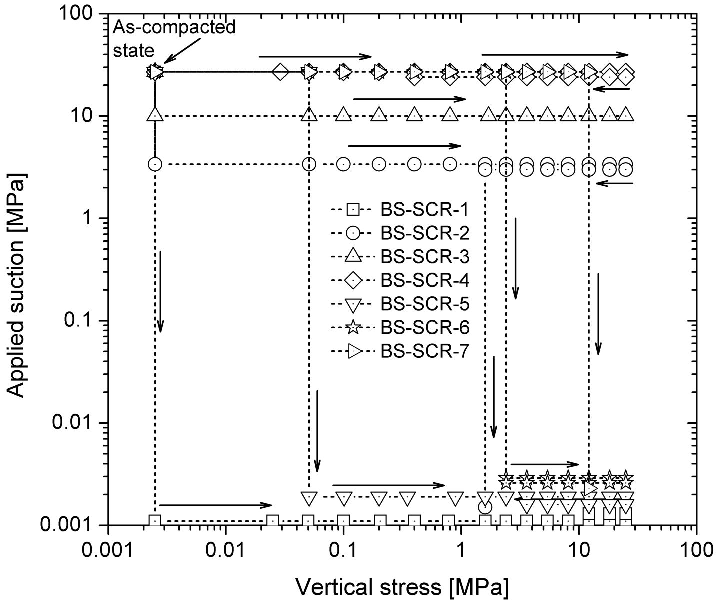

Figure 3.14: Generalised stress paths followed by one-dimensional swelling-compression-rebound tests (loading-unloading paths where the applied suction was less than 0.01 MPa were performed under saturated condition)

3.3.5.1 Barcelona isochoric cell

Barcelona isochoric cell mentioned in section 3.3.2.2 and 3.3.4 were used for determining the swelling pressure of saturated and unsaturated bentonite. The experimental set-up shown in Figure 3.10 was used to determine the swelling pressure of saturated bentonite. The bentonite sample was saturated with aqueous solution, i.e. 0.0001, 0.05, 1.0 to 2.0 M $CaCl_2$ solutions, meaning that different values of suction of hydrating fluid was applied. The Barcelona isochoric cell combined with the VET shown in Figure 3.11 was used for obtaining the swelling pressure of unsaturated bentonite. The three compacted bentonite samples were wetted with water vapour at a applied suction of 9.8, 39.5 and 85.6 MPa, respectively.

3.3.5.2 Chilled-mirror hygrometer technique

The chilled-mirror hygrometer used in this investigation was a water activity meter type 3TE purchased from Decagon Devices Inc. (Figure 3.16). This device uses the dew point technique to determine the relative humidity of a soil sample (Leong et al., 2003). The soil sample fills about half the capacity of a small container and is placed in the device

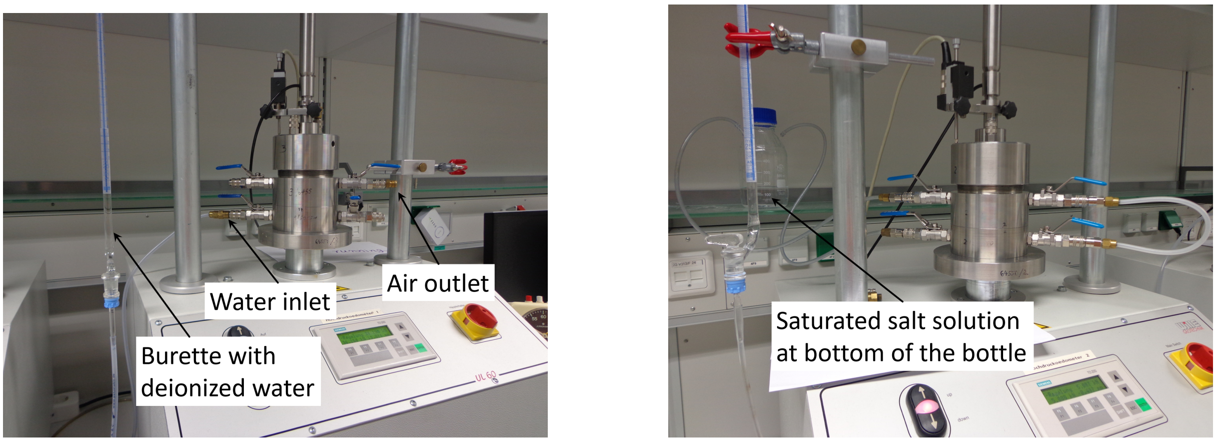

(a) (b)

Figure 3.15: Experimental set-up of one-dimensional swelling-compression-rebound tests in the case of (a) saturated condition and of (b) unsaturated condition

in a sealed chamber. The soil sample equilibrates with the water vapour in the air space above the soil sample. The chamber contains a mirror whose temperature is precisely controlled by a thermoelectric cooler. Detection of the exact point at which condensation first appears on the mirror is by a beam of light directed onto the mirror and reflected into a photo detector cell. The detector cell senses the change in reflectance when condensation occurs on the mirror and the temperature at which condensation occurs is recorded by a thermocouple attached to the mirror. The device is equipped with an internal fan that circulates the air within the sample chamber to reduce equilibrium time. The device also has a temperature controller to set the temperature of the sample at which relative humidity measurement is to be made.

The accuracy of AquaLab-3TE chilled-mirror hygrometer in terms of the relative humidity is ±0.3% (Decagon Devices, 2003). The accuracy of the device in terms of the total suction depends on the relative humidity of a soil sample or its total suction. For instance, if total suction of a soil sample was equal to 0.3 MPa, the total suction measured by the device could vary from 0 to 0.8 MPa at 22.5°C due to the accuracy of ±0.3%. If total suction of a soil sample was equal to 1.0 MPa, the total suction measured by the device could vary from 0.6 to 1.4 MPa at 22°C. If total suction of a soil sample was equal to 3.0 MPa, the total suction measured by the device could vary from 2.6 to 3.4 MPa at 22.5°C. This suggested that the accuracy of ±0.3% could cause an significant total suction measurement error (i.e. up to ±140%) if the total suction of a soil sample was less than 0.3 MPa.

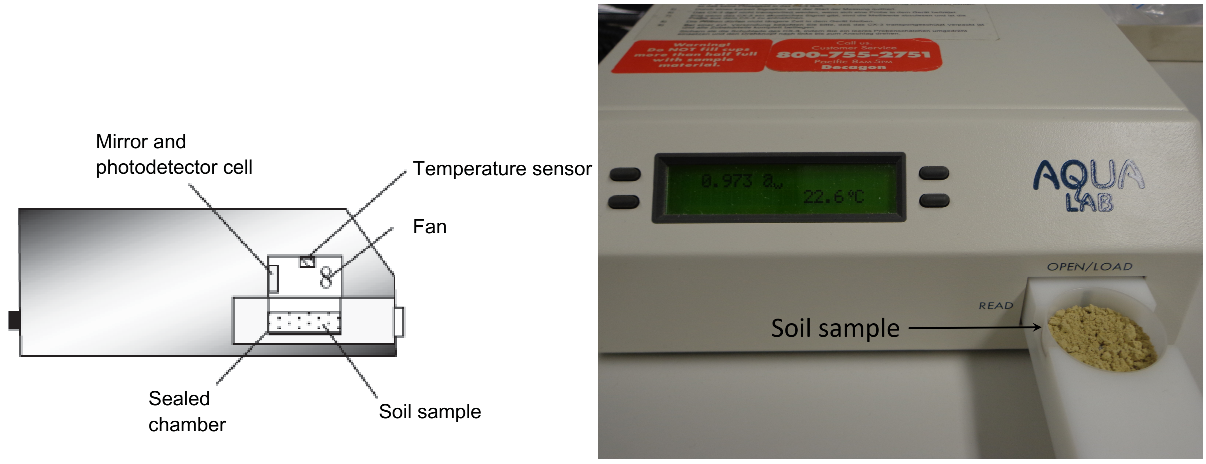

(a) (b)

Figure 3.16: Chilled-mirror hygrometer in the case of (a) schematic of the device (Leong et al., 2003) and (b) photograph

Prior to use, the chilled-mirror hygrometer is generally needed to be verified for its best performance in determining relative humidity. The verification is generally performed using standard salt solutions provided Decagon Devices Inc.. The reading for each standard salt solutions should be within ± 0.003 water activity of the standard salt solution. After the chiller-mirror hydrometer passes the verification, it can be used to measure the relative humidity of a soil sample. The total suction of the soil sample is calculated using Eq.(3.1).

$$\psi_{\mathrm{t}} = -\frac{RT_K}{M_{\mathrm{w}}\overline{v}_{\mathrm{w}}}\ln(RH) \tag{3.1}$$

Where: R is universal (molar) gas constant i.e., 8.31432 J/(mol K); T_K is absolute temperature i.e., $T_K = 273.15 + T$ (K), T = temperature, °C; $\overline{v}_{\mathrm{w}}$ is specific volume of water or the inverse of the density of water, m^3/kg; M_{w} is molecular mass of water vapour (i.e., 18.016 kg/kmol); RH is the measured relative humidity.

3.3.5.3 Experimental procedure for swelling pressure tests and subsequent total suction measurements

Table 3.9 presents the initial conditions of the compacted bentonite samples and wetting methods. Samples CB-0 to CB-6 with compaction dry densities varying between 1.20 to 1.83 $\mathrm{Mg/m}^3$ were hydrated by supplying deionized water. Samples CB-7, CB-8, CB-9,

Table 3.9: Initial conditions of the as compacted bentonite samples and the wetting methods during the swelling pressure tests

Sample no.	Initial compaction conditions				Wetting methods
-	Dry density (Mg/m^3)	Water content (%)	Degree of saturation (%)	Total suction (MPa)	-
CB-0	1.20	20.0	42.0	13.7	Deionized water
CB-1	1.41	20.0	56.2	13.7	Deionized water
CB-2	1.57	20.0	71.6	13.7	Deionized water
CB-3	1.57	20.0	71.8	13.7	Deionized water
CB-4	1.58	20.0	72.6	13.7	Deionized water
CB-5	1.66	20.0	81.6	13.7	Deionized water
CB-6	1.83	16.4$^\alpha$	86.2	52.4	Deionized water
CB-7	1.59	9.0	33.3	166.3	Deionized water
CB-8	1.59	9.0	33.2	166.3	0.5 M $CaCl_2$
CB-9	1.59	9.0	33.3	166.3	1.0 M $CaCl_2$
CB-10	1.59	9.0	33.3	166.3	2.0 M $CaCl_2$
CB-11	1.59	9.0	33.2	166.3	VET (10.1 MPa)
CB-12	1.59	9.0	33.3	166.3	VET (38.6 MPa)
CB-13	1.59	9.0	33.2	166.3	VET (85.6)

α, the targeted water content of 20% could not be achieved due to experimental error; VET means water vapour was used to hydrate the samples, values in brackets denote the applied suction by VET.

and CB-10 (dry density = 1.59 Mg/m^3) were hydrated with 0.0001, 0.5, 1.0 and 2.0M $CaCl_2$ solutions, respectively. Samples CB-2, CB3 and CB-4 had very similar compaction conditions (dry density = 1.57 Mg/m^3 and water content = 20%). The hydrating fluids were supplied from burettes attached to the bottom fluid reservoirs of Barcelona isochoric cell (Figure 3.10). The suctions of the $CaCl_2$ solutions were measured by using the chilled-mirror hygrometer described in section 3.3.5.2. During the swelling pressure tests, the $CaCl_2$ solutions were renewed periodically for minimizing the evaporation effect that may cause an increase the concentration of the solutions. Based on the finding reported by Tripathy et al. (2014a), the expulsion of ions from the bentonites samples were assumed to have negligible impact on the suctions of the hydrating fluids. Samples CB-11, CB-12, and CB-13 with compaction dry density of 1.59 Mg/m^3 were hydrated with water vapour at the applied suction of 9.8, 39.5, 85.6 MPa, respectively. Both swelling pressure and mass of the Barcelona cell were regularly measured during the water vapour equilibrium.

The swelling pressures tests for samples CB-0 to CB-10 were terminated once a variation of the swelling pressure was less than 5 kPa per day. However, the swelling pressure tests for samples CB-11 to CB-13 were terminated until a variation of the swelling pressure was less than 5 kPa per month and a varation of the mass of Barcelona isochoric cell was less than 0.01 g. Samples CB-0 and CB-4 were dismantled after about 17 and 19 days, respectively. For samples CB-1 to CB-3 and CB-5 to CB-10, the testing duration well exceeded 30 days. Samples CB-11, CB-12 and CB-13 were dismantled after about 343, 345 and 200 days, respectively.

Following termination of a test, the fluid supply to the sample was stopped. Subsequently, samples of the aqueous solution (i.e., the hydrating fluid) were collected (in duplicate) from the bottom fluid reservoir. The suctions of the fluid samples were measured by using the chilled-mirror hygrometer. Before dismantling the device, pressurized humid air (relative humidity = 100%) generated by deionized water was used to flush the bottom and top fluid reservoirs to minimize fluid uptake by samples CB-0 to CB-10 upon unloading. Afterwards, the sample was removed from the isochoric device for total suction (ψ_t) and water content measurements.

In order to explore the homogeneity of samples in terms of the water content and suction, the bentonite samples were cut into three parts that represented the top, middle and the bottom layers. The water contents and total suctions of the representative samples were measured by the oven drying method (105°C) and the chilled-mirror hygrometer, respectively. Sufficient care was exercised to minimize the evaporation water from the samples during preparing samples for final water content and suction measurements.

3.3.6 Desiccation tests and subsequent swelling pressure and permeability measurements

To examine the influence of preliminary desiccation on swelling pressure and hydraulic conductivity, elementary laboratory tests were carried out on compacted bentonite-based materials. This section presents the experimental techniques and procedure for desiccation tests and subsequent swelling pressure and permeability measurements.

The initial conditions of compacted bentonite-based materials used in the present study are presented in Table 3.10. The initial compaction dry density of compacted bentonite varied slightly from 1.56 to 1.59 Mg/m^3, whereas the initial compaction dry density of compacted bentonite-sand mixtures varied slightly from 1.79 to 1.82 Mg/m^3. The initial water content was 20% for the compacted bentonite specimens (100B-1 to 100B-17) and 9% for the compacted bentonote-sand mixture specimens (i.e. 50B-1 to 50B-11). In addition, the initial total suction was 20 MPa for the compacted bentonite specimens and 27 MPa for the compacted bentonote-sand mixture specimens.

3.3.6.1 Suction-controlled desiccation tests at 22 and 80°C

The drying tests were carried out using the VET. Schematic of the drying test set-up used in this study is shown in Figure 3.17. The drying phase was applied to all specimens except specimens 100B-9, 100B-15, 100B-16, 100B-17 and 50B-1. These five specimens were used as reference specimens and thus did not undergo the preliminary desiccation.

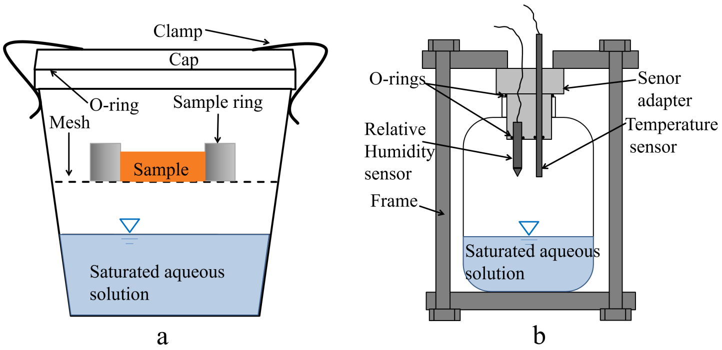

Figure 3.17: Schematic of (a) suction control device and (b) the device for measuring the suction of saturated aqueous solutions

A compacted specimen with the sample ring was placed on the plastic mesh that was fixed in the middle of the desiccator (Figure 3.17(a)). The saturated aqueous solution at

Table 3.10: Initial compaction conditions and suction paths followed in the drying test and subsequently swelling pressure and hydraulic conductivity tests for compacted bentonite-based specimens

Sample no.	Dry density	Water content	Drying phase		Saturating phase		
	ρ_{d0} [Mg/m^3]	w [%]	T [°C]	ψ_a [MPa]	T [°C]	P$_s$ √/-	k √/-
100B-1	1.588	20	105	1000	22	√	-
100B-2	1.582	20	80	700	80	√	√
100B-3	1.581	20	80	367	80	√	-
100B-4	1.586	20	80	219	80	√	-
100B-5	1.585	20	80	184	80	√	-
100B-6	1.590	20	80	104	-	-	-
100B-7	1.583	20	80	44	80	√	√
100B-8	1.588	20	80	39	-	-	-
100B-9*	1.576	20	-	-	80	√	√
100B-10	1.585	20	80	8	-	-	-
100B-11	1.567	20	22	346	22	√	-
100B-12	1.580	20	22	154	22	√	-
100B-13	1.580	20	22	83	22	√	-
100B-14	1.580	20	22	39	-	-	-
100B-15*	1.562	20	-	-	22-80-22-80-22	√	-
100B-16*	1.586	20	-	-	22	√	-
100B-17*	1.573	20	-	-	22	√	√
50B-1*	1.820	22	-	-	22-80-22-80-22	-	
50B-2	1.803	22	346	-	-	-	
50B-3	1.799	22	281	-	-	-	
50B-4	1.803	22	58	-	-	-	
50B-5	1.801	22	39	-	√	-	
50B-6	1.794	80	750	-	-	-	
50B-7	1.788	80	367	-	-	-	
50B-8	1.785	80	219	-	-	-	
50B-9	1.791	80	184	-	-	-	
50B-10	1.787	80	104	-	-	-	
50B-11	1.788	80	44	-	-	-	

$*$, reference specimens without undergoing preliminary desiccation; T, temperature; ψ_a, applied suction; P$_\mathrm{s}$, swelling pressure; k, saturated hydraulic conductivity; √ means that P$_\mathrm{s}$ or k was measured.

Table 3.11: Measured equilibrium suction (ψ_a) of the used saturated aqueous solutions at 22 and 80 °C

T [°C]	NaOH	LiCl	$MgCl_2$	$Mg(NO_3)_2$	$NaNO_2$	NaCl	KCl	K_2SO_4
				ψ [MPa]				
22	346	282	156	83	58	39	10	2
80	-	367	219	184	104	44	39	8

the bottom of the sealed desiccator provides a constant relative humidity (RH) at a given temperature. Different values of RH were applied by placing different salt solutions at the respective controlled temperature. The saturated aqueous solutions used in this study is presented in Table 3.11. The temperatures during the tests were controlled by placing the desiccator either in an oven with a temperature of 80 ± 0.1°C or in the constant temperature-controlled room with a temperature of 22 ± 0.1°C. For a given saturated aqueous solution at temperatures of 22 and 80°, the corresponding suction values were separately determined using the device shown in Figure 3.17(b). The device consists in a tightly closed container with a provision to insert two sensors for relative humidity and temperature measurements. Thus, the total suction applied by the saturated aqueous solutions at a given temperature can be determined by Eq.(3.1). The sensors used the present study were VAISALA HMP337 which consists of a humidity sensor based on correlation of humidity to dielectric characteristics (capacitive type RH sensor) and a thermocouple for temperature measurement. The measured RHs at two temperatures of 22 and 80° were found in agreement with that were reported by literature (Greenspan et al., 1977; Delage et al., 1998; Tang & Cui, 2005). According to the measured RH and temperature in this study, the applied total suctions (ψ_a) were calculated according to Eq.(3.1).

The applied suction values during the drying tests for each specimen are given in Table 3.10). Additionally, it is assumed that the dry state of a specimen after oven drying at a temperature of 105° corresponds to a suction of 1000 MPa (Fredlund et al., 2012). An oven with a temperature of 80° provided the suction of 700 MPa (Table 3.10)) which was determined by relative humidity and temperature measurements inside the atmosphere of the oven. During the drying tests, mass change of each specimen was periodically determined by taking it out of the container and weighing it on a balance with a readability of 0.001 g. Once the mass of the specimens reached equilibrium (variation of specimen mass less than 0.001 g), the diameter and height of each specimen were measured by a calliper and the dry density values were also calculated. The calculated dry densities, named dry density after desiccation, are summarize in Table 3.12.

3.3.6.2 Swelling pressure and permeability tests

After the desiccation tests were finished, all the dried specimens except specimens 100B-6, 100B-8, 100B-10, 100B-14 and 50B-2 to 50B-11 (Table 3.10) were transferred into an isochoric swelling pressure device as shown in Figure 3.18. Because the dessication caused the bond between clay particles and sand grains weakening or disappearing, many sand grains came off the surface of the dried bentonite-sand mixtures specimens (i.e. 50B-2 to 50B-11). This made it difficult to transfer the whole specimens into the isochoric swelling pressure device without mass loss and thus, the swelling pressure and hydraulic conductivity of the dried specimens 50B-2 to 50B-11 were not measured. Prior to use the isochoric cell, its load cell measurement was calibrated with respect to the non-isothermal test conditions. Details for the calibration can be found in the work of (Arifin, 2008). The swelling pressure tests were performed as one-step test by supplying deionized water at the respective temperatures used in the preliminary desiccation phase.

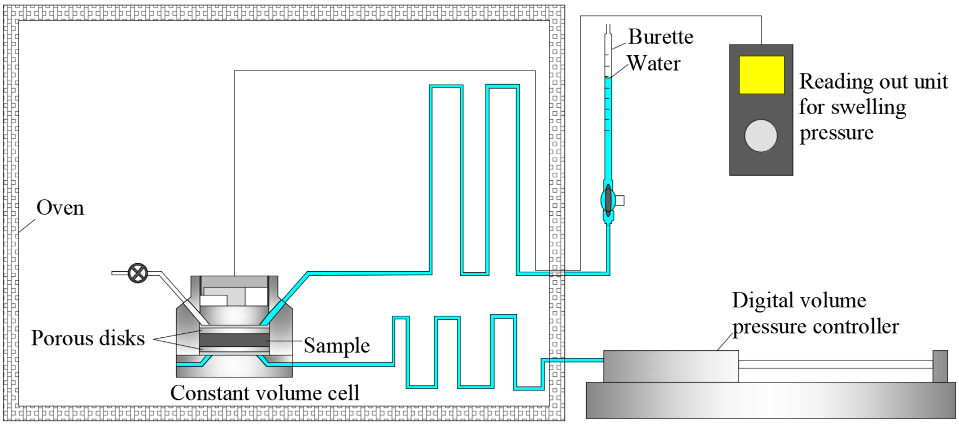

Figure 3.18: Experimental set-up for the swelling pressure and hydraulic conductivity tests

Due to the preliminary desiccation, all the bentonite specimens except specimen 100B-10 and the reference specimens (specimen 100B-9, specimen 100B-15 to specimen 100B-17) experienced volumetric shrinkage, leading to an increase in dry density. Consequently, these specimens had a smaller diameter than the diameter of 50 mm (inner diameter of sample ring) and a lower height than the height of 15.2 mm. The height of 15.2 mm corresponded to the net space height of sample ring when the isochoric swelling pressure device was assembled. The net space height of sample ring was 15.2 mm because the top porous combined with piston went inside the sample ring for 4.8 mm. Since small initial radial and vertical gaps existed at the start of hydration phase, the initial phase of the hydration corresponded to free swelling condition. Hydration of the desiccated specimens under constant volume conditions occurred until the initial radial and vertical gaps were filled with swollen clay particles.

The hydraulic conductivities of four saturated specimens (i.e. 100B-17, 100B-2, 100B-7 and 100B-9) were measured at the end of hydration phase at the respective temperature. Specimen 100B-17 was tested at 22°C and specimen 100B-2, 100B-7 and 100B-9 were tested at 80°C. The experimental set-up is shown in Figure 3.18. A constant water pressure head of 24 kPa was applied by a volume-pressure controller (VPS) at the bottom of specimens and the outflow at top of the specimen was measured by means of a burette. When the flows reached steady state, the saturated hydraulic conductivity was calculated according to Darcy's Law (Yong & Warkentin, 1975). The duration of each hydraulic conductivity test was about 45 days.

At the end of hydration test, the swelling pressure device was dismantled, and final dry densities of most specimens were determined by measuring the height and diameter of the specimens. The height and diameter measurements show that the preliminary volumetric shrinkage was fully recovered in case of the desiccated specimens. The final dry densities were found to be 0.8 to 5.7% smaller than dry densities after hydration (Table 3.12). This is mainly attributed to the expansion of the specimen after releasing the swelling pressure. Since dismantling the swelling pressure device and subsequently measuring specimen dimensions were not completed in the same span for each specimen, the error due to that cannot be quantified. Therefore, the dry density after saturation was used as relevant dry density to which the respective measured swelling pressure and hydraulic conductivity referred. The dry density after saturation was determined according to the water content and mass of a specimen before hydration and its volume after saturation under constant volume condition. The volume of a saturated specimen was determined based on the inner diameters (50-50.5 mm) of sample ring and the net space height (15.2 mm) of the sample ring.

Table 3.12: Dry densities at different testing stages

Sample no.	Dry density			
	After compaction	After desiccation [Mg/m^3]	After hydration	After dismantling
100B-1	1.588	1.740	1.563	1.474
100B-2	1.582	1.744	1.575	1.546
100B-3	1.581	1.738	1.574	1.548
100B-4	1.586	1.727	1.582	1.550
100B-5	1.585	1.698	1.588	1.558
100B-6	1.590	1.661	1.589	-
100B-7	1.583	1.660	1.576	1.564
100B-8	1.588	1.651	-	-
100B-9	1.576	-	1.576	1.555
100B-10	1.585	1.531	-	-
100B-11	1.567	1.732	1.572	1.510
100B-12	1.580	1.683	1.585	1.508
100B-13	1.580	1.666	1.572	1.504
100B-14	1.580	1.614	1.574	-
100B-15	1.562	-	1.562	1.483
100B-16	1.586	-	1.586	-
100B-17	1.573	-	1.573	1.506
50B-1	1.820	-	-	-
50B-2	1.803	1.770	-	-
50B-3	1.799	1.748	-	-
50B-4	1.803	1.798	-	-
50B-5	1.801	1.801	-	-
50B-6	1.794	1.781	-	-
50B-7	1.788	1.783	-	-
50B-8	1.785	1.773	-	-
50B-9	1.791	1.775	-	-
50B-10	1.787	1.768	-	-
50B-11	1.788	1.757	-	-

3.4 Summary

The basic properties of Calcigel bentonite and Hostun sand used in this investigation are presented in this chapter. The basic properties of the bentonite presented in the chapter include the specific gravity, the particle size distribution, the liquid limit, the plastic limit, the mineral constituents, the specific surface area and the cation exchange capacity.

Barcelona oedometer and isochoric cells equipped with the OT are presented in this chapter. The Barcelona oedometer and isochoric cells equipped with the OT are developed to determine the WRCs under confined conditions and to obtain the swelling pressure-suction relationship. These two cells are capable of applying the matric suction range from 0.001 to 13 MPa. Procedures used for sample preparation, determination of the WRCs under confined conditions, one-dimensional swelling-compression-rebound tests, multi-step swelling pressure tests, total suction measurements after swelling pressure tests, swelling pressure and permeability measurements after desiccation tests are also presented in this chapter.

4 Water retention curves (WRCs)

4.1 Introduction

The hydration of backfill and sealing materials used in the geological repository occur under different confinement conditions (unconfined, partially confined and completely confined conditions) (Pusch & Yong, 2006; Villar, 2007; Sellin & Leupin, 2013; Johannesson et al., 2014). In the past, great attention was paid to determining the WRCs under unconfined and constant volume conditions (Villar, 2007; Cui et al., 2008; Ye et al., 2009; Wang et al., 2013a; Romero et al., 2011; Gatabin et al., 2016; Tripathy et al., 2017). However, no systematic investigation into the effect of confinement conditions on the wetting WRCs of bentonite-sand mixtures used as backfill and sealing materials has been performed in the past.

This chapter mainly presents the experimental results and discussion with respect to the effect of different confinement conditions on the wetting WRCs of the bentonite-sand mixtures. The experimental methods are presented in see section 3.3.2. In this chapter, section 4.2.1 presents the evolution of swelling strain and swelling pressure during suction controlled wetting tests. Section 4.2.2 presents the wetting WRCs determined under different confinement conditions. Section 4.2.3 presents wetting-drying WRCs determined under unconfined and constant volume conditions. Section 4.2.4 presents microstructural characteristics determined from WRCs. Section 4.2.5 presents the applied suction versus measured total suction. Section 4.2.6 presents measured total suction-water curves. Section 4.3 presents concluding remarks.

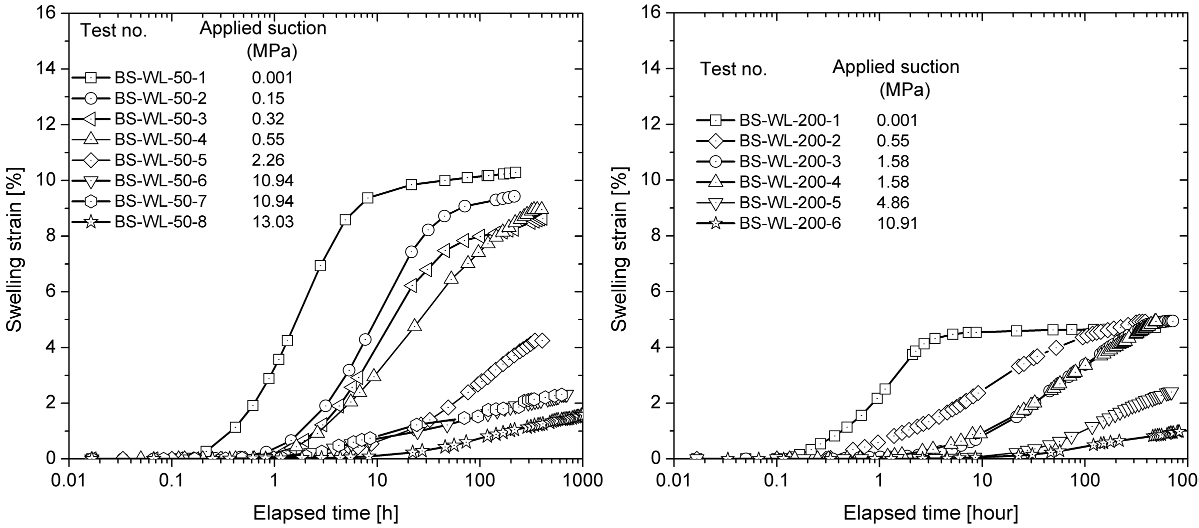

(a) (b)

Figure 4.1: Evolution of swelling strain of the compacted bentonite-sand mixtures wetted at different suctions for the tests performed under a vertical pressure of (a) 50 kPa and (b) 200 kPa

4.2 Results and discussion

4.2.1 Evolution of swelling strain and swelling pressure during water absorption

4.2.1.1 Evolution of swelling strain

Evolution of the swelling strain of the compacted bentonite-sand mixtures wetted at different suctions for the tests performed under a vertical pressure of (a) 50 kPa and (b) 200 kPa is presented in Figures 4.1(a) and 4.1(b), respectively. To assess the modified Barcelona oedometer cell, two replicable samples (i.e. BS-WL-50-6 and BS-WL-50-7) under the vertical pressure of 50 kPa were wetted at the applied suction of 10.94 MPa (Figure 4.1(a)). In addition, two replicable samples (i.e. BS-WL-200-3 and BS-WL-200-4) under the vertical pressure of 200 kPa were also wetted at the applied suction of 1.58 MPa (Figure 4.1(a)). According to Figures 4.1, the elapsed time-swelling strain curves were almost same when both the vertical pressure and the applied suction were same. These reproducible experimental results indicated that the modified Barcelona oedometer cell was capable of providing reliable experimental data.

The evolution of the swelling strain given in Figures 4.1 showed that the swelling strains monotonically increased with elapsed time, regardless of the applied vertical pressure and suction. Moreover, the evolution of the swelling strain shown in Figures 4.1 also showed that for a given the vertical pressure, the equilibrium swelling strains almost increased with decreasing the applied suctions. These two experimental findings suggested that the wetting paths followed by the samples BS-WL-50-1 to BS-WL-50-8 and BS-WL-200-1 to BS-WL-200-6 were far from their loading-collapse (LC) curves. Gens & Alonso (1992) stated that when the wetting path followed by a expansive clay was far from its LCs, the expansive clay upon wetting only exhibited swelling and the swelling capacity increased with a decrease in the suction. Thus, the swelling strains of the samples BS-WL-50-1 to BS-WL-50-8 and BS-WL-200-1 to BS-WL-200-6 monotonically increased with elapsed time and their equilibrium swelling strains almost increased with decreasing the applied suctions.

4.2.1.2 Evolution of swelling pressure

Evolution of swelling pressure of the compacted bentonite-sand mixtures for (a) wetting phase and (b) wetting-drying phases is shown in Figures 4.2(a) and 4.2(b), respectively. According to Figure 4.2(a), the swelling pressure monotonically increased with elapsed time, regardless of the applied suction, which was similar to development of swelling strain shown in Figures 4.1. In addition, Figure 4.2(a) also showed that the equilibrium swelling pressures almost increased with a decrease in the applied suction. The equilibrium swelling pressures for the applied suction of 11.45, 11.15, 3.78, 1.12, 0.55, 0.15 and 0.001 MPa were 201, 281, 374, 580, 567, 602 and 600 kPa, respectively. These two experimental findings suggested that the stress paths followed by the compacted bentonite-sand mixtures during the constant volume wetting tests were far from LC curves. Consequently, the swelling pressures of the compacted bentonite-sand mixtures monotonically increased with elapsed time and their equilibrium swelling pressures almost increased with decreasing the applied suctions.

The evolution of swelling pressure of the compacted bentonite-sand mixtures given in Figure 4.2(b) showed that the time-swelling pressure curves of the samples BS-WDCV-1 to BS-WDCV-4 were almost same during the wetting phase. These reproducible experimental results indicated that the Barcelona isochoric cell equipped with the OT was capable of providing reliable experimental data. When the samples BS-WDCV-1 to BS-WDCV-4 underwent the drying phase, their swelling pressures immediately dropped and fast reached new equilibrium. In the case of the applied suction of 10.9 MPa, the swelling

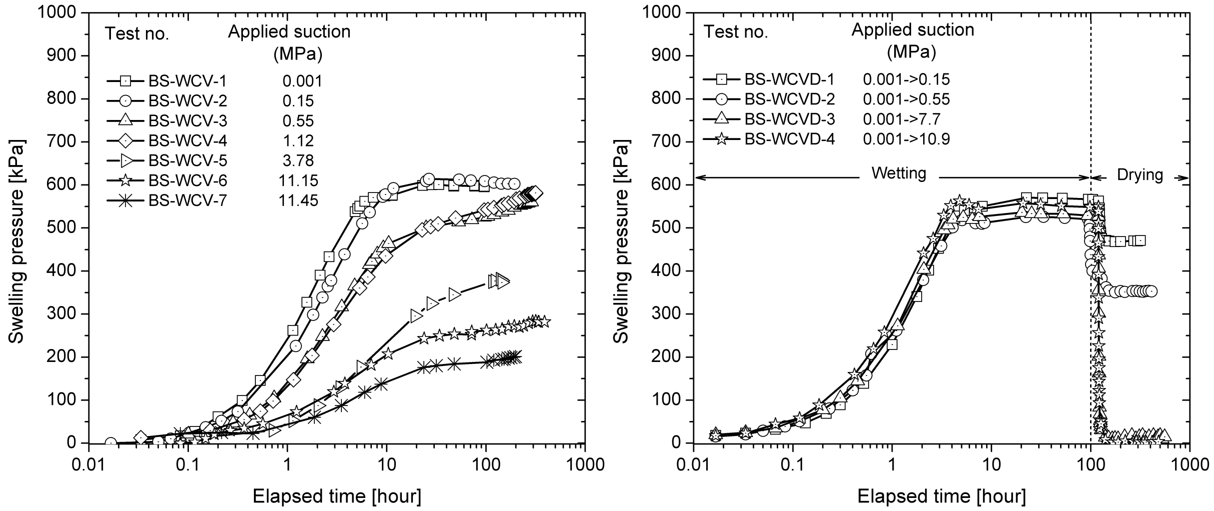

(a) (b)

Figure 4.2: Evolution of swelling pressure of the compacted bentonite-sand mixtures for (a) wetting phase and (b) wetting-drying phases

pressures of the samples BS-WDCV-4 to BS-WDCV-10 almost dissipated. Since the time-swelling pressure curves of samples BS-WDCV-4 to BS-WDCV-10 almost same, only the time-swelling pressure of sample BS-WDCV-4 was given in Figure 4.2(b). The samples BS-WDCV-4 to BS-WDCV-10 was found to almost lost the contact with the wall of the sample ring at the end of test. This result implied that if the applied suction during the drying process was greater than 10.9 MPa, the volume of the samples would decrease.

4.2.2 Wetting WRCs under different confinement conditions

After the swelling strains and the swelling pressures during the suction controlled wetting tests shown in Figures 4.1 and 4.2(a) reached equilibrium, the tests were terminated for final total suction and water content measurements. The water contents and the corresponding applied suctions (the suctions of the PEG solution) were used to establish wetting WRCs. The wetting WRCs under different confinement conditions are presented in Figure 4.3. In Figure 4.3(a), the wetting WRCs under unconfined condition were determined employing suction controlled wetting tests on oven-dried samples from slurry and as-compacted samples (see section 3.3.2.4). However, the wetting WRCs under a vertical pressure of 2.5 kPa condition were determined using suction controlled wetting tests on as-compacted samples BS-SCR-1 to BS-SCR-4 (see section 3.3.4.3). For comparison, a suction-water curve determined by Arifin (2008) is also presented in Figure 4.3(a).

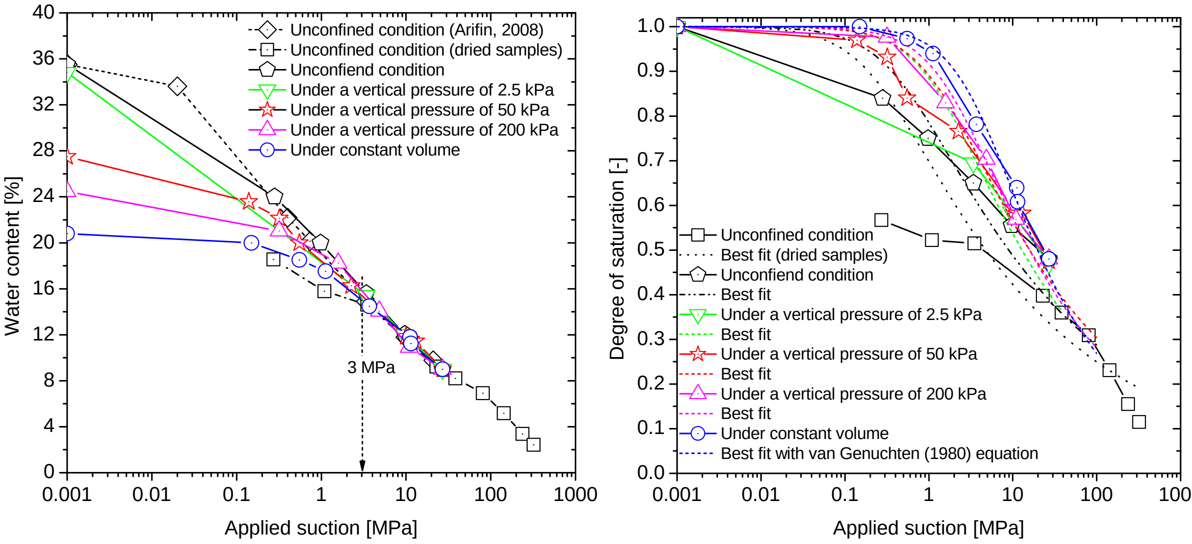

(a) (b)

Figure 4.3: Effect of confinement conditions on the wetting WRCs of bentonite-sand mixtures in the case of (a) suction-water content curve and (b) suction-degree of saturation curve

In his work, a compacted Calcigel bentonite-sand mixtures sample with the almost same initial conditions as those used in this study was gradually wetted by decreasing the applied suction in a stepwise manner under unconfined condition. In Figure 4.3(b), the applied suction versus degree of saturation were fitted with van Genuchten (1980) model (Eq.(4.1)) to obtain the best fit curves and the air-expulsion values. The air-expulsion values obtained under different confinement conditions are presented in Table 4.1.

van Genuchten (1980) model is given in Eq.(4.1):

$$S = \frac{1}{[1 + (\alpha\psi_{\mathrm{a}})^n]^{1-1/n}} \tag{4.1}$$

where S is the degree of saturation (-), ψ_{a} is the applied suction (MPa) and α (MPa^{-1}) and n (-) are fitting parameters. In addition, $1/\alpha$ corresponds to air-expulsion or air-entrance value.

The experimental data in Figure 4.3(a) showed that the suction of 3 MPa separated the suction-water content curves into the region independent of the confinement conditions and that dependent on the confinement conditions. The suction-water content curves over suction range greater than 3 MPa were unique and thus were independent of the confinement conditions. However, the suction-water content curves over suction range less than 3

Table 4.1: Effect of the confinement conditions on the air-expulsion values determined based on van Genuchten (1980) model

Confinement conditions	Fitting parameters		Air-expulsion value
	α (MPa^{-1})	n (-)	(MPa)
Under unconfined condition (a)	4.1969	1.2298	0.24
Under unconfined condition (b)	2.1800	1.2317	0.46
Under a vertical pressure of 2.5 kPa	0.7635	1.2986	1.31
Under a vertical pressure of 50 kPa	0.7611	1.2749	1.32
Under a vertical pressure of 200 kPa	0.5264	1.3120	1.90
Under constant volume	0.2648	1.4014	3.68

a: on oven-dried samples from slurry; b: on as-compacted samples

MPa varied significantly with the confinement conditions. From the unconfined condition to the completely confined condition (constant volume condition), water contents at a given applied suction less than 3 MPa significantly decreased.

In addition to the suction-water content curves, the suction-degree of saturation curves were also affected by the confinement conditions (Figure 4.3(b)). The suction-degree of saturation curves shifted from the left to the right with the confinement conditions varying from the unconfined condition to the completely confined condition (constant volume condition). Consequently, the air-expulsion values derived from best fitting the experimental data with van Genuchten (1980) model (Eq.(4.1)) increased with strengthening the confinement conditions (Table 4.1). The air-expulsion value was the minimum (0.24-0.46 MPa) for unconfined condition, but the maximum (3.68 MPa) for constant volume condition. In the case of the vertical pressures of 2.5 and 50 kPa conditions, the air-expulsion values were similar and about 1.3 MPa. In the case of the vertical pressure of 200 kPa condition, the air-expulsion value was a intermediate value, 1.90 MPa.

The experimental results in Figure 4.3 indicated that the confinement conditions significantly affect the wetting WRCs over suction range below 3 MPa and the air-expulsion values. Similar conclusions have been also drawn by Romero et al. (2011), Wang et al. (2013a) and Gatabin et al. (2016). For the wetting WRCs of bentonite-based materials, adsorptive and capillary mechanism dominant regions can be distinguished by a delimiting suction or water content (Romero et al., 2011). The delimiting suction corresponds to the water content that is sufficient to saturate the intra-aggregate pores but which leaves the inter-aggregate pores empty. The wetting WRCs over suction range above the delimiting suction is dominated by the adsorptive mechanism and the water in this region is held by the intra-aggregate pores. The intra-aggregate pores is almost independent of stress state(Romero & Simms, 2008). However, the wetting WRCs over suction range below the delimiting suction is dominated by the capillary mechanism and the water in this region is held by intra-aggregate and inter-aggregate pores. The capillary mechanism depends on the characteristic dimensions of interconnected inter-aggregate pores and thus on porosity or confinement conditions.

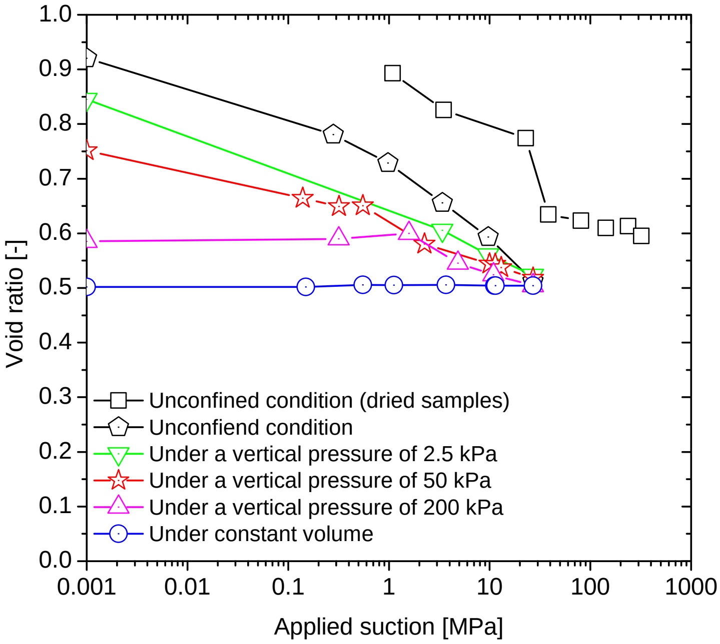

Figure 4.4: Variation of the total void ratio of bentonite-sand mixtures upon wetting under different confinement conditions

If the volume expansion is not or partially restricted, the total void ratio is allowed to increases with decreasing the suction (see Figure 4.4). In the case of constant volume condition, however, the volume expansion is completely restricted and thus the total void ratio keeps constant during wetting process. Moreover, the volume of intra-aggregate pore in the case of constant volume condition increases with decreasing the applied suction (Cui et al., 2002; Romero & Simms, 2008; Romero et al., 2011; Manca et al., 2015). Both a reduction in the total void ratio and an increase in the intra-aggregate pore volume would reduce the mean dimension of inter-aggregate pore and increase the air-expulsion value

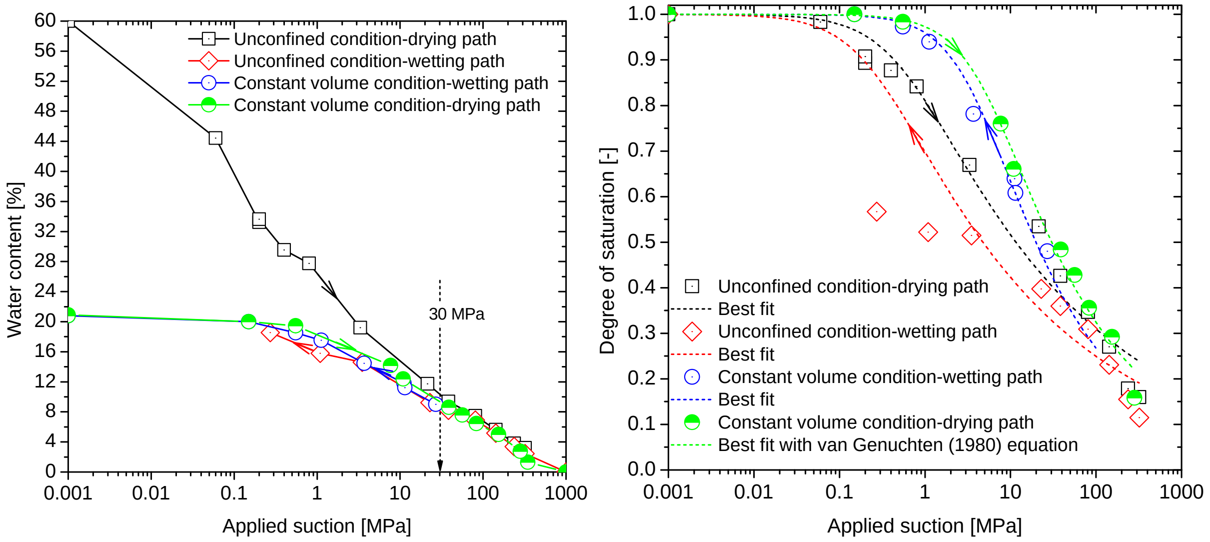

(a) (b)

Figure 4.5: Effect of confinement conditions on wetting-drying WRCs of bentonite-sand mixtures in the case of (a) suction-water content curve and (b) suction-degree of saturation curve

(Romero et al., 2011; Seiphoori et al., 2014). Thus, strengthening confinement conditions reduces total void ratio and increases the air-expulsion value.

4.2.3 Wetting-drying WRCs

The wetting-drying WRCs under unconfined and constant volume conditions are shown in Figure 4.5. The suction-degree of saturation curves shown in Figure 4.5(b) were obtained by best fitting the experimental data with van Genuchten (1980) equation. The air-entry and air-expulsion values are shown in Table 4.2.

Figure 4.5 showed that the confinement conditions (i.e. unconfined and constant volume conditions) significantly affected the wetting-drying WRCs or hysteresis loop. In case of the unconfined condition, the hysteresis loop was significant, particularly over suction range less than 30 MPa. However, the hysteresis loop was insignificant in case of the constant volume condition. The hysteresis nature of WRCs has been interpreted as a consequence of the well-know pore constriction effect, of soil deformability and of the permanent change of soil fabric (Lu & Likos, 2004; Nuth & Laloui, 2008; Seiphoori et al., 2014). In case of bentonite-sand mixtures, the irreversible soil deformability induced the hysteresis loop. A comparison of variation of total void ratios with applied suction under

Table 4.2: Effect of the different confinement conditions on the air-entry/expulsion values determined based on van Genuchten (1980) model

Constraint conditions	Fitting parameters		Air-entry/expulsion value
	α (MPa^{-1})	n (-)	(MPa)
Unconfined condition-drying path	1.8602	1.2244	0.54
Constant volume-drying path	0.1940	1.3782	5.16
Unconfined condition-wetting path	4.1969	1.2110	0.24
Constant volume-wetting path	0.2648	1.4014	3.68

unconfined condition and constant volume condition is presented in Figure 4.6. This comparison showed that the soil deformability during wetting-drying process was almost reversible in case of the constant volume condition. However, the soil deformability during wetting-drying process was irreversible in case of the unconfined condition, particularly over suction range greater than 30 MPa.

Moreover, Figure 4.5 also showed the confinement conditions considerably affected the air-entry value as well as the air-expulsion values (Table 4.2). The air-entry value in case of constant volume condition was equal to 5.16 MPa which was considerably greater than that (i.e. 0.54 MPa) in case of unconfined condition. This was due to the fact that the total void ratio under unconfined condition was significantly greater than that under constant volume condition (Figure 4.6). Both a reduction in the total void ratio and an increase in the intra-aggregate pore volume would reduce the mean dimension of inter-aggregate pore and increase the air-entry value (Romero et al., 2011; Seiphoori et al., 2014). As a consequence, the air-entry value in case of constant volume condition was considerably greater than that in case of unconfined condition.

In case of the suction range greater than 30 MPa, the suction-water content curves were almost unique (Figure 4.5(a)). This experimental result indicated that when the applied suction was greater than 30 MPa, the hydration and dehydration of bentonite-sand mixtures was almost reversible and thus, was independent of the confinement conditions. The suction of 30 MPa corresponds to the relative humidity of 80.2% at 22.5°C. In this condition, the water held by bentonite-sand mixtures is governed by bentonite or dominated by the montmorillonite in the bentonite. Montmorillonites dominated by divalent exchangeable cations (i.e. Ca, Mg montmorillonites) corresponds to two layers water state

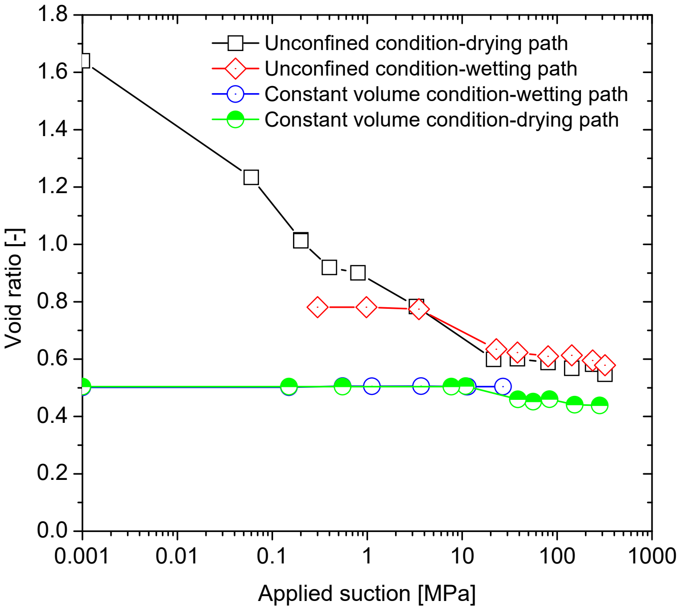

Figure 4.6: Variation of total void ratio of bentonite-sand mixtures upon wetting-drying under unconfined and constant volume conditions

under the condition of the relative humidity of 80.2% and the temperature of 22.5°C (Mooney et al., 1952; Madsen, 1998; Ferrage et al., 2007a). Therefore, the almost unique suction-water content curve over suction range greater than 30 MPa suggests that the hydration-dehydration of the interlayer of montmorillonite is almost reversible and independent of the confinement conditions

4.2.4 Determination of the intra-aggregate and inter-aggregate void ratios from WRCs

Navarro et al. (2017b) proposed a method for determining the intra-aggregate (microstructural) and inter-aggregate (macrostructural) water content of Na-bentonite using data from WRCs. According to their proposed method and reasonable modification, the microstructural and macrostructural void ratios of bentonite-sand mixtures were derived from the WRCs mentioned in the preceding sections.

4.2.4.1 Model introduction

To distinguish the microstructural water content values from the total water content values over suction-water content curves (i.e. Figures 4.3(a) and 4.5(a)), the total soil water content is assumed as the sum of macrostructural pore water and microstructural pore water. The macrostructural pore water partially fills the inter-aggregate voids and the microstructural water fills the intra-aggregate voids. Consequently, the following equation holds:

$$w = w_{\mathrm{M}} + w_{\mathrm{m}} \tag{4.2}$$

where w represents total water content (ratio of water mass to solid mass of soil particles), w_{M} represents macrostructural water content (ratio of macrostructural pore water mass to the solid mass of soil particles), w_{m} represents microstructural water content (ratio of microstructural pore water mass to the solid mass of soil particles).

Similarly, the relationship among total void ratio (e), macrostructural void ratio (e_{M}) and microstructural void ratio (e_{m}) is obtained and presented in the following equation:

$$e = e_{\mathrm{M}} + e_{\mathrm{m}} \tag{4.3}$$

where e is the ratio of total pore volume to solid volume of soil particles, e_{M} is the ratio of macrostructural pore volume to the solid volume of soil particles, e_{m} is the ratio of microstructural pore volume to the solid volume of soil particles.

It is assumed that the increase in microstructural void space from the dry state is equal to the increase in microstructural water, then the following relationship holds:

$$e_{\mathrm{m}} = G_{\mathrm{s}} w_{\mathrm{m}} = G_{\mathrm{s}}(w_{\mathrm{mC}} + \triangle w_{\mathrm{mO}}) = e_{\mathrm{mC}} + \triangle e_{\mathrm{mO}} \tag{4.4}$$

where G_{s} is the specific gravity of soil particles; w_{mC} and $\triangle w_{\mathrm{mO}}$ are crystalline microstructural water content and increase in microstructural water content caused by osmotic swelling, respectively; e_{mC} and $\triangle e_{\mathrm{mO}}$ are crystalline microstructural void ratio and increase in microstructural void ratio caused by osmotic swelling, respectively.

e_{mC} is determined by Eq.(4.5) that is similar to van Genuchten (1980) model (Eq.(4.1)).

$$e_{\mathrm{mC}} = \frac{e_{\mathrm{mCMAX}}}{[1 + (\alpha_{\mathrm{m}} s_{\mathrm{m}})^{n_{\mathrm{m}}}]^{l_{\mathrm{m}}}} \tag{4.5}$$

where e_{mCMAX} is the microstructural void ratio associated with the crystalline swelling at saturation, and α_{m} and l_{m} are fitting parameters. The relationship $n_{\mathrm{m}} = 1/(1 - l_{\mathrm{m}})$ (van

Genuchten, 1980) is assumed to be valid. In the equation above, s_{m} is the microstructural suction and can be determined by the following equation:

$$s_{\mathrm{m}} = s_{\mathrm{M}} + P \tag{4.6}$$

where s_{M} is the macrostructural suction which is equal to the difference between the gas pressure (P_{G}) and the pressure of macrostructural liquid (P_{L}) and P is the net mean stress.

$\triangle e_{\mathrm{mO}}$ is determined by Eq.(4.8)

$$\triangle\, e_{\mathrm{mO}} = -K_{\mathrm{m}} \ln\left(\frac{s_{\mathrm{m}} + P_{\mathrm{ATM}}}{s_{\mathrm{mO}} + P_{\mathrm{ATM}}}\right) \tag{4.7}$$

where K_{m} is a microstructural stiffness parameter (a value of 0.03 has been used in case of bentonite-sand mixtures), s_{mO} is the microstructural suction at which osmotic swelling begins to play a significant role (a value of 11 MPa has been used in this study), P_{ATM} is the atmosphere air pressure.

4.2.4.2 Determination of model parameters from wetting WRCs

For montmorillonites dominated by divalent exchangeable cations (e.g. Ca, Mg montmorillonites), the crystalline swelling is approximately complete when the suction reaches about 6 MPa (relative humidity of 95% at 22 °C) (Cases et al., 1997). The osmotic swelling or diffuse double layer swelling occurs at a suction of 26 MPa (Saiyouri et al., 2000, 2004) and plays a significant role at about 11 MPa (Slade & Quirk, 1991). Therefore, experimental data over suction range greater than 6 MPa shown in the wetting suction-water content curve determined under confined condition (Figure 4.5(a)) have been used to determine the model parameters of Eq.(4.5). The experimental data over suction range less than 11 MPa have been used to determine the increase in microstructural water content or void ratio caused by osmotic swelling. The microstructural void ratio (e_{m}) is then calculated according to Eq.(4.4) and finally the macrostructural void ratio (e_{M}) can be determined based on Eq.(4.3) at any given total void ratio (e).

The parameters identified to characterise the microstructural void ratio are summarized in Table 4.3. According to these parameters, the fitting and experimental data are presented in Figure 4.7. The model was capable of satisfactorily reproducing the experimental data over suction range greater than 6 MPa.

Table 4.3: Parameters identified to characterise the microstructural void ratio according the data in the wetting suction-water content curve determined under confined condition (Figure 4.5(a))

Parameter	Unit	Value
e_{mCMAX}	-	0.35
α_{m}	MPa^{-1}	0.057
l_{m}	-	1.546
K_{m}	-	0.03
s_{mO}	MPa	11
P_{ATM}	MPa	0.1
G_{s}	-	2.73

4.2.4.3 Variation of void ratio with applied suction

Figure 4.8 shows variations of the total, microstructural and macrostructural void ratios upon wetting for the different confinement conditions. In case of a vertical pressures of 2.5 (Figure 4.8(a)), both the total and microstructural void ratios increased with decreasing the applied suction. However, the macrostructural void ratio decreased with decreasing the applied suction from 27 to 3 MPa. Further decreasing the applied suction from 3 to 0.001 MPa resulted in an increase in the macrostructural void ratio. The variations of void ratios with decreasing the applied suction in case of a vertical pressure of 50 kPa (Figure 4.8(b)) were similar to those in case of a vertical pressure of 2.5 kPa. In case of a vertical pressure of 200 kPa (Figure 4.8(c)), both the total and microstructural void ratios increased with decreasing the applied suction. However, the macrostructural void ratio decreased with decreasing the applied suction. In case of the constant volume condition (Figure 4.8(d), the microstructural void ratio increased with decreasing the applied suction, whereas the macrostructural void ratio decreased with decreasing the applied suction.

The results shown in Figure 4.8 were expected, particularly in the case of constant volume condition. In the case of constant volume condition, the variation of void ratios with decreasing the applied suction derived from wetting WRCs is consistent with the experimental results reported by Cui et al. (2002); Romero & Simms (2008); Romero et al. (2011); Manca et al. (2015). They found that for compacted bentonite-sand mixtures,

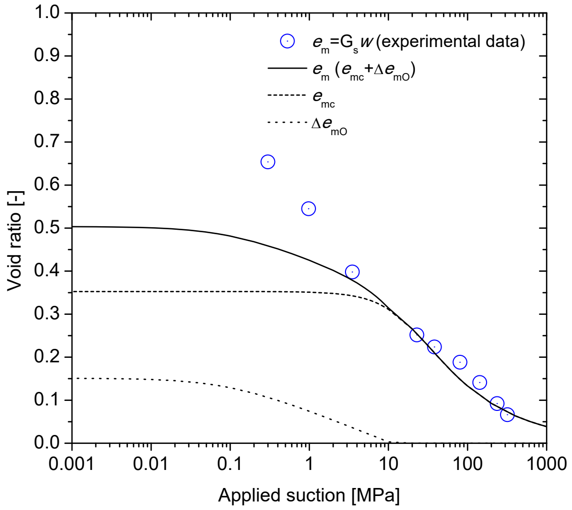

Figure 4.7: Fit of the applied suction-void ratios determined with Eq.(4.3) to Eq.(4.6) based on the experimental data from Figure 4.5(a)

the volume of intra-aggregate pore increased with decreasing the applied suction. The macrostructural void ratio continuously decreased with decreasing the applied suction in the case of constant volume condition. This consistence above suggested that the method for determining microstructural and macrostructural void ratios from wetting WRCs was qualitatively reliable, particularly the constant volume condition. However, either a series of MIP tests or simulation work is necessary to quantitatively asses the method for deriving the microstructural and macrostructural void ratios of bentonite-sand mixtures from WRCs.

A comparison of changes in void ratio with decreasing applied suction under different confinement conditions is presented Figure 4.9. As can be seen from Figure 4.9(a), the confinement conditions strongly affected the variation of the total void ratio with decreasing applied. When the volume expansion was partially restricted, the total void ratio (e) was allowed to increases with decreasing suction. In the case of constant volume condition, the total void ratio was constant during wetting process since the volume expansion was completely restricted.

According to Figure 4.9(b), the microstructural void ratio (e_{m}) increased with a reduction in applied suction, independent of the confinement conditions. Moreover, for a given applied suction, the confinement conditions had almost no effect on the microstructural void ratio , particularly for the suction range greater than 3 MPa.

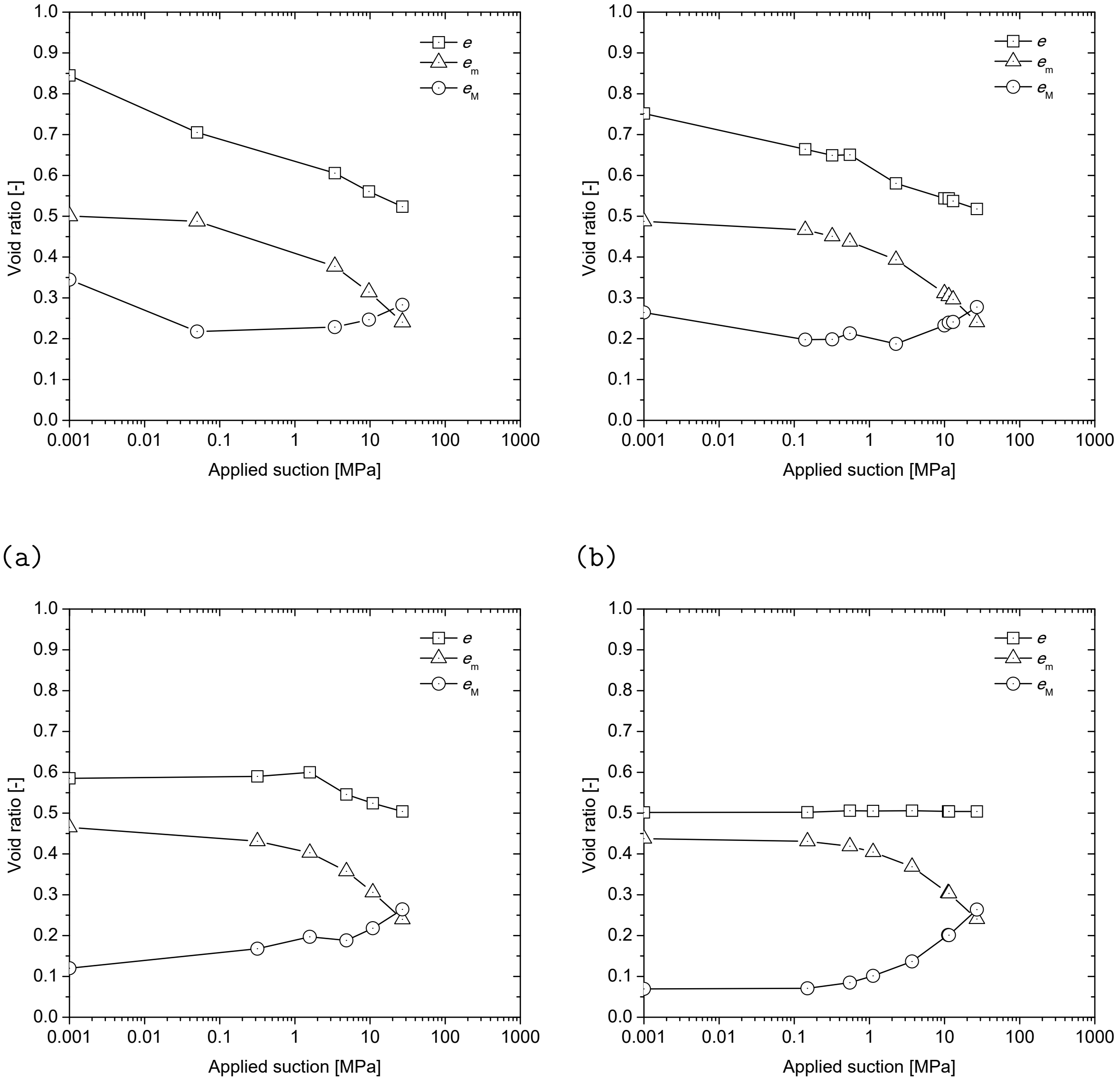

(a) (b)

(c) (d)

Figure 4.8: Variation of void ratio of bentonite-sand mixtures upon wetting under a vertical pressure of (a) 2.5, (b) 50, (c) 200 kPa and (d) constant volume condition

Unlike the change in microstructural void ratio, the variation of the macrostructural void ratio (e_{M}) with increasing the applied suction depended on both the applied suction and confinement conditions (Figure 4.9(c)). If the volume expansion was slightly restricted (i.e. swelling under the vertical pressures of 2.5 and 50 kPa), the macrostructural void ratio decreased with reducing the applied suction from 27 MPa (as-compacted state) to about 3 MPa. When the applied suction reduced from about 3 to 0.001 MPa, however, the macrostructural void ratio increased. If the volume expansion was strongly restricted (i.e. swelling under the vertical pressures of 200 kPa and constant volume), the macrostructural void ratio continuously decreased with decreasing the applied suction.

The decrease in the macrostructural void ratio with strengthening the confinement conditions was capable of explaining that the air-expulsion values derived from van Genuchten (1980) model decreased with strengthening the confinement conditions (Table 4.1). Strengthening the confinement conditions reduces the macrostructural void ratio. The decrease in macrostructural void ratio would reduce the mean dimension of inter-aggregate pore and the air-expulsion values (Romero et al., 2011; Seiphoori et al., 2014).

In addition to the variation of void ratios upon wetting, variation of void ratios upon drying in case of slurry samples under unconfined condition and compacted samples under constant volume condition was also determined. Figure 4.10 presents the variation of total, microstructural and macrostructural void ratios upon drying in case of slurry samples under unconfined condition and compacted samples under constant volume and unconfined conditions.

Figure 4.10(a) showed that for the slurry samples under unconfined conditions, the total, microstructural and macrostructural void ratios varied significantly with increasing the applied suction. Both the total void ratio and macrostructural void ratio decreased with increasing the applied suction from 0.001 to 0.54 MPa (air-entry value), whereas the microstructural void ratio remained almost unchanged over this suction range. This indicated that the shrinkage of the total void space over suction range below the air-entry value was dominated by the shrinkage of the macrostructural pore. When the applied suction increased from 0.54 to about 20 MPa, the total, macrostructural and microstructural void ratios decreased. This result suggested that the shrinkage of the total void space over suction range from 0.54 to 20 MPa was due to the shrinkages of both the macrostructural and microstructural pores. When the applied suction increased from 20 to 1000 MPa, the macrostructural void ratio increased, whereas the microstructural void ratio decreased. Moreover, the decrease in the microstructural void ratio was approximately equal to the increase in the macrostructural void ratio for a given increase in the applied suction. Con-

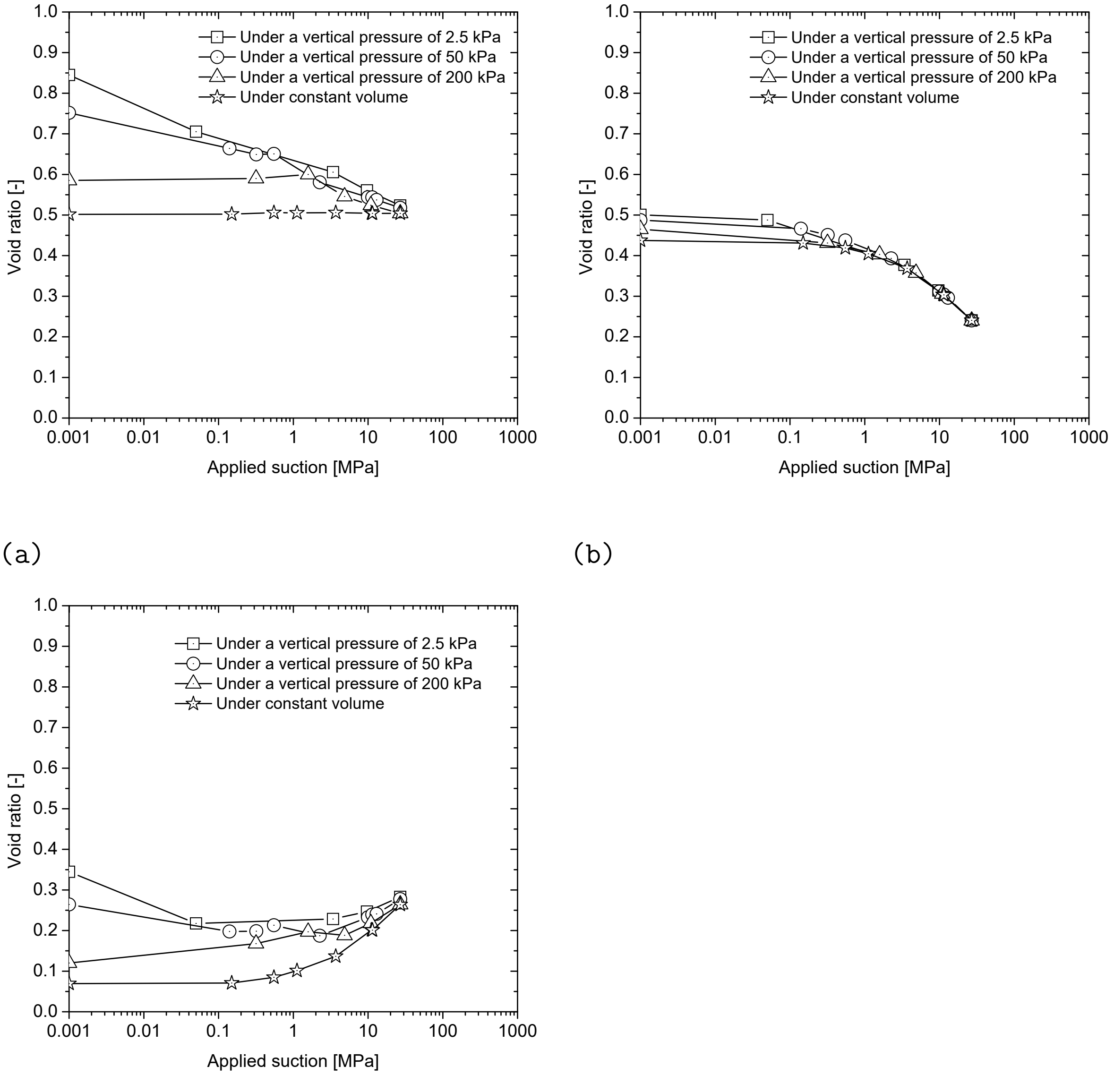

(a)

(b)

(c)

Figure 4.9: Effect of confinement conditions on changes in (a) total void ratio, (b) microstructural void ratio and (c) macrostructural void ratio with decreasing the applied suction for bentonite-sand mixtures

sequently, the total void ratio remained almost unchanged with decreasing the applied suction to greater than 20 MPa.

In case of the compacted samples under constant volume condition, the total void ratio varied insignificantly with increasing the applied suction, whereas both the microstructural and macrostructural void ratios varied significantly with decreasing the applied suction (Figure 4.10(b)). The total void ratio remained constant with increasing the applied suction from 0.001 to 40 MPa. Simultaneously, the microstructural void ratio decreased, whereas the macrostructural void ratio increased. The results above indicated for the suction range less than 40 MPa, the shrinkage of the microstructural pores induced the same magnitude of swelling of the macrostructural void ratio. Consequently, the total void ratio remained constant with increasing the applied suction from 0.001 to 40 MPa. When the applied suction increased from 40 to 60 MPa, the total, microstructural and macrostructural void ratios declined slightly. This result suggested that shrinkage of the microstructural pore and collapse of the macrostructural pore induced the slight decrease in the total void ratio. When the applied suction increased from 60 to 100 MPa, the total void ratio remained almost unchanged. Simultaneously, the microstructural void ratio decreased, whereas the macrostructural void ratio increased. These results indicated for the suction range greater than 60 MPa, the shrinkage of the microstructural pores induced almost same magnitude of swelling of the macrostructural void ratio. Consequently, the total void ratio remained almost constant with increasing the applied suction from 60 to 1000 MPa.

In the case of the compacted samples under constant volume condition, the air-entry value was about 5.2 MPa (Figure 4.10(b)). For the suction range less than 40 MPa, the shrinkage of the microstructural pores induced the same magnitude of swelling of the macrostructural void ratio. Thus, the air-entry value determined in the case of the compacted samples under constant volume condition was dominated by drainage of the microstructural pore water. However, the air-entry value (i.e. 0.54 MPa) determined in case of slurry samples under unconfined condition was controlled by drainage of the macrostructural pore water (Figure 4.10(a)). The mean dimension of the macrostructural pore is greater than that of the microstructural pore. Therefore, the air-entry value in case of the compacted samples under constant volume condition is considerably greater than that in case of slurry samples under unconfined condition.

A comparison of variation of void ratio with increasing the applied suction in case of slurry samples under unconfined condition and compacted samples under constant volume condition is shown Figure 4.11. Sample preparations and confinement conditions

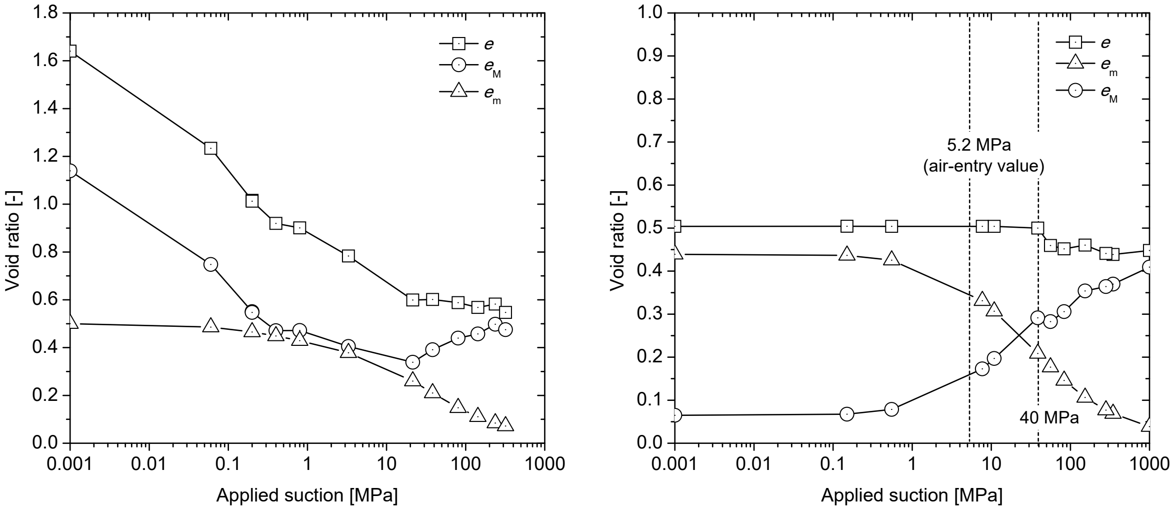

(a) (b)

Figure 4.10: Variation of void ratios of bentonite-sand mixtures upon drying in case of (a) slurry samples under unconfined condition and (b) compacted samples under constant volume and unconfined condition (the drying over suction range greater than 11 MPa occurred in unconfined condition)

had a significant effect on both total void ratio and macrostructural void ratio but had a insignificant effect on the microstructural void ratio. For a given suction, the total void ratios of the slurry samples undergoing the drying under confined condition was significantly greater than those of the compacted samples undergoing the drying under constant volume condition. Moreover, the total void ratios of the slurry samples decreased considerably with increasing the applied suction, whereas the total void ratios of compacted samples only decreased slightly over suction ranger greater than 40 MPa. The microstructural void ratios of the slurry samples undergoing the drying under confined condition was almost same with those of the compacted samples undergoing the drying under constant volume condition. As a consequence, the macrostructural void ratios of the slurry samples undergoing the drying under confined condition was significantly greater than those of the compacted samples undergoing the drying under constant volume condition. In addition, the macrostructural void ratios of the slurry samples under confined condition decreased with increasing the applied suction from 0.001 to 20 MPa and then increased with increasing the applied suction from 20 to 1000 MPa. However, the macrostructural void ratios of the compacted samples under constant volume condition continuously decreased with increasing the applied suction.

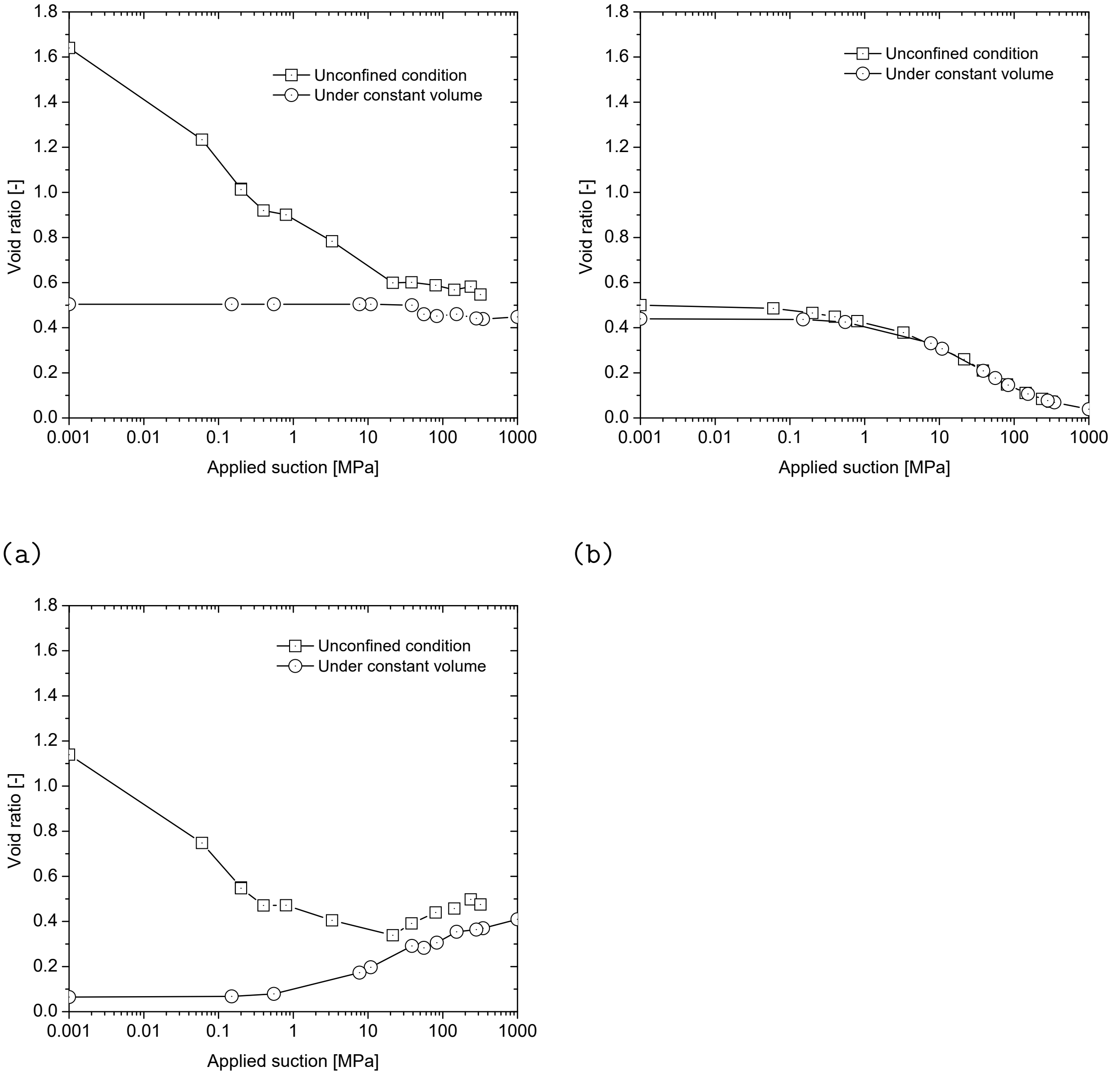

(a)

(b)

(c)

Figure 4.11: Variation of (a) total void ratio, (b) microstructural void and (c) macrostructural void ratio of bentonite-sand mixtures with increasing the applied suction in case of slurry samples under unconfined condition and compacted samples under constant volume condition

4.2.5 Applied suction versus measured total suction

The applied suction (the suctions of the PEG solution) versus the measured total suction plot is presented Figure 4.12. The measured total suction was found to be not equal to but considerably greater than the applied suction. The difference in the measured total suction and the applied suction varied from 0.1 to 4.6 MPa, depending on the vertical/swelling pressure and the applied suction. The effect of the vertical/swelling pressure and the applied suction on the difference in the measured total suction and the applied suction is shown in Figure 4.13. The difference in the measured total suction and the applied suction increased with the applied suction (Figure 4.13(a)). In addition, it also increased with the vertical or swelling pressure (Figure 4.13(b)).

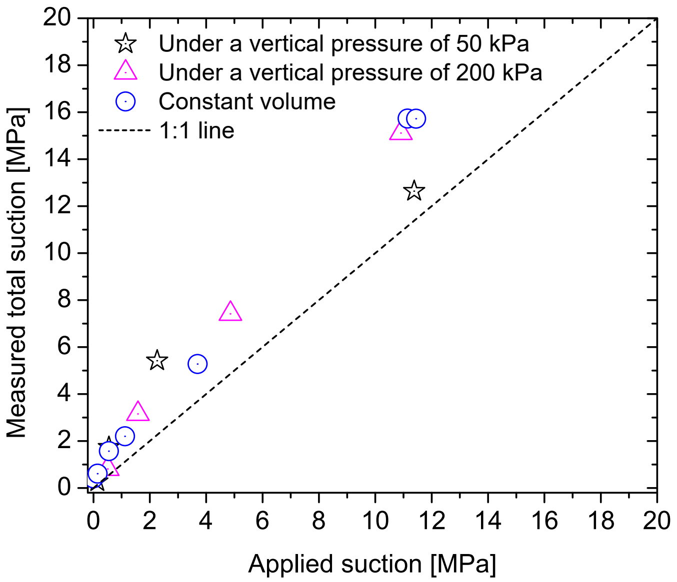

Figure 4.12: Applied suction versus measured total suction for compacted bentonite-sand mixtures wetted under the different confinement conditions

The excess of the measured total suction over the applied suction is mainly due to the restricted volume expansion conditions or the vertical pressures since the osmotic suction due to dissolved salts in Calcigel bentonite is less than 0.05 MPa (Arifin & Schanz, 2009). Regarding the effect of the vertical pressures on the difference between total suction and the applied suction will be discussed more in chapter 8. In addition, there might be a certain delay in reaching the hydraulic equilibrium when the swelling pressure/strain reached the steady state (Dueck, 2004). This certain delay in the hydraulic equilibrium might also induce the measured total suction greater than the applied suction.

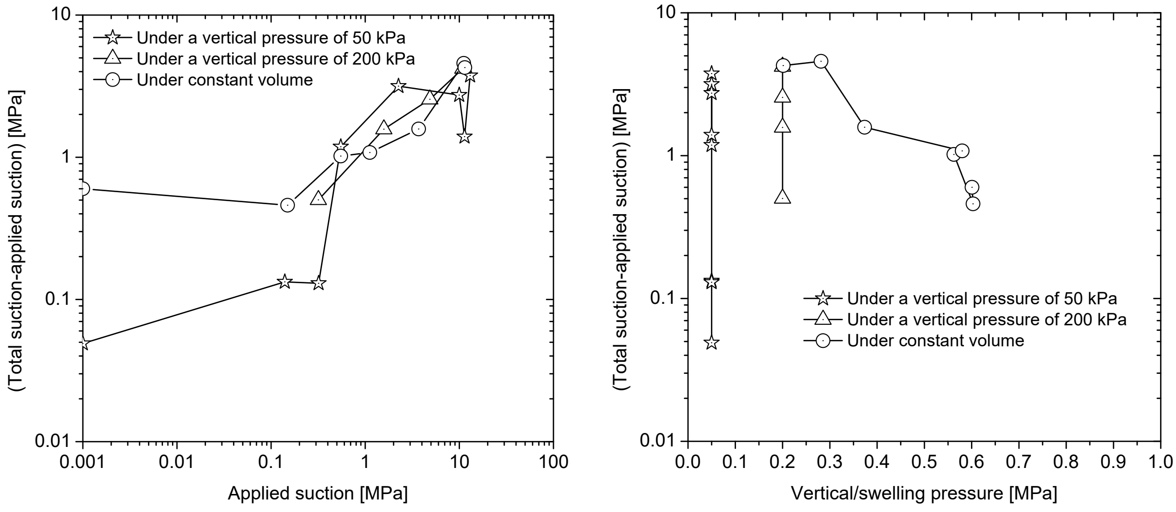

(a) (b)

Figure 4.13: Effect of (a) applied suction and (b) vertical pressure on the difference between the total suction of bentonite-sand mixtures and the applied suction

4.2.6 Total suction-water content curve

Figure 4.14 shows the measured total suction-water content curves determined under the different confinement conditions, i.e. unconfined condition, vertical pressures of 2.5, 50, 200 kPa and constant volume. Unlike the applied suction-water content curve presented in Figure 4.3(a), the total suction-water content curves were almost unique and thus, were independent of the confinement conditions. The unique total suction-water content curve could be characterized by the following equation:

$$w_{\mathrm{BS}} = -2.858\ln(\psi_{\mathrm{t}}) + 19.271 \tag{4.8}$$

where w_{BS} is the water content (%) of bentonite-sand mixtures and ψ_{t} is the measured total suction (MPa).

4.3 Summary

The influence of confinement conditions on the wetting WRCs of bentonite-sand mixtures and the hysteresis loop of the wetting-drying WRCs of bentonite-sand mixtures was experimentally examined in this chapter. The suction controlled wetting tests under

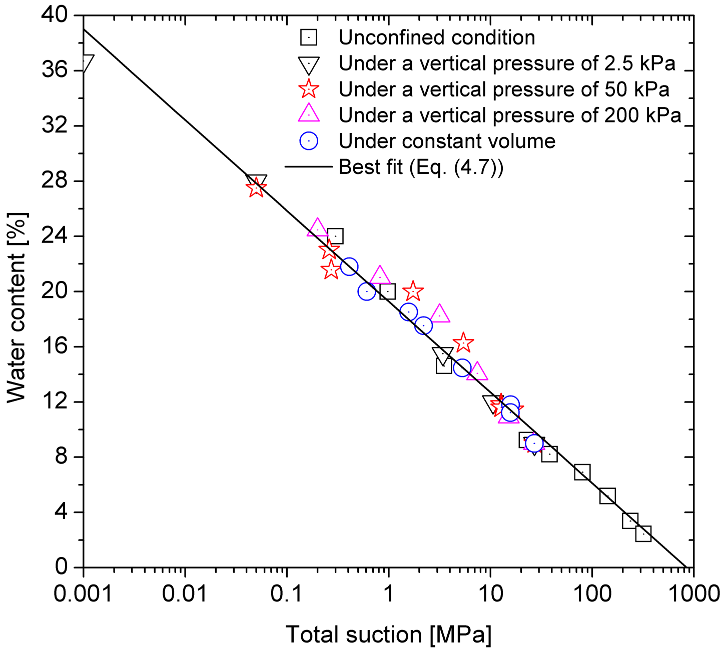

Figure 4.14: Wetting WRCs of bentonite-sand mixtures in the case of measured total suction-water content curve under different confinement conditions

different confinement conditions were carried out on the compacted bentonite-sand mixtures for determining wetting WRCs. The suction controlled wetting-drying tests under unconfined and constant volume conditions were performed on the bentonite-sand mixtures for determining wetting-drying WRCs. The variation of total, microstructural and macrostructural void ratios with suction were derived from WRCs. In addition, the total suctions after wetting tests were measured for comparing with the applied suction. The following conclusions were drawn in this chapter.

1. Swelling strains and swelling pressures upon suction controlled wetting monotonically increased with elapsed time and the equilibrium swelling strains and swelling pressures almost increased with decreasing the applied suctions. These experimental results are related to the initial compacted state and the stress path followed by compacted bentonite-sand mixtures upon wetting.

2. The confinement conditions were found to significantly affect the wetting WRCs over suction range below 3 MPa and the air-expulsion values. The air-expulsion value was the minimum (0.24-0.46 MPa) for the unconfined condition, but the maximum (3.68 MPa) for constant volume condition. In the case of the vertical pressures of 2.5 and 50 kPa conditions, the air-expulsion values were similar and about 1.3 MPa. In the case of the

vertical pressure of 200 kPa condition, the air-expulsion value was an intermediate value, 1.90 MPa. The effect of confinement conditions on wetting WRCs and air-expulsion values are due to their influence on microstructural characteristics of bentonite-sand mixtures.

3. The hysteresis loop of wetting-drying WRCs was found to be affected by the confinement conditions. In the case of the unconfined condition, the hysteresis loop of wetting-drying WRCs was significant, particularly over suction range less than 30 MPa. However, the hysteresis loop of wetting-drying WRCs was insignificant in the case of the constant volume condition. The air-entry value in the case of constant volume condition was considerably greater than that in the case of the unconfined condition.

4. According to the method proposed by Navarro et al. (2017b) and reasonable modification, the variation of total, microstructural and macrostructural void ratios with suction were successfully derived from the WRCs determined under different confinement conditions. The variation of total, microstructural and macrostructural void ratios with suction under different confinement conditions could qualitatively explain the effect of the confinement conditions on WRCs.

5. The measured total soil suction was found to be considerably greater than the applied suction. The difference in the measured total suction and the applied suction is mainly due to the confinement conditions or the vertical pressures. The wetting WRCs in terms of measured total suction-water content curves were almost unique and independent of the confinement conditions.

6. Since WRCs depend on the confinement conditions, water retention model should be developed to considerate their effect. The present study provides the experimental database for developing and calibrating water retention models for bentonite-based materials used in the geological repository for the disposal of radioactive wastes.

5 Swelling pressure-suction relationship

5.1 Introduction

The hydraulic boundary condition (suction and water phase) in the geological repository would affect the swelling capacity of compacted bentonite-sand mixtures used as the backfill and sealing materials. Though some researchers have studied the effect of suction on the swelling pressure of compacted bentonite-based materials (Kassiff & Shalom, 1971; Lloret et al., 2003; Agus et al., 2013; Wang et al., 2013b, 2014b; Yigzaw et al., 2016; Tripathy et al., 2017), few researchers have investigated the effect of water phase on the swelling pressure of compacted bentonite-sand mixtures. Moreover, determining the swelling pressure-suction relationship of compacted bentonite-sand mixtures with the OT and the VET is necessary for advancing the understanding of the insignificant development of swelling pressure within the suction range of 23 to 2 MPa (Agus et al., 2013). Since the WRCs define the relationship between the applied suction and either the water content or the degree of saturation, a linkage between the swelling pressure-suction relationship and WRCs is expected. However, the linkage between the swelling pressure-suction relationship and WRCs has not been explored yet.

The main objective of this chapter is to examine the effect of suction and water phase on the swelling pressure by performing two multi-step swelling pressure tests with the OT and the VET to control suction, respectively, on bentonite-sand mixtures. The experimental technique and procedure are shown in section 3.3.3. In this chapter, section 5.2.1 presents the effect of sample height and suction decrease path on the evolution of swelling pressures. Section 5.2.2 presents the influence of sample height, water phase and compaction dry density on swelling pressure-suction relationship. Section 5.2.3 presents an empirical method for obtaining swelling pressure-suction relationship from the wetting WRCs under constant volume condition. Section 5.2.4 shows the results of total suction measurements of saturated bentonite-sand mixtures after swelling pressure tests. Section 5.3 presents concluding remarks.

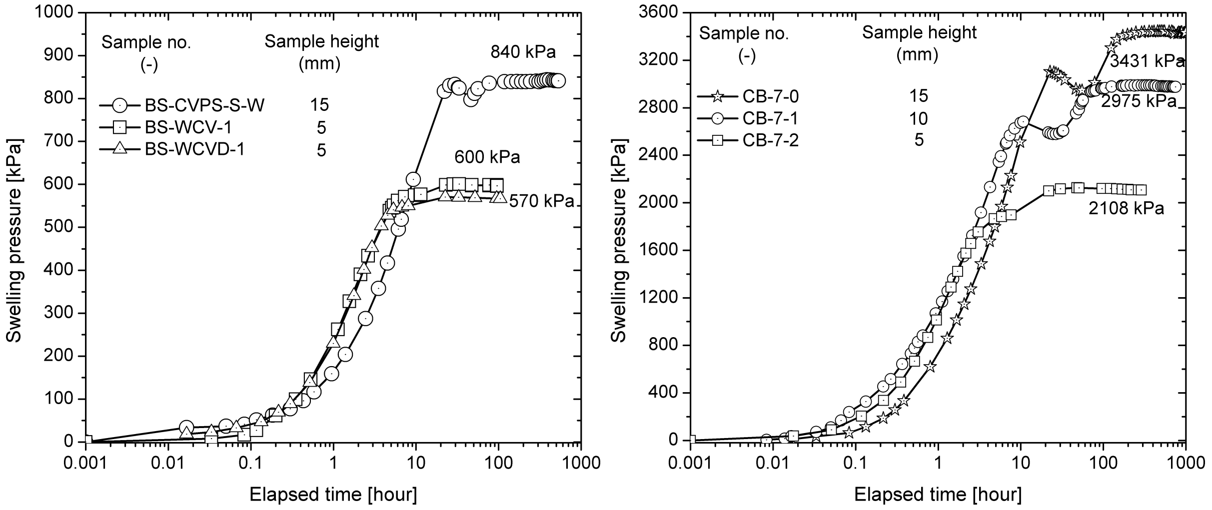

(a) (b)

Figure 5.1: Influence of sample height on evolution of swelling pressure of compacted (a) bentonite-sand mixtures and (b) bentonite saturated with deionized water

5.2 Results and discussion

5.2.1 Evolution of swellling pressures

5.2.1.1 Effect of sample height on evolution of swellling pressures

Influence of sample height on evolution of swelling pressure of (a) bentonite-sand mixtures and (b) bentonite saturated with deionized water is shown in Figures 5.1. Swelling pressure equilibrium time and equilibrium swelling pressure increased with sample height.

For the hydration of unsaturated compacted bentonite-sand mixtures with liquid water, the time required to reach the equilibrium swelling pressure depends upon the thickness of the samples. The greater the thickness of the sample is, the longer the fluid flow path (Mitchell & Soga, 2005). Therefore, the time required to reach equilibrium swelling pressure increases with the sample thickness or height.

The observed increase in the equilibrium swelling pressure with the sample thickness or height agrees with earlier findings reported by El-Sohby et al. (1989) and Jayalath et al. (2016). Increasing sample height while maintaining the same surface area (the same diameter) would allow a sample to expand more along the vertical direction of the sample (Jayalath et al., 2016). Consequently, the equilibrium swelling pressure increases with sample height.

5.2.1.2 Effect of suction decrease path on the evolution of swellling pressures

As mentioned in section 3.3.3, samples BS-CVPS-S-W, BS-CVPS-M-OT and BS-CVPS-M-VET with the same initial compaction conditions were saturated following three different suction decrease path. Sample BS-CVPS-S-W in constant volume condition was directly saturated with liquid water. However, samples BS-CVPS-M-OT and BS-CVPS-M-VET in constant volume condition were gradually saturated under suction controlled condition. The OT and the VET were used to decrease the suction of samples BS-CVPS-M-OT and BS-CVPS-M-VET, respectively.

According to the evolution of the swelling pressure for sample BS-CVPS-S-W shown in Figure 5.1 (a), its swelling pressure development followed a pattern of increase, decrease, increase and stabilization. When sample BS-CVPS-S-W was in contact with liquid water, its swelling pressure increased almost immediately and quickly reached a peak of 833 kPa (about 1 day). Subsequently, the swelling pressure dropped to 798 kPa, then increased and finally reached the stable value of 845 kPa. The time when the swelling pressure reached equilibrium was found be about 14 days.

The evolution of the swelling pressure for sample BS-CVPS-M-OT gradually saturated with liquid water by decreasing the applied suction with OT is shown in Figure 5.2. Swelling pressure development pattern and swelling pressure equilibrium time was affected by the applied suction. When the applied suction was kept at 13.06 MPa, the swelling pressure gradually increased to a peak of 317 kPa, then slightly decreased and finally reached an equilibrium value of 293 kPa. Time for obtaining this equilibrium swelling pressure was found to be equal to about 14 days. When the applied suction was kept at 4.78 MPa, the swelling pressure monotonically increased and then reached a stable value of 723 kPa. In this case, the swelling pressure equilibrium time was equal to about 22 days. While the applied suction was maintained at 1.02 MPa, the swelling pressure monotonically increased and reached the equilibrium value of 861 kPa. Time for obtaining this equilibrium swelling pressure was found to be about 14 days. While the applied suction was maintained at 0.55 MPa, the swelling pressure fast increased to a peak of 887 kPa, then decreased slightly and finally reached the stable value of 869 kPa. In the case of applied suction of 0.55 MPa, the swelling pressure equilibrium time was equal to about 7 days. When the applied suction was kept at 0.15 MPa, the swelling pressure fast increased to 884 kPa, then decreased slightly and finally reached the equilibrium value of 864 kPa. In this case, the swelling pressure equilibrium time was found to be equal to about 10 days. While sample BS-CVPS-M-OT was finally flooded by liquid water (the applied suction of 0.001 MPa), the swelling pressure quickly increased to 876 kPa, then dropped slightly and finally reached the equilibrium value of 859 kPa. Time for obtaining this equilibrium swelling pressure of 859 kPa was found to be equal to about 10 days.

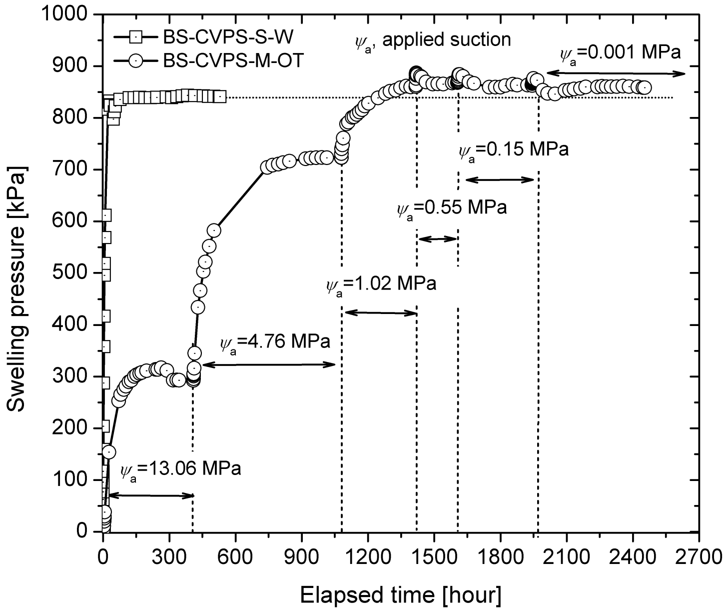

Figure 5.2: Evolution of swelling pressure of compacted bentonite-sand mixtures for sample BS-CVPS-M-OT gradually saturated with liquid water by decreasing the applied suction with osmotic technique

The evolution of the swelling pressure and the water content for sample BS-CVPS-M-VET gradually hydrated with water vapour and finally saturated with liquid water is presented in Figure 5.3. The swelling pressure development pattern was also affected by the applied suction when water vapour was used to hydrate the sample. In addition, swelling pressure equilibrium and water content equilibrium were quite time-consuming. When the applied suction was kept at 9.5 MPa, the swelling pressure gradually increased to a peak of 81 kPa, then slightly decreased, again increased and finally reached an equilibrium value of 134 kPa. The time when swelling pressure and water content reached equilibrium time was found be upto 260 days. When the applied suction was kept at 3.4 MPa, the swelling pressure monotonically increased and then slowly reached a stable value of 660 kPa. The time when swelling pressure and water content reached equilibrium was found be upto 386 days. While the sample BS-CVPS-M-VET was flooded by liquid water (the applied suction of 0.001 MPa), the swelling pressure quickly increased to 908 kPa, then dropped slightly and finally reached the equilibrium value of 880 kPa. In this case, the swelling pressure equilibrium time was about 10 days.

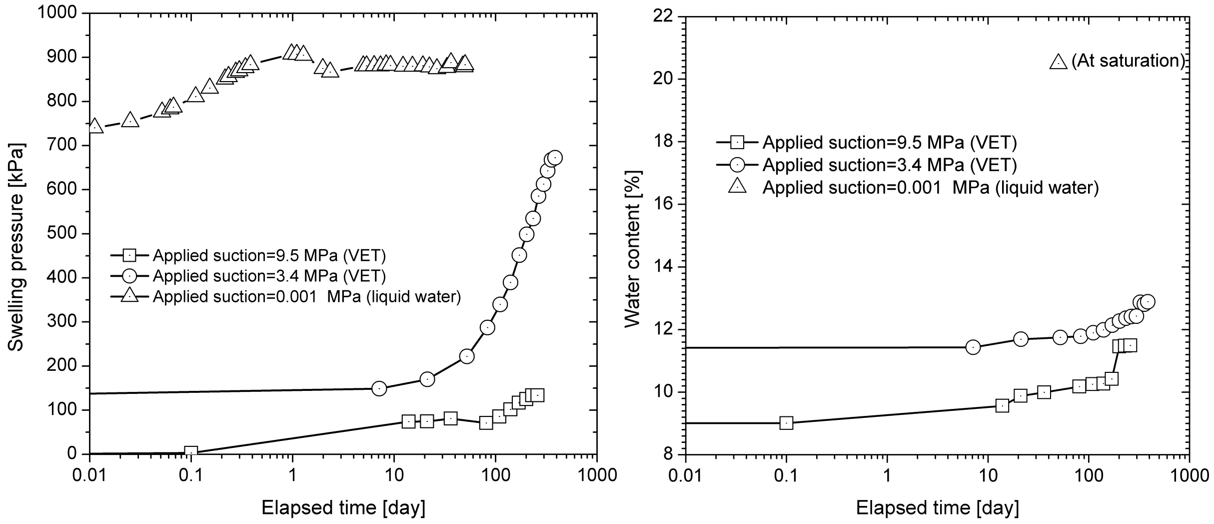

(a) (b)

Figure 5.3: Evolution of (a) the swelling pressure and (b) the water content for sample BS-CVPS-M-VET gradually hydrated with water vapour and finally saturated with liquid water

A comparison of the swelling pressure development in samples BS-CVPS-S-W, BS-CVPS-M-OT and BS-CVPS-M-VET indicated that although the swelling pressure development pattern was affected by the applied suction, the global swelling pressure development for each sample followed the pattern of increase, decrease, increase and stabilization. This swelling pressure development pattern is similar to those reported by many researchers e.g. Pusch (1982); Komine & Ogata (1994); Agus & Schanz (2005*b*); Imbert & Villar (2006); Schanz & Tripathy (2009); Yigzaw et al. (2016) on compacted bentonite-based materials. For this swelling pressure development pattern, the decrease in swelling pressure results from a collapse of the macro-structure on suction decrease. A further increase in the swelling pressure is due to the redistribution of water toward the microstructure.

The comparison of the swelling pressures at saturation for samples BS-CVPS-S-W, BS-CVPS-M-OT and BS-CVPS-M-VET showed that the swelling pressures at saturation were almost equal in quantity (i.e. 845 kPa for sample BS-CVPS-S-W, 859 kPa for sample BS-CVPS-M-OT and 880 kPa for sample BS-CVPS-M-VET). The almost constant swelling pressures at saturation are in agreement with the experimental results reported by Wang et al. (2014b) on a compacted bentonite-based material. However, (Yigzaw et al., 2016) indicated that for compacted bentonites, the direct water-flooding tests gave slightly higher swelling pressure values than progressive wetting under suction control tests.

5.2.2 Changes in swelling pressure with decreasing suction

5.2.2.1 Effect of sample height on swelling pressure-suction relationship

The effect of compacted bentonite-sand mixtures sample height on variation of swelling pressure with decreasing the applied suction is given in Figure 5.4. The experimental data for the height of 15 mm were from the constant volume swelling pressure tests on samples BS-CVPS-S-W and BS-CVPS-M-OT. However, the experimental data for the height of 5 mm were from the water retention measurement performed under constant volume condition on samples BS-WCV-1 to BS-WCV-7 (see section 4.2.1).

According to Figure 5.4, the swelling pressure values of compacted bentonite-sand mixtures upon wetting was dependent not only on the magnitude of applied suction but also on the sample height. The swelling pressure monotonically increased with decreasing the applied suction, which was independent of the sample height. For a given applied suction, the swelling pressures obtained from the samples with a height of 15 mm were greater than those obtained from the samples with with a height of 5 mm. The explanation for the effect of sample height on the magnitude of swelling pressure is presented in section 5.2.1.1.

The monotonic increase in swelling pressure with decreasing the applied suction is consistent with the findings reported by Kassiff & Shalom (1971); Agus et al. (2013); Wang et al. (2013b, 2014b); Tripathy et al. (2017). However, Lloret et al. (2003) and (Yigzaw et al., 2016) found that compacted bentonites exhibit not only expansion but also collapse upon gradually wetting. The behaviour of expansive clays upon gradually wetting depends on the initial compaction conditions (Gens & Alonso, 1992). When the initial stress state of an expansive clay is far from the loading-collapse (LC) curves, the expansive clay under constant volume condition exhibits the monotonic swelling upon wetting. When the initial stress state of an expansive clay is close to the LC curves, the expansive clay under constant volume condition exhibits the swelling upon wetting prior to reaching the LC curves. Once the LC curve is reached, the expansive clay under constant volume condition exhibits the collapse upon wetting. The collapse compresses the inter-aggregate pore and results in a movement of the LC curve to the right. Because of the movement of the LC curve to the right, further wetting under constant volume condition induces the expansive clay swelling again.

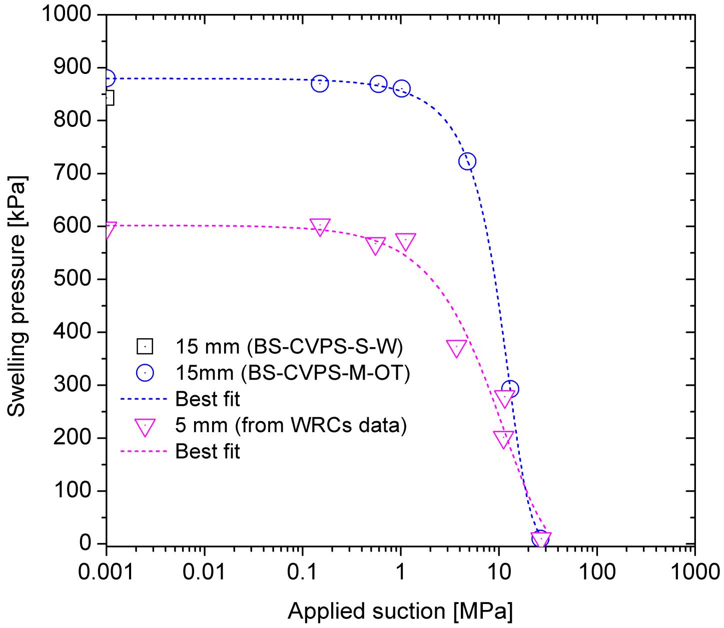

Figure 5.4: Dependence of changes in swelling pressure of compacted bentonite-sand mixtures with decreasing the applied suction on sample height

5.2.2.2 Effect of water phase during hydration on swelling pressure

Variation of swelling pressure with decreasing the applied suction for samples BS-CVPS-S-W, BS-CVPS-M-OT and BS-CVPS-M-VET is shown in Figure 5.5(a). The wetting WRCs determined under constant volume condition are presented in Figure 5.5(b). In Figure 5.5(b), the suction-water content curve with triangle corresponded to the experimental data of the sample BS-CVPS-M-VET and thus they were determined with the VET. The suction-water content curve with cycle corresponds to the experimental data from chapter 4 and they were determined with the OT.

According to intensification of swelling pressure with decreasing the applied suction, three zones titled crystalline-osmotic swelling zone, osmotic swelling zone and capillary zone could be distinguished on the applied suction-swelling pressure curves and applied suction-water content curves. The swelling pressure increase was found to be more intense within the suction range of 27 (initial as-compacted suction) to 3 MPa (the delimiting suction, see section 4.2). Saiyouri et al. (2000, 2004) stated tat for the hydration of compacted Ca-rich bentonite, the full development of crystalline swelling arises at a suction of 3 MPa, whereas osmotic swelling arises at a suction of 26 MPa. Therefore, the swelling pressure within suction range of 27 to 3 MPa was due to crystalline and osmotic swellings. Because the increase in swelling pressure with respective to a decrease in suction dissipated with decreasing the applied suction from 3 to 0.1 MPa, the swelling pressure within this suction range was due to osmotic swelling. Since the swelling pressure remained unchanged but the water content increased slightly with decreasing the applied suction from 0.1 to 0.001 MPa, the water content increase within this suction range was due to capillary effect. The volume of inter-aggregate pores decreases but might not dissipate as the compacted bentonite-based materials are gradually saturated (Cui et al., 2002; Agus & Schanz, 2005*b*; Romero et al., 2011; Manca et al., 2015). The saturation of inter-aggregate pores was dominated by capillary forces (Or & Tuller, 1999) and not expected to contribute to any swelling.

According to Figure 5.5, in crystalline-osmotic swelling zone, water phase affected the swelling pressure and the water content of compacted bentonite-sand mixtures. Within the crystalline-osmotic swelling zone, the swelling pressures and the water content caused by the hydration with liquid water were greater than those caused by the hydration with water vapour. Similar experimental results with respect to swelling pressure were also reported by Cuisinier & Masrouri (2005) on compacted bentonite-silt mixtures and Yigzaw et al. (2016) on compacted bentonites. The effect of water phase on the swelling pressure and the water content of compacted bentonite-sand mixtures is related to the swelling mechanisms. In the crystalline-osmotic swelling zone, the osmotic swelling may not develop when the compacted bentonite-sand mixtures is hydrated with water vapour. However, both crystalline swelling and osmotic swelling can develop in the crystalline-osmotic swelling zone when the compacted bentonite-sand mixtures is hydrated with liquid water. Therefore, in crystalline-osmotic swelling zone, the compacted bentonite-sand mixtures can exhibit more swelling and hold more water when the compacted bentonite-sand mixtures is hydrated with liquid water.

5.2.2.3 Swelling pressure-suction relationship at two different dry densities

In addition to this study, Agus et al. (2013) also investigated the variation of swelling pressure of compacted Calcigel bentonite-sand mixtures with gradually decreasing the applied suction. A comparison of variation of swelling pressure with decreasing the applied suction in this study and that of Agus et al. (2013) is shown in Figure 5.6. Calcigel bentonite used in their study had a similar material properties to that used in this study. In their study, two compacted Calcigel bentonite-sand mixtures samples with the dry density of 2.0 Mg/m^3 and water content of 9.1% was wetted under constant volume conditions. One sample was gradually wetted by decreasing suction in a stepwise manner from the initial value of 23 MPa to the value of 2 MPa using the VET. The other sample

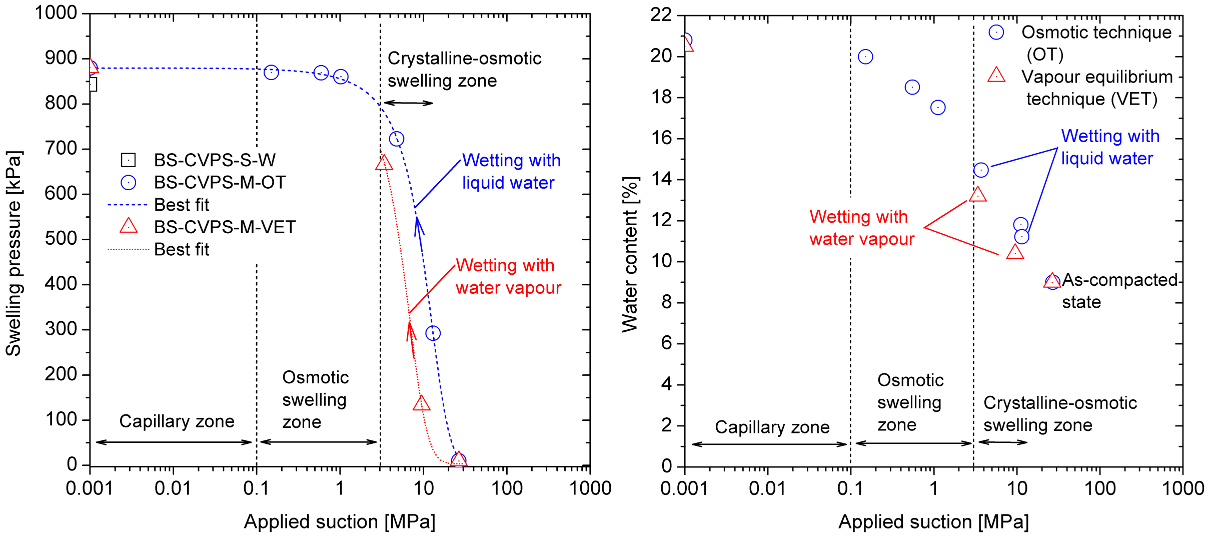

(a) (b)

Figure 5.5: Effect of water phase on changes in (a) swelling pressure and (b) water content of compacted bentonite-sand mixtures with decreasing the applied suction

was gradually saturated by decreasing suction in a stepwise manner from the initial value of 23 MPa to the value of 0.001 MPa using the ATT.

They found that compacted samples did not exhibit any collapse upon wetting and exhibited maximum swelling pressures at zero-equilibrium suction (Figure 5.6). This result is consistent with the experimental result found in the presented study. In addition, they also found that the increase in swelling pressure in the suction range from 23 to 2 MPa was insignificant, whereas the increase in swelling pressure in the suction range from 2 to 0.001 MPa was significant (Figure 5.6). The former contradicts the experimental result found in this study. Agus et al. (2013) stated that two reasons caused the insignificant development of swelling pressure within suction range of 23 to 2 MPa. The microstructural swelling was possibly compensated to a great extent collapse of macro-structure, leading to only very small magnitudes of swelling pressure. Moreover, inefficiency of the VET to apply desired suction may be also held responsible for insignificant increase in the swelling pressure.

The comparison of swelling pressure-suction relationships between two dry densities (Figure 5.6) indicates that the insignificant development of swelling pressure within suction range of 23 to 2 MPa reported by Agus et al. (2013) was due to inefficiency of the VET to apply desired suction. Since the compaction dry density of the samples used in this study was lower than that used in the study of Agus et al. (2013), the volume of macrostruc-

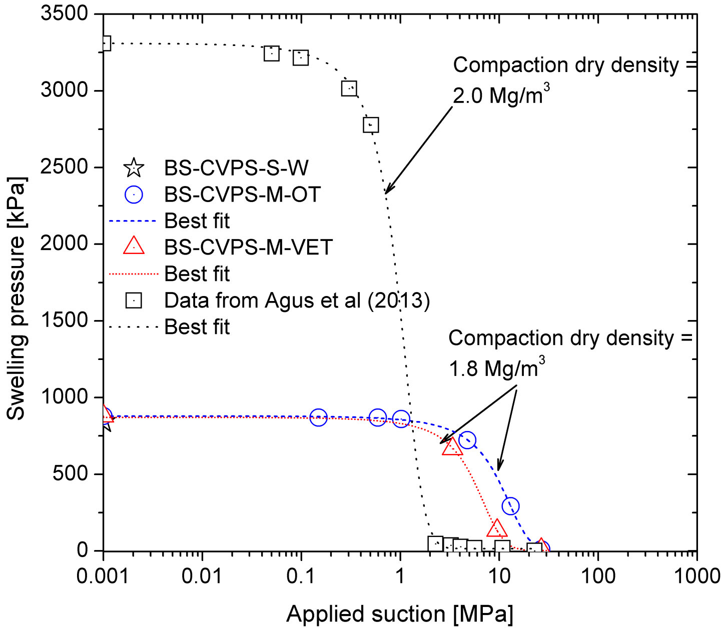

Figure 5.6: Comparison of changes in swelling pressure of compacted bentonite-sand (50/50) mixtures with decreasing the applied suction at two different dry densities

tural pore of the samples used in this study was greater than that used by Agus et al. (2013). If the microstructural swelling was really compensated to a great extent collapse of macro-structure, the significant development of swelling pressure within suction range of 27 to 3 MPa should not be observed in the present study. Thus, the inefficiency of the VET to apply desired suction induced the water equilibrium being not accomplished and further the insignificant development of swelling pressure within suction range of 23 to 2 MPa in the study of Agus et al. (2013).

5.2.3 Linkage between wetting WRCs and swelling pressure-suction relationhsiop

This section presents an empirical method for determining swelling pressure-suction relationship from the wetting WRCs (i.e. suction-water content curve and suction-degree of saturation curve) determined under constant volume condition. This empirical method is proposed based on the findings that in constant volume condition, water content, degree of saturation and swelling pressure of compacted bentonite-sand mixtures monotonically increases with gradually decreasing the applied suction.

5.2.3.1 Normalized water content/degree of saturation-suction relathionship

The applied suction against water content, degree of saturation and swelling pressure plots from wetting WRCs under constant volume condition (see Figures 4.2(a) and 4.3 in chapter 4) are shown in Figure 5.7. The water content (w), degree of saturation (S) and swelling pressure (P_{s}) were normalized according to Eq.(5.1), Eq.(5.2) and Eq.(5.3), respectively. In Eq.(5.1), w_{n}, w_{i} and w_{sat} are the normalized water content, initial water content and saturated water content, respectively. Similarly, S_{n} and S_{i} in Eq.(5.2) represent the normalized degree of saturation and initial degree of saturation, respectively. In Eq.(5.3), P_{sn} and P_{ssat} are the normalized swelling pressure and saturated swelling pressure, respectively.

$$w_{\mathrm{n}} = \frac{w - w_{\mathrm{i}}}{w_{\mathrm{sat}} - w_{\mathrm{i}}} \tag{5.1}$$

$$S_{\mathrm{n}} = \frac{S - S_{\mathrm{i}}}{1 - S_{\mathrm{i}}} \tag{5.2}$$

$$P_{\mathrm{sn}} = \frac{P_{\mathrm{s}}}{P_{\mathrm{ssat}}} \tag{5.3}$$

The applied suction against the normalized water content, degree of saturation and swelling pressure are presented in Figure 5.7(d). In Figure 5.7(d), the best fit curves were obtained using Eq.(5.4). In Eq.(5.4), y is normalized parameter corresponding to w_{n}, S_{n} or P_{sn}; a, b, c and d are fit parameters; ψ_{a} represents the applied suction. Fit parameters to characterise the applied suction against normalized water content, degree of saturation and swelling pressure plots are shown in Table 5.1.

$$y = \frac{a - b}{1 + e^{(\psi_{\mathrm{a}} - c)/d}} + b \tag{5.4}$$

As can be seen from Figure 5.7(d), the applied suction against the normalized water content, degree of saturation and swelling pressure plots distributed in a very narrow area. In addition, all the normalized parameters increased with decreasing the applied suction, which was similar to the variation of swelling pressure with decreasing the applied suction. The results above made it possible to predict swelling pressure-suction relationship according to the wetting WRCs determined under constant volume condition.

5.2.3.2 Swelling pressure-suction relationship obtained from wetting WRCs

For a given applied suction (ψ_{a}), the swelling pressure (P_{s}) was derived from Eq.(5.5). In Eq.(5.5), a saturated swelling pressure (P_{ssat}) of 845 kPa was used and corresponded

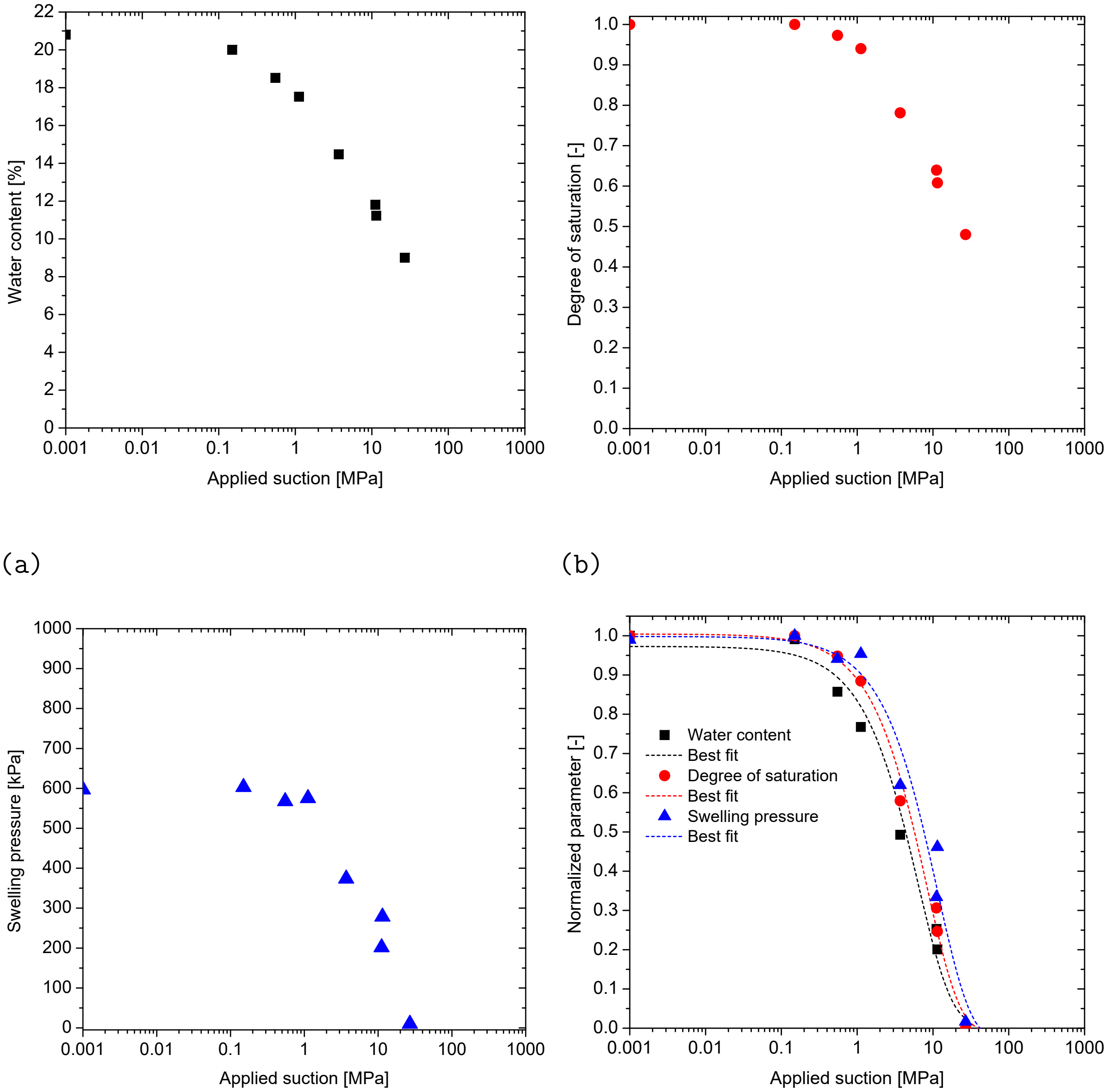

(a) (b)

(c) (d)

Figure 5.7: The applied suction against (a) water content (b) degree of saturation (c) swelling pressure and (d) normalized water content/degree of saturation/ swelling pressure plots for the compacted bentonite-sand mixtures wetted under constant volume condition

Table 5.1: Best-fit parameters to characterise the applied suction against normalized water content/degree of saturation/swelling pressure plots

Normalized parameter	Fitting parameter				Fit statistics
y	a	b	c	d	R^2
(-)	(-)	(-)	(MPa)	(MPa)	(-)
Normalized water content (w_n)	7659.4	0.0098	-57.9	6.45	0.99
Normalized degree of saturation (S_n)	869.3	-0.0090	-55.8	8.26	1.00
Normalized swelling pressure (P_{sn})	185.6	-0.0269	-59.3	11.43	0.99

to the saturated swelling pressure of the sample BS-CVPS-S-W. The parameters a, b, c and d were determined according to the normalized parameter (y) shown in Table 5.1.

$$P_s = P_{ssat} y = P_{ssat}[\frac{a-b}{1+e^{(\psi_a - c)/d}} + b] \tag{5.5}$$

Figure 5.8 presents the comparison of swelling pressure-suction relationships determined from the constant volume pressure tests (Figure 5.2) and derived from wetting WRCs determined under constant volume condition. The comparison indicated that the applied suction-swelling pressure curves derived from the constant volume wetting WRCs were quite similar to that measured, particularly the curves derived from degree of saturation and swelling pressure. Therefore, the method for deriving the swelling pressure-suction relationship from constant volume wetting WRCs was satisfactory according to Figure 5.8.

The procedure for determining swelling pressure-suction relationship based on wetting WRCs under constant volume condition is summarized in the following: several replicable samples with small size (e.g. a height of 5 mm) under constant volume condition are wetted at different applied suctions, respectively; after equilibrium is reached, the water content of each sample are measured to generate the applied suction against normalized water content and degree of saturation plots; a sample with the normal sample size (e.g. a height of 15 mm) and the same initial conditions as the replicable samples used for determining wetting WRCs is directly saturated with liquid water under constant volume condition to obtain the saturated swelling pressure; swelling pressure-suction relationship is determined according to the saturated swelling pressure and the applied suction against either normalized water content or normalized degree of saturation plots.

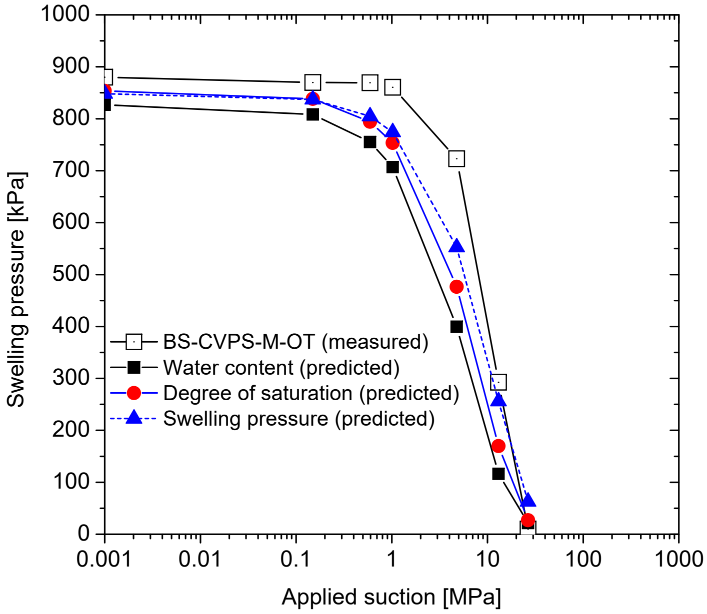

Figure 5.8: Comparison of swelling pressure-suction relationships determined from the multi-step swelling pressure test and derived from wetting WRCs under constant volume condition for compacted bentonite-sand mixtures

To further confirm the proposed method for deriving swelling pressure-suction relationship from wetting WRCs determined under constant volume condition, the experimental data reported in literature (i.e. Wang et al. (2013b); Tripathy et al. (2017)) were tested following the procedure above. For the study of Wang et al. (2013b), both swelling pressure-suction relationship and wetting WRCs under constant volume condition were measured on a compacted MX80 bentonite/sand mixture with a dry density of 1.67 Mg/m^3. In the study of Tripathy et al. (2017), both swelling pressure-suction relationship and wetting WRCs under constant volume condition were measured on a compacted MX80 bentonite with a dry density of 1.47 and 1.60 Mg/m^3.

A comparison of swelling pressure-suction relationships derived from the constant volume wetting WRCs and multi-step swelling pressure tests are presented in Figure 5.9 for the study of Wang et al. (2013b) and in Figure 5.10 for the study of Tripathy et al. (2017). The comparison indicated that the swelling pressure-suction relationships predicted can capture the main characteristics of those determined by multi-step swelling pressure tests. Moreover, for a given applied suction, the magnitude of swelling pressure predicted was similar to that measured.

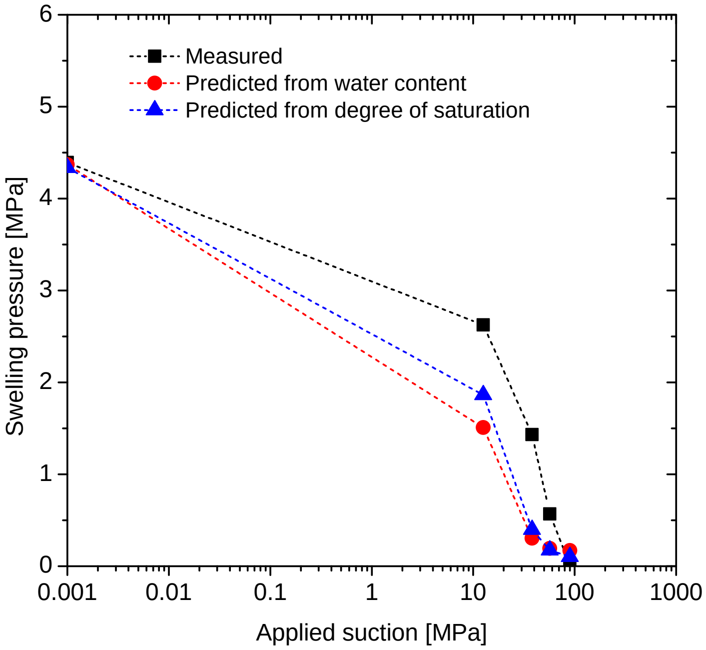

Figure 5.9: Comparison of swelling pressure-suction relationships determined from the multi-step swelling pressure test and derived from wetting WRCs under constant volume condition for compacted MX80 bentonite-sand mixtures (measuring data from Wang et al. (2013b))

5.2.4 Total suction of saturated bentonite-sand mixtures after swelling pressure tests

After releasing the swelling pressure, the measured final dry density, water content, degree of saturation and total suction are presented in Table 5.2. The final dry densities were found to smaller than the initial compaction dry density (i.e. 1.8 Mg/m^3). This is mainly attributed to the expansion of the specimen after releasing the swelling pressure.

For all samples but BS-WCV-1, the final water content remained nearly constant along the depth of the sample. Since the height of sample BS-WCV-1 was only 5 mm, only the average water content was measured. The degree of saturation of all samples tested was determined based on the final water contents, the dimensions of the samples and the volume-mass relationships. The degree of saturation of all samples indicated that the samples were fully saturated at the end of the swelling pressure tests.

In addition to the final water content, the total suction values for all samples but BS-WCV-1 were also very similar along the depth of the sample. Moreover, the total suction

Table 5.2: Swelling pressure and final conditions of saturated bentonite-sand mixtures

Sample no.	Swelling pressure	Final dry density[c]	Water content	Degree of saturation	Total suction[d]	Location[e]
(-)	(MPa)	(Mg/m^3)	(%)	(%)	(MPa)	(-)
BS-WCV-1[a]	0.60	1.74	21.5	100	0.54	n/a
BS-CVPS-S-W[b]	0.84	1.76	19.7	100	1.23	Top
			19.7		0.96	Middle
			20.6		0.82	Bottom
BS-CVPS-M-OT[b]	0.88	1.76	20.7	100	1.03	Top
			21.0		0.89	Middle
			20.8		0.89	Bottom
BS-CVPS-M-VET[b]	0.85	1.76	20.2	100	1.09	Top
			20.5		0.96	Middle
			20.8		0.82	Bottom

a, sample height was 5 mm; *b*, sample height was 15 mm; *c* was determined after releasing swelling pressure; *e* was determined by chilled-mirror hygrometer; *e* repre -sents sample collection location (see section 3.3.3).

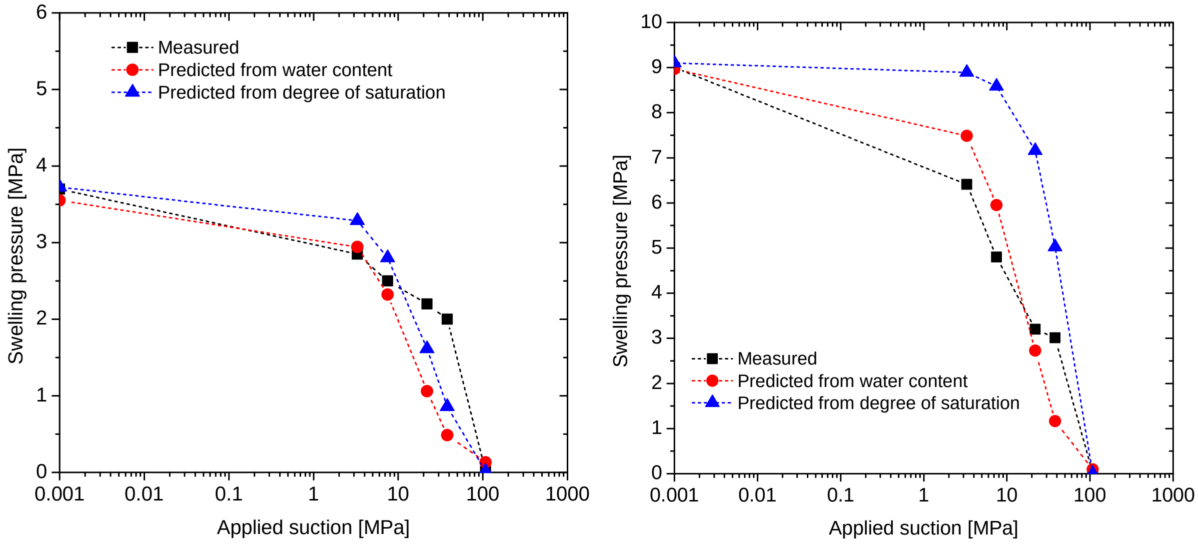

(a) (b)

Figure 5.10: Comparison of swelling pressure-suction relationships determined from the multi-step swelling pressure test and derived from wetting WRCs under constant volume condition for compacted MX80 bentonite with a density of (a) 1.47 and (b) 1.60 Mg/m^3 (data from Tripathy et al. (2017))

was found to be almost equal to the swelling pressure for any sample. The experimental results in Table 5.2 indicated that the total suction of saturated bentonite-sand mixtures was not zero but was almost equal to the swelling pressure. The detailed explanation for the measured total suction equal to the swelling pressure would be given in chapter 8.

The total suction versus water content (Table 5.2) were plotted on a plot of water content against the logarithm of the suction (Figure 5.11). According to Figure 5.11, the experimental data were almost located on the unique total suction-water content curve (Eq.(4.8)) found in chapter 4.

5.3 Summary

The main objective of this chapter is to examine the effect of suction and water phase on the swelling pressure by performing two multi-step swelling pressure tests with the OT and the VET to control suction, respectively, on compacted bentonite-sand mixtures. Moreover, one-step swelling pressure tests were also carried out on bentonite and bentonite-sand mixtures samples with different sample height. The linkage between swelling pressure-

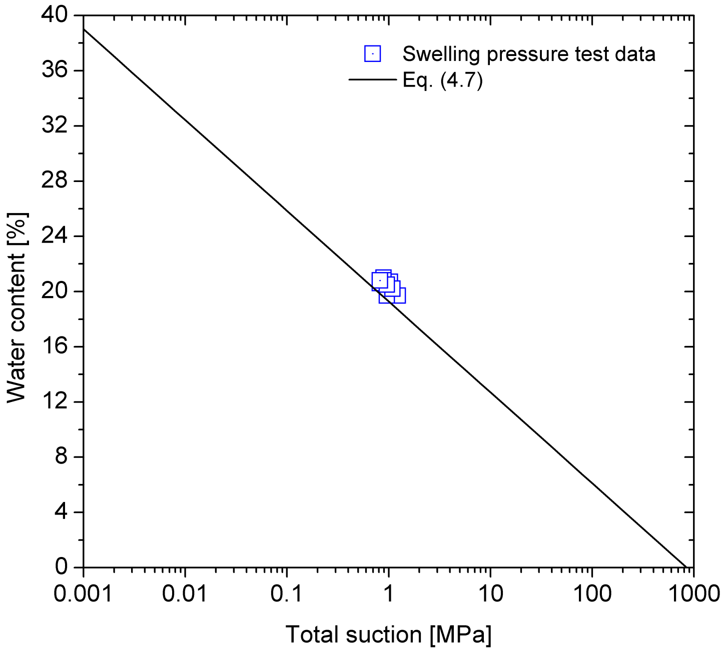

Figure 5.11: Measured total suction versus water content for saturated bentonite-sand mixtures

suction relationship and the wetting WRCs under constant volume condition was analysed based on experimental data. The following conclusions were drawn in this chapter.

1. When the compacted bentonite-based materials under constant volume condition were saturated with liquid water, the time taken for reaching swelling pressure equilibrium increased with the sample height. The increase in the time taken for reaching swelling pressure equilibrium with the sample height is due to the increase in the fluid flow path with an increase in the thickness of the sample. At saturation, the equilibrium swelling pressure was found to increase with the sample height, which agrees with the earlier findings.

2. The global swelling pressure development in compacted bentonite-sand mixtures followed the pattern of increase, decrease, increase and stabilization, regardless of suction decrease path. The decrease in swelling pressure results from a collapse of the macrostructure on the suction decrease, whereas the further increase in the swelling pressure is due to the redistribution of water toward the microstructure. Moreover, the magnitude of swelling pressure at saturation was found to be almost independent of the hydration path.

3. The swelling pressure of compacted bentonite-sand mixtures upon wetting was found to depend not only upon applied suction but also upon water phase. The swelling pressure monotonically increased with decreasing the applied suction, which was independent of the sample height and the suction decrease path. The monotonic increase in swelling pressure with decreasing the applied suction was due to the stress path followed by the samples during the wetting process far from the loading-collapse (LC) curves. Within the crystalline-osmotic swelling zone, the swelling pressures and the water content caused by the hydration with liquid water were greater than those caused by the hydration with water vapour. The effect of water phase on the swelling pressure and the water content of compacted bentonite-sand mixtures is related to the swelling mechanisms.

4. An empirical method for obtaining swelling pressure-suction relationship from the wetting WRCs under constant volume condition was proposed and validated based on the experimental data from this study and the literature. It should be noted that this method may not be appropriate for lightly compacted bentonite-based materials.

5. The measured total suctions of saturated bentonite-sand mixtures were not equal to zero but were almost equal to the swelling pressures for compaction dry density of 1.8 Mg/m^3. In addition, the measured total suction versus water content was almost located on the unique total suction-water content curve (Eq.(4.8)) found in chapter 4.

6 One-dimensional swelling-compression-rebound behaviour

6.1 Introduction

It is necessary to obtain the compressibility of compacted bentonite-based materials for calibrating constitutive models used in numerically simulating the hydraulic-mechanical behaviour of compacted bentonite-based materials. The main objective of this chapter is to determine the variation of yield stress and compression index with the applied suction for calibrating the Barcelona expansive model (BExM) used in chapter 7. The second objective of this chapter is to determine the total suction of saturated bentonite-sand mixtures after unloading for further validating the finding presented in chapter 5.

The present chapter presents the experimental results and discussion with respect to one-dimensional swelling-compression-rebound behaviour of compacted bentonite-sand mixtures. The experimental technique and procedure for one-dimensional swelling-compression-rebound tests have been shown in section 3.3.4. In this chapter, section 6.2.1 presents suction controlled swelling-compression rebound test results. Section 6.2.2 presents the one-dimensional swelling upon saturation at different constant vertical net stresses and subsequent compression-rebound experimental results. Section 6.2.3 presents a comparison of the coefficients of permeability determined from consolidation test and by permeability tests. Section 6.2.4 presents the results of the total suction and the water content measurements of saturated bentonite-sand mixtures after unloading. Section 6.3 presents concluding remarks.

6.2 Results and discussion

6.2.1 Suction controlled swelling-compression-rebound tests

The compacted bentonite-sand mixtures samples BS-SCR-1 to BS-SCR-4 (Table 3.7) had the same initial compaction conditions (dry density of 1.8 Mg/m^3 and total suction of 27 MPa). These samples were used to perform the suction controlled one-dimensional swelling-compression-rebound tests following the stress paths presented in Figure 3.14. The variation of swelling strain with time during the suction controlled one-dimensional swelling-compression-rebound tests for samples BS-SCR-1 to BS-SCR-3 is given in Figure 6.1.

According to Figure 6.1, the smaller the applied suction was, the greater the swelling strain rate was found. This was similar to the experimental results presented in Figures 4.1 chapter 4. The fastest hydration found on sample BS-SCR-1 was mainly due to the fact that sample BS-SCR-1 was saturated with liquid water, whereas samples BS-SCR-2 and BS-SCR-3 were wetted with water vapour. The diffusion of water vapour is extremely slow compared to water flow (Fredlund et al., 2012).

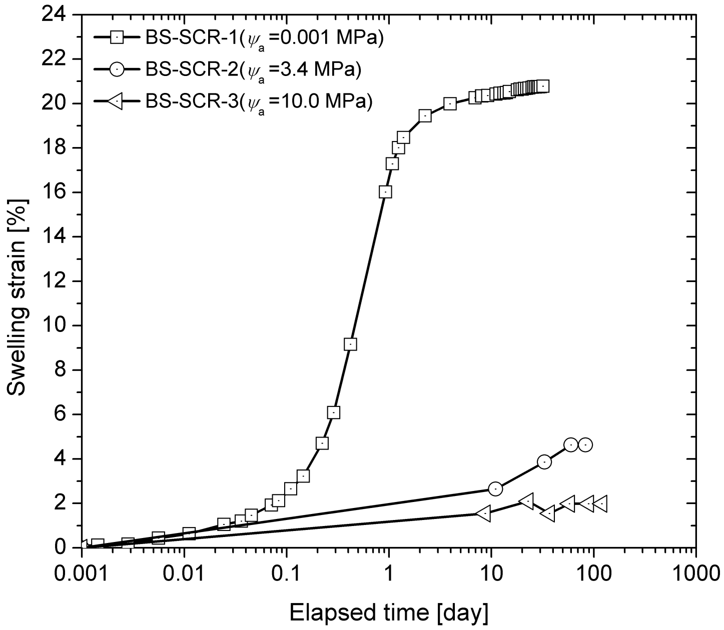

Figure 6.1: Evolution of swelling strain during the suction controlled one-dimensional swelling-compression-rebound tests on compacted bentonite-sand mixtures (the samples were hydrated under a vertical net stress of 2.5 kPa)

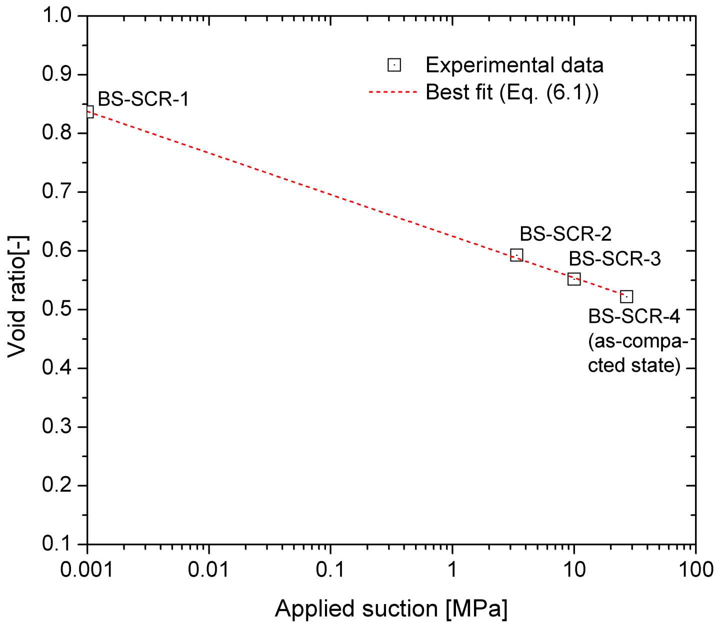

Figure 6.2: Relationship between the applied suction and final void ratio for compacted bentonite-sand mixtures hydrated under a vertical net stress of 2.5 kPa

The applied suction versus the final void ratio for samples BS-SCR-1 to BS-SCR-4 are shown on a semi-logarithmic plot (Figure 6.2). The experimental data were ideally located along a line which was characterized by the following relationship:

$$e = -0.031\ln(\psi_{\mathrm{a}}) + 0.625(R^2 = 1.0) \tag{6.1}$$

where e is the void ratio at equilibrium and ψ_{a} is the applied suction. According to Figure 6.2, the final swelling strain or void ratio at equilibrium increased with a decrease in the applied suction. The increase in the final void ratio with decreasing the applied suction is due to stress state and the stress paths followed by the samples BS-SCR-1 to BS-SCR-4 far from the loading-collapse curves in a two-dimensional (mean stress, suction) space (Gens & Alonso, 1992).

Once the swelling strains reached equilibrium, the samples BS-SCR-1 to BS-SCR-3 were subjected to suction controlled compression and rebound following the stress paths shown in Figures 4.1. The swelling-compression-rebound curves under various applied suctions are shown in Figure 6.3. This diagram shows the variations of void ration (e) with vertical net stress ($\sigma_{\mathrm{v}} - u_{\mathrm{a}}$) for a given applied suction (ψ_{a}). σ_{v} and u_{a} are vertical stress and the air pressure (equal to the atmosphere pressure), respectively.

The swelling-compression-rebound curves shown in Figure 6.3 indicated that the void ratio was as a function of the net vertical stress, applied suction and stress path. The dependency of the void ratio of compacted bentonite-sand mixtures on the net vertical stress, applied suction and stress path are consistent with the well-known fact that the volumetric behaviour of a soil depends on the net stress, suction and stress path (Alonso et al., 1990; Gens & Alonso, 1992; Fredlund & Rahardjo, 1993; Mitchell & Soga, 2005).

Prior to compression, the samples BS-SCR-1 to BS-SCR-4 exhibited significantly different the initial void ratios since the initial swelling strain upon wetting increased linearly with deceasing the applied suction (Figure 6.2). For each sample or any given applied suction, the compression curves were characterized by a linear branch with low compressibility (elastic domain) followed by a second branch with higher compressibility (plastic domain). The elastic and plastic branches of the compression curve were delimited by a yield point corresponding the yield stress or preconsolidation stress. Unlike the compression curves, the rebound curves were found to be approximately linear for a given applied suction.

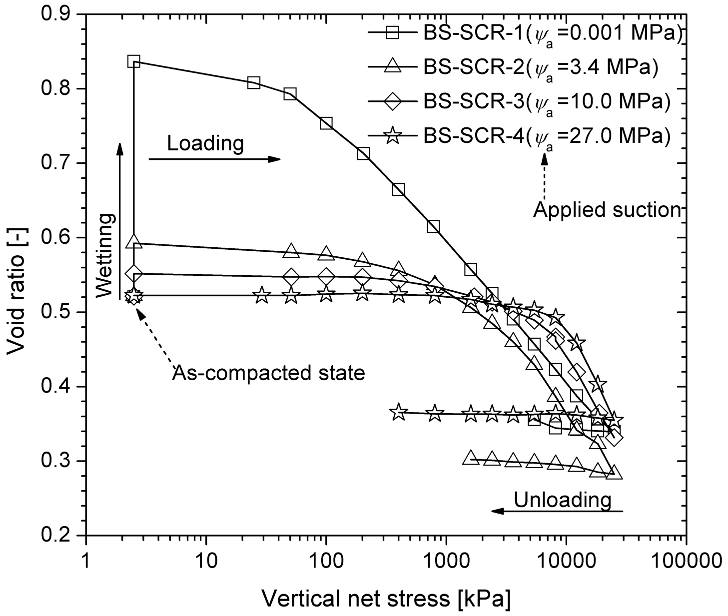

Figure 6.3: Swelling-compression-rebound curves of compacted bentonite-sand mixtures obtained under suction controlled condition

The compression-rebound curves at the constant suction of 0.001, 3.4, 10.0 and 27.0 MPa are presented in Figure 6.4 to determine the yield stress, compression index and swelling index. A clear pre and post yield response was found, defining a preconsolidation stress or yield stress which delimited elastic domain and plastic domain. The compression index

(C_c) corresponded to the slope of the plastic domain, whereas the swelling index (C_s) corresponded to the slope of the elastic domain or rebound curve. According to Figure 6.4, both the yield stress and swelling index were affected by the applied suction, whereas the compression index was affected not only by the applied suction but also by the vertical net stress.

The variation of yield stress with the applied suction is shown in Figure 6.5. In addition, the experimental data obtained by Agus (2005) on compacted bentonite-sand (50/50) mixtures with a initial compaction dry density of 2.0 Mg/m^3 are also given in this figure. It should be noted that the bentonite used in this study and that used by Agus (2005) were Calcige and had the similar mineral composition, material properties and initial water content (about 9%).

For a for given applied suction, the greater the initial compaction dry density was, the greater the yield stress was. The increase in the yield stress with the initial compaction dry density suggested that the bentonite-sand mixtures hardened with increasing the initial compaction dry density.

The increase in the yield stress with an increase in the initial compaction dry density is due to an increase in the static compaction pressure which in turn affects the pore-size distribution (PSD) of compacted bentonite-based materials (Pusch, 1980*a*; Lloret et al., 2003). Studies on the pore size distribution (PSD) of the compacted bentonite-based materials have shown double porosity structure with intra-aggregate and inter-aggregate pores (Cui et al., 2002; Lloret et al., 2003; Agus & Schanz, 2005*b*; Delage et al., 2006; Romero et al., 2011; Wang et al., 2013a; Manca et al., 2015). As the dry density increases, the inter-aggregate pore size decreases, whereas the intra-aggregate pore size remains almost constant (Lloret et al., 2003; Romero & Simms, 2008; Li & Zhang, 2009; Wang et al., 2013a; Seiphoori et al., 2014). The yield stress is controlled by the inter-aggregate pore size and increases with a decrease in the inter-aggregate pore size (Gens & Alonso, 1992). Therefore, the yield stress increases with an increase in the initial compaction dry density.

Moreover, Figure 6.5 also showed that the yield stress increased with the applied suction, indicating that suction contributes to stiffening of compacted benonite against external loading. The increase in the yield stress of bentonite-sand mixtures with the applied suction is consistent with earlier findings reported in literature on bentonite-based materials (Lloret et al., 2003; Cuisinier & Masrouri, 2005; Agus, 2005; Wang et al., 2013a). The increase in the yield stress of bentonite-sand mixtures with the applied suction can be well explained according to Barcelona basic model (Alonso et al., 1990).

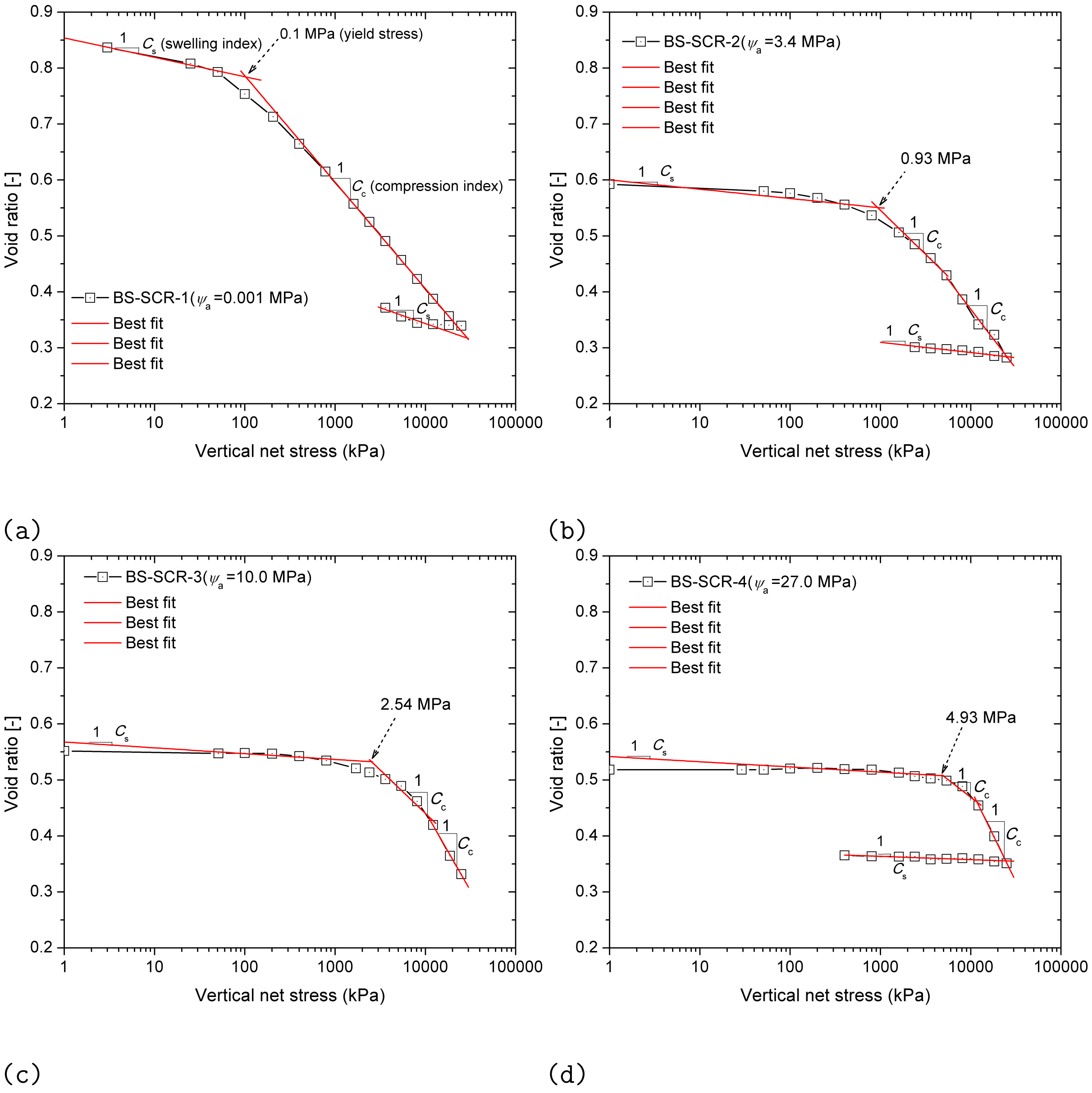

(a) (b)

(c) (d)

Figure 6.4: One-dimensional loading-unloading tests at a constant suction of (a) 0.001, (b) 3.4, (c) 10.0 and (d) 27.0 MPa on compacted bentonite-sand mixtures

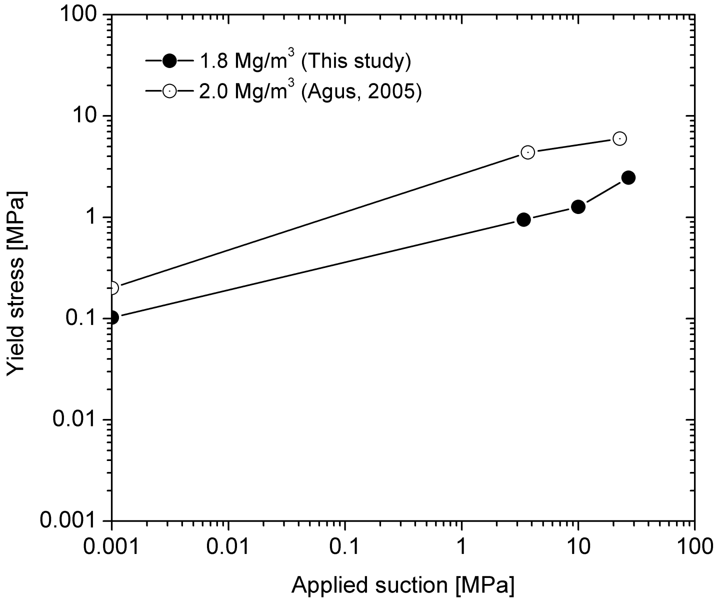

Figure 6.5: Changes in yield stress with the applied suction for compacted bentonite-sand mixtures

The changes in swelling index with the applied suction are presented in Figure 6.6(a). For each given applied suction, two values of the swelling index were determined from rebound curve and elastic loading curve, respectively. The swelling indexes decreased with an increase in the applied suction, regardless of determining the swelling index either from elastic curve or from rebound curve. The dependency of swelling index on suction indicated that the general assumption made in numerical simulation that swelling index of compacted bentonite-based materials may be not appropriate.

Moreover, the swelling index determined from the elastic loading curve was found to similar to that determined from the rebound curve, especially for the applied suction greater than 3 MPa. This suggested that at relatively high applied suction, e.g. as-compacted state, the irrecoverable volumetric strain disappeared after one cycle of loading and unloading.

Changes in compression index (C_c) with suction are presented in Figure 6.6(b). For the case of saturated condition (ψ_a=0.001 MPa), the compression index was a constant and independent of vertical net stress. However, for the case of unsaturated condition, the compression index were affected by both the vertical net stress and the applied suction. When the vertical net stress was less than 10 MPa, the compression index decreased with increasing the applied suction. When the vertical net stress was greater than 10 MPa, the compression index increased with increasing the applied suction.

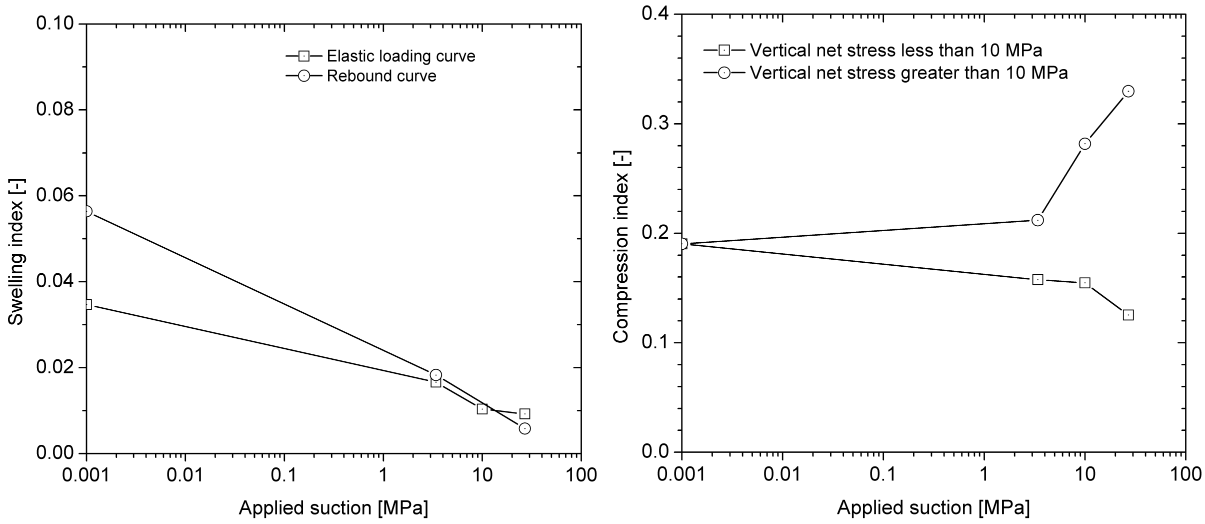

(a) (b)

Figure 6.6: Changes in (a) swelling index and (b) compression index with the applied suction for compacted bentonite-sand mixtures

The variation of compression index with suction on compacted bentonite-based material had been studied by Agus (2005); Cuisinier & Masrouri (2005); Wang et al. (2013a). Agus (2005) stated that the compression index of compacted Calcigel bentonite-sand mixtures decreased with an increase in the applied suction. However, Wang et al. (2013a) found that the change in the compression index of compacted MX80 bentonite-sand mixtures with respect to suction appeared to be non-monotonic. The compression index of compacted MX80 bentonite-sand mixtures decreased with increasing the applied suction from 0.001 to 12.6 MPa. When the applied suction was increased from 12.6 to 38 MPa, the compression index of compacted MX80 bentonite-sand mixtures increased. Cuisinier & Masrouri (2005) found that the compression index of compacted bentonite-silt mixture was not influenced significantly by the controlled suctions. Alonso et al. (1990) stated that for compacted soils, the slope of the compression lines decreased with increasing suction based on Barcelona basic model. Thus, the dependence of compression index on both applied suction and the vertical net stress can not be explained according to Barcelona basic model (Alonso et al., 1990).

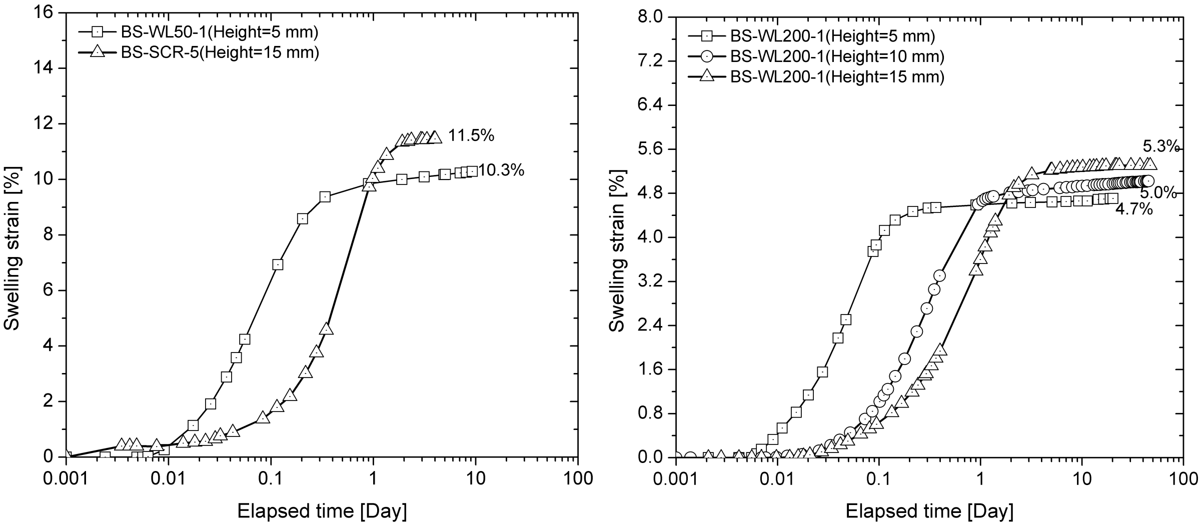

(a) (b)

Figure 6.7: Evolution of swelling strain with time for compacted bentonite-sand mixtures samples with a height of 5, 10 and 15 mm in case of saturating under a constant vertical net stress of (a) 50 kPa and (b) 200 kPa

6.2.2 Saturation under constant vertical stresses and subsequent compression-rebound tests

6.2.2.1 Effect of sample heights on swelling deformation

The development of swelling strain with time for compacted bentonite-sand mixtures samples with a height of 5, 10 and 15 mm is shown in Figure 6.7. The sample heights affected the swelling strain rate and the final swelling strain. The swelling strain rates decreased with with an increase in the sample height. The increase in the time taken for reaching swelling deformation equilibrium with the sample height is due to the increase in the fluid flow path with an increase in the thickness of the sample. However, the final swelling strain increased with the sample heights. The effect of sample heights on the magnitude of swelling strain is due to is due to the fact that increasing the sample height while maintaining the same surface area (the same diameter) would induce more swelling along vertical direction of the sample (Jayalath et al., 2016).

6.2.2.2 Effect of the vertical net stresses on volumetric response

Evolution of the vertical strain with time for samples BS-SCR-1, BS-SCR-5, BS-WL200-1, BS-SCR-6 and BS-SCR-7 saturated under a vertical stress of 0.003, 0.05, 0.2, 2.4 and 12.2 MPa, respectively, is presented in Figure 6.8. The volumetric response of compacted bentonite-sand mixtures samples upon saturating was affected by the vertical net stressed prior to saturating. When the vertical stress prior to saturating was less than about 2.4 MPa, the samples exhibited swelling upon saturating. Moreover, the smaller the vertical net stress was, the smaller the swelling strain rate was but the greater the equilibrium swelling strain was. Since the swelling rate decreased with a decrease in the vertical net stress, the time to reach the equilibrium swelling strain increased with a decrease in the vertical net stress. When the vertical stress was equal to 2.4 MPa, the sample exhibited very slight swelling followed by slight collapse during saturating. When the vertical stress was greater than 2.4 MPa (i.e. 12.4 MPa), the sample exhibited significant collapse upon saturating. The dependency of volumetric response of compacted bentonite-sand mixtures samples upon saturating on the vertical net stress can be well explained according to BExM (Gens & Alonso, 1992).

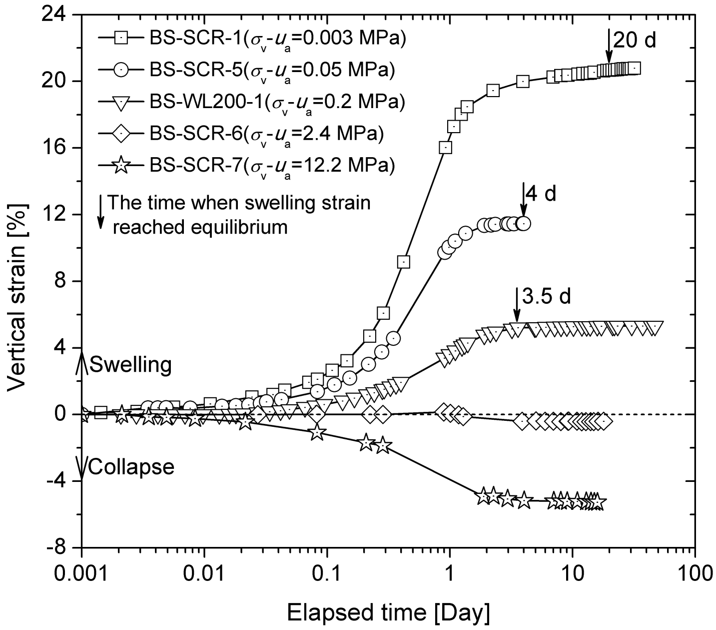

Figure 6.8: Evolution of vertical strain with time for compacted bentonite-sand mixtures saturated under constant vertical net stresses (all the samples with a height of 15 mm)

The equilibrium void ratios at saturation versus the vertical net stressed shown in Figure 6.8 are presented in Figure 6.9 on a semi-logarithmic plot. In addition, experimental data obtained by Agus (2005) on compacted bentonite-sand mixtures with a initial dry density of 2.0 Mg/m^3 are also given in Figure 6.9.

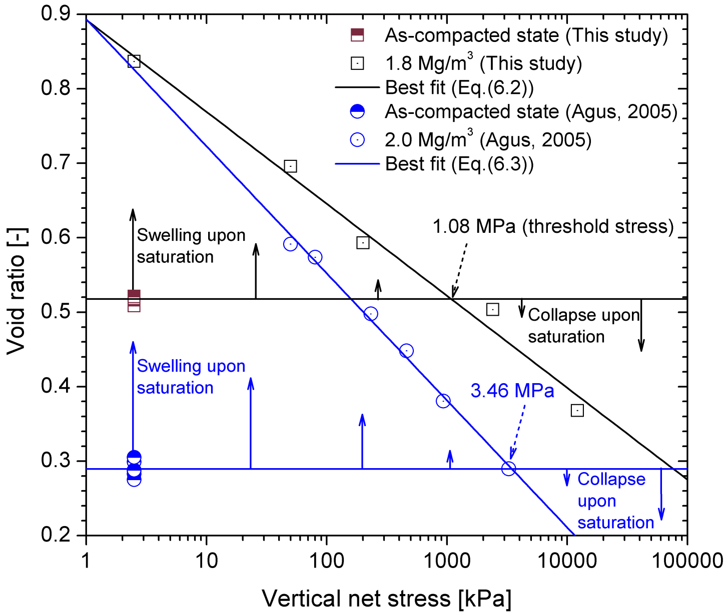

Figure 6.9: Changes in void ratio of saturated bentonite-sand mixtures with increasing the vertical net stress where the compacted bentonite-sand mixtures is saturated with deionized water

For a given dry density, the experimental data were approximately located along a straight line. The straight line was characterized by Eq.(6.2) in case of the dry density of 1.8 Mg/m^3 (present study) and by Eq.(6.3) in case of the dry density of 2.0 Mg/m^3. Eq.(6.2) and Eq.(6.3) intersected at the vertical net stress of 1 kPa and void ration of 0.893. This suggested that the void ratio of compacted bentonite-sand mixtures upon saturating under unconfined condition was the maximum and was independent of the initial compaction dry density. This maximum void ratio was expected to depend on mineral composition of bentonite and on the nature of exchangeable cation in the bentonite.

If two horizontal straight lines passing through the initial void ratios were added into Figure 6.9, the straight lines characterized by Eq.(6.2) and Eq.(6.3) would be divided into two parts: swelling upon saturation and collapse upon saturation. The vertical net stress at the intersection of one horizontal straight line and the corresponding straight line characterized by Eq.(6.2) or Eq.(6.3) was a threshold stress. When a vertical net stress was less than the threshold stress, the saturation under the vertical net stress induced bentonite-sand mixtures swelling. When a vertical net stress was greater than the threshold stress, the saturation under the vertical net stress resulted in bentonite-sand mixtures collapse. According to Figure 6.9, the threshold stress was equal to 1.08 MPa for the initial dry density of 1.8 $\mathrm{Mg/m^3}$ and to 3.46 MPa for the initial dry density of 2.0 $\mathrm{Mg/m^3}$. This suggested that high compaction or dry density increased the threshold stress. Consequently, the compacted bentonite-sand mixtures with high initial dry density exhibited swelling upon saturation under large range of vertical net stress.

$$e = -0.054\ln(\sigma_\mathrm{v} - u_\mathrm{a}) + 0.893(R^2 = 0.98) \tag{6.2}$$

$$e = -0.074\ln(\sigma_\mathrm{v} - u_\mathrm{a}) + 0.893(R^2 = 0.99) \tag{6.3}$$

6.2.2.3 Compression-rebound curves

Once the samples BS-SCR-1, BS-SCR-5 and BS-SCR-6 reached the equilibrium void ratio or vertical strain under the different vertical net stresses, they were subjected to loading and unloading following the stress paths presented in Figures 4.1. The swelling/collapse-compression-rebound curves of the samples BS-SCR-1, BS-SCR-5, BS-SCR-6 and BS-SCR-7 are shown in Figure 6.10. In addition, the relationship between the vertical net stress and the equilibrium void ratio characterized by Eq.(6.2) is also given in Figure 6.10.

According to Figure 6.10, two swelling pressures (i.e. P_s1=1.08 and P_s2=2.48 MPa) were determined with "swelling-under-load" method and "free swelling-load" method, respectively (see section 2.7 for details). The former method was consistently reported to give a lower value of swelling pressure than the latter method (Sridharan et al., 1986a; El-Sohby et al., 1989; Agus, 2005). Compared to the two methods above, the constant volume method provided the lowest value of swelling pressure (i.e. 0.86 MPa, see section 5.2 for details). The constant volume method gives swelling pressures that have been reported to be intermediate between "free swelling-load" method and "swelling-under-load" (Sridharan et al., 1986a) method or to be the lowest values (El-Sohby et al., 1989; Agus, 2005). The phenomenon that the three methods determine different values of swelling pressures can be well explained according to stress-path dependency of swelling pressure introduced by Gens & Alonso (1992).

The swelling pressure P_s1 shown in Figure 6.10 corresponded to a threshold vertical net stress. When the vertical net stress was less than P_s1, the compression strain due to loading was less than subsequent swelling strain due to the saturation under the vertical net stress. Consequently, samples BS-SCR-1 and BS-SCR-5 exhibited swelling upon saturation when

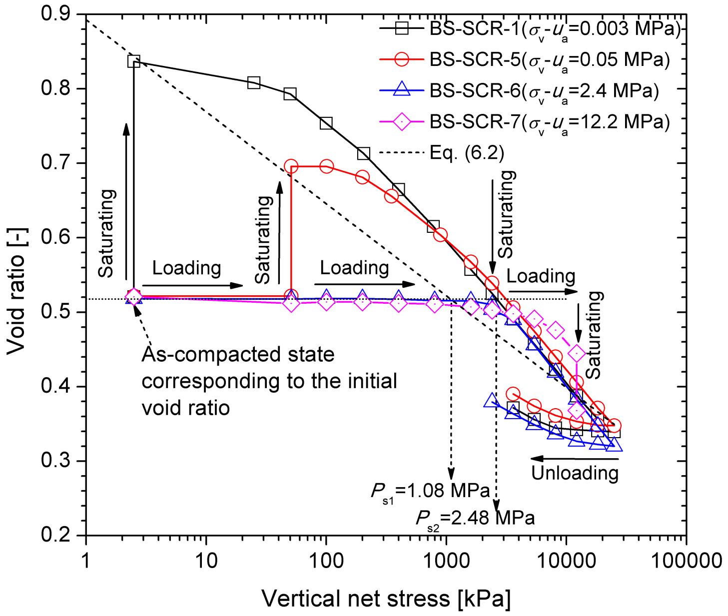

Figure 6.10: Swelling-compression-rebound curves of compacted bentonite-sand mixtures in the case of saturation occurring under various vertical net stresses ($\sigma_{\mathrm{v}} - u_{\mathrm{a}}$ in brackets represents the vertical net stresses at which the samples are saturated with deionized water)

the vertical net stress was less than the threshold vertical net stress (P_{s1}). When the vertical net stress was equal to P_{s1}, the compression strain due to loading would be equal to subsequent swelling strain due to the saturation under the vertical net stress. As a consequence, the sample would not exhibit any swelling or compression upon saturation. When the vertical net stress was greater than P_{s1}, the compression strain due to loading was greater than subsequent swelling strain due to the saturation under the vertical net stress. As a result, samples BS-SCR-6 and BS-SCR-7 exhibited collapse up on saturating.

The compression curves of saturated bentonite-sand mixtures presented in Figure 6.10 showed that the elastic loading curves depended on the stress history, whereas the saturated virgin consolidation curves were almost linear and unique. In the case of sample BS-SCR-7, the collapse upon saturating under the vertical net stress of 12.2 MPa almost followed the saturated normal consolidation curve.

Since the stress history affected elastic loading curves, both the swelling indexed derived from the elastic loading curves and the yield stresses depended on the stress history. Figures 6.4(a) and 6.11 show the swelling indexed and yield stresses determined from

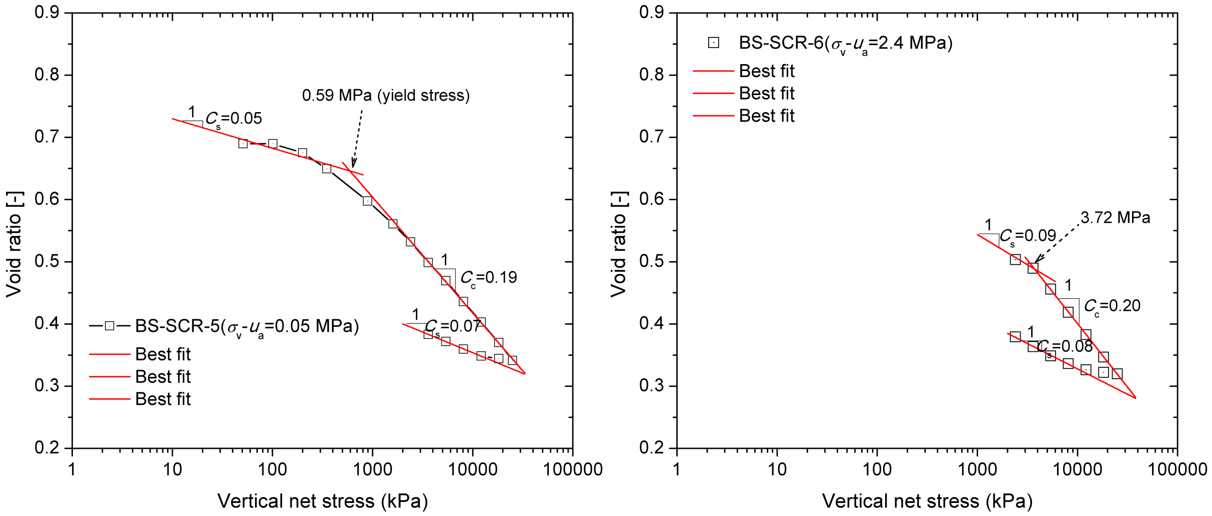

(a) (b)

Figure 6.11: Compression-redound curves of saturated samples (a) BS-SCR-5 and (b) BS-SCR-6

the compression-rebound curves of saturated samples BS-SCR-1, BS-SCR-5 and BS-SCR-6.

The yield stress was 0.1 MPa for sample BS-SCR-1 saturated under the vertical net stress of 0.003 MPa, 0.59 MPa for sample BS-SCR-5 saturated under the vertical net stress of 0.05 MPa and 3.72 MPa for sample BS-SCR-6 saturated under the vertical net stress of 2.4 MPa. Therefore, yield stress increased with the vertical net stresses where the samples were saturated with deionized water. At saturation, the increase in yield stress due to an increase in the vertical net stress can be well explained according to either Barcelona basic model (Alonso et al., 1990) or Barcelona expansive model (Gens & Alonso, 1992).

The compression indexes (C_c) of samples BS-SCR-1, BS-SCR-5 and BS-SCR-6 were found to be equal to 0.19, 0.19 and 0.20 respectively. Thus, the compression index of saturated bentonite-sand mixtures was approximately constant and independent of stress paths. Moreover, the compression indexes determined in the present investigation were found to be equal to the value of 0.19 reported by Agus (2005) on compacted bentonite-sand mixtures with a initial dry density of 2.0 Mg/m^3. Thus, the compression index of saturated bentonite-sand mixtures was also independent of the initial compaction dry densities.

The swelling indexes of saturated samples BS-SCR-1, BS-SCR-5 and BS-SCR-6 versus the vertical net stresses where samples were saturated are shown in Figures 6.12. The swelling indexes increased with an increase in the vertical net stress, regardless of determining the

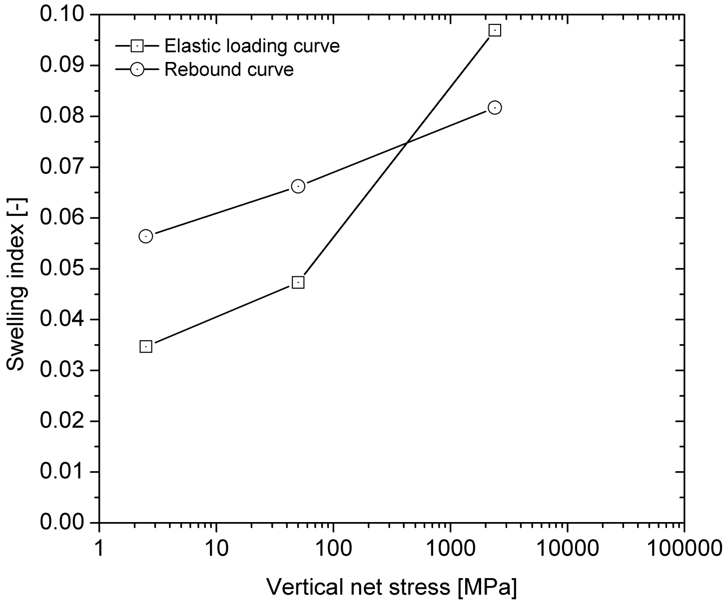

Figure 6.12: Changes in swelling index of saturated bentonite-sand mixtures with the vertical net stress where the bentonite-sand mixtures samples are saturated with deionized water

swelling index either from elastic loading curve or from rebound curve. Therefore, stress paths affected the swelling index of saturated bentonite-sand mixtures. Moreover, the swelling indexes derived from the elastic loading were found similar to those derived from the rebound curve.

6.2.3 Coefficient of permeability of saturated bentoniite-sand mixture

The result of oedometer tests on sample BS-SCR-1 was used to determine the saturated coefficient of permeability as a function of bentonite dry density. The coefficient of permeability (k) was determined according to the following equation:

$$k = \gamma_{\mathrm{w}} C_{\mathrm{v}} \frac{\triangle e}{(1+e) \triangle (\sigma_{\mathrm{v}} - u_{\mathrm{a}})} \tag{6.4}$$

where γ_{w} is unit volume weight of water, KN/m^3 and C_{v} is consolidation coefficient, m^2/s. C_{v} was calculated based on Eq.(6.5).

$$C_{\mathrm{v}} = \frac{T_{\mathrm{v}} H^2}{t} \tag{6.5}$$

In Eq.(6.5), T_v is a dimensionless time factor, depending on the degree of consolidation; H is the drainage path which is equal to half the sample height for double-sided drainage and to the full sample height for one-sided drainage; t is time corresponding to the particular degree of consolidation. In the present investigation, square-root-of-time or Taylor's method (Taylor, 1942; ASTM-D698, 1996) was used to determine T_v and t and further calculate C_v.

For each vertical net stress, the void ratio was converted into bentonite dry density to compare the calculated coefficient of permeability and measured ones. The bentonite dry density (ρ_db) was determined using the following Eq.(6.6) (Agus, 2005; Wang et al., 2013a).

$$\rho_\mathrm{db} = \frac{(B/100)\rho_\mathrm{m} G_\mathrm{ss}\rho_\mathrm{w}}{G_\mathrm{ss}\rho_\mathrm{w}(1 + w_\mathrm{BS}/100) - \rho_\mathrm{m}(1 - B/100)} \tag{6.6}$$

In Eq.(6.6), $B(\%)$ is the bentonite content, ρ_m is the mixture density, G_ss is the specific gravity of sand, ρ_w, is the liquid water density and w_BS is the water content of bentonite-sand mixtures.

The bentonite dry density versus coefficient of permeability data are presented in Figures 6.13. In addition to the data calculated from the oedometer test result, the hydraulic conductivities of saturated Calcigle bentonite reported by Khan (2012) has been also given in Figures 6.14 for comparison. It should be noted that both the bentonite used in this study and that used by Khan (2012) were Calcige and had the similar mineral composition and material properties.

As expected, the coefficient of permeability or hydraulic conductivity decreased with an increase in the bentonite dry density. Moreover, the coefficient of permeabilities determined from oedometer test result was quite similar to those measured by permeability tests for a given bentonite dry density.

6.2.4 Total suction of saturated samples after unloading

After releasing the vertical stress under undrained condition, the final dry density, water content and total sucton of the samples BS-SCR-1, BS-SCR-2, BS-SCR-5, BS-SCR-6 and BS-SCR-7 were measured. The measured dry density, water content, degree of saturated and total suction are shown in Table 6.1. It should be noted that after the vertical net stress was unloaded to 1.6 MPa, the sample BS-SCR-2 was saturated with deionized water under the constant vertical net stress of 1.6 MPa. The final dry density and degree of

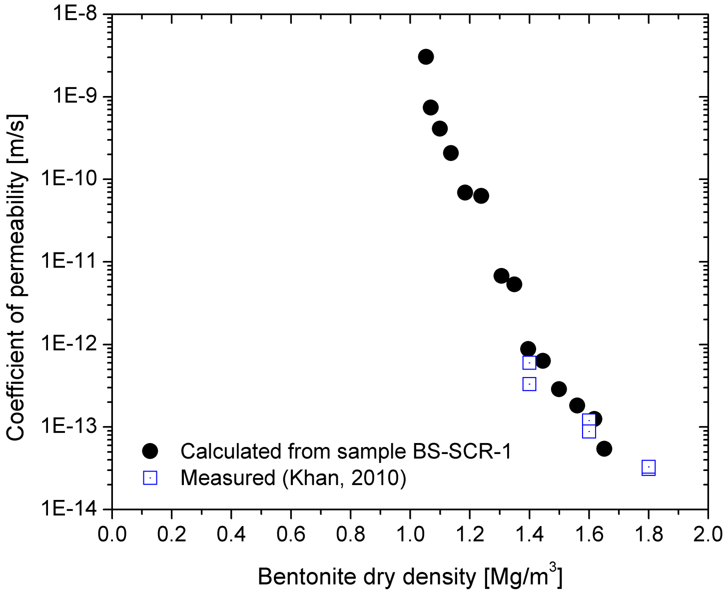

Figure 6.13: Bentonite dry density versus saturated coefficient of permeability

saturated were determined according to measured water content and the sample volume after releasing the vertical stresses.

The degree of saturation of all samples indicated that all samples were saturated at the end of the one-dimensional swelling-compression-rebound tests. Moreover, the experimental results in Table 6.1 also showed that the total suctions of saturated bentonite-sand mixtures were not equal to zero but were significant values, depending on water content. If the experimental data in terms of total suction versus water content were plotted in a semi-logarithmic plot (Figure 6.14), it is found that the experimental data were located on the unique total suction-water content curve (Eq.(4.8)) found in chapter 4.

6.3 Summary

The one-dimensional swelling-compression-rebound behaviour of compacted bentonite-sand mixtures was experimentally determined in this chapter. One-dimensional swelling-compression-rebound tests were performed under suction controlled conditions. Changes in yield stress, compression index and swelling index with applied suction were determined from the compression-rebound curves at different applied suction. The effect of the stress level during wetting process on the yield stress, the compression index and the swelling index of saturated bentonite-sand mixtures is also experimentally examined

Table 6.1: Final conditions of saturated bentonite-sand mixtures after releasing the vertical stress

Sample no.	$(\sigma_\mathrm{v} - u_\mathrm{a})$	Dry denisty	Water content	Degree of saturation	Total suction*
(-)	(MPa)	(Mg/m^3)	(%)	(%)	(MPa)
BS-SCR-1	3.60	1.99	14.6	100	4.57
BS-SCR-2	1.60	1.96	14.9	100	3.80
BS-SCR-5	2.40	1.94	14.7	98	4.85
BS-SCR-6	3.60	1.96	14.5	100	4.71
BS-SCR-7	12.15	1.93	14.5	96	4.99

$(\sigma_\mathrm{v} - u_\mathrm{a})$ was the vertical net stress before removing samples from oedometer, $*$ was determined by chilled-mirror hygrometer.

in this chapter. The coefficient of permeability as a function of bentonite dry density was determined according to the consolidation test of bentonite-sand mixtures and was compared with that measured by permeability tests. Moreover, total suction and water content measurements after unloading were also performed on saturated bentonite-sand mixtures samples. The following conclusions were drawn in this chapter.

1. The yield stress of bentonite-sand mixture was found to increase with initial compaction dry density and applied suction. The increase in the yield stress with an increase in the initial compaction dry density can be explained according to the linkage between dry density, inter-aggregate pore volume and yield stress. The increase in the yield stress with an increase in the applied suction agrees with the findings reported in the literature and can be well explained according to Barcelona basic model.

2. The compression index was found to depend not only on applied suction but also on vertical net stress. The dependency of compression index on vertical net stress and applied suction cannot be explained based on Barcelona basic model.

3. It was found that the swelling indexes decreased with an increase in the applied suction, regardless of determining the swelling index either from the elastic curve or from the rebound curve. The dependency of swelling index on suction indicated that the general assumption that swelling index of compacted bentonite-based materials is constant may be not appropriate.

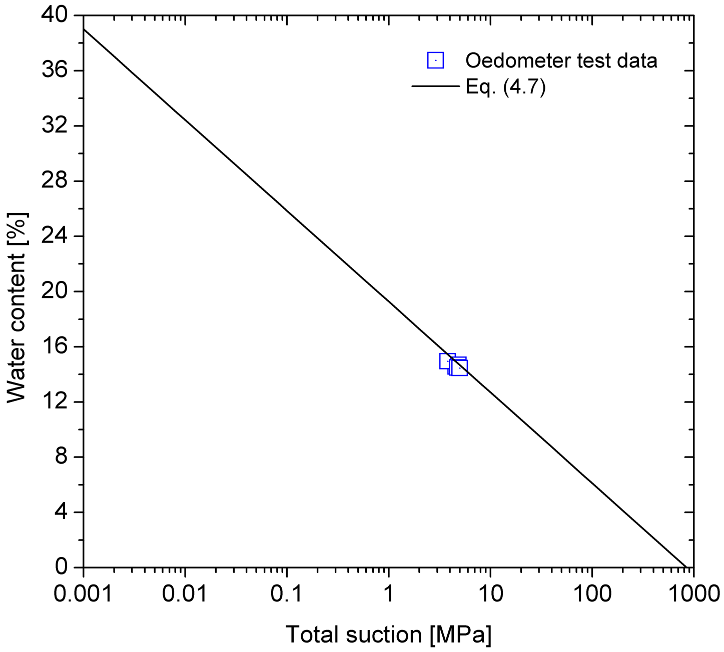

Figure 6.14: Measured total suction versus water content for bentonite-sand mixtures

4. The swelling deformation of compacted bentonite-sand mixture upon saturating increased with the sample heights. The effect of sample heights on the magnitude of swelling deformation may be due to the fact that increasing the sample height while maintaining the same surface area (the same diameter) would induce more swelling along the vertical direction of the sample.

5. The ”free swelling-load” method, ”swelling-under-load” method and ”constant volume” method determined the maximum, intermediate and minimum swelling pressures, respectively. The dependency of swelling pressure on experimental methods can be well explained according to the stress-path dependency of swelling pressure.

6. The compression index of saturated bentonite-sand mixtures was almost independent of stress paths and initial compaction dry density. The Barcelona basic model can explain why the compression index of saturated bentonite-sand mixtures is independent of stress paths.

7. The coefficient of permeability as a function of bentonite dry density determined from consolidation tests was found to well agree with that measured by permeability tests reported in the literature. The coefficient of permeabilities determined in this chapter provides hydraulic parameters for calibrating the hydraulic model used in the numerical simulation.

8. The measured total suctions of saturated bentonite-sand mixtures were not equal to zero but were significant values, depending on water content. The measured total suction versus water content was found to be located on the unique total suction-water content curve (Eq.(4.8)) found in chapter 4.

7 Numerical simulation of hydro-mechanical behaviour

7.1 Introduction

The objective of this chapter is to verify the assumption that the method for determining microstructural characteristics from the wetting WRCs based on the method proposed by Navarro et al. (2017b) on Na-bentonite is reliable on Ca-rich bentonite. Numerical simulation of a multi-step swelling pressure test was performed to verify the method for deriving microstructural characteristics from wetting WRCs on Ca-rich bentonite. This chapter presents the numerical simulation and simulation results with respect to the hydraulic-mechanical behaviour of compacted bentonite-sand mixtures. Barcelona expansive model (BExM) is first introduced and parameters used in this mechanical model are then determined based on the experimental data reported in Chapters 4, 5 and 6. The hydro-mechanical (HM) responses of the compacted bentonite-sand mixtures upon saturation are numerically simulated using Code_Bright (UPC, 2017). Finally, the simulation results are compared with experimental results.

7.2 Barcelona expansive model (BExM)

The BExM is a elastoplastic constitutive law for expansive soils, especially for unsaturated expansive soils (Gens & Alonso, 1992; Alonso et al., 1999). For this model, two levels of soil structure are defined: macrostructural level (macro) and microstructural level (micro). The macrostructural level corresponds to the inter-aggregate pores, whereas the microstructural level corresponds to the intra-aggregate pores (Gens & Alonso, 1992). According to the concept above, the void ratio (e) is composed of two parts:

$$e = e_{\mathrm{M}} + e_{\mathrm{m}} \tag{7.1}$$

where e_{M} and e_{m} are micro and macrostructural void ratios, respectively.

According to the concept basis for BExM (Gens & Alonso, 1992), the swelling of active clay minerals takes place at the microstructural level and the macrostructural level is responsible for major structural rearrangement. The assumptions adopted in this model are listed in the following:

- the microstructural level is mainly saturated and the effective stress concept holds;
- the microstructural behaviour is elastic and volumetric;
- mechanical, hydraulic and chemical equilibrium exists between microstructure and macrostructure;
- coupling between microstructure and macrostructure results in possible build-up of macrostructural elastoplastic strains when elastic microstructural strains take places.

Based on the assumptions above, the increment of volumetric microstructural strain ($d\epsilon^{\mathrm{e}}_{\mathrm{vm}}$) depends only on the increment of mean effective stress ($d(p+s)$). p and s are mean net stress and matric suction, respectively. Thus, the microstructural volumetric elastic strain is calculated by the following equations.

$$d\epsilon^{\mathrm{e}}_{\mathrm{vm}} = \frac{de_{\mathrm{m}}}{1+e_{\mathrm{m}}} = \frac{d(p+s)}{K_{\mathrm{m}}} \tag{7.2}$$

with

$$K_{\mathrm{m}} = \frac{(1+e_{\mathrm{m}})(p+s)}{\kappa_{\mathrm{m}}} \tag{7.3}$$

In these equations, K_{m} is the microstructural bulk modulus against effective stress changes which is linearly dependent of the logarithmic effective net stress $(p+s)$ and κ_{m} is the slope of the unloading/reloading line in e_{m}-$\ln(p+s)$ diagram.

In the case of macrostructural level, the macrostructural level volumetric elastic strain ($d\epsilon^{\mathrm{e}}_{\mathrm{vM}}$) is expressed as a function of mean net stress and suction:

$$d\epsilon^{\mathrm{e}}_{\mathrm{vM}} = \frac{dp}{K_{\mathrm{t}}} + \frac{ds}{K_{\mathrm{s}}} \tag{7.4}$$

With

$$K_{\mathrm{t}} = \frac{(1+e_{\mathrm{M}})(p)}{\kappa} \tag{7.5}$$

and

$$K_{\mathrm{s}} = \frac{(1+e_{\mathrm{M}})(s+p_{\mathrm{atm}})}{\kappa_{\mathrm{s}}} \tag{7.6}$$

where K_{t} and K_{s} are the macrostructural bulk modulus against mean net stress changes and the macrostructural bulk modulus against suction changes, respectively; κ is the slopes of the unloading/reloading line in e_{M}-ln(p) diagram; p_{atm} is the atmosphere pressure; κ_{s} is the slope of the reversible wetting-drying lines in e_{M}-ln(s) diagram.

The total volumetric elastic strain ($d\epsilon_{\mathrm{v}}^{\mathrm{e}}$) is the sum of $d\epsilon_{\mathrm{vm}}^{\mathrm{e}}$ and $d\epsilon_{\mathrm{vM}}^{\mathrm{e}}$.

The changes in preconsolidation mean net stress or yield stress (p_0) with suction is shown by a loading-collapse (LC) yield curve characterized by Eq.(7.7) in the p-s plane (Figure 7.1).

$$p_0 = p_{\mathrm{c}}(\frac{p_{\mathrm{o}}^*}{p_{\mathrm{c}}})^{\dfrac{\lambda(0)-\kappa}{\lambda(s)-\kappa}} \tag{7.7}$$

with

$$\lambda(s) = \lambda(0)[r + (1-r)\mathrm{e}^{-\beta s}] \tag{7.8}$$

In equations above, p_{o}^* is the saturated preconsolidation mean net stress, p_{c} is the reference stress, $\lambda(s)$ is the slope of the normal compressive line at suction s, $\lambda(0)$ is the slope of the saturated virgin consolidation line and r and β are model parameters.

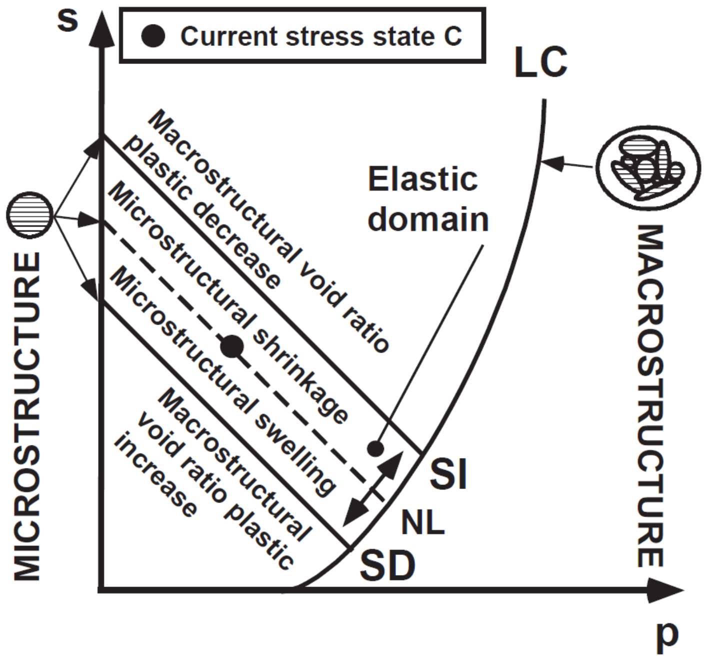

Figure 7.1: BExM yield loci in p-s plane (Alonso etal., 1999)

Eq.(7.7) describes the yield conditions of the macro-structure. The plastic strain depends on the wetting-drying paths or microstructural deformation, the applied confining stress and the density of materials. BExM characterizes the plastic strains by means of two additional yield curves: suction increase (SI) and suction decrease (SD) curves which are presented in Figure 7.1. These two yield curves are defined by Eq.(7.9) and Eq.(7.10), respectively. In these equations, s_{I} and s_{D} are hardening parameters.

$$p + s - s_{\mathrm{I}} = 0 \tag{7.9}$$

$$p + s - s_{\mathrm{D}} = 0 \tag{7.10}$$

For a reason of simplicity, it is generally assumed that the SI and SD yield curves are always activated. This assumption was commonly adopted by several researchers (e.g. Alonso et al. (1999, 2005); Sánchez et al. (2005); Wang et al. (2013b)) during simulating the thermo-hydro-mechanical behaviour of expansive clays. When SI and SD yield curves are activated, plastic strains take place. The plastic strains are characterized by the following equations:

$$d\epsilon^{\mathrm{P}}_{\mathrm{vMSI}} = f_{\mathrm{I}} d\epsilon^{\mathrm{e}}_{\mathrm{vm}} \tag{7.11}$$

$$d\epsilon^{\mathrm{P}}_{\mathrm{vMSD}} = f_{\mathrm{D}} d\epsilon^{\mathrm{e}}_{\mathrm{vm}} \tag{7.12}$$

where f_{I} and f_{D} are micro-macro coupling functions which depends on (p/p_0). p_0 corresponds to the current preconsolidation net stress at the current value of suction as characterized by the LC yield curve.

In BExM, it is assumed that SI and SD hardening is controlled by $d\alpha_1 = d\epsilon^{\mathrm{P}}_{\mathrm{vMSI}} + d\epsilon^{\mathrm{P}}_{\mathrm{vMSD}}$. LC hardening is assumed to be dependent on $d\alpha_2 = d\epsilon^{\mathrm{P}}_{\mathrm{vMSI}} + d\epsilon^{\mathrm{P}}_{\mathrm{vMSD}} + d\epsilon^{\mathrm{P}}_{\mathrm{vMCL}}$. Here $d\epsilon^{\mathrm{P}}_{\mathrm{vMCL}}$ is the volumetric plastic strain due to the activation of LC. Hardening laws are defined as the following equations:

$$ds_{\mathrm{I}} = \frac{K_{\mathrm{m}} d\alpha_1}{f_{\mathrm{I}}} \tag{7.13}$$

$$ds_{\mathrm{D}} = \frac{K_{\mathrm{m}} d\alpha_1}{f_{\mathrm{D}}} \tag{7.14}$$

$$d\alpha_2 = \frac{\lambda(s) - \kappa}{1 + e_{\mathrm{M}}} \frac{dp_0}{p_0} \tag{7.15}$$

7.3 Parameter determination

The model parameters were determined according to the experimental results presented in Chapters 4, 5 and 6 on compacted bentonite-sand mixtures. The microstructure of the compacted bentonite-sand mixtures was derived from the wetting WRCs (for details, please see section 4.2.4). The derived results allow determining not only the initial macro- and microstructural void ratios (e_{M} and e_{m}) but also the changes in e_{m} with mean effective stress ($p + s$). This further allows determining the κ_{m}. The variations of volume upon wetting and loading-unloading presented in Chapters 4 and 6 were used to determine the model parameters related to the hydro-mechanical behaviour. It should be noted that the symbol p adopted in the BExM corresponds to mean net stress. Since the experimental results from oedometer tests were used to determine model parameters, the symbol p used in the following corresponds to vertical net stress.

According to the microstructural data derived from wetting WRCs (i.e. Figure 4.8), the e_{M} and e_{m} were equal to 0.27 and 0.24, respectively, for the as-compacted bentonite-sand mixtures with an initial suction of 27 MPa and a dry density of 1.8 Mg/m^3.

The variation of microstructural void ratio of bentonite-sand mixtures upon wetting under constant volume condition (i.e. Figure 4.8(b)) was used to determine κ_{m} according to Eq.(7.9). Eq.(7.16) was used to fit effective stress versus microstructural void ratio in the diagram shown in Figure 7.2. In Eq.(7.16), both κ_{m} and c were fit parameters and κ_{m} was found to be equal to 0.50.

$$e_{\mathrm{m}} = \kappa_{\mathrm{m}} \ln(p + s) + c \tag{7.16}$$

The parameters for the LC yield curve characterized by Eq.(7.7) and Eq.(7.8) were determined based on the suction controlled compression tests presented in Chapter 6. Since κ_{m} was known, e_{M}-ln(p) curves could be obtained from the compression curves at a suction of 0.001 (at saturation), 3.4, 10.0 and 27.0 MPa. The κ, λ and p_{o} could be then determined based on e_{M}-ln(p) curves. For example, Figure 7.3 shows the method for determining the κ, λ and p_{o} in case of saturated condition. The values of κ varied from 0.004 to 0.016 with suction and the mean value of 0.01 was used in the simulation. The values of λ at a suction of 0.001, 3.4, 10.0 and 27.0 MPa were 0.083, 0.063, 0.033 and 0.027, respectively. In case of p_{o}, its value was equal to 0.4 MPa for a suction of 0.001 MPa, 0.53 MPa for a suction of 3.38 MPa, 1.13 MPa for a suction of 10 MPa and 3.34 MPa for a suction of 27 MPa. According to the values of κ, λ and p_{o}, Eq.(7.7) and Eq.(7.8) were calibrated. The calibrated parameters are presented in Table 7.1.

The macrostructural volumetric strain upon wetting or drying is composed of volumetric elastic strain (Eq.(7.4)) and volumetric plastic strain due to the interaction between the micro and macrostructures (Eq.(7.9) to Eq.(7.12)). For simplicity, the macrostructural

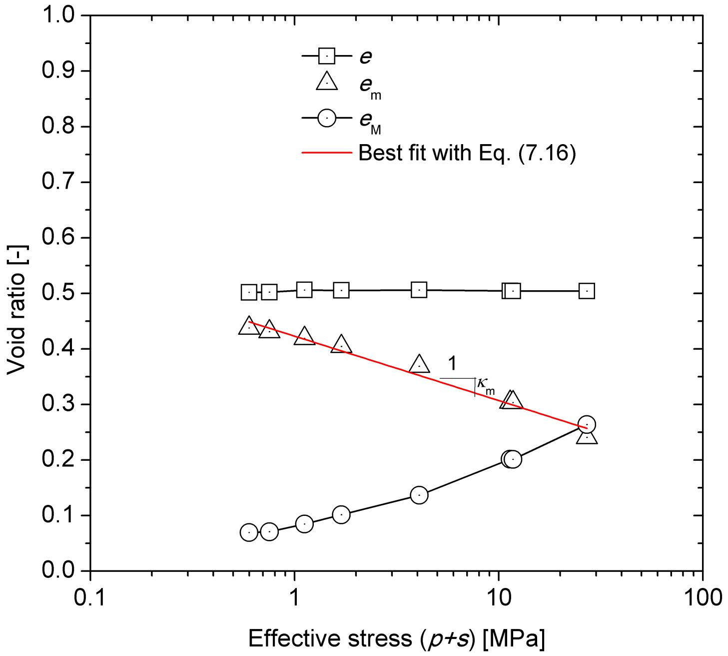

Figure 7.2: Variation of microstructural void ratio of bentonite-sand mixtures with the effective stress under constant volume condition

volumetric elastic strain due to suction changes was assumed not significant and a insignificant value of κ_s=0.001 was used in the present simulation work. This assumption was commonly adopted by several researchers (e.g. Alonso et al. (1999, 2005); Sánchez et al. (2005); Wang et al. (2013b)) during simulating the thermo-hydro-mechanical behaviour of expansive clays.

The microstructural void ratio was determined according to Eq.(7.2) and Eq.(7.3). The f_D was calculated by fitting the void ratio values in Figure 4.8 with Eq.(7.4), Eq.(7.7) and Eq.(7.10): $f_\mathrm{D} = -0.4 + 0.5(1 - p/p_0)^2$. The f_I was determined by fitting the changes in void ratio values with increasing the suction in Figure 4.11 with Eq.(7.4), Eq.(7.7) and Eq.(7.9): $f_\mathrm{I} = -0.4 + 0.5(p/p_0)^{0.5}$.

For Code-Bright, the van Genuchten (1980) model (Eq.(7.17)) were used to characterize the water retention of a soil. The parameters used to calibrate water retention model were obtained from the wetting WRCs determined under constant volume condition (Figure 4.5). The parameters obtained are shown in Table 7.1.

$$S_\mathrm{e} = \frac{S_\mathrm{l} - S_\mathrm{rl}}{S_\mathrm{ls} - S_\mathrm{rl}} = [1 + (\frac{P_\mathrm{g} - P_\mathrm{l}}{P_\mathrm{o}})^{\frac{1}{1-\lambda}}]^{-\lambda} \tag{7.17}$$

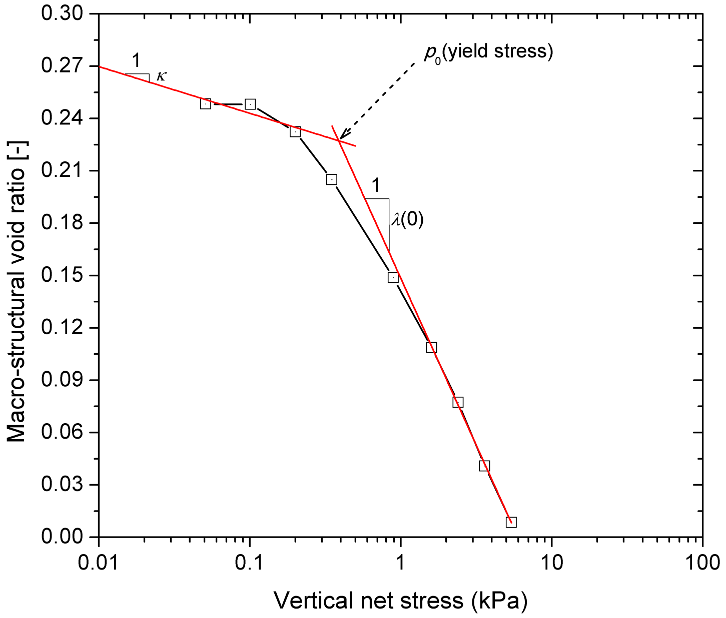

Figure 7.3: Variation of macrostructural void ratio of bentonite-sand mixtures with vertical net stress at saturated condition

In Eq.(7.17), S_e, S_l, S_rl and S_ls are effective degree of saturation, degree of saturation at suction of $P_\mathrm{g} - P_\mathrm{l}$, residual degree of saturation and maximum or saturated degree of saturation, respectively. In addition, λ is the shape function for retention curve and P_o corresponds to the air entry or expulsion value.

Kozeny-Carmen relationship (Eq.(7.18)) was used to describe the dependency of water permeability on porosity ϕ. In Eq.(7.18), $\mathbf{k}$ is the intrinsic permeability, $\mathbf{k}_\mathrm{o}$ is the intrinsic permeability for matrix ϕ_o and ϕ_o is the reference porosity. If ϕ_o is equal to 0, permeability will be constant. In case of ϕ_o equal to 0, the $\mathbf{k}_\mathrm{o}$ was determined according to the coefficient of permeability shown in Figure 6.14. The value of $\mathbf{k}_\mathrm{o}$ is presented in Table 7.1. In this table, $(k_{11})_\mathrm{o}$, $(k_{22})_\mathrm{o}$ and $(k_{33})_\mathrm{o}$ are the first, second and third principle intrinsic permeability.

$$\mathbf{k} = \mathbf{k}_\mathrm{o} \frac{\phi^3}{(1+\phi)^2} \frac{(1-\phi_\mathrm{o})^2}{\phi_\mathrm{o}^3} \tag{7.18}$$

Table 7.1: Parameters used in the present simulation

Initial state parameter		Mechanical parameter		Hydraulic parameter	
e	0.51	κ	0.01	P_o	3.67 MPa
e_m	0.24	κ_s	0.001	λ	0.24
s_0	27 MPa	κ_m	0.05	S_rl	0
p_o^*	0.4 MPa	$\lambda(0)$	0.083	S_ls	1
		p_c	0.21 MPa	$(k_{11})_\mathrm{o}$	6.75 E-20 m^2
		r	0.30	$(k_{22})_\mathrm{o}$	
		β	0.16	$(k_{33})_\mathrm{o}$	

7.4 Results and discussion

The changes in swelling pressure of compacted bentonite-sand mixtures upon gradually saturating was simulated using Code_bright. Following the suction decrease path followed by sample BS-CVPS-M-OT (see Table 3.7), the numerical simulation was performed under constant volume condition.

7.4.1 Variation of microstructure with decreaing suction

During simulating the swelling pressure test performed under constant volume condition, the variation of micro and macrostructural void ratios was calculated. The changes of micro and macrostructural void ratios with decreasing the suction are presented in Figure 7.4. The dotted lines represent the results from simulation and the lines with symbols represent the results derived from the wetting WRCs. According to Figure 7.4, the consistence between the simulated and derived values was well for both micro and macrostructural void ratios.

7.4.2 Water retention

Since the BExM assumes that the microstructural pores remain always saturated, the amount of water in the microstructural pores can be determined from the microstructural void ratio calculated in the simulation. Moreover, the amount of water in the micro and macrostructural pores can be determined from degree of saturation calculated in the

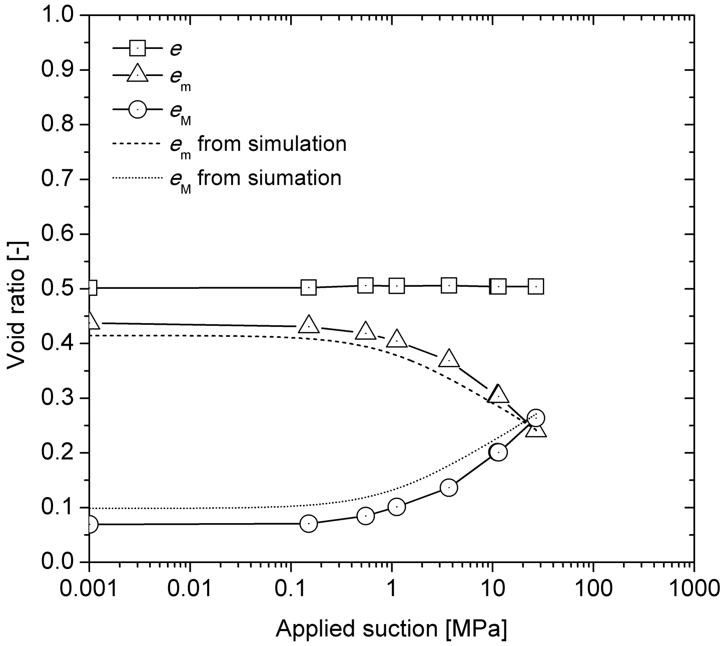

Figure 7.4: Variation of micro and macrostructural void ratios of compacted bentonite-sand mixtures with a decrease in the applied suction

simulation. The variation of the determined microstructural water content (WC_{m}) and total water content with a decrease in suction is presented in Figure 7.5. In addition to the WRCs determined from simulation, Figure 7.5 also presents the wetting WRC measured under constant volume condition.

According to Figure 7.5, the simulated WRCs could capture the main feature of the measured WRCs. In addition, for a given suction, the difference in total water content and microstructural water corresponded to the water content in macrostructural pore. Both micro and macrostructural pore waters increased with decreasing the suction. When the suction decreased to less than 0.86 MPa corresponding to the swelling pressure at saturation, the increase in microstructural water content almost disappeared. Thus, the increase in water content was mainly due to the increase in macrostructural water content when the suction decreased to less than 0.86 MPa.

7.4.3 Variation of swelling pressure with decreasing suction

Figure 7.6 presents a comparison of swelling pressure-suction relationships obtained from numerical simulation result and experimental results (see Chapter 5). According to Figure 7.6, the changes in swelling pressure upon gradually saturating obtained by the experi-

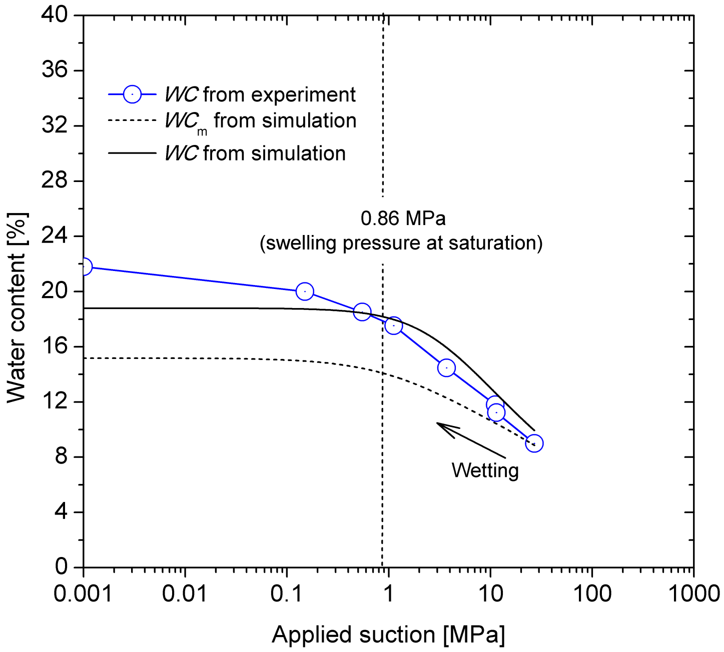

Figure 7.5: Variation of the measured water content, simulated water content and simulated microstructural water content (WC_{m}) of compacted bentonite-sand mixtures with decreasing suction

ments could be very well reproduced by the simulation. This, in turn, suggested that the method for deriving the variation of microstructural void ration from the wetting WRCs were effective and reliable.

The increase in swelling pressure with a decrease in the applied suction could be well explained according to the BExM. Initially, a suction decrease induces the swelling of aggregates and an increase in the microstructural void ratio (Figure 7.4 or 7.5). To remain the constant volume condition, a decrease in macrostructural void ratio which is equal to the increase in the microstructural void ratio (Figure 7.4) takes place. Since the SD and SI yield curves were assumed to be always activated in the presented simulation, LC yield curve moves towards upside (Figure 7.6). The upside movement of LC yield curve with decreasing the suction leads to the hardening of the materials (Gens & Alonso, 1992; Alonso et al., 1999, 2005). Since stress paths followed by the multi-step swelling pressure tests do not touch the modified LC curve, the swelling pressure increases monotonically with a decrease in the applied suction (Figure 7.6).

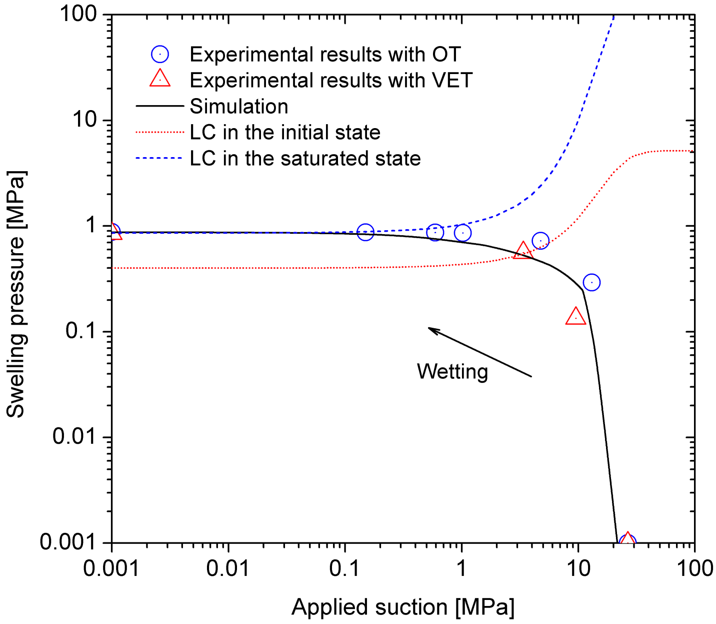

Figure 7.6: A comparison of swelling pressure-suction relationships obtained from the numerical simulation and experimental measurements

7.5 Summary

Numerical simulation of a multi-step swelling pressure test was performed to verify the method for deriving microstructural characteristics from wetting WRCs on Ca-rich bentonite. The model parameters used in the numerical simulation were determined according to the experimental results obtained in the previous chapters. The changes in microstructural void ratio, microstructural water content and swelling pressure with decreasing the applied suction were numerically simulated and compared with the experimental results. According to the simulation and simulation results, the following conclusions were drawn in this chapter.

1. The variation of the micro and macrostructural void ratios with decreasing the applied suction was well reproduced by the simulation and the simulated WRCs could capture the main feature of the measured WRCs. Moreover, the changes in swelling pressure upon gradually saturating obtained by the multi-step swelling pressure tests could be very well reproduced by the numerical simulation.

2. The consistency between the numerical simulation results and experimental results confirms the assumption that the method for determining microstructural characteristics from the wetting WRCs based on the method proposed by Navarro et al. (2017b) on

Na-bentonite is reliable on Ca-rich bentonite. The method for deriving microstructural characteristics from wetting WRCs is helpful in understanding the effect of the mechanical boundary conditions in repositories on the hydration of backfill and sealing materials.

8 Linkage between swelling pressure, total suction and applied suction

8.1 Introduction

The linkage between swelling pressure, the total suction of bentonite-based materials and applied suction (suction and suction of hydrating fluids) allows quantitatively estimating the effect of hydro-chemical boundary conditions on the swelling capacity of buffer, backfill and sealing materials. This chapter examines the linkage between swelling pressure, total suction and applied suction under saturated condition and unsaturated condition. In the case of saturated bentonite-based materials, an equation describing the linkage between the swelling pressure, the total suction of saturated bentonite-based materials and the suction of hydrating fluids is derived based on the thermodynamics of soil moisture (section 8.2). The derived equation is then validated according to laboratory tests involving swelling pressure tests and total suction measurements after the swelling pressure tests on the bentonite (section 8.3.1). The experimental technique and procedure of swelling pressure tests and total suction measurements are shown in section 3.3.5. In addition, the experimental data for bentonite-sand mixtures presented in chapters 4, 5 and 6 are used to validate the derived equation (section 8.3.2). In the case of the unsaturated bentonite-based materials, the linkage between swelling pressure, the total suction of the bentonite-based materials and applied suction is experimentally examined based on the experimental data obtained in this thesis (section 8.3.3). Moreover, this chapter also presents a relationship between the measured total suction and water content in bentonite-based materials in section 8.3.4. Concluding remarks are presented in section 8.4.

8.2 Theoretical considerations

Total potential of soil-water from the thermodynamics of soil moisture has been discussed by numerous researchers (Edlefsen & Anderson, 1943; Low & Deming, 1953; Bolt & Miller, 1958; Mitchell, 1962; Yong & Warkentin, 1975; Iwata et al., 1995). Iwata et al. (1995) stated that the total water potential (μ) in clays relative to the potential of the free pure water at the same temperature and external pressure is comprised of the potentials due to surface tension (μ_{c}), van der Waals fore (μ_{f}), solutes (μ_0), electric field (μ_{e}), temperature (μ_{T}), pressures (μ_{P}), and gravimetrical field (μ_{g}) (Eq.(8.1)).

$$\mu = \mu_{\mathrm{c}} + \mu_{\mathrm{f}} + \mu_0 + \mu_{\mathrm{e}} + \mu_{\mathrm{T}} + \mu_{\mathrm{P}} + \mu_{\mathrm{g}} \tag{8.1}$$

Detailed description about these potentials could be found in the work of Iwata et al. (1995). Since μ_{c}, μ_{f}, μ_0, μ_{e} and μ_{P} are the potentials which are closely related the discussion in this paper, their definitions were given in the following paragraphs.

Curved surfaces of water are formed in soils pores under the unsaturated condition. The water menisci gives rise to a decrease in the total potential of the water and this decrease is described by surface tension effect or capillary potential (Eq.(8.2)),

$$\mu_{\mathrm{c}} = \frac{2\sigma}{r}\overline{v}_{\mathrm{w}} = -(u_{\mathrm{a}} - u_{\mathrm{w}})\overline{v}_{\mathrm{w}} \tag{8.2}$$

where $\overline{v}_{\mathrm{w}}$ denotes the partial specific volume of water, r is the radius of curvature of the water menisci, σ is the surface tension, u_{a} is pore air pressure and and u_{w} is pore water pressure.

Van der Waals force effect is given in Eq.(8.3),

$$\mu_{\mathrm{f}} = -\frac{A}{z^{\alpha}} \tag{8.3}$$

where A and α are constant and z is the distance from the surface of the clay particle to water molecular.

Various solutes in the soil solution decrease the total potential of water in soil. In case of a non-ideal solution, the solute effect or osmotic potential is presented by Eq.(8.4).

$$\mu_0 = -\frac{RT}{1000}\Sigma\pi_{\mathrm{j}}n_{\mathrm{j}} \tag{8.4}$$

where π_{j} is the osmotic coefficient, n_{j} is the molarity of the solute j.

Clay minerals have electric charge and the soil solution is affected by the electric field induced by those charges. The change of total potential of water in soil because of electric displacement is shown in the following equation:

$$\mu_{\mathrm{e}} = \int_0^D \frac{D\overline{\upsilon}_{\mathrm{w}}}{4\pi}(\frac{1}{\overline{\epsilon}_{\mathrm{w}}} - 1)dD \tag{8.5}$$

where $\overline{\epsilon}_{\mathrm{w}}$ donates the partial dielectric constant of water in soil and D represents the electric displacement at the point where the water exists. The value of D is influenced by the shape and size of the clay particles which adsorb the water, the surface density of electric charge and the distance between the surface and the water.

A state of equilibrium where the total potential of water in clay equals at any point in the system is maintained by a pressure (P). P compensates for the drop in the total potential of the water near the clay particle due to surface tension, van der Waals fore, solutes, electric field, temperature and gravimetrical field. Moreover, P at equilibrium is approximately equal to net mean stress.

$$\mu_{\mathrm{P}} = P\overline{\upsilon}_{\mathrm{w}} \tag{8.6}$$

The applicability of the potentials above can be examined in the light of a constant volume swelling pressure test on compacted bentonite-based materials. Studies on the pore size distribution (PSD) of the compacted bentonite-based materials have shown dual-structure pore size distributions with inter-aggregate pores and intra-aggregate pores (Sridharan et al., 1971; Pusch & Yong, 2006; Lloret et al., 2003; Delage et al., 2006; Romero & Simms, 2008; Seiphoori et al., 2014). The inter-aggregate pores and intra-aggregate pores are generally identified with macrostructural porosity and microstructural porosity, respectively, during analysing compacted clays (Alonso et al., 1990; Gens & Alonso, 1992; Musso et al., 2013; Măsin & Khalili, 2016; Navarro et al., 2017a,b). Similarly, total potential of macrostructural pore water (μ_{M}) and total potential of microstructural pore water (μ_{m}) can be defined during analysing the constant volume swelling pressure test on compacted bentonite-based materials.

An experimental sketch of the swelling pressure test device and structures of compacted bentonite-based materials (macro and micro structures) are shown in Figure 8.1. A compacted sample under constant volume condition is wetted by an aqueous solution. The upon saturation of the sample in the measuring system (Figure 8.1) during a swelling pressure test, the macro-pores are filled with the aqueous solution. In addition, the micropores are also filled with water that may also includes some solutes. At saturation,

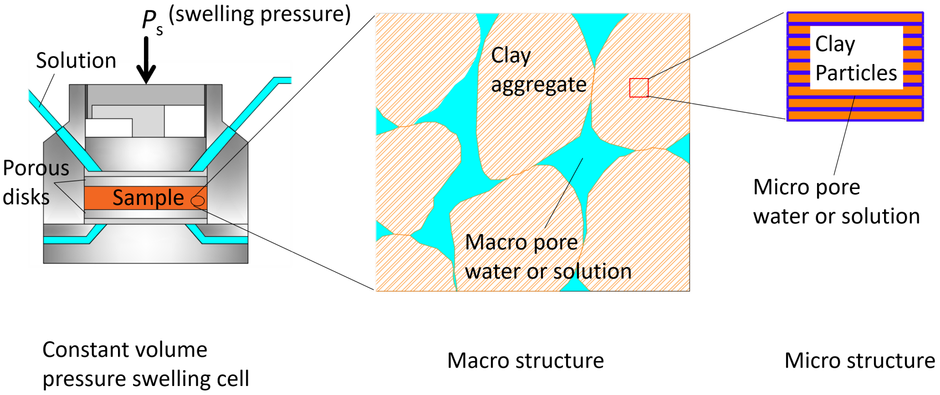

Figure 8.1: Schematics of swelling pressure measurement using constant volume test set up and structures of compacted clay sample

the water potential due to surface tension (μ_{c}) gets eliminated. Considering that the temperature and the atmospheric pressure change little during an isothermal swelling pressure test, the potentials due to temperature (μ_{T}) and atmosphere pressure can be neglected. Since the scale of this system is very small, it is reasonable to neglect the gravitational potential (μ_{g}). Therefore, the total potential of macrostructural pore water (μ_{M}) is reduced to only the potential due to solutes (μ_0^{M}) and is given by Eq.(8.7). In a swelling pressure test, μ_0^{M} corresponds to the total water potential of the external fluid (μ_{a}). In suction terms, the total suction of the hydrating fluid is ψ_{a} (applied suction).

$$\mu_{\mathrm{M}} = \mu_0^{\mathrm{M}} = \mu_{\mathrm{a}} = -\psi_{\mathrm{a}}\overline{v}_{\mathrm{w}} \tag{8.7}$$

Similarly, the total potential of microstructural pore water (μ_{m}) is given by Eq.(8.8).

$$\mu_{\mathrm{m}} = \mu_{\mathrm{f}}^{\mathrm{m}} + \mu_0^{\mathrm{m}} + \mu_{\mathrm{e}}^{\mathrm{m}} + P\overline{v}_{\mathrm{w}} \tag{8.8}$$

According to the thermodynamics of soil moisture, at equilibrium the total potential of the water at any given points in the system has a constant value. Thus, Eq.(8.9) can be obtained.

$$\mu_{\mathrm{m}} = \mu_{\mathrm{M}} \tag{8.9}$$

By rearranging Eqs.(8.7), (8.8), and (8.9), Eq.(8.10) can be obtained:

$$\mu_{\mathrm{f}}^{\mathrm{m}} + \mu_{\mathrm{e}}^{\mathrm{m}} + \mu_0^{\mathrm{m}} = -\psi_{\mathrm{a}}\overline{v}_{\mathrm{w}} - P\overline{v}_{\mathrm{w}} \tag{8.10}$$

It is generally assumed that $\overline{v}_{\mathrm{w}}$ does not depend on pressure and is a constant, nearly 1 m^3/Mg. A simplification of Eq.(8.10) yields Eq.(8.11).

$$-\frac{1}{\overline{v}_{\mathrm{w}}}(\mu_{\mathrm{f}}^{\mathrm{m}} + \mu_{\mathrm{e}}^{\mathrm{m}} + \mu_0^{\mathrm{m}}) - \psi_{\mathrm{a}} = P \tag{8.11}$$

Since $(\mu_{\mathrm{f}}^{\mathrm{m}}+\mu_{\mathrm{e}}^{\mathrm{m}})$ and μ_{0}^{m} correspond to the hydration effect and osmotic effect, respectively, thus they correspond to matric potential and osmotic potential, respectively. Because $(\mu_{\mathrm{f}}^{\mathrm{m}}+\mu_{\mathrm{e}}^{\mathrm{m}}+\mu_{0}^{\mathrm{m}})$ corresponds the sum of matric and osmotic potentials in case of saturated clays, the value of which can be approximately determined from Kelvin's equation (i.e., Eq.(8.12)).

$$\mu_{\mathrm{f}}^{\mathrm{m}}+\mu_{\mathrm{e}}^{\mathrm{m}}+\mu_{0}^{\mathrm{m}}=\frac{RT}{M_{\mathrm{w}}}\ln(RH) \tag{8.12}$$

In Eq.(8.12), R is the molar gas constant, M_{w} is the molecular mass of water, and (RH) is the relative humidity. In suction terms, total suction (ψ_{t}) of the saturated bentonite-based materials under constant volume condition is given in Eq.(8.13):

$$\psi_{\mathrm{t}}=-\frac{RT}{M_{\mathrm{w}}\overline{v}_{\mathrm{w}}}\ln(RH) \tag{8.13}$$

After Eqs.(8.11), (8.12), and (8.13) are combined, Eq.(8.14) can be obtained in suction and pressure terms, where P_{s} represents swelling pressure.

$$\psi_{\mathrm{t}}-\psi_{\mathrm{a}}=P=P_{\mathrm{s}} \tag{8.14}$$

Similar relationship to Eq.(8.14) has been reported by several researchers. Croney (1952); Kassiff & Shalom (1971); Towenr (1981) suggested a similar relationship to Eq. (14) for a saturated clay under compression and no water content changes, i.e.

$$s+U=P \tag{8.15}$$

where s is the matric suction measured under zero load, corresponding to ψ_{t} in Eq.(8.14); U is the pore water pressure measured under load, corresponding to $-\psi_{\mathrm{a}}$ in Eq.(8.14); P is the total external all-round pressure, corresponding to P_{s} in Eq.(8.14). If the aqueous solution in Fig. 1 is pure water ($\psi_{\mathrm{a}}=0$), then Eq.(8.14) is reduced to the thermodynamic equations developed by Low and his co-works (Low & Anderson, 1958; Viani et al., 1983; Low, 1987). In addition, a similar expression has been also given by Navarro et al. (2017a) (see Eq.(8.7) in the case of saturation condition).

To validate Eq.(8.14) experimentally, separate measurements of P_{s}, ψ_{a} and ψ_{t} are necessary. The former two can be directly determined by a swelling pressure device and chilled mirror hygrometer, respectively. However, the latter one can not be directly determined by placing a relative humidity sensor in a constant volume swelling pressure device. In constant volume condition, the water potential determined by the relative humidity sensor is total water potential (μ_{m} or μ_{M}). This can be confirmed by constant volume infiltration experimental results reported by Cui et al. (2008); Ye et al. (2009); Mokni & Barnichon

(2016); Villar et al. (2016). They found that the relative humidity above the wetting face reached nearly 100% after long-term of supplying water. This indicates that the water potential determined by the relative humidity sensor in constant volume condition is equal to the water potential of hydrating fluid (water). Thus, removal of swelling pressure is necessary for determining ψ_{t} or $(\mu_{\mathrm{f}}^{\mathrm{m}} + \mu_{\mathrm{e}}^{\mathrm{m}} + \mu_{0}^{\mathrm{m}})$.

If the hydrating fluid (Figure 8.1) is removed before releasing the swelling pressure, subsequent removal of swelling pressure can be considered as undrained unloading. Consequently, the water content of the saturated bentonite sample will not change after releasing the swelling pressure. Since $\mu_{\mathrm{f}}^{\mathrm{m}}$ and $\mu_{\mathrm{e}}^{\mathrm{m}}$ are dominated by water content or volume (Eq.(8.3) and Eq.(8.4)), it is reasonable to assume that they will not change after releasing the swelling pressure. According to Eq.(8.5), μ_{0}^{m} are dominated by the molarity of solutes. Because the unloading does not change the mass of solutes and the water content, μ_{0}^{m} remains after releasing the swelling pressure. This is also true for μ_{0}^{M}. Thus, $(\mu_{\mathrm{f}}^{\mathrm{m}} + \mu_{\mathrm{e}}^{\mathrm{m}} + \mu_{0}^{\mathrm{m}})$ or ψ_{t} remains unchanged before and after releasing the swelling pressure.

Moreover, undrained unloading will induce an negative pore water pressure or capillary suction $(u_{\mathrm{a}} - u_{\mathrm{w}})$ (Lambe & Whitman, 1969; Nagaraj et al., 1994; Singhal et al., 2015). Since the effective stress of a soil sample remains during undrained unloading, a decrease in the net mean stress will be balanced by an equal increase in $(u_{\mathrm{a}} - u_{\mathrm{w}})$ (Lambe & Whitman, 1969; Nagaraj et al., 1994). Thus, the total potential of macrostructural pore water after releasing swelling pressure $(\mu_{\mathrm{M}}^{\mathrm{un}})$ changes to the expression shown in Eq.(8.16).

$$\mu_{\mathrm{M}}^{\mathrm{un}} = \mu_{0}^{\mathrm{M}} - (u_{\mathrm{a}} - u_{\mathrm{w}})\overline{v}_{\mathrm{w}} = \mu_{0}^{\mathrm{M}} - P_{\mathrm{s}}\overline{v}_{\mathrm{w}} = -(\psi_{\mathrm{a}} + P_{\mathrm{s}})\overline{v}_{\mathrm{w}} \tag{8.16}$$

Because of the removal of the swelling pressure, the total potential of microstructural pore water $(\mu_{\mathrm{m}}^{\mathrm{un}})$ is reduced to Eq.(8.17).

$$\mu_{\mathrm{m}}^{\mathrm{un}} = \mu_{\mathrm{f}}^{\mathrm{m}} + \mu_{\mathrm{e}}^{\mathrm{m}} + \mu_{0}^{\mathrm{m}} = -\psi_{\mathrm{t}}\overline{v}_{\mathrm{w}} \tag{8.17}$$

Comparison of Eq.(8.16) and Eq.(8.17) indicates that the total potential of macrostructural pore water is still equal to the total potential of microstructural pore water after releasing the swelling pressure. In other word, the thermodynamic equilibrium remains during undrained unloading, which certifies that there is no water exchange between macro-pore and micropore water or that the assumption of undrained unloading is reasonable. Thus, after releasing the swelling pressure, measured total suction of saturated bentonite will be equal to not only the capillary suction due to releasing swelling pressure but also the total suction (ψ_t) of the saturated bentonite under constant volume condition. Consequently, ($\mu_\mathrm{f}^\mathrm{m} + \mu_\mathrm{e}^\mathrm{m} + \mu_0^\mathrm{m}$) or ψ_t can be also determined by a chilled mirror hydrometer after releasing swelling pressure.

8.3 Results and discussion

8.3.1 Linkage between swelling pressure, total suction of saturated bentonites and suction of hydrating fluids

8.3.1.1 Swelling pressure

The elapsed time versus swelling pressure test results for the bentonite samples CB-0 to CB-7 are shown in Figure 8.2(a). Similarly, Figure 8.2(b) presents the evolution of swelling pressures in case of the samples CB-7, CB-8, CB-9, and CB-10 that were hydrated with 0.0001, 0.5, 1.0 and 2.0 M $CaCl_2$ solutions, respectively. Swelling pressure equilibrium time was defined as the time when variation of swelling pressure started to be less than 5 kPa per day. The swelling pressure equilibrium time was found to increase with an increase in the sample dry density (Figure 8.2(a)). The equilibrium time for sample CB-0 (dry density = 1.2 Mg/m^3) was about 60 h, whereas it was found to be about 440 h for sample CB-6 with a compaction dry density of 1.83 Mg/m^3. For a given dry density of 1.59 Mg/m^3, the type of hydrating fluid (i.e., water or $CaCl_2$ solutions) had no significant influence on the equilibrium time. In this case, the swelling pressure equilibrated in about 270 h.

An increase in the swelling pressure equilibrium time with an increase in the dry density is attributed to an increase in the static compaction pressure which in turn affects the pore-size distribution and permeability of compacted bentonites (Pusch, 1980*a*; Lloret et al., 2003). Studies on the pore size distribution (PSD) of the compacted clays have shown dual-structure pore size distributions with intra-aggregate and inter-aggregate pores (Sridharan et al., 1971; Pusch & Yong, 2006; Delage et al., 2006). As the dry density increases, the inter-aggregate pore size decreases, whereas the intra-aggregate pore size remains almost constant (Lloret et al., 2003; Romero & Simms, 2008; Li & Zhang, 2009; Wang et al., 2013a; Seiphoori et al., 2014). The flow of liquid water in compacted bentonites initially occurs within the inter-aggregate pores and then in the intra-aggregate pores. The diffusion of water molecule into the interlayer of particles causes crystalline swelling

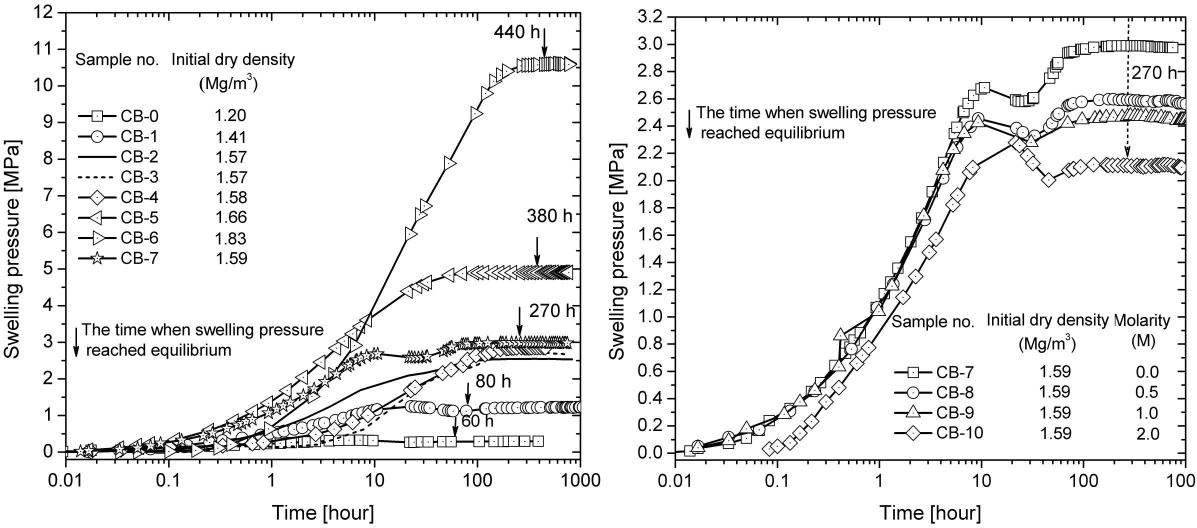

(a) (b)

Figure 8.2: Elapsed time versus swelling pressure for the samples (a) saturated with deionized water and (b) saturated with $CaCl_2$ solutions of different concentrations

in dry bentonites (Norrish, 1954). Further increase in the water content (beyond crystalline swelling) causes osmotic swelling (Van Olphen, 1977). Since the permeability of the compacted bentonites is mainly governed by the inter-aggregate pores, a reduction in size of the inter-aggregate pores either due to an increase in compaction dry density or due to swelling decelerates the development of swelling pressure.

The effects of sample dry density and concentration of the hydrating fluid on the equilibrium swelling pressure are presented in Figures 8.3(a) and 8.3(b), respectively. The magnitude of swelling pressure at equilibrium was found to be influenced by the sample dry density and $CaCl_2$ concentration. As can be seen from Figure 8.3(a), with deionized water as the hydrating fluid the swelling pressure increased from 0.3 to about 10.5 MPa with an increase in the dry density from 1.20 to 1.83 Mg/m^3. The differences in the swelling pressures of samples CB-2, CB-3, and CB-4 (dry density = 1.57 Mg/m^3) remained less than about 0.5 MPa. The swelling pressure increase was found to be more intense within a range of dry density of 1.50 to 1.83 Mg/m3. Based on the diffuse double layer theory as applicable to interacting clay platelet systems, a dry density of 1.50 Mg/m^3 for Calcigel bentonite corresponds to a clay platelet separation distance of about 0.94 nm (Schanz & Tripathy, 2009). Schanz & Tripathy (2009) stated that for compaction dry densities greater than 1.50 Mg/m^3 the swelling pressures of Calcigel bentonite is influ-

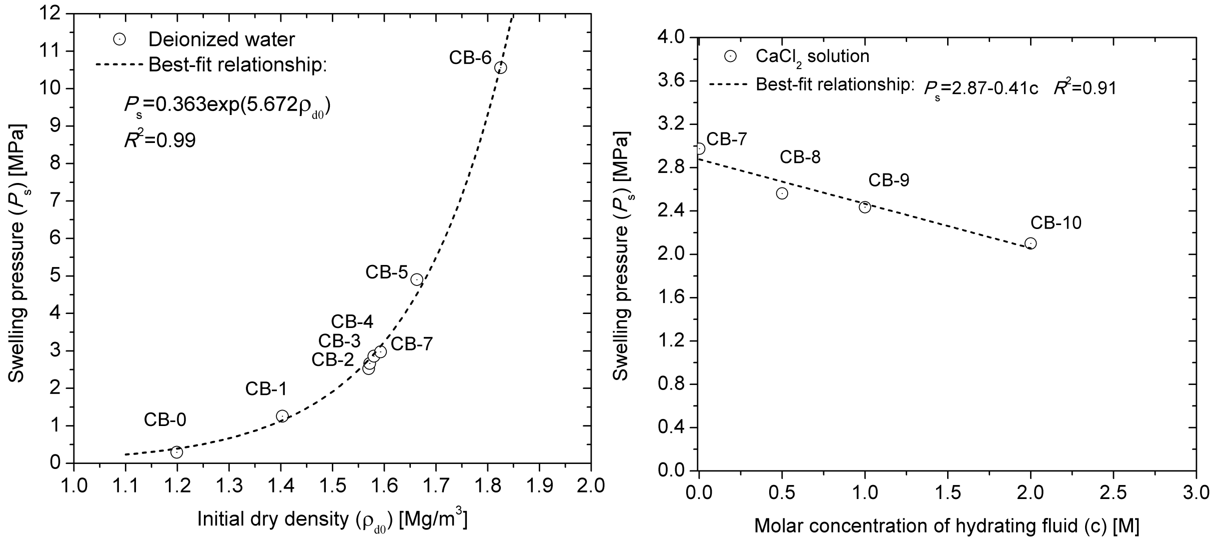

(a) (b)

Figure 8.3: Effects of (a) initial dry density and (b) $CaCl_2$ concentration on swelling pressure

enced by the presence of significant amount of divalent exchangeable cations that produce greater hydration energy at close particle spacing.

In the case of samples with a constant dry density of 1.59 Mg/m^3, the swelling pressure decreased with an increase in $CaCl_2$ concentration (Figure 8.3(b)). A reduction in the swelling pressure from 2.98 to 2.10 MPa was found to occur (i.e. a decrease of about 30%) when the concentration of $CaCl_2$ was increased from 0.0001 to 2.0 M. Similar experimental results concerning the influence of dry density and salt solution concentration on the swelling pressure have been reported by several researchers (Pusch, 1980*b*; Bucher & Max, 1989; Pusch et al., 1990; Karnland et al., 2005; Villar & Lloret, 2008; Castellanos et al., 2008; Zhu et al., 2013; Tripathy et al., 2014b).

8.3.1.2 Water content and total soil suction profiles

The profiles of the water content and total suction for the bentonite samples CB-0 to CB-6 that were saturated with deionized water are presented in Figure 8.4. Similarly, the profiles of the water content and total suction for the samples CB-7 to CB-10 that were saturated with $CaCl_2$ solutions are shown in Figure 8.5. Due to the water uptake by the samples during the swelling pressure tests, the water contents of the samples at the end of the swelling pressure tests were found to be higher than the initial water contents

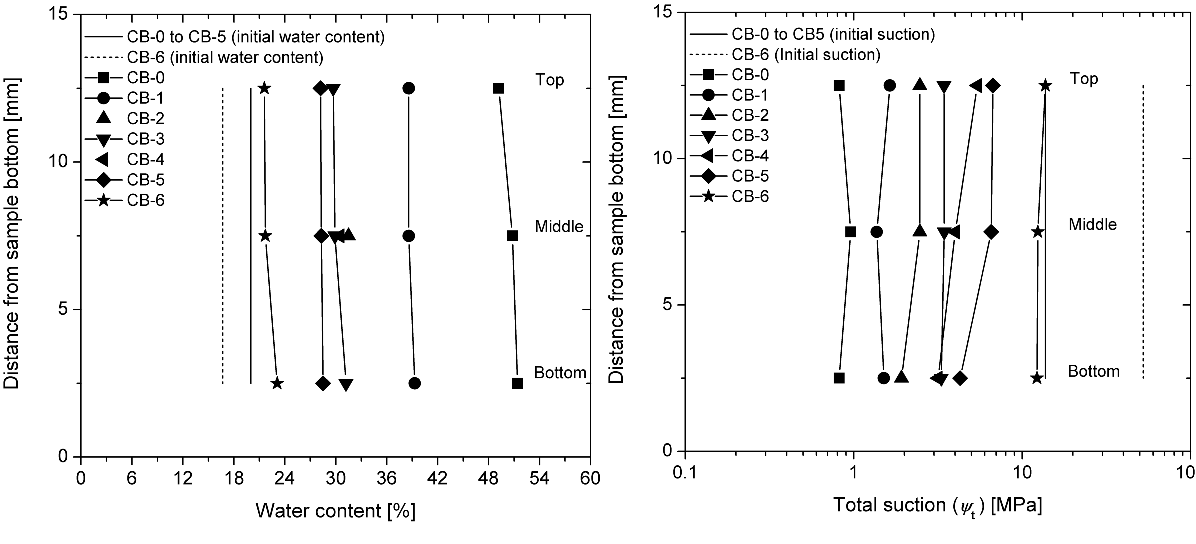

(a) (b)

Figure 8.4: Profiles of (a) water content and (b) total suction for the swelling pressure tests with deionized water (water contents of CB-2 and CB-4 correspond to mean water contents)

(Figures 8.4(a) and 8.5(a)). For any sample, the final water content remained nearly constant along the depth of the sample. The degree of saturation of all samples tested was determined based on the final water contents, the dimensions of the samples and the volume-mass relationships. The degree of saturation of all samples indicated that the samples were fully saturated at the end of the swelling pressure tests.

As compared to the initial total suctions, the total suctions of the samples at the end of the swelling pressure tests were found to have decreased (Figures 8.4(b) and 8.5(b)). The suction profiles in most cases were found to be uniform. A variation of suction along the depth of sample CB-4 was noted, in which case the total suction towards the top of the sample was found to be greater than that occurred towards the bottom (Figure 8.4(b)). The variation of the total suction along the depth of sample CB-4 is attributed to a lesser testing time (19 days) as against samples CB-2 and CB-3 that had similar compaction conditions, but tested for longer durations (more than 32 days). The test results demonstrated that while an equilibrium in terms of swelling pressure was attained by sample CB-4 in less than about 12 days (Figures 8.2(a)), however, an equilibrium in terms of total suction required a much longer testing time as seen from the test results of samples CB-3 and CB-4.

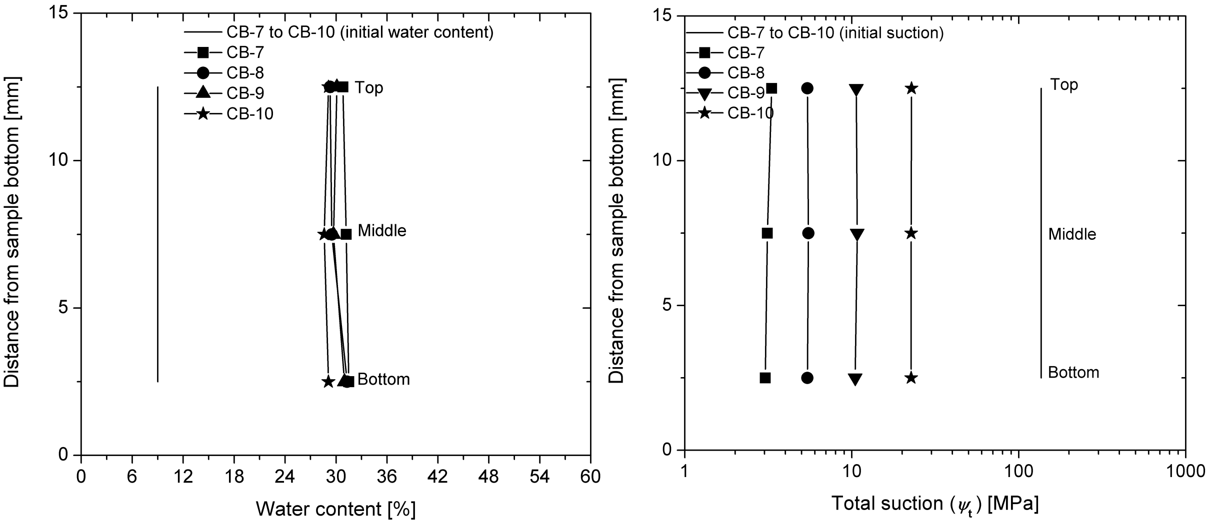

(a) (b)

Figure 8.5: Profiles of (a) water content and (b) total suction for the swelling pressure tests with $CaCl_2$ solutions

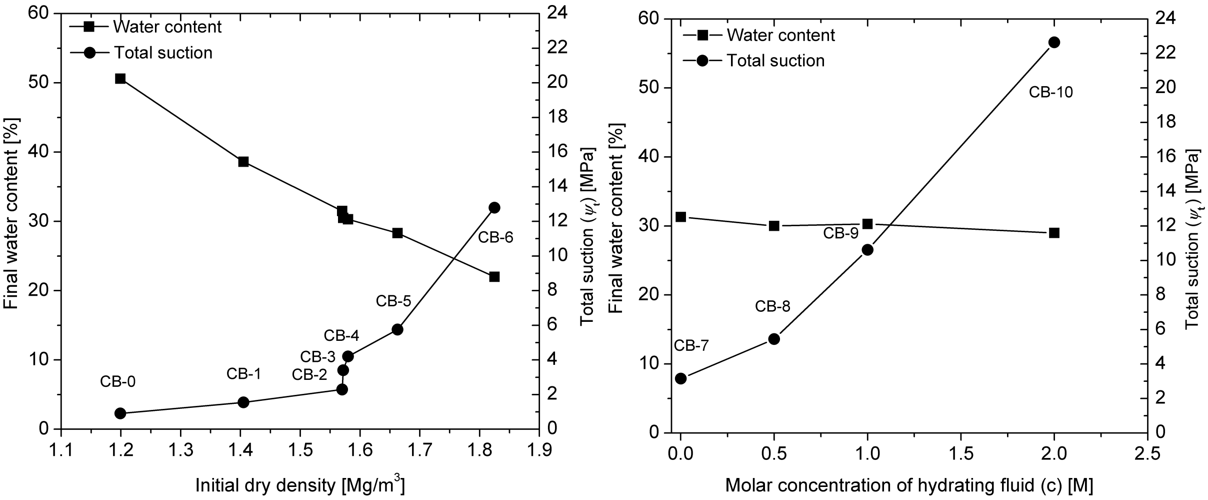

(a) (b)

Figure 8.6: Effects of (a) initial dry density and (b) $CaCl_2$ concentration on the water content and total suction of the saturated bentonite samples after swelling pressure tests

The effect of dry density on the final water content and total suction of the samples tested with deionized water is shown in Figure 8.6(a). The average values of the final water contents and total suctions were used in Figure 8.6(a). With an increase in the dry density, the final water content decreased and the total suction was found to increase.

The decrease in the saturated water content with dry density is due to a decrease in the void ratio of the bentonite. The amount of water present in the saturated bentonite affects the total suction and the magnitude of total suction depends on the dry density of the bentonite. At high dry densities, the capillary effect disappears and the electrical double layer is suppressed, but the short-range adsorption effects (surface and ion hydration within the interlayers) remain (Yong, 1999; Schanz & Tripathy, 2009). In this case, matric suction due to the short-range adsorption effects contribute to the total suction and its magnitude increases with a decrease in the thickness of water layer within the interlayers. At low dry densities, the matric suction due to the short-range adsorption effects disappears, whereas the one due to the electrical double layer forces remains. Its magnitude decreases with an increase in the water content or a decrease in the dry density (Yong, 1999; Tripathy et al., 2014a).

The concentration of $CaCl_2$ in the hydrating fluid affected the measured total suctions of samples CB-7 to CB-10 (Figure 8.6(b)). Since the samples had the same dry density, the saturated water contents remained similar regardless of the concentration of the hydrating fluid. However, the total suction increased significantly with an increase in the $CaCl_2$ concentration. With an increase in the $CaCl_2$ concentration from 0.0001 to 2.0 M, the total suction increased from 3.2 to 22.7 MPa. The increase in the total suction with the $CaCl_2$ concentration is attributed primarily to an increase in osmotic suction caused by an increase in amount of dissolved salts ($CaCl_2$) in the pore fluid (Rao & Thyagaraj, 2007; Musso et al., 2013).

8.3.1.3 Total suction and swelling pressure

The experimental results presented in Figures 8.3 and 8.6 demonstrated that both swelling pressure and total soil suction were dependent on the dry density of the bentonite and salt concentration of the hydrating fluid. The measured total suction versus swelling pressure plot is shown in Figures 8.7. For the bentonite samples that were hydrated with deionized water (samples CB-0 to CB-7), with an exception of sample CB-0, the measured total suction was nearly equal to the swelling pressure. For sample CB-0, the measured total suction (0.8 MPa) was greater than the swelling pressure (0.3 MP), which was probably due to a significant total suction measurement error. As mentioned in the section of materials and methods, the total suction measurement error was upto ±140% if the total suction of a soil was less than 0.3 MPa. If the total suction of a soil sample was equal to 0.3 MPa, the total suction measured by the device could vary from 0 to 0.8 MPa at 22°C due to the accuracy of the chilled-mirror hygrometer. This significant error (i.e. ±140%) could overestimate the real total suction of sample CB-0. In case of the samples that were hydrated with $CaCl_2$ solutions (samples CB-8 to CB-10), the measured total suction was considerably greater than the corresponding swelling pressure. The test results demonstrated that if the hydrating fluid was water ($\psi_a = 0.001$ MPa), there was a good agreement between the measured swelling pressures and the total suctions of the bentonite. Disagreement between total suction and swelling pressure was only observed for the samples that were hydrated with solutions having high salt concentration.

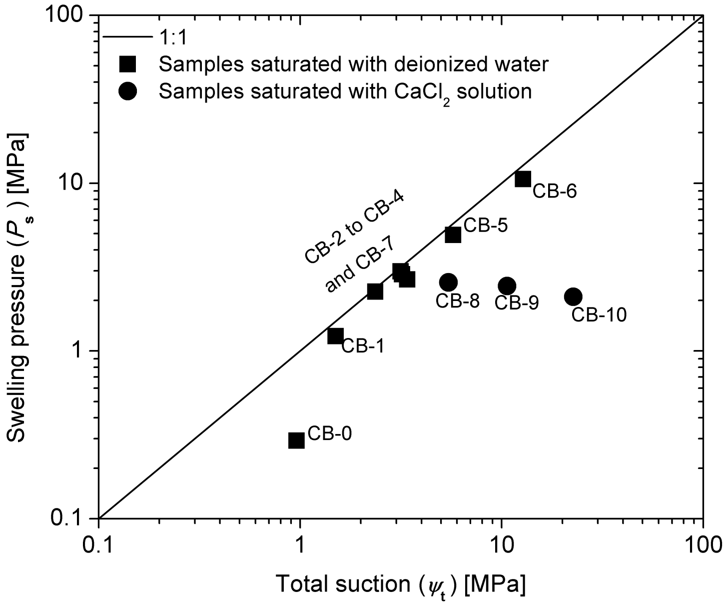

Figure 8.7: Total suction versus swelling pressure plot for saturated bentonite samples at the end of swelling pressure tests

8.3.1.4 Suction of hydrating fluid and total suction

The suctions of the aqueous solutions used for hydrating the bentonite samples versus the measured total suctions of the samples are presented in Figure 8.8. As can be expected, the measured total suctions of the samples that were saturated with deionized water (samples CB-0 to CB-7) far exceeded the suction of water ($\psi_a = 0.001$ MPa). The measured total suctions of these samples increased from 0.8 MPa to 12.8 MPa with an increase in the dry density from 1.2 to 1.83 Mg/m^3 (Fig. 7a). For samples CB-8 to CB-10 that were saturated with $CaCl_2$ solutions, the total suctions were found to be greater than the suctions of aqueous solutions, too. For these samples, the total suction increased from 5.4 to 22.7 MPa with an increase in the suction of $CaCl_2$ solutions from 3.0 to 20.6 MPa.

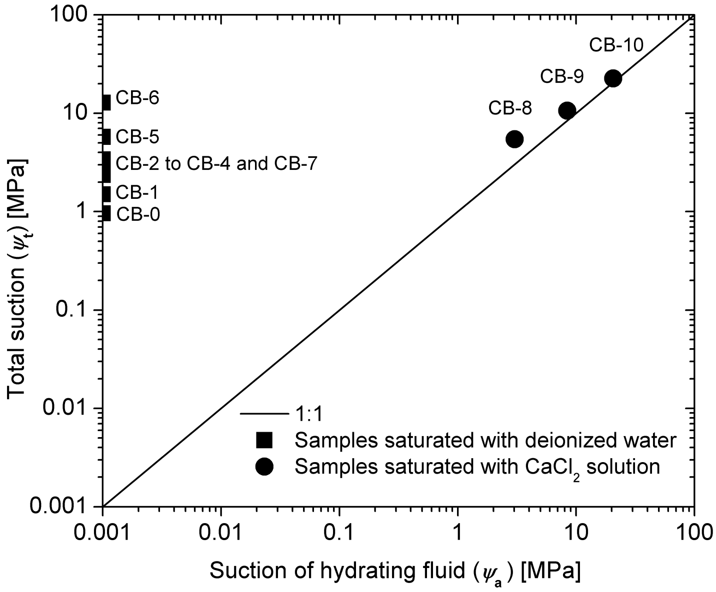

Figure 8.8: Suction of hydrating fluid versus total suction of the saturated samples at the end of the swelling pressure tests

8.3.1.5 Swelling pressure and difference in total suction and suction of hydrating fluid

The swelling pressures (P_s) of the samples are plotted against the differences in total suctions ($\psi_t - \psi_a$) of saturated bentonite samples and suctions of the hydrating fluids in Figure 8.9. The results for the bentonite samples that were tested with water as the hydrating fluid are presented in Figure 8.9(a), whereas the results for samples that were hydrated with $CaCl_2$ solutions are given in Figure 8.9(b). Moreover, the test results reported by Karnland et al. (2005) on a Na bentonite are also shown in Figure 8.9(a) for the tests with water and in Figure 8.9(b) for the tests with various NaCl solutions. In their study, the compacted Na bentonite samples under constant volume condition were saturated with a concentration from 0.0001 to 3 M NaCl solutions. After the swelling pressures reached equilibrium, the samples were extracted from constant volume device for

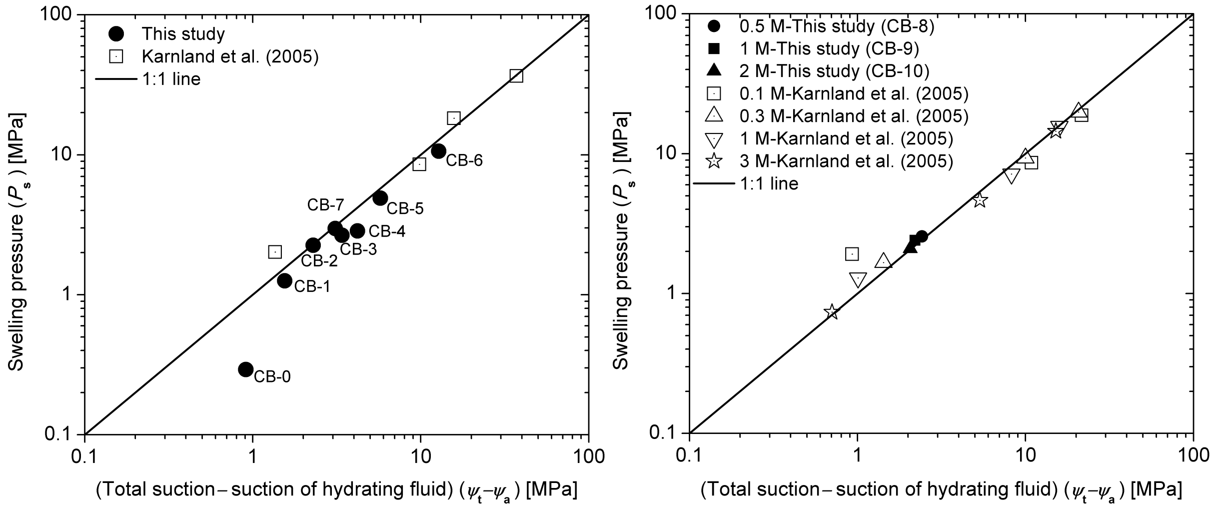

(a) (b)

Figure 8.9: Difference in total suction of saturated bentonites and suction of hydrating fluid versus swelling pressure in the case of tests with (a) deionized water and (b) various salt solutions

total suction measurement. Details for the material and experimental methods and results could be found in their publication. Because the suctions of the various concentrations of NaCl were not measured in their study, these suctions were determined based on a method proposed by Lang (1976).

With the exception of sample CB-0, the difference in the total suction of a sample and suction of the hydrating fluid used to saturate the sample was nearly equal to the swelling pressure for both bentonites. The results presented in Figure 8.9 validated Eq.(8.14) that was derived based on thermodynamics of soil moisture considerations. For sample CB-0, the difference in the total suction and suction of deionized water used to saturate the sample was found to be greater than the swelling pressure. For this sample, the swelling pressure and the total suction was 0.3 MP and 0.8 MPa, respectively. As mentioned in the section of total suction and swelling pressure, the significant total suction measurement error (i.e. ±140%) could overestimate the real total suction of sample CB-0. Consequently, the difference in the total suction of sample CB-0 and suction of deionized water used to saturate the sample was found to be greater than the swelling pressure.

The results in Figure 8.9 show that there is a strong linkage between swelling pressure, total suction of saturated bentonite and suction of hydrating fluid. Measurements of any two parameters would be sufficient to assess the unknown parameter. The linkage between these three parameters indicates that total suction of a bentonite due to the adsorptive and osmotic forces would not dissipate when the bentonite under constant volume condition is saturated with aqueous solution.

8.3.2 Linkage between swelling pressure and total suction of saturated bentonite-sand mixtures

The difference in the total suction of saturated bentonite-sand mixture and suction of hydrating fluid versus swelling pressure in the case of tests with deionized water are presented in Figure 8.10. The experimental data shown in Figure 8.10 were collected from the swelling pressure test results presented in Table 5.2, chapter 5 and from the consolidation test results given in Table 6.1, chapter 6. In case of the consolidation test results, the vertical net stress was assumed to be equal to swelling pressure. In addition, the experimental data reported by Arifin (2008) for a heavily compacted bentonite-sand mixture are also presented in Figure 8.10.

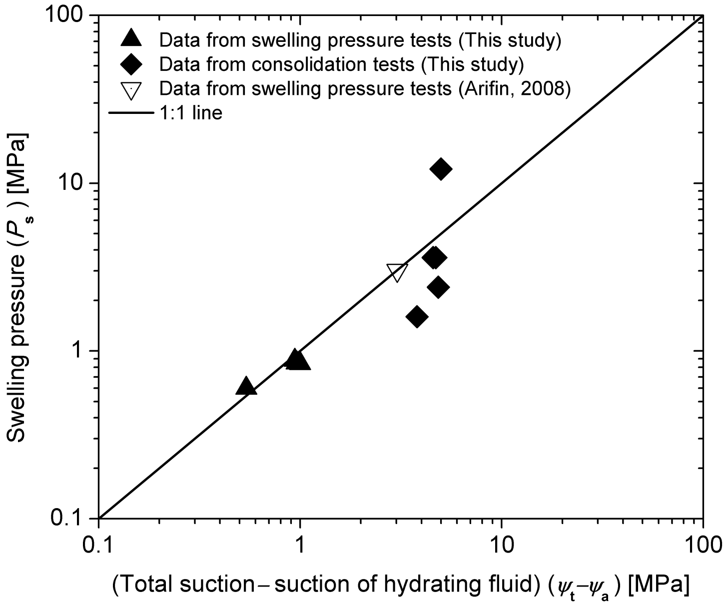

Figure 8.10: Difference in total suction of saturated bentonite-sand mixture and suction of hydrating fluid versus swelling pressure in the case of tests with deionized water

According to Figure 8.10, the difference in the total suction of a sample and suction of the hydrating fluid used to saturate the sample was almost equal to the swelling pressure for bentonite-sand mixture. The results presented in Figure 8.10 validated Eq.(8.14) that was derived based on thermodynamics of soil moisture considerations.

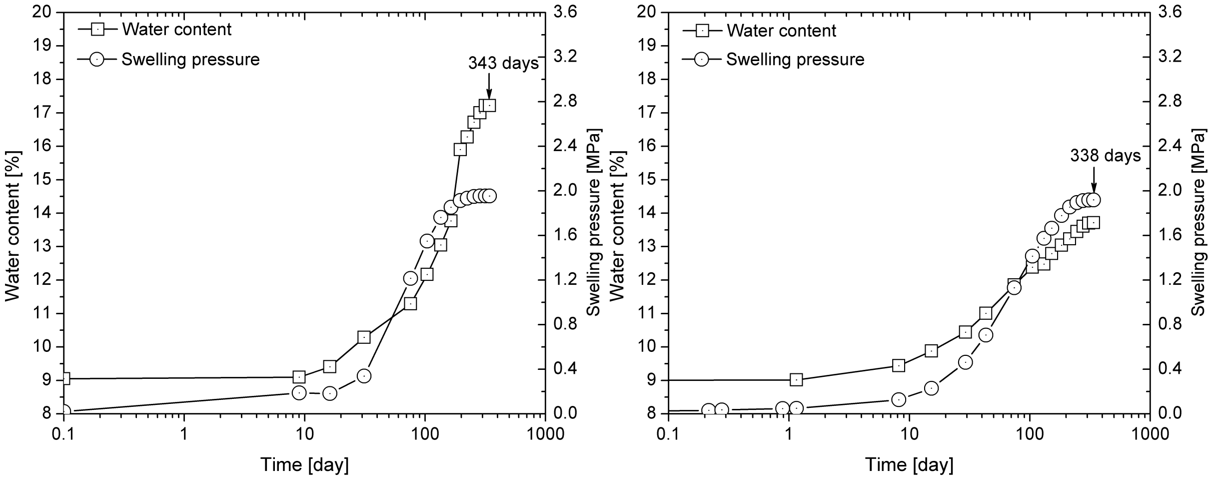

(a) (b)

Figure 8.11: Evolution of water content and swelling pressure for compacted bentonoite samples CB-11 and CB-12 wetted with water vapour under a controlled suction of (a) 10.1 MPa and (b) 38.6 MPa

8.3.3 Linkage between swelling pressure, total suction of unsaturated bentonite-based materials and applied suction

The evolution of water content and swelling pressure for compacted bentonoite samples CB-11 and CB-12 hydrated with water vapour under a controlled suction of (a) 10.1 MPa and (b) 38.6 MPa is shown in Figure 8.11. Equilibrium time was defined as the time when both water content and swelling pressure reached constant. For both samples, the establishment of equilibrium took nearly one year and thus, was extremely slow. In addition, the equilibrium water content and swelling pressure depended on the applied suction. For the case of the controlled suction of 10.1 MPa, the equilibrium water content and swelling pressure were 17.2% and 1.95 MPa, respectively. In the case of the controlled suction of 38.3 MPa, the equilibrium water content and swelling pressure were 13.7% and 1.92 MPa, respectively.

After both water content and swelling pressure reached equilibrium, the samples CB-11 and CB-12 were expelled from the isochoric cell for further measuring their total suctions and water contents. The equilibrium water content, swelling pressure and the measured total suctions are summarized in Table 8.1.

According to Table 8.1, the applied suction was not equal to but significantly less than the measured total suction, which was consistent with the finding presented in section

Table 8.1: Swelling pressure and final conditions of unsaturated bentonite

Sample no.	Applied suction[a]	Swelling pressure	Final dry density[b]	Water content	Degree of saturation[b]	Total suction[a]
(-)	(MPa)	(MPa)	(Mg/m^3)	(%)	(%)	(MPa)
CB-11	10.1	1.95	1.53	17.2	57.5	28.12
CB-12	38.6	1.92	1.53	13.7	46.0	45.77

a was determined by chilled-mirror hygrometer; *b* was determined after releasing swelling pressure.

4.2.5 for bentonite-sand mixture. In addition, the difference in the total suction and the applied suction was found to be not equal to but significantly greater than the swelling pressure. The same conclusion could be also drawn for bentonite-sand mixture according to the experimental results presented in section 4.2.5. Therefore, Eq.(8.14) was not effective in unsaturated condition and a modified equation, i.e. Eq.(8.18), was proposed according to the experimental results above.

$$\alpha(\psi_{\mathrm{t}} - \psi_{\mathrm{a}}) = P_{\mathrm{s}} \tag{8.18}$$

with

$$0 \leq \alpha \leq 1 \tag{8.19}$$

In Eq.(8.18), α is a parameter expressing the fraction of the difference in total suction between microstructural pore and macrostructural pore which is effective in inducing the swelling pressure. α increases with the normalized degree of saturation S_{n} (see Eq.(5.2)) and increases to the maximum value, 1, when the bentonite-based materials reach saturation.

According to the experimental data presented in Table 8.1 and section 4.2.5, α could be determined using Eq.(5.2) and Eq.(8.18). The normalized degree of saturation versus parameter α is shown in Figure 8.12. α increased with increasing the normalized degree of saturation. Moreover, the relationship between α and the normalized degree of saturation could be characterized by Eq.(8.20) where a, k and c are fitting parameters. Thus, α was a function of the normalized degree of saturation.

$$\alpha = ae^{-e^{-k(S_{\mathrm{n}}-c)}} \tag{8.20}$$

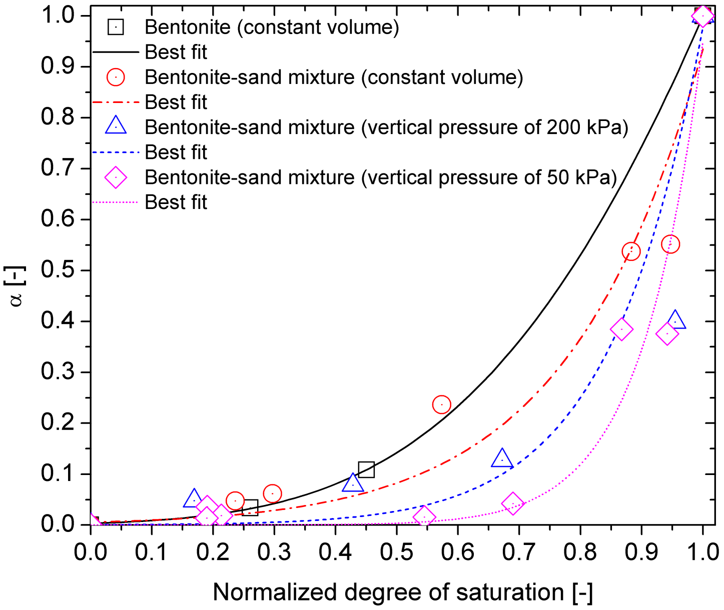

Figure 8.12: Normalized degree of saturation versus parameter α

8.3.4 Relationship between total suction and water content in bentonite-based materials

The experimental data in terms of the measured total suction versus water content for compacted bentonite samples (i.e. CB-0 to CB-7, CB-11 and CB-12) wetted with deionized water and water vapour are presented in Figure 8.13. In addition, the drying-wetting WRCs of bentonite determined under unconfined condition are also given in Figure 8.13. The measured total suction versus water content for samples CB-0 to CB-7, CB-11 and CB-12 were almost located on the wetting WRC, suggesting that the relationship between total suction and water content was unique for bentonite. The similar experimental results could be also found in previous chapters (i.e. Figures 4.14, 5.11 and 6.14) for bentonite-sand mixture.

Experimental data in terms of the measured total suction versus bentonite water content for both bentonite samples and bentonite-sand mixtures samples are presented in Figure 8.14. In addition, the experimental data corresponding to the wetting WRCs are also presented in Figure 8.14. In Figure 8.14, symbols with half filling represent the experimental data of bentonite samples, whereas the other symbols represent the experimental data of bentonote-sand mixture samples.

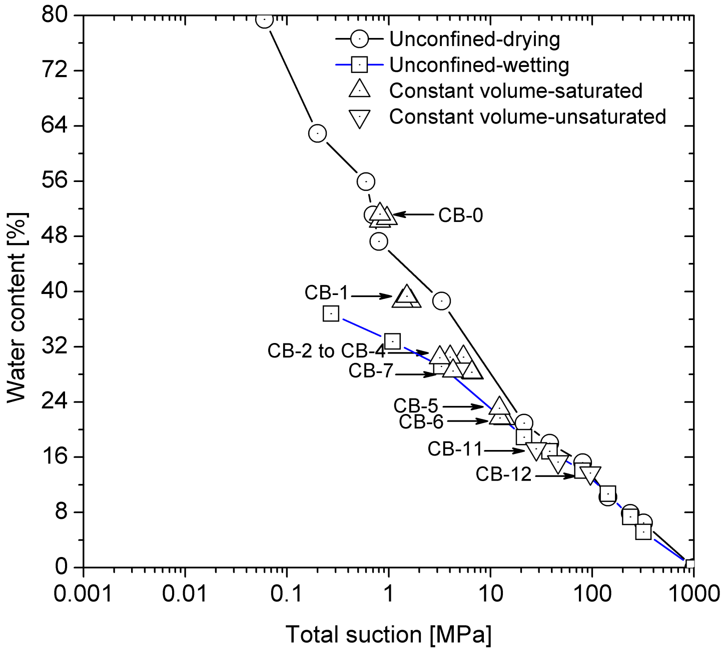

Figure 8.13: Total suction versus water content for bentonite

According to Figure 8.14, there was an unique relationship between the measured total suction and bentonite water content. Furthermore, this unique relationship could be characterized by Eq.(8.21). In Eq.(8.21), w_{b} is the bentonite water content (%) and a and b are fitting parameters. According to the best fit performed in Figure 8.14, the fitting parameters a and b are equal to -6.0 and 39.7, respectively. Because the relationship between the total suction and water content for bentonite was unique and independent of the boundary conditions, Eq.(8.21) provided a method for determining the total suction of bentonite based on water content.

$$w_{\mathrm{b}} = b\ln(\psi_{\mathrm{t}}) + a \tag{8.21}$$

8.4 Summary

Swelling pressure tests and suction measurements were performed on bentonite-based materials to explore the quantitative effect of hydro-chemical boundary conditions on swelling capacity of buffer, backfill and sealing materials. The link between swelling pressure, total suction and applied suction was examined under saturated and unsaturated conditions. For saturated bentonite-based materials, an equation describing the link between swelling pressure, total suction and the suction of aqueous solutions used to saturate

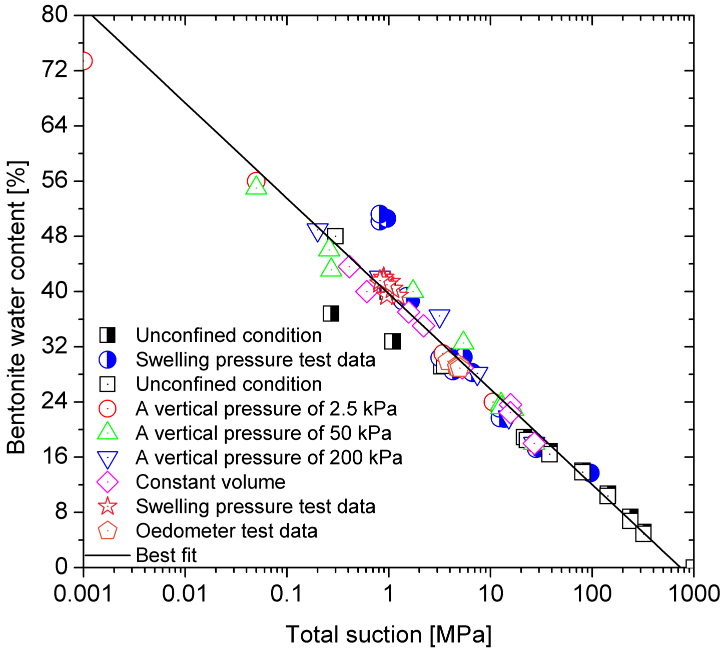

Figure 8.14: Total suction versus bentonite water content (symbols with half filling are the experimental data of bentonite, whereas the other symbols are the experimental data of bentonote-sand mixtures)

bentonite-based materials was derived based on the thermodynamics of soil-moisture. To validate the derived equation, laboratory tests involving swelling pressure tests with aqueous solutions and subsequent total suction measurements were carried out on compacted bentonite-based materials. For unsaturated bentonite-based materials, laboratory tests involving swelling pressure tests with suction control and subsequent total suction measurements were performed on compacted bentonite-based materials. According to the theoretical considerations, the experimental results and discussion, the following conclusions were drawn in this chapter.

1. An equation describing the linkage between the swelling pressure of saturated bentonite-based materials, total suction of saturated bentonite-based materials and the suction of hydrating fluids was proposed based on the thermodynamics of soil moisture. The linkage between these three parameters indicates that total suction of bentonite-based materials due to the adsorptive and osmotic forces would not dissipate when the bentonite-based materials under constant volume condition are saturated with aqueous solution.

2. When compacted bentonite under constant volume condition was saturated with liquid water, the time taken for the swelling pressure to reach an equilibrium increased with an

increase in the dry density of the bentonite. The increase in the time taken for reaching swelling pressure equilibrium with the dry density was attributed to a decrease in the permeability of the bentonite at high compaction dry densities.

3. In addition to the swelling pressure of the saturated bentonite, the total suction of the saturated bentonite was significantly affected by the compaction dry density of the bentonite and the salt concentration of the hydrating fluids, too. The increase in the total suction of the saturated bentonite with the compaction dry density results from the decrease in the amount of water present in the saturated bentonite. The increase in the total suction of the saturated bentonite with the salt concentration of the hydrating fluids is attributed primarily to an increase in the osmotic suction caused by an increase in the amount of dissolved salts in the macrostructural pore fluids.

4. The total suction of the saturated bentonite was nearly equal to the swelling pressure in case of water as the hydrating fluid. However, the total suction was significantly greater than the swelling pressure in case of $CaCl_2$ solutions as the hydrating fluid. Moreover, the total suction of the saturated bentonite was found to be greater than the suction of the hydrating fluids.

5. Based on the experimental results from this study and those reported in the literature it is found that the difference in the total suction of saturated bentonites and suction of aqueous solutions used to saturate the bentonites is approximately equal to the swelling pressure. In addition, the difference in the total suction of saturated bentonite-sand mixture and suction of aqueous solutions used to saturate the bentonite-sand mixture was also found to be approximately equal to the swelling pressure. The present finding extends the relationship suggested by Croney (1952); Kassiff & Shalom (1971); Towenr (1981); Karnland et al. (2005). Moreover, the present finding provides the framework for establishing quantitative linkage between swelling pressure of bentonite-based material and chemical boundary condition in the deep geological repository.

6. In unsaturated condition, the difference in the total suction and the applied suction was found to be not equal to but significantly greater than the swelling pressure for both bentonite and bentonite-sand mixture. A modified equation (i.e. Eq.(8.18)) characterizing the linkage between swelling pressure, total suction and applied suction in the case o unsaturated bentonite-based materials was proposed according to the experimental data. Future study should explore the physical meaning of parameter α in Eq.(8.18).

7. A unique relationship between the measured total suction and bentonite water content was found in bentonite-based materials. This unique linkage between total suction and

bentonite water content provides a method for determining the total suction of bentonite-based materials from measuring the water content of bentonite-based materials. The modified equation (Eq.(8.18)) and the unique relationship between the measured total suction and bentonite water content provide the framework for quantitatively estimating the effect of hydro-chemical boundary conditions on the swelling capacity of buffer, backfill and sealing materials.

9 Effect of desiccation on swelling pressure and permeability

9.1 Introduction

In the geological repository, compacted bentonite-based buffer blocks will be under thermal gradient for about three months before being wetted with water from the host rock (Johannesson et al., 2014). The effect of desiccation on the swelling behaviour and the permeability of clays have been only addressed in the frame of studies regarding cyclic wetting-drying behaviour (Osipov et al., 1987; Day, 1994; Al-Homoud et al., 1995; Alonso et al., 1999; Albrecht & Benson, 2001; Akcanca & Aytekin, 2014). However, the influence of the desiccation at elevated temperature on the swelling behaviour and the permeability of compacted bentonite-based materials has not been explored.

The objective of this study is to experimentally study the effect of the desiccation at elevated temperature on the swelling behaviour and the permeability of compacted bentonite-based materials. The experimental method is presented in section 3.3.6. In this chapter, sections 9.2.1 and 9.2.2 present measured water content and shrinkage strain, respectively, during the suction controlled desiccation tests. Section 9.2.3 presents swelling pressure test results for bentonite specimens dried under different suctions. Section 9.2.4 presents permeability test results for bentonite specimens dried under different suctions. Section 9.3 presents concluding remarks.

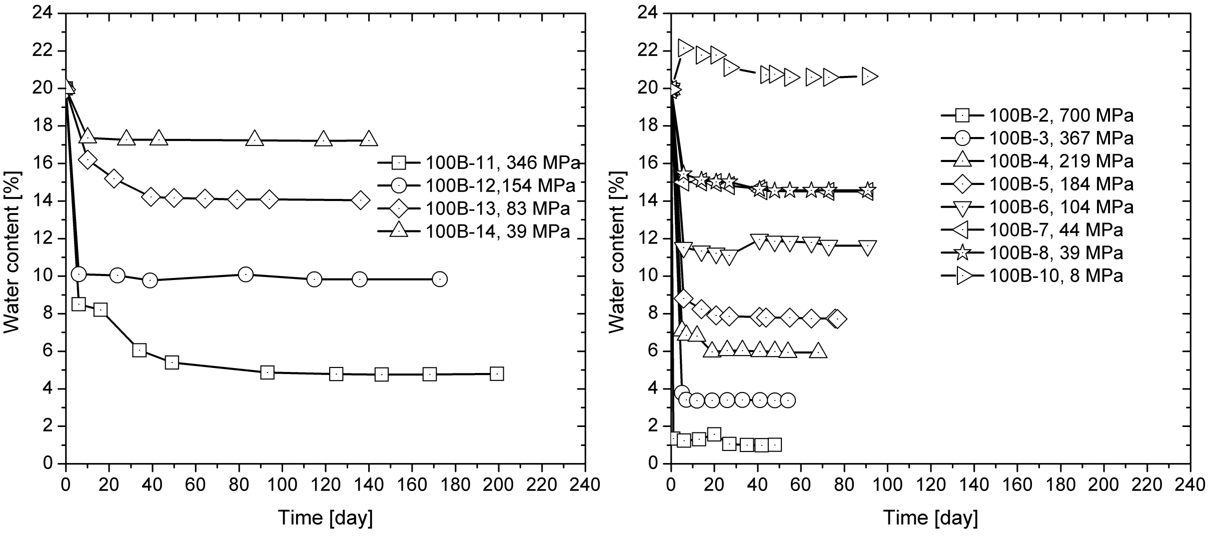

(a) (b)

Figure 9.1: Measured water content of compacted bentonite with elapsed time during the suction-controlled desiccation at (a) 22 and (b) 80°C (sample no. and applied suctions are given in legends)

9.2 Results and discussion

9.2.1 Desiccation-equilibrium water content and suction-water content relationship

Evolution of water content of compacted bentonite with time at different applied suctions is presented in Figure 9.1(a) for the drying tests at 22°C and in Figure 9.1(b) for the drying tests at 80°C. The equilibrium water contents of all specimens except for 100B-10 were found to be less than the initial water content of 20% since the applied suctions were greater than the initial suction of 14 MPa. For specimen 100B-10, its equilibrium water content (i.e. 20.7%) at an applied suction of 8 MPa was slightly greater than the initial water content. This implied that the suction corresponding to the water content of 20% at 80°C was greater than 8 MPa but less than 14 MP.

Similarly, evolution of water content of compacted bentonite-sand mixture with time at different applied suctions is presented in Figure 9.2(a) for the drying tests at 22°C and in Figure 9.2(b) for the drying tests at 80°C. According to Figures 9.2, the equilibrium water contents of all specimens were found to be less than the initial water content of 9% since the applied suctions were greater than the initial suction of 27 MPa.

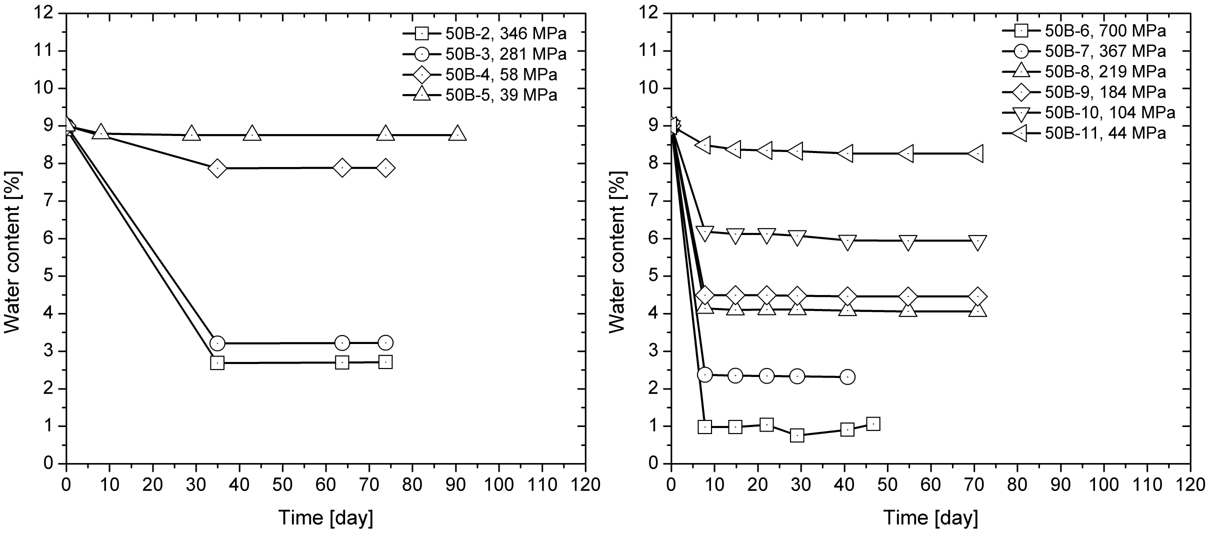

(a) (b)

Figure 9.2: Measured water content of compacted bentonite-sand mixture with elapsed time during the suction-controlled desiccation at (a) 22 and (b) 80°C (sample no. and applied suctions are given in legends)

A comparison of the suction-water content relationships at 22 and 80°C is shown in Figure 9.3(a) for compacted bentonote and in in Figure 9.3(b) for compacted bentonote-sand mixture. The comparison revealed that for a given applied suction, the measured water content was slightly smaller for the specimens subjected to 80°C than for the specimens subjected to 22°C. Similar experimental result was also reported by Villar et al. (2010) on compacted bentonite. The dependency of water retention on temperature is due to temperature dependency on surface tension and additional thermal disturbance altering clay fabric and intra-aggregate fluid chemistry (Romero et al., 2001; Villar et al., 2010).

In addition, the comparison of the suction-water content relationships at two temperatures also showed that for a given water content, the specimen suction was found to be smaller at the higher temperature. The experimental result above implies that once a thermal gradient is applied to the bentonite-based buffer materials with homogeneous initial water content, the suction of the buffer zone close to heating source decrease and thus a suction or hydraulic gradient occurs. This hydraulic gradient due to the thermal gradient, in turn, induce water movement from the low suction region to the high suction region of the buffer zone.

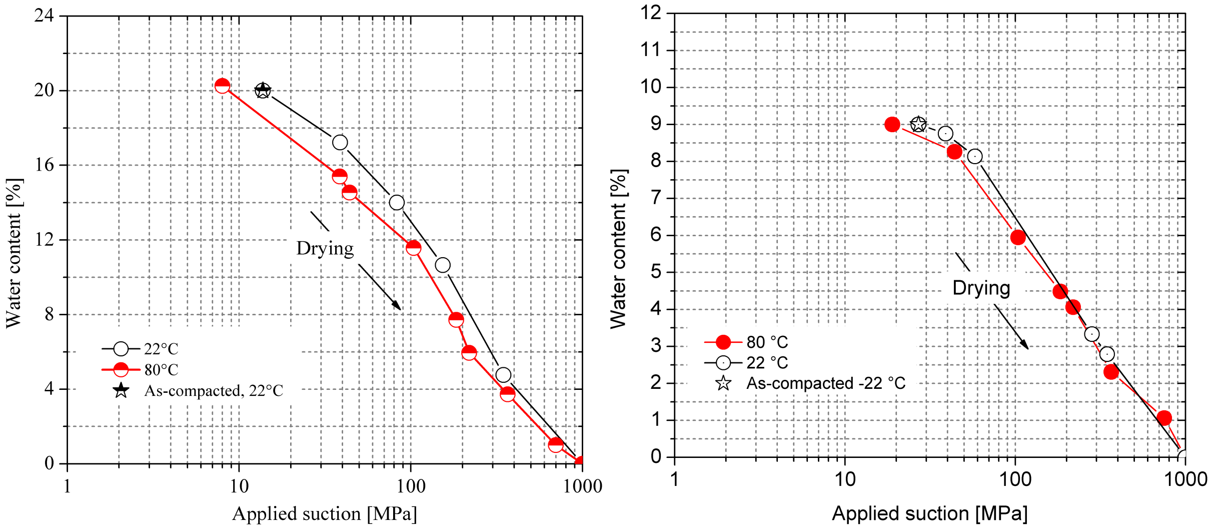

(a) (b)

Figure 9.3: Suction-water content relationships at 22 and 80°C for (a) compacted bentonite and (b) compacted bentonite-sand mixture

9.2.2 Desiccation-shrinkage strain

The measured axial, radial and volumetric strains against the applied suction for both temperatures are presented in Figures 9.4(a), 9.4(b) and 9.4(c), respectively, for compacted bentonite. Similarly, the measured axial, radial and volumetric strains against the applied suction for both temperatures are presented in Figures 9.5(a), 9.5(b) and 9.5(c), respectively, for compacted bentonite-sand mixture.

For a given temperature, the compacted bentonite exhibited significant volumetric shrinkage upon drying (Figures 9.4). From the initial state corresponding to 14 MPa suction and zero strain, the axial, radial and volumetric strains of compacted bentonite increased linearly with increasing suction up to about 400 MPa for a given temperature. Beyond the suction range of 400 MPa, a further suction increase did not induce further strains for a given temperature.

Unlike the compacted bentonite, the compacted bentonite-sand mixture exhibited slight volumetric swelling upon drying (Figures 9.5) for a given temperature. As the applied suction increased at a given temperature, the compacted bentonite-sand mixtures swelled slightly along the axial direction of specimens but remained almost unchanged along the radial direction of specimens.

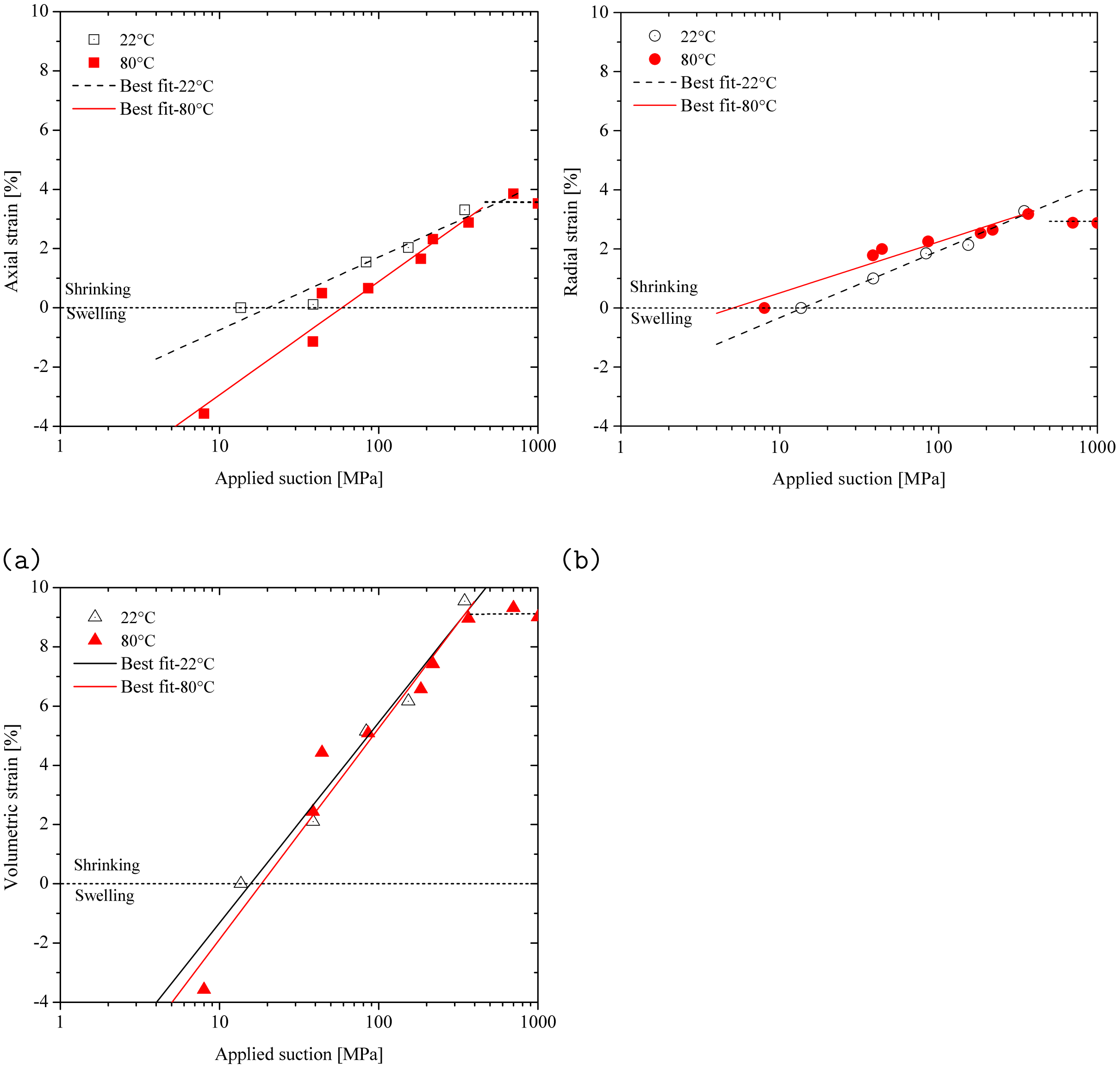

(a)

(b)

(c)

Figure 9.4: Applied suction versus (a) axial, (b) radial and (c) volumetric strains of compacted bentonite at 22 and 80°C

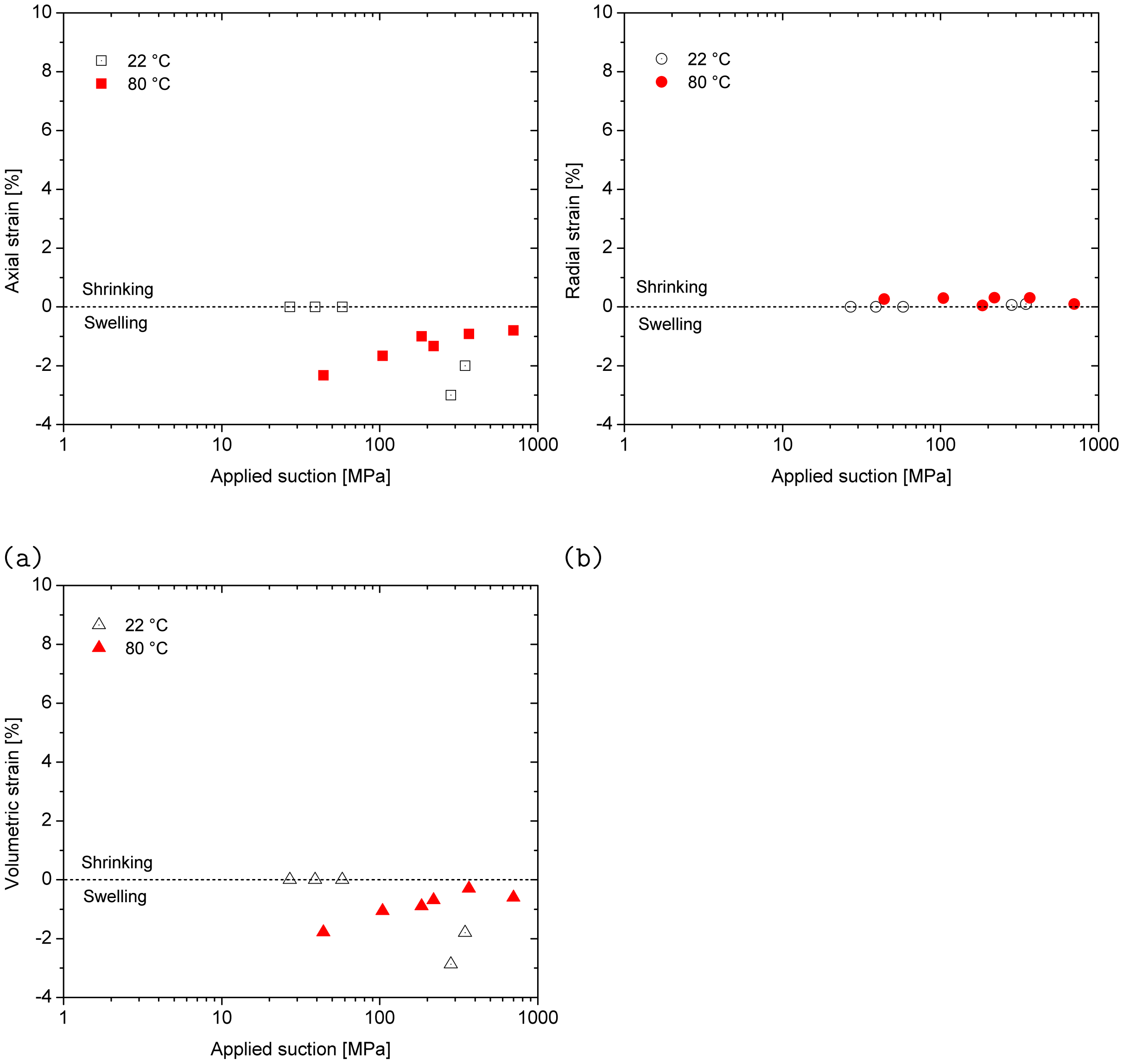

(a)

(b)

(c)

Figure 9.5: Applied suction versus (a) axial, (b) radial and (c) volumetric strains of compacted bentonite-sand mixture at 22 and 80°C

The shrinking/swelling behaviour of compacted bentonite-based materials upon drying was due to the competing effects of the shrinkage of clay particles due to dehydration and the swelling along axial direction due to dissipating the friction between the specimen and the specimen ring. For compacted bentonite, its initial water content (20%) was greater than its shrinkage limit (10%). Consequently, dehydration due to increasing the applied suction at a given temperature would result in volume reduction. For the case of compacted bentonite-sand mixtures, dehydration due to increasing the applied suction at a given temperature would not result in any more volume reduction since the initial water content (9%) of compacted bentonite-sand mixtures was less than the shrinkage limit (12%). Simultaneously, the dehydration due to increasing the applied suction at a given temperature would reduce the post-compaction residual lateral stresses due to the lateral restraint provided by the specimen ring. The decrease in post-compaction residual lateral stresses would decrease the friction between the specimen and the specimen ring. As the friction between the specimen ring and the lateral surface of the specimen decrease, the specimen tends to swell along the axial direction of the specimen (Dueck et al., 2014; Jayalath et al., 2016). When the volume reduction due to dehydration is greater than the volume increase due to the decrease in the friction between the specimen ring and the specimen, the volume of the specimens decreases upon drying. When the volume reduction due to dehydration is less than the volume increase due to the decrease in the friction forces between the specimen ring and the specimen, the volume of the specimens increases upon drying.

It should be noted that after the bentonite-sand mixture specimens underwent the dessication, it was observed that many sand grains came off the surface of the dried specimens. This suggested that the dessication caused the bond between clay particles and sand grains weakening or disappearing. This made it difficult to transfer the whole specimens into the isochoric swelling pressure device without mass loss. Consequently, the swelling pressure and hydraulic conductivity of the dried specimens 50B-2 to 50B-11 were not measured in this investigation.

9.2.3 Swelling pressure

9.2.3.1 Effect of temperature on swelling pressure

The influence of temperature on evolution of swelling pressure of compacted bentonite-based materials saturated with deionized water is presented in Figures 9.6. The swelling pressure of compacted bentonite-based materials saturated with deionized water decreased

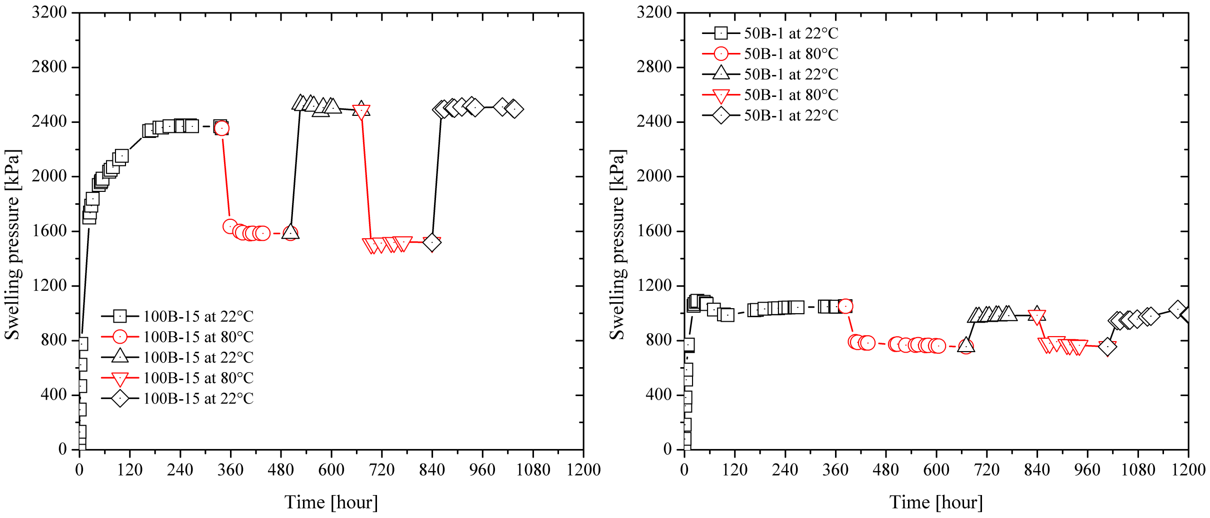

(a) (b)

Figure 9.6: The effect of temperatures on swelling pressure at saturation for (a) compacted bentonite and (b) compacted bentonite-sand mixture

with an increase in temperature. Moreover, the decrease in swelling pressure due to an increase in temperature was reversible. The similar experimental result was also reported by (Arifin, 2008) on heavily compacted bentonite-sand mixture.

The reversible decrease in swelling pressure of compacted bentonite-based materials due to an increase in temperature is attributed to the transfer of microstructural pore water to the macrostructural pore water triggered by temperature (Villar et al., 2010). Since the microstructural pore water (interlayer water and inter-particle water) dominates the crystalline swelling and DDL swelling, the decrease in microstructural pore water reduces the crystalline swelling and/or DDL swelling and the swelling pressure. Moreover, the microstructural pore is reversible upon drying-wetting cycles (Gens & Alonso, 1992). Therefore, the decrease in swelling pressure due to an increase in temperature was reversible.

9.2.3.2 Effect of desiccation on swelling pressure

Evolution of swelling pressure with elapsed time is presented in Figure 9.7(a) for the tests at 22°C and in Figure 9.7(b) for the tests at 80°C. The equilibrium swelling pressure was established faster at the elevated hydration temperature of 80°C. The swelling pressure equilibrium time for the specimens tested at 22°C was about 300 h, whereas the swelling pressure equilibrium time for specimens hydrated at 80°C was about 100 h. In addition,

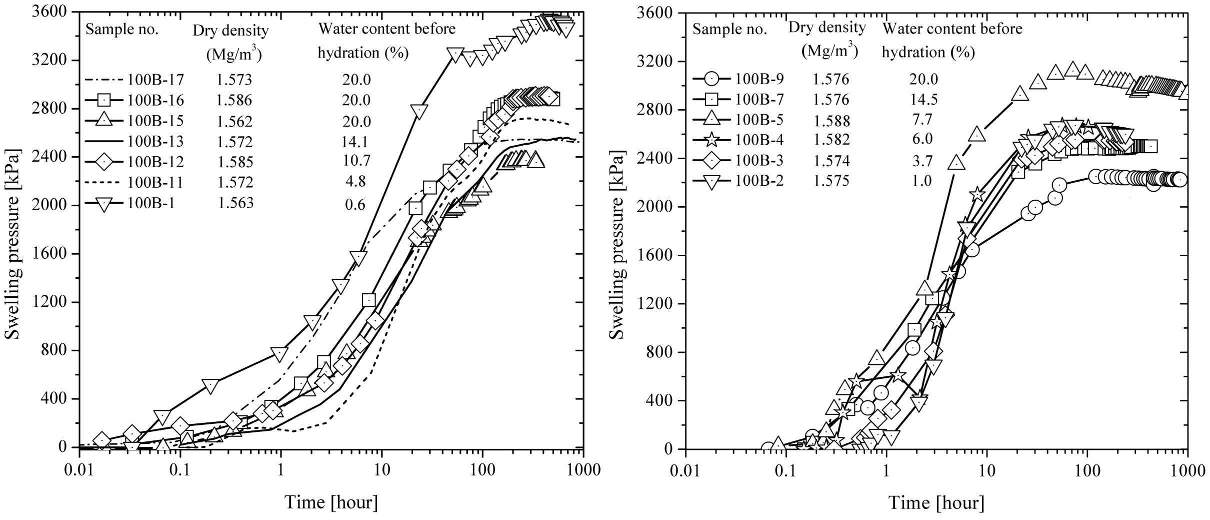

(a) (b)

Figure 9.7: Evolution of swelling pressure of compacted bentonite with elapsed time in the case of saturating with deionized water at (a) 22 and (b)80°C

for a given temperature, dry density and water content before hydration had almost no influence on the swelling pressure equilibrium time but affected the magnitude of the equilibrium swelling pressure.

The equilibrium swelling pressures as a function of dry density of saturated the specimens are shown in Figure 9.8. The data in literature (Schanz & Tripathy, 2009; Baille et al., 2010) were obtained from constant volume swelling pressure tests performed at 20°C on compacted Calcigel bentonite with the mineral composition and material properties similar to the bentonite used in this study. According to Figure 9.8, the swelling pressures in this study were found to be in a reasonable agreement with the data from literature. In addition, temperature had an insignificant influence on the swelling pressure-dry density relationship. For a given dry density, swelling pressures measured at 80°C were slightly less than those measured at 22°C, which could be also found in Figure 9.9.

For a given dry density and temperature, effect of water content before hydration on swelling pressure is presented in Figure 9.9. The swelling pressure increased with decreasing the water content before hydration for a given temperature and dry density. This experimental result indicated that the desiccated specimens exhibited the greater swelling pressure compared with the reference specimens (i.e. 100B-9, 100B-15, 100B-16 and 100B-17) since the reference specimens did not undergo desiccation and had the highest water content. Moreover, the difference in swelling pressure between the desiccated

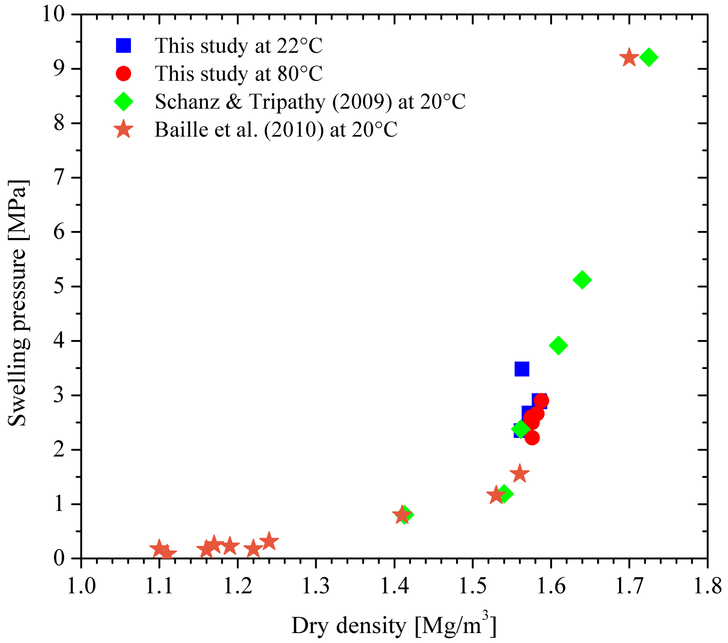

Figure 9.8: Dependence of swelling pressure of compacted bentonite on dry density after hydration

specimen and reference specimen depended on their difference in water content or the applied suction during desiccation. For specimen 100B-1 dried at an applied suction of 1000 MPa, its swelling pressure increased by 46% compared to the reference specimen 100B-15. For specimen 100B-2 dried at an applied suction of 700 MPa, its swelling pressure increased by 18% compared with the reference specimen 100B-9. In the case of specimens 100B-11 and 100B-12 dried at an applied suction of 346 and 154 MPa, respectively, their swelling pressures only increased by 7 and 1%, respectively. The experimental results in Fig.9 indicated that desiccation increased the swelling pressure of compacted bentonite. Furthermore, the increase in the swelling pressure was significant when the compacted bentonite (i.e. specimens 100B-1 and 100B-2) underwent the extreme desiccation at an applied suction greater than 700 MPa.

The increase in swelling pressure due to desiccation may be relevant to the influence of desiccation on the fabric of bentonite. Desiccation, particularly the extreme desiccation at an applied suction of above 700 MPa, can destroy the dispersed aggregates and results in great swelling upon subsequent hydration phase. Osipov et al. (1987); Day (1994) found that drying-wetting cycles could significantly increase the swelling of clays and that the dispersed clay structure was destroyed during the drying-wetting cycles. The destruction of large aggregates and the disorientation of structural elements of clays resulted in great

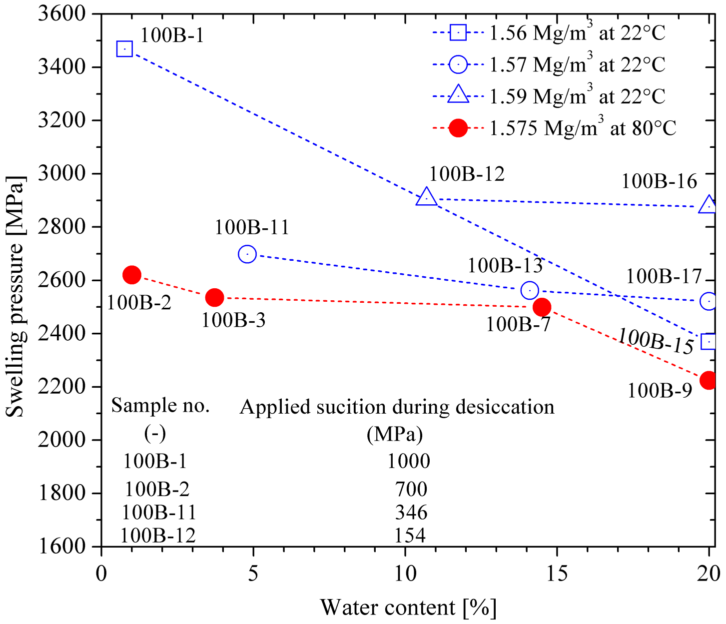

Figure 9.9: Dependence of swelling pressure of compacted bentonite on the water content before hydration for a given temperature and dry density

swelling. In addition, Gens & Alonso (1992) and Baille et al. (2010) stated that a decrease in initial water content or an increase in initial suction leaded to greater swelling pressures for a given dry density, which was related to the effect of initial water content or suction on the fabric of expansive clays.

In addition, the increase in swelling pressure due to desiccation could be also explained according to the BExM (Gens & Alonso, 1992; Alonso et al., 1999). Because of the interaction between micro and macrostructure (Figure 7.1), microstructural shrinkage due to the suction controlled desiccation could induce an irreversible decrease of macrostructural void ratio. This irreversible decrease of macrostructural void ratio due to suction increase occurs when suction increase (SI) yield curve is activated. Because the coupling between loading-collapse (LC) and SI curves exists, the irreversible decrease of macrostructural void ratio due to suction increase results in LC curve shifting from the left side to the right side in $p - s$ plane (Figure 7.1). Since the magnitude of swelling upon saturating increases with the distance between the current stress state and LC curve, the desiccation due to suction increase tends to increase the swelling pressure for a given dry density.

9.2.4 Hydraulic conductivity

The measured hydraulic conductivities of saturated specimens 100B-2, 100B-7, 100B-9 and 100B-17 are shown in Figure 9.10. Specimens 100B- 17 and 100B-9 were the reference samples, thus did not undergo desiccation and were hydrated at 22 and 80°C, respectively. The data from Khan (2012) were obtained from constant volume permeability test performed at 20°C on compacted Calcigel bentonite specimen with initial compaction conditions similar to the specimen 100B-17. The magnitudes of their hydraulic conductivity were found to be similar (1.2×10^{-13} m/s for the specimen in Khan (2012) and 7.7×10^{-13} m/s for specimen 100B-17). However, the hydraulic conductivity of specimen 100B-17 was significantly lower than that of specimen 100B-9 (4.6×10^{-12} m/s). This indicates that hydraulic conductivity increases with temperature, given that the two reference specimens had a similar dry density and the same water content before hydration. The experimental result above is consistent with the earlier finding that the saturated hydraulic conductivity of compacted bentonites increased with increasing temperature (Pusch, 1980*a*; Villar et al., 2010; Ye et al., 2013).

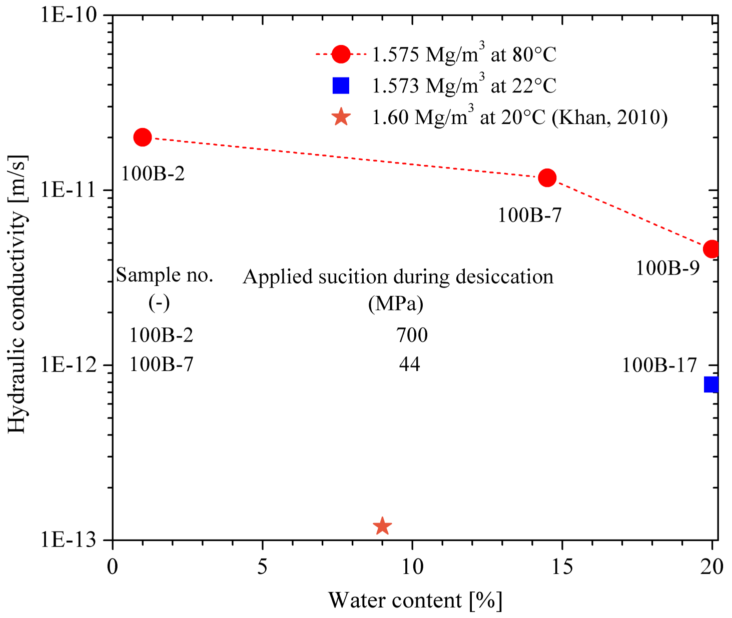

Figure 9.10: Dependence of hydraulic conductivity of compacted bentonite on the water content before hydration for a given temperature and dry density

In addition, experimental data in Figure 9.10 also showed that for the given temperature of 80°C and dry density, the hydraulic conductivity increased with decreasing the water content before hydration. The reference specimen 100B-9 had the highest water content (i.e. 20%) but exhibited the lowest hydraulic conductivity (4.6×10^{-12} m/s) compared with specimens 100B-7 and 100B-2. Specimen 100B-7 dried at applied suction of 44 MPa had a water content of 14.5% and showed a hydraulic conductivity of 1.2×10^{-11} m/s. Specimen 100B-2 dried at applied suction of 700 MPa had the lowest water content (i.e. 1%) but exhibited the highest hydraulic conductivity (2.0×10^{-11} m/s). Compared to the hydraulic conductivity of the reference specimen 100B-9, the hydraulic conductivities of specimens 100B-7 and 100B-2 increased by 156 and 334%, respectively. The experimental results above indicated that desiccation increased the hydraulic conductivity of compacted bentonite. Moreover, the increase in the hydraulic conductivity was considerable when the compacted bentonite (i.e. specimen 100B-2) underwent the extreme desiccation at an applied suction greater than 700 MPa.

The increase in hydraulic conductivity due to desiccation may be due to the fact that the inhomogeneity induced by shrinkage and subsequent temporary unconfined swelling may induce weaker zones with reduced dry density and slightly higher permeability. The volumetric shrinkage due to desiccation leads to reduced specimen dimensions. Therefore, the initial stage of hydration corresponded to free swelling conditions (without volume constraint). Hydration of the desiccated specimens under constant volume conditions occurred until the initial radial and vertical gaps were filled with swollen bentonite particle. The initial unconfined swelling results in a redistribution of bentonite particles into the former radial and axial gap and thus a change in local dry densities of the specimen. The zone of the former gap may have a reduced dry density as compared to the inner core of the specimen and provide a preferential flow pathway. Consequently, the desiccated specimens exhibited a higher permeability compared with the reference sample without desiccation. Study related to the effect of initial technical voids on hydraulic conductivity of compacted bentonite-based material indicates that at the same bentonite dry density or void ratio, the specimens with a higher technical void showed a higher hydraulic conductivity (Wang et al., 2013a).

9.3 Summary

The effect of desiccation on hydro-mechanical behaviour (swelling pressure and hydraulic conductivity) of compacted bentonite-based materials (bentonite and bentonite-sand mixture) was experimentally examined at 22 and 80°C. For a given temperature, the suction-controlled desiccation tests were carried out on compacted specimens to obtain desiccated samples. After the compacted specimens reached water equilibrium at applied suction, they were placed in the swelling pressure device to perform the constant volume swelling pressure tests. When the swelling pressure reached equilibrium, permeability tests were finally conducted on four saturated specimens. The following conclusions were drawn in the present chapter.

1. For a given suction, the water retention of compacted bentonite-based materials at 22°C was slightly greater than that at 80°C. The dependency of water retention on temperature is due to temperature dependency on surface tension and additional thermal disturbance altering clay fabric and intra-aggregate fluid chemistry

2. It was found that the compacted bentonite exhibited significant volumetric shrinkage upon drying from the as-compacted state, whereas the compacted bentonite-sand mixture exhibited slight volumetric swelling upon drying from the as-compacted state. The shrinking/swelling behaviour of compacted bentonite-based materials upon drying from the as-compacted state is due to the competing effects of the shrinkage of clay particles due to dehydration and the swelling due to dissipating the friction between the specimen ring and the specimen.

3. The decrease in swelling pressure of compacted bentonite-based materials due to an increase in temperature was found to be reversible. The reversible decrease in swelling pressure of compacted bentonite-based materials caused by an increase in temperature is due to the fact that the water transfer between microstructural pore and the macrostructural pore triggered by temperature change is reversible.

4. Desiccation was found to slightly increase swelling pressure of compacted bentonite, especially when the compacted bentonite underwent the extreme desiccation at the applied suction greater than 700 MPa. The increase in swelling pressure due to desiccation may be relevant to the influence of desiccation on the fabric of bentonite.

5. Desiccation was found to slightly increase hydraulic conductivity of compacted bentonite, especially when the compacted bentonite underwent the extreme desiccation at the applied suction greater than 700 MPa. The increase in hydraulic conductivity induced by desiccation may be due to the fact that the inhomogeneity induced by shrinkage and subsequent temporary unconfined swelling may induce weaker zones with reduced dry density and slightly higher permeability.

6. The desiccation due to the thermo-hydraulic boundary conditions in the geological repository could slightly increase the swelling capacity and the permeability of bentonite buffer. However, it should be noted that the conclusions drawn here are based on the results of Calcigel bentonite specimens with a dry density of 1.56-1.59 Mg/m^3. Extension

of the experimental program to a wide range of initial dry densities and other bentonite materials would be useful to further substantiate the present conclusions.

10 Conclusions and recommendations

10.1 Conclusions

Compacted bentonite-based materials (bentonite and bentonite-sand mixtures) are often selected as buffer, backfill and sealing materials in the geological repository for the disposal of radioactive wastes because these materials exhibit several valuable properties (e.g. adequate swelling capacity, low water permeability). To study the influence of the thermo-hydro-mechanical-chemical boundary conditions prevailing in the geological repository on the hydro-mechanical behaviour of buffer, backfill and sealing materials, laboratory tests under controlled-boundary condition were performed on bentonite-based materials (bentonite and bentonite-sand mixtures).

Water retention measurements were carried out under different confinement conditions (unconfined, constant vertical stress and constant volume conditions) on bentonite-sand (50/50) mixtures to obtain the water retention curves (WRCs) under different mechanical boundary conditions. To explain the effect of mechanical boundary conditions on the WRCs of bentonite-sand (50/50) mixtures, microstructural characteristics of bentonite-sand (50/50) were derived from wetting WRCs based on the method proposed by Navarro et al. (2017b) on Na-bentonite.

Multi-step swelling pressure tests were performed on compacted bentonite-sand (50/50) mixtures to study the effect of hydraulic boundary conditions (water phase and suction) on the swelling capacity of backfill and sealing materials. Compacted bentonite-sand (50/50) mixtures were gradually hydrated with either liquid water or water vapour during the multi-step swelling pressure tests.

Numerical simulation of a multi-step swelling pressure test was performed to verify the method for deriving microstructural characteristics from wetting WRCs on Ca-rich bentonite. The wetting WRCs under constant volume condition was used to calibrate the hydraulic model used in the numerical simulation. It is assumed that the method for determining microstructural characteristics from the wetting WRCs based on the method proposed by Navarro et al. (2017b) on Na-bentonite is reliable on Ca-rich bentonite. The microstructural characteristics and suction-controlled one-dimensional swelling-compression-rebound test results were used to calibrate the mechanical model used in the numerical simulation.

Swelling pressure tests and suction measurements were performed on bentonite-based materials to explore the quantitative effect of hydro-chemical boundary conditions on the swelling capacity of buffer, backfill and sealing materials. The link between swelling pressure, total suction and applied suction was examined under saturated and unsaturated conditions. For saturated bentonite-based materials, an equation describing the link between swelling pressure, total suction and the suction of aqueous solutions used to saturate bentonite-based materials was derived based on the thermodynamics of soil-moisture. To validate the derived equation, swelling pressure tests with aqueous solutions and total suction measurements were carried out on compacted bentonite-based materials. For unsaturated bentonite-based materials, laboratory tests involving swelling pressure tests with suction control and subsequent total suction measurements were performed on compacted bentonite-based materials.

Swelling pressure and permeability tests were performed on desiccated bentonite samples and reference bentonite sample to study the effect of the desiccation due to the thermo-hydraulic boundary conditions on the swelling capacity and the permeability of bentonite buffer. The desiccated bentonite samples were obtained by subjecting as-compacted bentonite samples to suction-controlled desiccation at constant temperature.

According to the experimental results, the numerical simulation and the theoretical considerations, the following main conclusions were drawn in this thesis:

1. The confinement conditions significantly affect the wetting WRCs of bentonite-sand (50/50) mixtures. The air-expulsion values significantly increased with changing the confinement conditions from unconfined condition to constant volume condition. In addition, the confinement conditions also strongly affect the hysteresis loop of the wetting-drying WRCs. The hysteresis loop of the wetting-drying WRCs was significant in the case of unconfined condition, whereas the hysteresis loop of the wetting-drying WRCs was insignificant in case of the constant volume condition. The effect of confinement conditions on the WRCs of bentonite-sand mixtures (50/50) is due to their influence on the macrostructural voids of bentonite-sand (50/50) mixtures. Thus, mechanical boundary conditions strongly affect the hydration of backfill and sealing materials and hydraulic model taking account of mechanical boundary conditions should be developed to better simulate the hydration of backfill and sealing materials.

2. The magnitudes of the swelling pressure of compacted bentonite-sand (50/50) mixtures upon wetting depend not only on the magnitude of applied suction but also on water phase (water vapour and liquid water). For the applied suction range greater than 3 MPa, the swelling pressures due to the hydration with liquid water were greater than those due to the hydration with water vapour. The effect of suction and water phase on the swelling pressure is related to swelling mechanisms. Therefore, hydraulic boundary conditions (water phase and suction) affect the swelling capacity of backfill and sealing materials.

3. The present study proposes and validates an empirical method for determining swelling pressure-suction relationship from the wetting WRCs under constant volume condition. The empirical method provides an alternative method for estimating the effect of the hydraulic boundary condition related to suction on the swelling capacity of buffer, backfill and sealing materials.

4. The comparison of multi-step swelling pressure test results and numerical simulation results showed that the numerical simulation reproduced the multi-step swelling pressure test results very well. The consistency between the numerical simulation results and experimental results confirms the assumption that the method for determining microstructural characteristics from the wetting WRCs based on the method proposed by Navarro et al. (2017b) on Na-bentonite is reliable on Ca-rich bentonite. The method for deriving microstructural characteristics from wetting WRCs is helpful in understanding the effect of the mechanical boundary conditions in the geological repository on the hydration of backfill and sealing materials.

5. Based on the experimental results from this study and those reported in the literature, the difference between the total suction of saturated bentonite-based materials and the suction of the aqueous solutions used to saturate the bentonite-based materials is approximately equal to the swelling pressure of saturated bentonite-based materials. The link between these three parameters indicates that the total suction of bentonite-based materials caused by the adsorptive and osmotic forces will not dissipate when the bentonite-based materials are saturated with aqueous solutions under constant volume condition. The present finding extends the relationship suggested by Croney (1952); Kassiff & Shalom (1971); Towenr (1981); Karnland et al. (2005). Moreover, the link between these three parameters provides the framework for establishing a quantitative link between the swelling capacity of buffer, backfill and sealing materials and the chemical boundary condition in the geological repository.

6. For the unsaturated bentonite-based materials, the experimental results indicate that the difference between the total suction of bentonite-based materials and the applied

suction was not equal to but significantly greater than the swelling pressure of bentonite-based materials. The equation describing the link between the total suction, the suction of the aqueous solutions and the swelling pressure for saturated bentonite-based materials was modified to consider the link between the total suction, the applied suction and the swelling pressure for unsaturated bentonite-based materials. Moreover, a unique relationship between the measured total suction and bentonite water content was found for bentonite-based materials. The modified equation and the unique relationship between the measured total suction and bentonite water content provide the framework for quantitatively estimating the effect of hydro-chemical boundary conditions on the swelling capacity of buffer, backfill and sealing materials.

7. Desiccation slightly increases the swelling pressure and the hydraulic conductivity of saturated bentonite, especially when the compacted bentonite undergoes the extreme desiccation at the applied suction greater than 700 MPa. The increase in swelling pressure due to desiccation may be relevant to the influence of desiccation on the fabric of bentonite. The increase in hydraulic conductivity induced by desiccation may be due to the fact that the inhomogeneity induced by shrinkage and subsequent temporary unconfined swelling may induce weaker zones with reduced dry density and slightly higher permeability. Therefore, the desiccation due to the thermo-hydraulic boundary conditions in the geological repository could slightly increase the swelling capacity and the permeability of bentonite buffer.

10.2 Recommendations

1. Since the WRCs are closely related to the confinement conditions, water retention model should be developed to considerate their influence.

2. To further confirm Eq.(8.14) describing the link between the swelling pressure of saturated bentonite-based materials, the total suction of bentonite-based materials and applied suction, the aqueous solutions including complex solutes and similar to the groundwater in the geological repository should be checked in the future by performing laboratory tests involving constant volume swelling pressure tests and total suction measurements.

3. The link between swelling pressure, total suction and applied suction for unsaturated bentonite-based materials should be reconsidered in the future to explore the physical meaning of parameter α in Eq.(8.18).

4. Extension of the experimental program to a wide range of initial densities and other bentonite materials would be useful to further substantiate the influence of desiccation on the swelling capacity and the permeability of bentonite buffer.

Bibliography

Agus, S., Arifin, Y., Tripathy, S. & Schanz, T. (2013), ‘Swelling pressure-suction relationship of heavily compacted bentonite-sand mixtures’, *Acta Geotech.* **8**(2), 155–165.

Agus, S. S. (2005), An experimental study on hydro-mechanical characteristics of compacted bentonite-sand mixtures, PhD thesis, Bauhaus-University Weimar.

Agus, S. S. & Schanz, T. (2005*a*), ‘Comparison of four methods for measuring total suction’, *Vadose Zone J.* **4**(4), 1087–1095.

Agus, S. S. & Schanz, T. (2005*b*), Effect of shrinking and swelling on microstructures and fabric of a compacted bentonite-sand mixture, *in* ‘Proceedings of the International Conference on Problematic Soils’, Vol. 32, pp. 543–550.

Agus, S. S. & Schanz, T. (2008), ‘A method for predicting swelling pressure of compacted bentonites’, *Acta Geotech.* **3**(2), 125–137.

Agus, S. S., Schanz, T. & Fredlund, D. G. (2010), ‘Measurements of suction versus water content for bentonite-sand mixtures’, *Can. Geotech. J.* **47**(5), 583–594.

Akcanca, F. & Aytekin, M. (2014), ‘Impact of wetting–drying cycles on the hydraulic conductivity of liners made of lime-stabilized sand–bentonite mixtures for sanitary landfills’, *Environ Earth sci.* **72**(1), 59–66.

Åkesson, M., Jacinto, A., Gatabin, C., Sanchez, M. & Ledesma, A. (2009), ‘Bentonite THM behaviour at high temperatures: experimental and numerical analysis’, *Géotechnique* **59**(4), 307–318.

Al-Badran, Y. M. H. (2011), Volumetric yielding behavior of unsaturated fine-grained soils, PhD thesis, Ruhr-Universität Bochum.

Al-Homoud, A., Basma, A., Husein Malkawi, A. & Al Bashabsheh, M. (1995), ‘Cyclic swelling behavior of clays’, *Int. J. Geotech. Eng.* **121**(7), 562–565.

Albrecht, B. A. & Benson, C. H. (2001), ‘Effect of desiccation on compacted natural clays’, *J. Geotech. Geoenviron. Eng.* **127**(1), 67–75.

Albrecht, B., Benson, C. & Beuermann, S. (2003), ‘Polymer capacitance sensors for measuring soil gas humidity in drier soils’, *Geotech. Test. J.* **26**(1), 3–11.

Alonso, E. E., Gens, A. & Josa, A. (1990), ‘A constitutive model for partially saturated soils’, *Géotechnique.* **40**(3), 405–430.

Alonso, E., Romero, E., Hoffmann, C. & García-Escudero, E. (2005), ‘Expansive bentonite–sand mixtures in cyclic controlled-suction drying and wetting’, *Eng. Geol.* **81**(3), 213–226.

Alonso, E., Vaunat, J. & Gens, A. (1999), ‘Modelling the mechanical behaviour of expansive clays’, *Eng. Geol.* **54**(1), 173–183.

Arifin, Y. F. (2008), Thermo-hydro-mechanical behavior of compacted bentonite-sand mixtures: an experimental study, PhD thesis, Bauhaus-University Weimar.

Arifin, Y. F. & Schanz, T. (2009), ‘Osmotic suction of highly plastic clays’, *Acta Geotech.* **4**(3), 177–191.

ASTM-D3977 (1997), Standard test methods for determining sediment concentration in water samples, Standard D3977-97, ASTM International, West Conshohocken, PA.

ASTM-D422 (2007), Standard test method for particle-size analysis of soils, Standard D422-63, ASTM International, West Conshohocken, PA.

ASTM-D4318 (2000), Standard test methods for liquid limit, plastic limit, and plasticity index of soils, Standard D4318-00, ASTM International, West Conshohocken, PA.

ASTM-D4943 (2010), Standard test method for shrinkage factors of soils by the wax method, Standard D4943-08, ASTM International, West Conshohocken, PA.

ASTM-D5298 (2010), Standard test method for measurement of soil potential (suction) using filter paper, Standard D5298-10, ASTM International, West Conshohocken, PA.

ASTM-D6836 (2003), Standard test methods for determination of the soil water chararcteristic curve for desorption using a hanging column, pressure extractor, chilled mirror hygrometer, and/or centrifuge, Standard D6836-02, ASTM International, West Conshohocken, PA.

ASTM-D698 (1996), Standard test method for one-dimensional consolidation properties of soils, Standard D2435-96, ASTM International, West Conshohocken, PA.

ASTM-D698 (2007), Standard test methods for laboratory compaction characteristics of soil using standard effort (12 400 ft-lbf/ft^3 (600 kN-m/m^3)), Standard D698-07, ASTM International, West Conshohocken, PA.

ASTM-D854 (2002), Standard test methods for specific gravity of soil solids by water pycnometer, Standard D854-02, ASTM International, West Conshohocken, PA.

ASTM-E104 (2007), Standard practice for maintaining constant relative humidity by means of aqueous solutions, Standard E104-02, ASTM International, West Conshohocken, PA.

Bag, R. (2011), Coupled thermo-hydro-mechanical-chemical behaviour of MX80 bentonite in geotechnical applications, PhD thesis, Cardiff University.

Baille, W. (2014), Hydro-Mechanical Behaviour of Clays Significance of Mineralogy, PhD thesis, Ruhr-UniversitLät Bochum.

Baille, W., Tripathy, S. & Schanz, T. (2010), ‘Swelling pressures and one-dimensional compressibility behaviour of bentonite at large pressures’, *Appl. Clay Sci.* **48**(3), 324 – 333.

Baille, W., Tripathy, S. & Schanz, T. (2014), ‘Effective stress in clays of various mineralogy’, *Vadose Zone J.* **13**(5), 1–10.

Ballew, H., Clark, D., Crooks, G., Ho, S., Markee, C., Martinez, F., Milner, D., Partee, J. & Simmons, J. (2002), *The ABC’s of filtration and bioprocessing for the third millennium*, Rancho Dominguez, CA: Spectum Laboratories Inc.

Bergaya, F., Theng, B. & Lagaly, G., eds (2006), *Handbook of clay science. In: Developments in Clay Science*, Vol. 1, Elsevier, Amsterdam.

Bishop, A. W. & Donald, I. (1961), The experimental study of partly saturated soil in the triaxial apparatus, *in* ‘Proceedings of the 5th International Conference on Soil Mechanics and Foundation Engineering, Paris’, Vol. 1, pp. 13–21.

Blatz, J. & Graham, J. (2000), ‘A system for controlled suction in triaxial tests’, *Géotechnique* **50**(4), 465–470.

Bolt, G. (1956), 'Physico-chemical analysis of the compressibility of pure clays', *Géotechnique.* **6**(2), 86–93.

Bolt, G. & Miller, R. (1958), 'Calculation of total and component potentials of water in soil', *Eos.* **39**(5), 917–928.

Bray, H. & Redfern, S. (1999), 'Kinetics of dehydration of Ca-montmorillonite', *Phys. Chem. Miner.* **26**(7), 591–600.

Bucher, F. & Max, M. (1989), 'Bentonite as a containment barrier for the disposal of highly radioactive wastes', *Appl. Clay Sci.* **4**(2), 157–177.

Caglar, B., Afsin, B., Tabak, A. & Eren, E. (2009), 'Characterization of the cation-exchanged bentonites by XRPD, ATR, DTA/TG analyses and BET measurement', *Chem. Eng. J.* **149**(1), 242–248.

Cardoso, R., Romero, E., Lima, A. & Ferrari, A. (2007), A comparative study of soil suction measurement using two different high-range psychrometers, *in* 'Experimental unsaturated soil mechanics', Springer, pp. 79–93.

Cases, J., Bérend, I., François, M., Uriot, J., Michot, L. & Thomas, F. (1997), 'Mechanism of adsorption and desorption of water vapor by homoionic montmorillonite; 3, the Mg (super 2+), Ca (super 2+), and Ba (super 3+) exchanged forms', *Clays Clay Miner.* **45**(1), 8–22.

Castellanos, E., Villar, M., Romero, E., Lloret, A. & Gens, A. (2008), 'Chemical impact on the hydro-mechanical behaviour of high-density FEBEX bentonite', *Phys. Chem. Earth.* **33**, S516–S526.

Cerato, A. & Lutenegger, A. (2002), 'Determination of surface area of fine-grained soils by the ethylene glycol monoethyl ether (EGME) method', *Geotech. Test. J.* **25**, 315–321.

Collins, K. t. & McGown, A. (1974), 'The form and function of microfabric features in a variety of natural soils', *Géotechnique* **24**(2), 223–254.

Croney, D. (1952), 'The movement and distribution of water in soils', *Géotechnique.* **3**(1), 1–16.

Cui, Y.-J., Tang, A. M., Loiseau, C. & Delage, P. (2008), 'Determining the unsaturated hydraulic conductivity of a compacted sand–bentonite mixture under constant-volume and free-swell conditions', *Phys. Chem. Earth.* **33**, S462–S471.

Cui, Y., Loiseau, C. & Delage, P. (2002), Microstructure changes of a confined swelling soil due to suction controlled hydration, *in* 'Proc. 3rd Int. Conf. on Unsaturated Soils', pp. 593–598.

Cuisinier, O. & Masrouri, F. (2004), 'Testing the hydromechanical behavior of a compacted swelling soil', *Geotech. Test. J.* **27**(6), 598–606.

Cuisinier, O. & Masrouri, F. (2005), 'Hydromechanical behaviour of a compacted swelling soil over a wide suction range', *Engineering Geology* **81**(3), 204 – 212.

Day, R. W. (1994), 'Swell-shrink behavior of compacted clay', *Int. J. Geotech. Eng.* **120**(3), 618–623.

Decagon Devices, I. (2003), *Water Activity Meter Operator's Manual for Aqualab Series 3*, Decagon Devices, Inc.

Decagon Devices, I. (2010), *WP4C Dew Point PotentiaMeter Operator's Manual*, Decagon Devices, Inc.

Delage, P. & Cui, Y. J. (2008a), 'An evaluation of the osmotic method of controlling suction', *Geomech. Geoeng.* **3**(1), 1–11.

Delage, P. & Cui, Y. J. (2008b), 'A novel filtration system for polyethylene glycol solutions used in the osmotic method of controlling suction', *Can. Geotech. J.* **45**(3), 421–424.

Delage, P., Howat, M. & Cui, Y. (1998), 'The relationship between suction and swelling properties in a heavily compacted unsaturated clay', *Eng. Geol.* **50**(1), 31–48.

Delage, P., Marcial, D., Cui, Y. J. & Ruiz, X. (2006), 'Ageing effects in a compacted bentonite: a microstructure approach', *Géotechnique.* **56**(5), 291–304.

Delage, P., Romero, E. & Tarantino, A. (2008c), Recent developments in the techniques of controlling and measuring suction in unsaturated soils, *in* 'Unsaturated Soils. Advances in Geo-Engineering', CRC Press, pp. 44–63.

Delage, P., Suraj De Silva, G. & Vicol, T. (1992), Suction controlled testing of non saturated soils with an osmotic consolidometer, *in* 'Proc. 7th Int. Conf. Expansive Soils', pp. 206–211.

Derkowski, A., Drits, V. A. & McCarty, D. K. (2012), 'Rehydration of dehydrated-dehydroxylated smectite in a low water vapor environment', *Am. Mineral.* **97**(1), 110–127.

Dueck, A. (2004), Hydro-mechanical properties of a water unsaturated sodium bentonite. Laboratory study and theoretical interpretation, PhD thesis, Lund University.

Dueck, A., Börgesson, L. & Wadsö, L. (2001), Constant volume tests with suction control performed on a swelling clay, *in* 'Proc. 6th Int. Workshop Key Issues in Waste Isolation Research, Paris', pp. 83–101.

Dueck, A., Goudarzi, R. & Börgesson, L. (2014), Buffer homogenisation, status report 2, Technical report, Swedish Nuclear Fuel and Waste Management Co.

Edlefsen, N. E. & Anderson, A. B. (1943), *Thermodynamics of soil moisture*, University of California.

El-Sohby, M. A., Mazen, S. O. & Abou-Taha, M. A. (1989), Effect of apparatus deformability on swelling pressure, *in* 'Proceedings of the 12th International Conference on Soil Mechanics and Foundation Engineering', pp. 589–592.

Ferrage, E., Kirk, C. A., Cressey, G. & Cuadros, J. (2007a), 'Dehydration of Ca-montmorillonite at the crystal scale. part i: Structure evolution', *Am. Mineral.* **92**(7), 994–1006.

Fredlund, D. G. & Rahardjo, H. (1993), *Soil mechanics for unsaturated soils*, John Wiley & Sons.

Fredlund, D. G., Rahardjo, H. & Fredlund, M. D. (2012), *Unsaturated soil mechanics in engineering practice*, John Wiley & Sons, Inc.

Gatabin, C., Talandier, J., Collin, F., Charlier, R. & Dieudonné, A.-C. (2016), 'Competing effects of volume change and water uptake on the water retention behaviour of a compacted MX-80 bentonite/sand mixture', *Appl. Clay Sci.* **121-122**, 57 – 62.

Gee, G., Campbell, M., Campbell, G. & Campbell, J. (1992), 'Rapid measurement of low soil water potentials using a water activity meter', *Soil Sci. Soc. Am. J.* **56**(4), 1068–1070.

Gens, A. & Alonso, E. E. (1992), 'A framework for the behaviour of unsaturated expansive clays', *Can. Geotech. J.* **29**(6), 1013–1032.

Greenspan, L. et al. (1977), 'Humidity fixed points of binary saturated aqueous solutions', *J. Res. Nat. Bur. Stand.* **81**(1), 89–96.

Grim, R. E. (1968), *Clay mineralogy*, McGraw-Hill.

Hilf, J. W. (1956), An investigation of pore water pressure in compacted cohesive soils, Technical report, United States Department of the Interior Bureau of Reclamation.

Hoffmann, C., Alonso, E. & Romero, E. (2007), 'Hydro-mechanical behaviour of bentonite pellet mixtures', *Phys. Chem. Earth.* **32**(8), 832 – 849.

Imbert, C. & Villar, M. V. (2006), 'Hydro-mechanical response of a bentonite pellets/powder mixture upon infiltration', *Appl. Clay Sci.* **32**(3), 197–209.

Iwata, S., Tabuchi, T., Warkentin, B. P. et al. (1995), *Soil-water interactions: mechanisms and applications*, Marcel Dekker, Inc.

Jayalath, C., Gallage, C. & Miguntanna, N. (2016), 'Factors affecting the swelling pressure measured by the oedemeter method', *International Journal of GEOMATE* **11**(24), 2397–2402.

Jobmann, M., Flügge, J., Gazul, R., Hammer, J., Herold, P., Krone, J., Kuate Simo, E., Kühnlenz, T., Laggiard, E., Lommerzheim, A., Meleshyn, A., Müller, C., Rübel, A., Wolf, J. & Zhao, H. (2017), Investigation on long-term safety aspects of a radioactive waste repository in a diagenetic clay formation, Technical report, DBE Technology GmbH.

Jobmann, M., Flügge, J., Hammer, J., Herold, P., Krone, J., Kühnlenz, T., Li, S., Lommerzheim, A., Meleshyn, A. & Wolf, J. (2015), Site-specific evaluation of safety issues for high-level waste disposal in crystalline rocks, Technical report, DBE Technology GmbH.

Johannesson, L., Kristensson, O. & Åkesson, M. (2014), Tests and simulations of THM processes relevant for the buffer installation, Technical report.

Karnland, O., Muurinen, A. & Karlsson, F. (2005), Bentonite swelling pressure in NaCl solutions-experimentally determined data and model calculations, *in* A. L. Eduardo E. Alonso, ed., 'Advances in Understanding Engineering Clay Barriers', pp. 241–256.

Kassiff, G. & Shalom, A. B. (1971), 'Experimental relationship between swell pressure and suction', *Géotechnique.* **21**(3), 245–255.

Khalili, N., Geiser, F. & Blight, G. E. (2004), 'Effective stress in unsaturated soils: Review with new evidence', *Int. J. Geomech.* **4**(2), 115–126.

Khan, M. I. (2012), Hydraulic conductivity of moderate and highly dense expansive clays, PhD thesis, Ruhr-UniversitLät Bochum.

Komine, H. & Ogata, N. (1994), 'Experimental study on swelling characteristics of compacted bentonite', *Can. Geotech. J.* **31**(4), 478–490.

Komine, H. & Ogata, N. (1996), 'Prediction for swelling characteristics of compacted bentonite', *Can. Geotech. J.* **33**(1), 11–22.

Komine, H. & Ogata, N. (2003), 'New equations for swelling characteristics of bentonite-based buffer materials', *Can. Geotech. J.* **40**(2), 460–475.

Krahn, J. & Fredlund, D. (1972), 'On total, matric and osmotic suction', *Soil Sci.* **114**, 339–348.

Laird, D. A. (1996), 'Model for crystalline swelling of 2:1 phyllosilicates', *Clays Clay Miner.* **44**(4), 553–559.

Laird, D. A. (2006), 'Influence of layer charge on swelling of smectites', *Appl. Clay Sci.* **34**(1), 74–87.

Lambe, T. W. & Whitman, R. V. (1969), *Soil mechanics*, John Wiley & Sons.

Lang, A. (1976), 'Osmotic coefficients and water potentials of sodium chloride solutions from 0 to 40°C', *Aust. J. Chem.* **20**(9), 2017–2023.

Lang, L. Z., Xiang, W., Huang, W., Cui, D. S. & Schanz, T. (2017), 'An experimental study on oven-drying methods for laboratory determination of water content of a calcium-rich bentonite', *Applied Clay Science* **150**, 153 – 162.

Leong, E.-C., Tripathy, S. & Rahardjo, H. (2003), 'Total suction measurement of unsaturated soils with a device using the chilled-mirror dew-point technique', *Géotechnique.* **53**(2), 173–182.

Leong, E. C., Tripathy, S. & Rahardjo, H. (2004), 'A modified pressure plate apparatus', *Geotech. Test. J.* **27**(3), 322–331.

Li, X. & Zhang, L. (2009), 'Characterization of dual-structure pore-size distribution of soil', *Can. Geotech. J.* **46**(2), 129–141.

Lins, Y., Schanz, T. & Fredlund, D. G. (2009), 'Modified pressure plate apparatus and column testing device for measuring SWCC of sand', *Geotech. Test. J.* **32**(5), 450–464.

Liu, L. (2013), 'Prediction of swelling pressures of different types of bentonite in dilute solutions', *Colloids Surf., A* **434**, 303–318.

Lloret, A., Villar, M. V., Sanchez, M., Gens, A., Pintado, X. & Alonso, E. E. (2003), 'Mechanical behaviour of heavily compacted bentonite under high suction changes', *Géotechnique.* **53**(1), 27–40.

Lorenz, P. M. (1999), 'Determination of the cation exchange capacity (CEC) of clay minerals using the complexes of copper (II) ion with triethylenetetramine and tetraethylenepentamine', *Clays Clay Miner* **47**, 386–388.

Low, P. & Deming, J. M. (1953), 'Movement and equilibrium of water in heterogeneous systems with special reference to soils', *Soil Sci.* **75**(3), 187–202.

Low, P. F. (1987), 'Structural component of the swelling pressure of clays', *Langmuir* **3**(1), 18–25.

Low, P. F. & Anderson, D. M. (1958), 'Osmotic pressure equations for determing thermodynamic properties of soil water', *Soil Sci.* **86**(5), 251–253.

Lu, N. & Likos, W. J. (2004), *Unsaturated soil mechanics*, Wiley.

Madsen, F. (1998), 'Clay mineralogical investigations related to nuclear waste disposal', *Clay Miner.* **33**(1), 109–129.

Manca, D., Ferrari, A. & Laloui, L. (2015), 'Fabric evolution and the related swelling behaviour of a sand/bentonite mixture upon hydro-chemo-mechanical loadings', *Géotechnique* **66**(1), 41–57.

Manheim, F. (1966), 'A hydraulic squeezer for obtaining interstitial water from consolidated and unconsolidated sediments', *US Geological Survey Professional Paper* **550**, 256–261.

Marcial, D., Delage, P. & Cui, Y. J. (2002), 'On the high stress compression of bentonites', *Can. Geotech. J.* **39**(4), 812–820.

Măsin, D. & Khalili, N. (2016), 'Swelling phenomena and effective stress in compacted expansive clays', *Can. Geotech. J.* **53**(1), 134–147.

McQUEEN, I. S. & Miller, R. F. (1968), 'Calibration and evaluation of a wide-range gravimetric method for measuring moisture stress', *Soil Science* **106**(3), 225–231.

Mesri, G. & Olson, R. E. (1971), 'Consolidation characteristics of montmorillonite', *Géotechnique* **21**(4), 341–352.

Meter Group, I. (2018), *Water Activity Meter Operator's Manual for Series 4, 4TE, 4TEV, DUO and TEV DUO*, Decagon Devices, Inc.

Mitchell, J. (1962), Components of pore water pressure and their engineering significance, *in* 'Clays and Clay Minerals: Proceedings of the Ninth National Conference', Elsevier, pp. 162–184.

Mitchell, J. K. & Soga, K. (2005), *Fundamentals of soil behavior*, Wiley New York.

Mokni, N. & Barnichon, J.-D. (2016), 'Hydro-mechanical analysis of SEALEX in-situ tests–Impact of technological gaps on long term performance of repository seals', *Eng. Geol.* **205**, 81–92.

Monroy, R., Ridley, A., Dineen, K. & Zdravkovic, L. (2007), 'The suitability of the osmotic technique for the long-term testing of partly saturated soils', *Geotech Lett.* **30**(3), 1–7.

Mooney, R., Keenan, A. & Wood, L. (1952), 'Adsorption of water vapor by montmorillonite. ii. effect of exchangeable ions and lattice swelling as measured by X-ray diffraction', *J. Am. Chem. Soc.* **74**(6), 1371–1374.

Morodome, S. & Kawamura, K. (2009), 'Swelling behavior of Na-and Ca-montmorillonite up to 150 °C by in situ X-ray diffraction experiments', *Clays Clay Miner.* **57**(2), 150–160.

Morodome, S. & Kawamura, K. (2011), 'In situ X-ray diffraction study of the swelling of montmorillonite as affected by exchangeable cations and temperature', *Clays Clay Miner.* **59**(2), 165–175.

Musso, G., Romero, E. & Vecchia, G. (2013), 'Double-structure effects on the chemo-hydro-mechanical behaviour of a compacted active clay', *Géotechnique* **63**(3), 206–220.

Nagaraj, T. & Murthy, B. S. (1985), 'Compressibility of partly saturated soils', *J. Geotech. Eng.* **111**(7), 937–942.

Nagaraj, T. S., Murthy, B. R. S. & Vatsala, A., eds (1994), *Analysis and Prediction of Soil Behaviour*, New Age International (P) Ltd., New Delhi.

Navarro, V., De la Morena, G., Yustres, Á., González-Arteaga, J. & Asensio, L. (2017a), 'Predicting the swelling pressure of MX-80 bentonite', *Appl. Clay Sci.* **149**, 51–58.

Navarro, V., Morena, G. D., Arteaga, J. G., Yustres, Á. & Asensio, L. (2017b), ‘A microstructural effective stress definition for compacted active clays’, *Geomech. Energy Environ.* .

Ng, C. W. & Pang, Y. (2000), ‘Influence of stress state on soil-water characteristics and slope stability’, *J. Geotech. Geoenviron. Eng.* **126**(2), 157–166.

Nguyen-Tuan, L. (2014), Coupled Thermo-Hydro-Mechanical Analysis: Experiment and Back Analysis, PhD thesis, Ruhr-Universität Bochum.

Norrish, K. (1954), ‘The swelling of montmorillonite’, *Discuss. Faraday Soc.* **18**, 120–134.

Nuth, M. & Laloui, L. (2008), ‘Advances in modelling hysteretic water retention curve in deformable soils’, *Comput. Geotech.* **35**(6), 835 – 844.

OECD (1995), ‘The environmental and ethical basis of geological disposal of long-lived radioactive wastes–A collective opinion of the radioactive waste management committee of the oecd nuclear energy agency’.

OECD (2003), ‘Engineered barrier systerms and the safety of deep geological reporsitories–State-of-the-art Report’.

Önal, M. & Sarıkaya, Y. (2007), ‘Thermal behavior of a bentonite’, *J. Therm. Anal. Calorim.* **90**(1), 167–172.

Or, D. & Tuller, M. (1999), ‘Liquid retention and interfacial area in variably saturated porous media: Upscaling from single-pore to sample-scale model’, *Water Resour. Res.* **35**(12), 3591–3605.

Osipov, V., Bik, N. N. & Rumjantseva, N. (1987), ‘Cyclic swelling of clays’, *Appl. Clay Sci.* **2**(4), 363–374.

Phene, C., Hoffman, G. & Rawlins, S. (1971a), ‘Measuring soil matric potential in situ by sensing heat dissipation within a porous body: I. theory and sensor construction’, *Soil Sci. Soc. Am. J.* **35**(1), 27–33.

Phene, C., Rawlins, S. & Hoffman, G. (1971b), ‘Measuring soil matric potential in situ by sensing heat dissipation within a porous body: II. experimental results’, *Soil Sci. Soc. Am. J.* **35**(2), 225–229.

Pintado, X., Hassan, M. M. & Martikainen, J. (2013), Thermo-hydro-mechanical tests of buffer material, Technical report, Posiva Oy.

Pintado, X., Lloret, A. & Romero, E. (2009), 'Assessment of the use of the vapour equilibrium technique in controlled-suction tests', *Can. Geotech. J.* **46**(4), 411–423.

Pusch, R. (1980*a*), Permeability of highly compacted bentonite, Technical report, SKB.

Pusch, R. (1980*b*), Swelling pressure of highly compacted bentonite, Technical report, SKB.

Pusch, R. (1982), 'Mineral-water interactions and their influence on the physical behavior of highly compacted Na bentonite', *Can. Geotech. J.* **19**(3), 381–387.

Pusch, R., Karnland, O. & Hokmark, H. (1990), GMM-a general microstructural model for qualitative and quantitative studies of smectite clays, Technical report, SKB Stockholm, Sweden.

Pusch, R. & Yong, R. (2003), 'Water saturation and retention of hydrophilic clay buffer-microstructural aspects', *Appl. Clay Sci.* **23**(1-4), 61–68.

Pusch, R. & Yong, R. N. (2006), *Microstructure of smectite clays and engineering performance*, CRC Press.

Rao, S. M. & Thyagaraj, T. (2007), 'Swell-compression behaviour of compacted clays under chemical gradients', *Can. Geotech. J.* **44**(5), 520–532.

Richards, B. (1965), Measurement of free energy of soil moisture by the psychrometric technique, using thermistors, Technical report.

Richards, L. (1941), 'A pressure-membrane extraction apparatus for soil solution', *Soil Sci* **51**(5), 377–386.

Richards, L. & Ogata, G. (1958), 'Thermocouple for vapor pressure measurement in biological and soil systems at high humidity', *Science* **128**(3331), 1089–1090.

Ridley, A. & Burland, J. (1993), 'A new instrument for the measurement of soil moisture suction', *Géotechnique.* **43**(2), 321–4.

Romero, E. (1999), Characterisation and thermo-hydro-mechanical behaviour of unsaturated boom clay: an experimental study, PhD thesis, Universitat Politècnica de Catalunya.

Romero, E., Della Vecchia, G. & Jommi, C. (2011), 'An insight into the water retention properties of compacted clayey soils', *Géotechnique* **61**(4), 313–328.

Romero, E., Gens, A. & Lloret, A. (2001), 'Temperature effects on the hydraulic behaviour of an unsaturated clay', *Geotech. Geol. Eng.* **19**(3), 311–332.

Romero, E. & Simms, P. H. (2008), 'Microstructure investigation in unsaturated soils: a review with special attention to contribution of mercury intrusion porosimetry and environmental scanning electron microscopy', *Geotech. Geol. Eng.* **26**(6), 705–727.

Rothfuchs, T., Hartwig, O. C. L., Hellwald, K., Komischke, M., Miehe, R. & Zhang, C. L. (2012), Self-sealing barriers of clay/mineral mixtures in a clay repository: SB experiment in the Mont Terri rock laboratory, Technical report, Gesellschaft für Anlagen-und Reaktorsicherheit (GRS).

Rothfuchs, T., Jockwer, N., Miehe, R. & Zhang, C. L. (2005), Self-sealing barriers of clay/mineral mixtures in a clay repository: SB experiment in the Mont Terri rock laboratory, Technical report, Gesellschaft für Anlagen-und Reaktorsicherheit (GRS).

Saiyouri, N., Hicher, P. Y. & Tessier, D. (2000), 'Microstructural approach and transfer water modelling in highly compacted unsaturated swelling clays', *Mech. Cohesive-Frict. Mater.* **5**(1), 41–60.

Saiyouri, N., Tessier, D. & Hicher, P.-Y. (2004), 'Experimental study of swelling in unsaturated compacted clays', *Clay Miner.* **39**(4), 469–479.

Salles, F., Bildstein, O., Douillard, J., Jullien, M., Raynal, J. & Van Damme, H. (2010), 'On the cation dependence of interlamellar and interparticular water and swelling in smectite clays', *Langmuir* **26**(7), 5028–5037.

Sánchez, M., Gens, A., do Nascimento Guimarães, L. & Olivella, S. (2005), 'A double structure generalized plasticity model for expansive materials', *Int. J. Numer. Anal. Methods Geomech.* **29**(8), 751–787.

Schanz, T., Khan, M. I. & Al-Badran, Y. (2013), 'An alternative approach for the use of ddl theory to estimate the swelling pressure of bentonites', *Appl. Clay Sci.* **83**, 383–390.

Schanz, T. & Tripathy, S. (2009), 'Swelling pressure of a divalent-rich bentonite: Diffuse double-layer theory revisited', *Water Resour. Res.* **45**(5), W00C12.

Segad, M., Hanski, S., Olsson, U., Ruokolainen, J., Akesson, T. & Jonsson, B. (2012a), 'Microstructural and swelling properties of Ca and Na montmorillonite: (in situ) observations with Cryo-TEM and SAXS', *J. Phys. Chem. C.* **116**(13), 7596–7601.

Segad, M., Jönsson, B. & Cabane, B. (2012b), ‘Tactoid formation in montmorillonite’, *J. Phys. Chem. C.* **116**(48), 25425–25433.

Seiphoori, A., Ferrari, A. & Laloui, L. (2014), ‘Water retention behaviour and microstructural evolution of MX-80 bentonite during wetting and drying cycles’, *Géotechnique.* **64**(9), 721–734.

Sellin, P. & Leupin, O. X. (2013), ‘The use of clay as an engineered barrier in radioactive-waste management–a review’, *Clays Clay Miner.* **61**(6), 477–498.

Singhal, S., Houston, S. L. & Houston, W. (2015), ‘Swell pressure, matric suction, and matric suction equivalent for undisturbed expansive clays’, *Can. Geotech. J.* **52**(3), 356–366.

Slade, P. & Quirk, J. (1991), ‘The limited crystalline swelling of smectites in CaCl2, MgCl2, and LaCl3 solutions’, *J. Colloid Interface Sci.* **144**(1), 18–26.

Spanner, D. (1951), ‘The Peltier effect and its use in the measurement of suction pressure’, *J. Exp. Bot.* pp. 145–168.

Sridharan, A., Altschaeffl, A. & Diamond, S. (1971), ‘Pore size distribution studies’, *J.Soi. Mech. Found. Div.* **97**(5), 771–787.

Sridharan, A. & Choudhury, D. (2002), ‘Swelling pressure of sodium montmorillonites’, *Géotechnique* **52**(6), 459–462.

Sridharan, A. & Jayadeva, M. (1982), ‘Double layer theory and compressibility of clays’, *Géotechnique.* **32**(2), 133–144.

Sridharan, A., Rao, A. S. & Sivapullaiah, P. V. (1986a), ‘Swelling pressure of clays’, *Geotech. Test. J.* **9**(1), 24–33.

Sridharan, A. & Rao, G. V. (1973), ‘Mechanisms controlling volume change of saturated clays and the role of the effective stress concept’, *Géotechnique.* **23**(3), 359–382.

Sridharan, A., Rao, S., Murthy, N. et al. (1986b), ‘Compressibility behaviour of homoionized bentonites’, *Geotechnique* **36**(4), 551–564.

Środoń, J. & MaCarty, D. K. (2008), ‘Surface area and layer charge of smectite from CEC and EGME/H_2O-retention measurements’, *Clays Clay Miner.* **56**(2), 155–174.

Stannard, D. I. (1992), ‘Tensiometers–theory, construction, and use’, *Geotech. Test. J.* **15**(1), 48–58.

Steudel, A. & Emmerich, K. (2013), ‘Strategies for the successful preparation of homoionic smectites’, *Appl. Clay Sci.* **75-76**, 13 – 21.

Tang, A.-M. & Cui, Y.-J. (2005), ‘Controlling suction by the vapour equilibrium technique at different temperatures and its application in determining the water retention properties of MX80 clay’, *Can. Geotech. J.* **42**(1), 287–296.

Taylor, D. W. (1942), *Research on consolidation of clays*, Vol. 82, Massachusetts Institute of Technology.

Towenr, G. D. (1981), ‘The correction of in situ tensiometer readings for overburden pressures in swelling soils’, *J. Soil Sci.* **32**(4), 499–504.

Tripathy, S., Bag, R. & Thomas, H. R. (2014b), ‘Effects of post-compaction residual lateral stress and electrolyte concentration on swelling pressures of a compacted bentonite’, *Geotech. Geol. Eng.* **32**(4), 749–763.

Tripathy, S. & Rees, S. (2013), ‘Suction of some polyethylene glycols commonly used for unsaturated soil testing’, *Geotech. Test. J.* **36**(5), 1–13.

Tripathy, S. & Schanz, T. (2007), ‘Compressibility behaviour of clays at large pressures’, *Can. Geotech. J.* **44**(3), 355–362.

Tripathy, S., Sridharan, A. & Schanz, T. (2004), ‘Swelling pressures of compacted bentonites from diffuse double layer theory’, *Can. Geotech. J.* **41**(3), 437–450.

Tripathy, S., Tadza, M. Y. M. & Thomas, H. R. (2014a), ‘Soil-water characteristic curves of clays’, *Can. Geotech. J.* **51**(8), 869–883.

Tripathy, S., Tadza, M., Yuhyi, M. & Thomas, H. R. (2011), ‘On the intrusion of polyethylene glycol during osmotic tests’, *Geotech Lett.* **1**(3), 47–51.

Tripathy, S., Thomas, H. & Bag, R. (2017), ‘Geoenvironmental application of bentonites in underground disposal of nuclear waste: characterization and laboratory tests’, *J. Hazard. Toxic Radioact. Waste.* p. D4015002.

Tu, H. & Vanapalli, S. K. (2016), ‘Prediction of the variation of swelling pressure and one-dimensional heave of expansive soils with respect to suction using the soil-water retention curve as a tool’, *Can. Geotech. J.* **53**(8), 1213–1234.

UPC (2017), *Code-Bright tutorial manual*, Department of Civil and Environmental Engineering of the Polytechnic University of Catalonia (UPC).

van Genuchten, M. T. (1980), ‘A closed-form equation for predicting the hydraulic conductivity of unsaturated soils’, *Soil Sci. Soc. Am. J.* **44**, 892–898.

Van Olphen, H. (1977), *An introduction to clay colloid chemistry: for clay technologists, geologists, and soil scientists*, 2 edn, Wiley, New York.

Vanapalli, S. K., Fredlund, D. G. & Pufahl, D. E. (1999), ‘The influence of soil structure and stress history on the soil-water characteristics of a compacted till’, *Géotechnique* **49**(2), 143–159.

Vanapalli, S. K., Lu, L., Sedano, J. I. & Oh, W. (2012), Swelling characteristics of sand-bentonite mixtures, *in* ‘Unsaturated Soils: Research and Applications’, Springer, pp. 77–84.

Vanapalli, S., Lu, L. & Oh, W. (2010), Estimation of swelling pressure and 1-d heave in expansive soils, *in* ‘Proceedings of the 5th International Conference on Unsaturated Soils, Barcelona, Spain, September’, pp. 6–8.

Velde, B. (1992), *Introduction to clay minerals: chemistry, origins, uses and environmental significance*, Chapman, Hall, London.

Viani, B. E., Low, P. F. & Roth, C. B. (1983), ‘Direct measurement of the relation between interlayer force and interlayer distance in the swelling of montmorillonite’, *Journal of Colloid and Interface Science* **96**(1), 229 – 244.

Villar Galicia, M. (2002), ‘Thermo-hydro-mechanical characterisation of a bentonite from Cabo de Gata a study applied to the use of bentonite as sealing material in high level radioactive waste repositories’, *Publicación técnica.(Empresa Nacional de Residuos Radiactivos.)* (4), 15–258.

Villar, M. (1999), ‘Investigation of the behaviour of bentonite by means of suction-controlled oedometer tests’, *Eng. Geol.* **54**, 67–73.

Villar, M. (2007), ‘Water retention of two natural compacted bentonites’, *Clays Clay Miner.* **55**(3), 311–322.

Villar, M. & Lloret, A. (2004), ‘Influence of temperature on the hydro-mechanical behaviour of a compacted bentonite’, *Appl. Clay Sci.* **26**(1), 337 – 350.

Villar, M. V., Gómez-Espina, R. & Lloret, A. (2010), ‘Experimental investigation into temperature effect on hydro-mechanical behaviours of bentonite’, *J. Rock Mech. Geotech. Eng.* **2**(1), 71–78.

Villar, M. V. & Lloret, A. (2008), ‘Influence of dry density and water content on the swelling of a compacted bentonite’, *Appl. Clay Sci.* **39**(1), 38–49.

Villar, M. V., Martín, P. L., Romero, F. J., Iglesias, R. J. & Gutiérrez-Rodrigo, V. (2016), ‘Saturation of barrier materials under thermal gradient’, *Geomech. Energy Environ.* .

Waclawska, I. (1984), ‘Dehydration and dehydroxylation of smectites 1. dehydration and dehydroxylation kinetics’, *Mineral Pol.* **15**(1-2), 91–107.

Wang, Q., Cui, Y.-J., Tang, A. M., Barnichon, J.-D., Saba, S. & Ye, W.-M. (2013), ‘Hydraulic conductivity and microstructure changes of compacted bentonite/sand mixture during hydration’, *Eng. Geol.* **164**, 67–76.

Wang, Q., Cui, Y.-J., Tang, A. M., Delage, P., Gatmiri, B. & Ye, W.-M. (2014b), ‘Long-term effect of water chemistry on the swelling pressure of a bentonite-based material’, *Appl. Clay Sci.* **87**, 157–162.

Wang, Q., Tang, A. M., Cui, Y.-J., Barnichon, J.-D. & Ye, W.-M. (2013b), ‘Investigation of the hydro-mechanical behaviour of compacted bentonite/sand mixture based on the BExM model’, *Computers and Geotechnics* **54**, 46–52.

Wang, Q., Tang, A. M., Cui, Y.-J., Delage, P., Barnichon, J.-D. & Ye, W.-M. (2013a), ‘The effects of technological voids on the hydro-mechanical behaviour of compacted bentonite-sand mixture’, *Soils Found.* **53**(2), 232–245.

Wang, Q., Tang, A. M., Cui, Y.-J., Delage, P. & Gatmiri, B. (2012), ‘Experimental study on the swelling behaviour of bentonite/claystone mixture’, *Engineering Geology* **124**(Supplement C), 59 – 66.

Wiederhold, P. R. (1997), *Water vapor measurement: methods and instrumentation*, CRC Press.

Williams, J. & Shaykewich, C. (1969), ‘An evaluation of polyethylene glycol (peg) 6000 and peg 20,000 in the osmotic control of soil water matric potential’, *Can. J. Soil Sci.* **49**(3), 397–401.

Xie, M. L., Miehe, R., Kasbohm, J., Herb, H. J., Meyer, L. & Ziesche, U. (2012), Bentonite as barrier material for the sealing of underground disposal sites: Bentonite barriers new experiments and state of the art, Technical report, Bundesanstalt für Geowissenschaften und Rohstoffe (BGR).

Ye, W.-M., Cui, Y.-J., Qian, L.-X. & Chen, B. (2009), ‘An experimental study of the water transfer through confined compacted GMZ bentonite’, *Eng. Geol.* **108**(3), 169–176.

Ye, W.-M., Wan, M., Chen, B., Chen, Y., Cui, Y. & Wang, J. (2013), ‘Temperature effects on the swelling pressure and saturated hydraulic conductivity of the compacted GMZ01 bentonite’, *Environ Earth sci.* **68**(1), 281–288.

Ye, W.-M., Zhang, Y., Chen, B., Zheng, Z., Chen, Y.-G. & Cui, Y.-J. (2012a), ‘Investigation on compression behaviour of highly compacted GMZ01 bentonite with suction and temperature control’, *Nucl. Eng. Des.* **252**, 11–18.

Ye, W., Wan, M., Chen, B., Chen, Y., Cui, Y. & Wang, J. (2012b), ‘Temperature effects on the unsaturated permeability of the densely compacted GMZ01 bentonite under confined conditions’, *Eng. Geol.* **126**, 1–7.

Yigzaw, Z., Cuisinier, O., Massat, L. & Masrouri, F. (2016), ‘Role of different suction components on swelling behavior of compacted bentonites’, *Appl. Clay Sci.* **120**, 81–90.

Yong, R. (1999), ‘Soil suction and soil-water potentials in swelling clays in engineered clay barriers’, *Eng. Geol.* **54**(1), 3–13.

Yong, R. N. & Mohamed, A. M. O. (1992), ‘A study of particle interaction energies in wetting of unsaturated expensive; clays’, *Can. Geotech. J.* **29**(6), 1060–1070.

Yong, R. N. & Warkentin, B. P. (1975), *Soil Properties and Behaviour. In: Developments in Geotechnical Engineering*, Vol. 5, Elsevier, Amsterdam.

Zhu, C.-M., Ye, W.-M., Chen, Y.-G., Chen, B. & Cui, Y.-J. (2013), ‘Influence of salt solutions on the swelling pressure and hydraulic conductivity of compacted GMZ01 bentonite’, *Eng. Geol.* **166**, 74–80.

Schriftenreihe des Lehrstuhls für Grundbau, Boden- und Felsmechanik der Ruhr-Universität Bochum

Herausgeber: H.L. Jessberger

1 (1979) **Hans Ludwig Jessberger**
Grundbau und Bodenmechanik an der Ruhr-Universität Bochum

2 (1978) **Joachim Klein**
Nichtlineares Kriechen von künstlich gefrorenem Emschermergel

3 (1979) **Heinz-Joachim Gödecke**
Die Dynamische Intensivverdichtung wenig wasserdurchlässiger Böden

4 (1979) **Poul V. Lade**
Three Dimensional Stress-Strain Behaviour and Modeling of Soils

5 (1979) **Roland Pusch**
Creep of soils

6 (1979) **Norbert Diekmann**
Zeitabhängiges, nichtlineares Spannungs-Verformungsverhalten von gefrorenem Schluff
unter triaxialer Belastung

7 (1979) **Rudolf Dörr**
Zeitabhängiges Setzungsverhalten von Gründungen in Schnee, Firn und Eis
der Antarktis am Beispiel der deutschen Georg-von-Neumayer- und Filchner-Station

8 (1984) **Ulrich Güttler**
Beurteilung des Steifigkeits- und Nachverdichtungsverhaltens von
ungebundenen Mineralstoffen

9 (1986) **Peter Jordan**
Einfluss der Belastungsfrequenz und der partiellen Entwässerungsmöglichkeiten auf die Verflüssigung von Feinsand

10 (1986) **Eugen Makowski**
Modellierung der künstlichen Bodenvereisung im grundwasserdurchströmten
Untergrund mit der Methode der finiten Elemente

11 (1986) **Reinhard A. Beine**
Verdichtungswirkung der Fallmasse auf Lastausbreitung in nichtbindigem
Boden bei der Dynamischen Intensivverdichtung

12 (1986) **Wolfgang Ebel**
Einfluss des Spannungspfades auf das Spannungs-Verformungsverhalten
von gefrorenem Schluff im Hinblick auf die Berechnung von Gefrierschächten

13 (1987) **Uwe Stoffers**
Berechnungen und Zentrifugen-Modellversuche zur Verformungsabhängigkeit
der Ausbaubeanspruchung von Tunnelausbauten in Lockergestein

14 (1988) **Gerhard Thiel**
Steifigkeit und Dämpfung von wassergesättigtem Feinsand unter Erdbebenbelastung

15 (1991) **Mahmud Thaher**
Tragverhalten von Pfahl-Platten-Gründungen im bindigen Baugrund, Berechnungsmodelle und Zentrifugen-Modellversuche

16 (1992) **Rainer Scherbeck**
Geotechnisches Verhalten mineralischer Deponieabdichtungsschichten bei ungleichförmiger Verformungswirkung

17 (1992) **Martin M. Bizialiele**
Torsional Cyclic Loading Response of a Single Pile in Sand

18 (1993) **Michael Kotthaus**
Zum Tragverhalten von horizontal belasteten Pfahlreihen aus langen Pfählen in Sand

19 (1993) **Ulrich Mann**
Stofftransport durch mineralische Deponieabdichtungen: Versuchsmethodik und Berechnungsverfahren

20 (1992) **Festschrift anlässlich des 60. Geburtstages von Prof. Dr.-Ing. H. L. Jessberger**
20 Jahre Grundbau und Bodenmechanik an der Ruhr-Universität Bochum

21 (1993) **Stephan Demmert**
Analyse des Emissionsverhaltens einer Kombinationsabdichtung im Rahmen der Risikobetrachtung von Abfalldeponien

22 (1994) **Diethard König**
Beanspruchung von Tunnel- und Schachtausbauten in kohäsionslosem Lockergestein unter Berücksichtigung der Verformung im Boden

23 (1995) **Thomas Neteler**
Bewertungsmodell für die nutzungsbezogene Auswahl von Verfahren zur Altlastensanierung

24 (1995) **Ralph Kockel**
Scherfestigkeit von Mischabfall im Hinblick auf die Standsicherheit von Deponien

25 (1996) **Jan Laue**
Zur Setzung von Flachfundamenten auf Sand unter wiederholten Lastereignissen

26 (1996) **Gunnar Heibrock**
Zur Rissbildung durch Austrocknung in mineralischen Abdichtungsschichten an der Basis von Deponien

27 (1996) **Thomas Siemer**
Zentrifugen-Modellversuche zur dynamischen Wechselwirkung zwischen Bauwerken und Baugrund infolge stoßartiger Belastung

28 (1996) **Viswanadham V. S. Bhamidipati**
Geosynthetic Reinforced Mineral Sealing Layers of Landfills

29 (1997) **Frank Trappmann**
Abschätzung von technischem Risiko und Energiebedarf bei Sanierungsmaßnahmen für Altlasten

30 (1997) **André Schürmann**
Zum Erddruck auf unverankerte flexible Verbauwände

31 (1997) **Jessberger, H. L. (Herausgeber)**
Environment Geotechnics, Report of ISSMGE Technical Committee TC 5 on Environmental Geotechnics

Herausgeber: Th. Triantafyllidis

32	(2000)	**Triantafyllidis, Th. (Herausgeber)** Boden unter fast zyklischer Belastung: Erfahrung und Forschungsergebnisse (Workshop)
33	(2002)	**Christof Gehle** Bruch- und Scherverhalten von Gesteinstrennflächen mit dazwischenliegenden Materialbrücken
34	(2003)	**Andrzej Niemunis** Extended hypoplastic models for soils
35	(2004)	**Christiane Hof** Über das Verpressankertragverhalten unter kalklösendem Kohlensäureangriff
36	(2004)	**René Schäfer** Einfluss der Herstellungsmethode auf das Verformungsverhalten von Schlitzwänden in weichen bindigen Böden
37	(2005)	**Henning Wolf** Zur Scherfugenbänderung granularer Materialien unter Extensionsbeanspruchung
38	(2005)	**Torsten Wichtmann** Explicit accumulation model for non-cohesive soils under cyclic loading
39	(2008)	**Christoph M. Loreck** Die Entwicklung des Frischbetondruckes bei der Herstellung von Schlitzwänden
40	(2008)	**Igor Arsic** Über die Bettung von Rohrleitungen in Flüssigböden
41	(2009)	**Anna Arwanitaki** Über das Kontaktverhalten zwischen einer Zweiphasenschlitzwand und nichtbindigen Böden

Herausgeber: T. Schanz

42 (2009) **Yvonne Lins**
Hydro-Mechanical Properties of Partially Saturated Sand

43 (2010) **Tom Schanz (Herausgeber)**
Geotechnische Herausforderungen beim Umbau des Emscher-Systems
Beiträge zum RuhrGeo Tag 2010

44 (2010) **Jamal Alabdullah**
Testing Unsaturated Soil for Plane Strain Conditions: A New Double-Wall Biaxial Device

45 (2011) **Lars Röchter**
Systeme paralleler Scherbänder unter Extension im ebenen Verformungszustand

46 (2011) **Yasir Al-Badran**
Volumetric Yielding Behavior of Unsaturated Fine-Grained Soils

47 (2011) **Usque ad finem**
Selected research papers

48 (2012) **Muhammad Ibrar Khan**
Hydraulic Conductivity of Moderate and Highly Dense Expansive Clays

49 (2014) **Long Nguyen-Tuan**
Coupled Thermo-Hydro-Mechanical Analysis: Experimental and Back Analysis

50 (2014) **Tom Schanz (Herausgeber)**
Ende des Steinkohlenbergbaus im Ruhrrevier: Realitäa und Perspektiven für die
Geotechnik Beiträge zum RuhrGeo Tag 2014

51 (2014) **Usque ad finem**
Selected research papers

52 (2014) **Houman Soleimani Fard**
Study on the Hydro-Mechanical Behaviour of Fiber Reinforced Fine Grained Soils
with Application to the Preservation of Historical Monuments

53 (2014) **Wiebke Baille**
Hydro-Mechanical Behavior of Clays - Significance of Mineralogy

54 (2014) **Qasim Abdulkarem Jassim Al-Obaidi**
Hydro-Mechanical Behavior of Collapsible Soils

55 (2015) **Veselin Zarev**
Model Identification for the Adaption of Numerical Simulation Models - Application
to Mechanized Shield Tunneling

56 (2015) **Meisam Goudarzy**
Micro and Macro Mechanical Assessment of Small and Intermediate Strain Properties
of Granular Material

57 (2016) **Oliver Detert**
Analyse einer selbstregulierenden interaktiven Membrangründung für Schüttkörper
auf geringtragfähigen Böden

58 (2016) **Yang Yang**
Analyses of Heat Transfer and Temperature-induced Behaviour in Geotechnics

59	(2016)	**Alborz Pourzargar** Application of suction stress concept to partially saturated compacted soils
60	(2017)	**Hanna Haase** Multiscale analysis of clay-polymer composites for Geoenvironmental applications
61	(2017)	**Kavan Khaledi** Constitutive modeling of rock salt with application to energy storage caverns
62	(2017)	**Nina Silvia Müthing** On the consolidation behavior of fine-grained soils under cyclic loading
63	(2017)	**Elham Mahmoudi** Probabilistic analysis of a rock salt cavern with application to energy storage systems
64	(2017)	**Negar Rahemi** Evaluation of liquefaction behavior of sandy soils using critical state soil mechanics and instability concept
65	(2018)	**Chenyang Zhao** A contribution to modeling of mechanized tunnel excavation
67	(2019)	**Linzhi Lang** Hydro-mechanical behaviour of bentonite-based materials used for disposal of radioactive wastes

Curriculum Vitae

Personal Information

Name	Linzhi Lang
Date of birth	January 15, 1988
Nationality	P.R. China
Gender	Male
Email	Linzhi.Lang@rub.de

Education

2014–2019 **Ph.D. in Geotechnical Engineering**, *Ruhr-Universität Bochum*, Germany.
Supervisor: Prof. Dr.-Ing. habil. Tom Schanz and Prof. Dr. Jörg Renner
Dissertation: Hydro-mechanical behaviour of bentonite-based materials used for disposal of radioactive wastes

2012–2014 **Ph.D. in Geological Engineering**, *China University of Geosciences (Wuhan)*, China.
Supervisor: Prof. Dr. Wei Xiang
Ph.D. project: Study on the model and mechanism of adsorbed water adsorption kinetics of cohesive soil

2008–2012 **Bachelor of Engineering Geology**, *China University of Geosciences (Wuhan)*, China.

Research Activities

2018.04-07 **Visiting Scholar**, *Cardiff University*, UK.
Cooperator: Prof. Snehasis Tripathy

Project Experience

Germany

2014–2018 **DFG Project: Scha 675/16-1 and FOR 444**, *Transient water transport in expansive soils under coupled hydraulic, mechanical and thermal boundary conditions: Experimental and numerical study*, Ruhr-Universität Bochum, Germany.

China

2012–2014 **Faculty of Engineering** , China University of Geosciences (Wuhan), China.

Publications

Journal paper

1. L.Z. Lang, S. Tripathy, W. Baille, T. Schanz & A. Sridharan (2019), Linkage between swelling pressure, total suction of saturated bentonites and suction of saturating aqueous solution, *Applied Clay Science* 171, 82-91
2. L.Z. Lang, W. Baille, S. Tripathy & T. Schanz (2018), Experimental study of influence of preliminary desiccation on swelling pressure and hydraulic conductivity of compacted bentonite, *Clay Minerals*, 1-12. doi:10.1180/clm.2018.53
3. L.Z. Lang, W. Xiang, W. Huang, D.S. Cui & T. Schanz (2017), An experimental study on oven-drying

methods for laboratory determination of water content of a calcium-rich bentonite, *Applied Clay Science* 150, 153-162

4. W. Huang, Q.B. Liu, W. Xiang, L.Z. Lang, D.S. Cui & J.E. Wang (2018), Hydration mechanism and microscopic water retention model of clay at high suction range, *Chinese Journal of Geotechnical Engineering* 40(7): 1268-1276.(In Chinese)
5. D.S. Cui, W. Xiang, Q. Chen, Q.B. Liu, L.Z. Lang & Y.P. Wu (2014), Pore characteristics of sliding zone soils of Huangtupo landslide by vacuum freeze-dried and dried methods, *Earth Science–Journal of China University of Geosciences* 39(10): 1431-1437.(In Chinese)
6. H.L. Jia, Q.B. Liu, W. Xiang, W.L. Zhang & L.Z. Lang (2013), Damage evolution model of saturated sandstone under freeze-thaw cycles, *Chinese Journal of Rock Mechanics and Engineering* S2: 3049-3055.(In Chinese)
7. L.Z. Lang, H.L. Jia & Y. Guo (2012a), Elementary analysis of failure mechanism and mechanical properties of sandstone under freeze-thaw cycling condition, *Water Resources and Power* 30(11): 118-121. (In Chinese)
8. L.Z. Lang, W. Xiang, R.R. Lou & H.L. Jia (2012b), Research and application on mathematic models for determining pre-consolidation pressure, *Journal of Engineering Geology* 20(5): 657-662. (In Chinese)
9. L.Z. Lang, P.Y. Chen, L.Z. Nie & L.D. Wu (2011), Research on preconsolidation pressure and its application based on Gaussian model, *Water Resources and Power* 29(7): 47-52. (In Chinese)
10. P.Y. Chen, & L.Z. Lang (2010), Advantage analysis of linear combination construction of background value in GM(1,1) model, *Journal of Southwest China Normal University (Natural Science Edition)* 35(6): 95-99. (In Chinese)
11. L.Z. Lang, X.S. Duan, & P.Y. Chen (2010), Numerical simulation of U-tube and analysis of constant heat flux models, *Journal of Shandong Jianzhu University* 25(5): 539-542. (In Chinese)

Conference paper

1. L.Z. Lang, W. Baille, S. Tripathy & T. Schanz (2018), Correlation between applied suction, total suction and swelling pressure in compacted bentonite-based materials, *8th International Conference on Unsaturated Soils* August 3–5, 2018, HongKong, China, Unsat2018_111.
2. L.Z. Lang, W. Xiang, A. Rawat, & W. Baille (2017), Identifying pore waters in clays based on isothermal adsorption of water vapour, *9. CMM Tagung 2017: Material–Prozesse–Systeme* September 20-21, 2017, Karlsruhe, Germany. 11-27.
3. W. Baille, L.Z. Lang, S. Tripathy, & T. Schanz (2016), Influence of effective stress on swelling pressure of expansive soils, *3rd European Conference on Unsaturated Soils* September 12–14, 2016, Paris, France, E3S Web Conf. 9, 14016.
4. L.Z. Lang, A. Rawat, W. Baille, & T. Schanz (2016), Effect of desiccation on hydro-mechanical behaviour of compacted bentonite based buffer material, *8th Mid-European Clay Conference* July 4–8, 2016, Kosice, Slovakia.
5. L.Z. Lang, W. Xiang, A. Rawat, W. Huang & W. Baille (2015), Effect of temperature under vacuum drying on rehydration of Ca-rich bentonite, *8. CMM Tagung 2015: Material–Prozesse–Systeme* October 8, 2015, Karlsruhe, Germany, 11–25.